EXPERIMENTAL INVESTIGATION OF FORCED CONVECTIVE BOILING OF HYDROCARBONS AND HYDROCARBON MIXTURES

by

Dipl.-Ing.

Thomas Kandlbinder

A thesis submitted in partial fulfilment of the requirements for the degree of Doctor of Philosophy of the University of London and for the Diploma of Imperial College of Science, Technology and Medicine

Department of Chemical Engineering and Chemical Technology, Imperial College of Science, Technology and Medicine, London, SW7 2AZ

November 1997

1 BIBL. LONDIN. UNIV

Abstract

Experimental results have been obtained for flow boiling in a vertical tube (tube inner diameter 25.4 mm, length 8.5 m) using hydrocarbons as test fluids. Local pressures, wall and bulk temperatures and heat flux were measured in order to calculate heat transfer coefficients. The test fluids were pure n-pentane and iso-octane, two binary mixtures of n-pentane and iso-octane with mole fractions of 0.7/0.3 and 0.35/0.65 respectively and a ternary mixture of n-pentane/n-hexane/iso-octane with a mole fraction of 0.2/0.22/0.58. Wide operating conditions were covered, with mass fluxes of 100 to 500 kg/m^{2}s, pressure of 0.23 to 1.5 MPa and heat fluxes of 10 to 100 kW/m^2.

The wide range of conditions highlighted separate regions where the nucleate boiling and purley convective heat transfer mechanisms dominated. Tests to examine the effect of pressure and the effect of inlet subcooling were conducted; for the pure components, characteristic peaks in heat transfer coefficient were observed at near-zero qualities, the heat transfer coefficient increasing at a given local quality with decreasing inlet subcooling. This effect was not observed with the mixtures. For the mixtures, characteristic decreases in heat transfer coefficients with increase in quality were observed and it is hypothesised that this is due to differential concentration of the heavier phase in the liquid film in annular flow. The two-phase heat transfer data, both for the pure components and mixtures were compared with common existing forced convective boiling correlations. In the nucleate boiling dominant region the heat transfer coefficient decreased with increasing quality. This trend is predicted by the Kandlikar (1990b) correlation. Results for single-phase heat transfer experiments in the fully turbulent and mixed convection, i.e. with relaminarisation, regions are given and compared with correlations. Dryout data were also compared with predictions from an annular flow model which considers entrainment and deposition.

Meinen Eltern Johann
und Brigitta gewidmet

Acknowledgements

This work was supported by the Engineering and Physical Research Council (EPSRC) and supervised by Professor G. F. Hewitt at the Department of Chemical Engineering, Imperial College of Science, Technology and Medicine. The experimental work was performed in the Heat Transfer and Fluid Flow Service (HTFS) High Pressure Boiling Facility at AEA Technology plc., Harwell.

I wish to express my thanks and appreciation to:

Professor G. F. Hewitt for providing me with the opportunity to do this work, and furthermore for his guidance and support throughout which have been invaluable.

HTFS for the provision of the facility.

My colleagues and friends Andrew Lintern and Richard Stevenson.

The EPSRC for their financial support.

Finally and most importantly my dear friends who supported and encouraged me throughout my stay in the UK.

Contents

Abstract 3

Acknowledgements 6

Nomenclature 22

1 Introduction 28

1.1 Overview of thesis 30

2 Literature survey 31

2.1 Forced convective boiling of pure components 31

2.1.1 The flow boiling process in a vertical tube from single-phase to two-phase 32

2.1.2 Observations in flow boiling 33

2.1.3 Concepts modelling the interaction of nucleate boiling and convective heat transfer. Classification of boiling models . 35

2.1.4 Suppression of nucleate boiling 37

2.1.5 Nucleate boiling during forced convection 38

2.1.6 Correlations 39

2.1.7 Other correlations 44

2.1.8 Flow history 44

2.1.9 Heat transfer in the intermittent flow regime 44

2.1.10 Void fraction and thermodynamic disequilibrium in sub-cooled boiling 45

2.2 Nucleate pool boiling 47
2.2.1 Bubble dynamics 48
2.2.2 Bubble growth, bubble departure and frequency 49
2.2.3 Heat transfer mechanisms, models 50
2.2.4 Correlations 51
2.2.5 Transfer of pool boiling methods to forced convective boiling 52
2.2.6 Dissolved gas effects 53
2.3 The evaporation of mixtures 55
2.3.1 The temperature – composition diagram 55
2.3.2 Difference in bubble growth dynamics between pure fluids and mixtures 55
2.3.3 Pool boiling of multicomponent mixtures 57
2.4 Forced convective boiling of mixtures 60
2.4.1 Experiments 60
2.4.2 Correlations: 66

3 Description of experimental apparatus, measuring devices and error analysis 82

3.1 The apparatus 82
3.1.1 History of rig 83
3.1.2 Modifications to the rig 83
3.2 The test section and its instrumentation 85
3.2.1 Pressure measurement 87
3.2.2 Temperature measurement 87
3.2.3 The calculation of the inner wall temperature 89
3.2.4 Flow measurement 91
3.2.5 Heat balances for single phase experiments 92
3.2.6 Density measurement 92
3.2.7 Test section heating 93
3.2.8 Overall uncertainity in the heat transfer coefficient 93

3.2.9 Stability of operating conditions during experiments 94
3.3 Operation of rig and conduction of experiments 95
3.3.1 Data collection 95
3.3.2 Procedure for boiling experiments 95

4 Analysis of experimental results **102**
4.1 Single phase heat transfer in vertical heated upflow 102
4.1.1 Effect of bulk thermocouples on the wall temperature profile 103
4.1.2 Fully turbulent heat transfer 103
4.1.3 Property correction 105
4.1.4 Entrance effect correction 106
4.1.5 Buoyancy effects on heat transfer: Mixed convection . . . 107
4.2 Forced convective boiling results for pure components 110
4.2.1 Assessment of the effect of the thermocouple pockets on the flow in the tube and the heat transfer 110
4.2.2 Calculation of heat transfer coefficient from the measurements 112
4.2.3 Effect of dissolved gas 114
4.2.4 Sensible heating profiles 116
4.2.5 Results of the main experiments and parametric trends . . 117
4.2.6 Peak in heat transfer coefficient at near zero quality 119
4.2.7 Comparison of single component data with existing empirical and semi-empirical predictive methods 121
4.2.8 Dryout 126
4.3 Forced convective boiling results for mixtures 130
4.3.1 Observations and parametric trends for mixtures 131
4.3.2 Comparison of correlations with mixture data 136

5 Conclusions **206**

6 Future work **209**
6.1 Analytical work 209

6.2 Experimental work 210

A Physical properties of hydrocarbons **212**

B Properties and dimensions of the test section **216**

C Statistical analysis of the experiments **221**

D Data storage **222**

References **223**

List of Figures

2.1 Flow boiling map with flow patterns, adapted from Steiner and Taborek (1992) 70

2.2 The effect of quality (left) on the heat transfer coefficient and (right) the effect of superheat on the heat flux. 71

2.3 Typical temperature profile for flow boiling in a horizontal tube, adapted from Reid et al. (1987). 71

2.4 Experimental heat transfer coefficient from Reid et al. (1987) on the effect of tube diameter, mass flux and heat flux. 72

2.5 Forced convection enhancement factor (F) and nucleate boiling suppression factor (S) as used in the Chen (1966) correlation. . . . 72

2.6 Kandlikar (1990a) flow boiling map for different liquid/vapour density ratios and Bo numbers. 73

2.7 Correlation chart of Shah (1976). 73

2.8 Effect of heat flux on relation between entrained liquid flow rate and quality for fixed mass flux and tube length (Sun and Hewitt, 1996). 74

2.9 Flow pattern and heat transfer regimes for flow boiling in a vertical tube, adapted from Spindler (1994). 74

2.10 Nucleate pool boiling process, Hsu and Graham (1986). 75

2.11 The nucleate boiling heat transfer mechanisms: bubble agitation (top), liquid exchange mechanism (middle) and micro layer evaporation (bottom). Adapted from Collier and Thome (1994). . . . 75

2.12 Temperature gradient at the wall for nucleate pool boiling (left) and for forced convection (right). 76
2.13 Temperature – Composition diagram for a nonazeotropic mixture, (water–methanol). 76
2.14 Temperature – Composition diagram, reduction in effective wall superheat due to mixture effects. 77
2.15 Variation of heat transfer coefficient with composition for binary mixture (Happel and Stephan, 1974). 77
2.16 Hihara and Saito (1988) data for the two different mixtures with different boiling ranges: low boiling range (left) and large boiling range (right). 78
2.17 Murata and Hashizume (1991) experimental data for pure component and binary mixtures at different mass fluxes and two heat fluxes. 78
2.18 Niederkrüger et al. (1992) horizontal tube flow boiling data (D = 14 mm) for a SF2/CF2Cl2 mixture. 79
2.19 Fujita and Tsutsui's (1995) results for the binary mixture R134a/ R123 and the pure components of R134a and R123 at a pressure of 0.6 MPa and mass flux of 300 kg/m^{2}s. 80
2.20 Comparison of pure component and binary mixture results from Celata et al. (1995): (top) subcooled boiling region and (middle and bottom) two-phase region. 81

3.1 Schematic diagram of the HPBR facility. 99
3.2 Installation of the wall thermocouples. 99
3.3 Installation of the test section thermocouples. 100
3.4 Temperature profile across the test section wall: without heat generation but with heat loss to the surroundings (left); with internal heat generation and heat losses (right). 100
3.5 Heat loss experiments. 101
3.6 Stability of DC supply. 101

4.1 Detailed drawing of the bulk thermocouple pocket. 139
4.2 Single phase run at a pressure of 1.66 MPa, mass flux of 292.8 kg/m^{2}s and a heat flux of 29.9 kW/m^2 showing a wall temperature peak. 139
4.3 Single phase run at a pressure of 1.77 MPa, mass flux of 170.2 kg/m^{2}s and a heat flux of 13.8 kW/m^2 showing the effect of wall thermocouple pockets. 140
4.4 Fully turbulent single phase run at a pressure of 0.24 MPa, mass flux of 505.8 kg/m^{2}s and a heat flux of 39.3 kW/m^2. 140
4.5 Ratio of the experimental to predicted heat transfer coefficient (Dittus-Boelter (1930) and Petukhov (1963)) plotted against the Reynolds and Prandtl number. 141
4.6 Ratio of the experimental to predicted heat transfer coefficient (Gnielinski (1976) and ESDU (1967)) plotted against the Reynolds and Prandtl number. 141
4.7 Plots of the experimental versus the predicted fully turbulent single phase heat transfer coefficients for different methods. 142
4.8 Single phase experimental results compared with the correlation of Jackson (1979). 143
4.9 Single phase experimental results compared with the correlation of Petukhov (1977) 144
4.10 Single phase experimental results compared with the correlation of Rouai (1987). 145
4.11 Test section with thermocouple pocket (hypodermic tube) and pressure tapping. 146
4.12 Schematic diagram of the entrance to the test section. 146
4.13 Solubility chart of the solubility of N_2 in n-pentane, from Landolt-Börnstein (1976). 147
4.14 n-pentane experiments with a Helium pressure of 0.14 MPa in the main storage tank. 148

4.15 n-pentane experiments with a Nitrogen pressure of 0.08 MPa in the main storage tank. 149
4.16 n-pentane experiments with a Nitrogen pressure of 0.24 MPa in the main storage tank. 150
4.17 Comparison of measured bulk fluid temperatures with the calculations from heat balances. 151
4.18 Effect of pressure on heat transfer coefficient, subcooling of about 14 °C. 152
4.19 Effect of pressure on heat transfer coefficient, subcooling of about 35 °C. 153
4.20 The effect of subcooling for two inlet suboolings with variation in heat flux. Subcooling of around 10 °C (left) and subcooling of around 23 °C (right). 154
4.21 The effect of variation in inlet temperature at a pressure of 1.0 MPa, mass flux of 500 kg/m^{2}s and a heat flux of 40 kW/m^2. . . . 155
4.22 The effect of variation in inlet temperature at a pressure of 0.24 MPa, mass flux of 500 kg/m^{2}s and a heat flux of 40 kW/m^2. . . . 156
4.23 Enhancement factor as a function of reciprocal Martinelli parameter calculated from various correlations compared with n-pentane experiments at a pressure of 0.23 MPa and a mass flux of 300 kg/m^{2}s; F_l (left) and F_{lo} (right). 157
4.24 Chen (1966) correlation compared with n-pentane data for pressures of 0.23 and 1.0 MPa, mass fluxes of 200 and 500 kg/m^{2}s and for various heat flux levels. 157
4.25 Steiner and Taborek (1992) correlation compared with n-pentane data for pressures of 0.23 and 1.0 MPa, mass fluxes of 200 and 500 kg/m^{2}s and for various heat flux levels. 158
4.26 Shah (1982) correlation compared with n-pentane data for pressures of 0.23 and 1.0 MPa, mass fluxes of 200 and 500 kg/m^{2}s and for various heat flux levels. 158

4.27 Kandlikar (1990b) correlation compared with n-pentane data for pressures of 0.23 and 1.0 MPa, mass fluxes of 200 and 500 kg/m^{2}s and for various heat flux levels. 159
4.28 Chen (1966) correlation compared with iso-octane data for pressures of 0.23 and 0.3 MPa, mass fluxes of 200 and 500 kg/m^{2}s and for various heat flux levels. 159
4.29 Steiner and Taborek (1992) correlation compared with iso-octane data for pressures of 0.23 and 0.6 MPa, mass fluxes of 200 and 500 kg/m^{2}s and for various heat flux levels. 160
4.30 Shah (1982) correlation compared with iso-octane data for pressures of 0.23 and 0.6 MPa, mass fluxes of 200 and 500 kg/m^{2}s and for various heat flux levels. 160
4.31 Kandlikar (1990b) correlation compared with iso-octane data for pressures of 0.23 and 0.6 MPa, mass fluxes of 200 and 500 kg/m^{2}s and for various heat flux levels. 161
4.32 Predicted versus experimental heat transfer coefficients for n-pentane data (for the Chen, Steiner and Taborek, Shah and Kandlikar correlations). 162
4.33 Predicted versus experimental heat transfer coefficients for iso-octane data (Chen, Steiner and Taborek, Shah and Kandlikar correlations). 162
4.34 Hysteresis effects for change in heat flux. 163
4.35 Hysteresis effects for change in inlet temperature: Increasing inlet temperature. 163
4.36 Hysteresis effects for change in inlet temperature: Decreasing inlet temperature. 164
4.37 Measured heat transfer coefficient and wall temperature and calculated film parameters for a typical n-pentane dryout experiment. 165
4.38 Measured heat transfer coefficient and wall temperature and calculated film parameters for a typical iso-octane dryout experiment. 166

4.39 Comparisons of experimental dryout results with predictions from the GRAMP code. 167
4.40 Experimental dryout qualities plotted against boiling length (left: n-pentane; right: iso-octane). 168
4.41 Comparison of entrainment and film thickness with and without initial entrainment at the onset of annular flow. 168
4.42 The effect of inlet temperature on the heat transfer coefficient for Mixture 1 at a pressure of 0.22 MPa, mass flux of 500 kg/m^{2}s and a heat flux of 40 kW/m^2. 169
4.43 Interface and wall temperatures and calculated heat transfer coefficients based on various levels of initial entrainment and on heavier phase concentration in the liquid film (Mixture 1 data, pressure 0.23 MPa). 170
4.44 Interface and wall temperatures and calculated heat transfer coefficients based on various levels of initial entrainment and on heavier phase concentration in the liquid film (Mixture 1 data, pressure 0.32 MPa). 170
4.45 Interface and wall temperatures and calculated heat transfer coefficients based on various levels of initial entrainment and on heavier phase concentration in the liquid film (Mixture 1 data, pressure 0.61 MPa). 171
4.46 Interface and wall temperatures and calculated heat transfer coefficients based on various levels of initial entrainment and on heavier phase concentration in the liquid film (Mixture 1 data, pressure 1.02 MPa). 171
4.47 Palen (1983) correlation compared with Mixture 1 data for pressures of 0.23 and 1.0 MPa, mass fluxes of 200 and 500 kg/m^{2}s for various heat flux levels. 172

4.48 Kandlikar (1991) correlation compared with Mixture 1 data for pressures of 0.23 and 1.0 MPa, mass fluxes of 200 and 500 kg/m^{2}s for various heat flux levels. 172
4.49 Murata (1993) correlation compared with Mixture 1 data for pressures of 0.23 and 1.0 MPa, mass fluxes of 200 and 500 kg/m^{2}s for various heat flux levels. 173
4.50 Predicted versus experimental heat transfer coefficient for the binary mixture (Palen, 1983). 173
4.51 Predicted versus experimental heat transfer coefficient for the binary mixture (Kandlikar, 1991). 174
4.52 Predicted versus experimental heat transfer coefficient for the binary mixture (Murata, 1993). 174
4.53 Operating conditions for boiling experiments as used in the following charts of the main series, Figures 4.54 to 4.83. 175
4.54 Temperature profiles plotted against tube length for the n-pentane boiling experiments at a pressure of 0.23 and 0.3 MPa. 176
4.55 Temperature profiles plotted against tube length for the n-pentane boiling experiments at a pressure of 0.6 and 1 MPa. 177
4.56 Heat transfer coefficients plotted against quality for the n-pentane boiling experiments at a pressure of 0.23 and 0.3 MPa. 178
4.57 Heat transfer coefficients plotted against quality for the n-pentane boiling experiments at a pressure of 0.6 and 1 MPa. 179
4.58 F enhancement factor plotted against $1/X_{tt}$ for the n-pentane boiling experiments at a pressure of 0.23 and 0.3 MPa. 180
4.59 F enhancement factor plotted against $1/X_{tt}$ for the n-pentane boiling experiments at a pressure of 0.6 and 1 MPa. 181
4.60 Temperature profiles plotted against tube length for the iso-octane boiling experiments at a pressure of 0.23 and 0.3 MPa. 182
4.61 Temperature profiles plotted against tube length for the iso-octane boiling experiments at a pressure of 0.6 and 1 MPa. 183

4.62 Heat transfer coefficients plotted against quality for the iso-octane boiling experiments at a pressure of 0.23 and 0.3 MPa. 184
4.63 Heat transfer coefficients plotted against quality for the iso-octane boiling experiments at a pressure of 0.6 and 1 MPa. 185
4.64 F enhancement factor plotted against $1/X_{tt}$ for the iso-octane boiling experiments at a pressure of 0.23 and 0.3 MPa. 186
4.65 F enhancement factor plotted against $1/X_{tt}$ for the iso-octane boiling experiments at a pressure of 0.6 and 1 MPa. 187
4.66 Temperature profiles plotted against tube length for Mixture 1 boiling experiments at a pressure of 0.23 and 0.3 MPa. 188
4.67 Temperature profiles plotted against tube length for Mixture 1 boiling experiments at a pressure of 0.6 and 1 MPa. 189
4.68 Heat transfer coefficients plotted against equilibrium quality for Mixture 1 boiling experiments at a pressure of 0.23 and 0.3 MPa. 190
4.69 Heat transfer coefficients plotted against equilibrium quality for Mixture 1 boiling experiments at a pressure of 0.6 and 1 MPa. . . 191
4.70 F enhancement factor plotted against $1/X_{tt}$ for the Mixture 1 boiling experiments at a pressure of 0.23 and 0.3 MPa. 192
4.71 F enhancement factor plotted against $1/X_{tt}$ for Mixture 1 boiling experiments at a pressure of 0.6 and 1 MPa. 193
4.72 Temperature profiles plotted against tube length for Mixture 2 boiling experiments at a pressure of 0.23 and 0.3 MPa. 194
4.73 Temperature profiles plotted against tube length for Mixture 2 boiling experiments at a pressure of 0.6 and 1 MPa. 195
4.74 Heat transfer coefficients plotted against quality for Mixture 2 boiling experiments at a pressure of 0.23 and 0.3 MPa. 196
4.75 Heat transfer coefficients plotted against equilibrium quality for Mixture 2 boiling experiments at a pressure of 0.6 and 1 MPa. . . 197
4.76 F enhancement factor plotted against $1/X_{tt}$ for the Mixture 2 boiling experiments at a pressure of 0.23 and 0.6 MPa. 198

4.77 F enhancement factor plotted against $1/X_{tt}$ for the Mixture 2 boiling experiments at a pressure of 0.6 and 1 MPa. 199
4.78 Temperature profiles plotted against tube length for Mixture 3 boiling experiments at a pressure of 0.23 and 0.3 MPa. 200
4.79 Temperature profiles plotted against tube length for Mixture 3 boiling experiments at a pressure of 0.6 and 1 MPa. 201
4.80 Heat transfer coefficients plotted against quality for Mixture 3 boiling experiments at a pressure of 0.23 and 0.3 MPa. 202
4.81 Heat transfer coefficients plotted against quality for the Mixture 3 boiling experiments at a pressure of 0.6 and 1 MPa. 203
4.82 F enhancement factor plotted against $1/X_{tt}$ for Mixture 3 boiling experiments at a pressure of 0.23 and 0.3 MPa. 204
4.83 F enhancement factor plotted against $1/X_{tt}$ for Mixture 3 boiling experiments at a pressure of 0.6 and 1 MPa. 205

A.1 Properites of n-pentane and iso-octane at saturation as a function of pressure 213
A.2 Properites of n-pentane and iso-octane at saturation as a function of pressure 214
A.3 Temperature–composition diagram for the binary mixture n-pentane/iso-octane at different pressures 215
A.4 Boiling ranges for the mixtures used plotted against pressure . . . 215

B.1 Thermal conductivity and electrical resistivity of stainless steel 321 218
B.2 Measured test section thickness 219
B.3 The definition of the roughness parameters 219
B.4 Definition of roughness parameter R_a 220
B.5 Measured roughness of test section for two locations (left: Position 1; right: Position 2) 220

List of Tables

2.1 Experiments on forced convective boiling of mixtures in horizontal tubes: Authors and range of operating conditions 61

2.2 Experiments on forced convective boiling of mixtures in vertical tubes: Authors and range of operating conditions 62

3.1 Correction factors for the wall thermocouples 97

3.2 Estimated uncertainities of the measured values needed for the calculation of the heat transfer coefficient 98

3.3 Test matrix for two-phase experiments 98

4.1 Comparison of average and mean errors of the single-phase heat transfer correlations compared with present data for single phase heat transfer 105

4.2 Operating conditions of single phase experiments 110

4.3 Statistical performance of pure component forced convective boiling correlations 124

4.4 Statistical performance of mixture forced convective boiling correlations 137

4.5 The description of the displayed items in the graphs of the main series, Figures 4.54 to 4.83 138

A.1 Properties for the pure hydrocarbons n-pentane, iso-octane and n-hexane 212

B.1 Roughness parameters for the two measured locations of the test section 217
B.2 Description of the roughness parameters according to the German standard DIN 4768 218

Nomenclature

Symbol	Quantity	SI unit
A	Constant introduced in Stephan and Körner (1969) correlation, eq. 2.47	-
A_o	Constant introduced in Stephan and Körner (1969) correlation, eq. 2.47	-
A_1	Constant introduced in Murata (1993) correlation, eq. 2.61	-
B_o	Parameter introduced in Schlünder (1983) correlation, eq. 2.49	-
C	Droplet concentration, introduced in Section 4.2.8	kg/m^3
C_d	Constant in eq. 2.63	
C_{offset}	Thermocouple offset	°C
c_p	Specific heat capacity	$J/(kgK)$
(dp_F/dz)	Frictional pressure gradient	N/m^3
D	Diameter	m
D_{12}	Mass diffusivity	m^2/s
D_d	Deposition rate, introduced in Section 4.2.8	kg/m^2s
D_d	Bubble departure diameter	m
E	Entrainment rate, introduced in Section 4.2.8	kg/m^2s
E	Enhancement factor	-
$e(j)$	Relative deviation of experimental to predicted values	-
f_{err}	Error function	-
Δf_{err}	Relative error	-
F	Enhancement factor	-
F_M	Mixture correction factor	-
F_{nbf}	Nucleate flow boiling correction factor, eq. 2.26	-

Symbol	Quantity	SI unit
F_{fl}	Fluid dependence factor in Kandlikar (1990b) correlation	-
F_p	Nucleate pool boiling pressure correction, eq. 2.62	-
F_{pf}	Nucleate flow boiling pressure correction in Steiner and Taborek (1992) correlation	-
F_{pn}	Nucleate pool boiling pressure correction in Gorenflo (1991) correlation	-
$f_2(Fr_{lo})$	Correction factor for gravitational effects, in Kandlikar (1990b) correlation	-
f_o	Fanning friction factor	-
G	Parameter in Shah (1982) correlation	-
g	Gravitational acceleration	m/s^2
h	Specific enthalpy	J/kg
h_{LV}	Specific latent heat of vaporisation	J/kg
I	Electrical current	A
K	Parameter in Petukhov correlation, eq. 4.4	-
K_S	Parameter defined in eq. 2.51	-
k	Droplet mass transfer coefficient, introduced in Section 4.2.8	m/s
L	Length	m
$\dot{M}$	Mass flow rate	kg/s
$\dot{m}$	Mass flux	$kg/(m^2s)$
$\tilde{M}$	Molecular weight	kg/kmol
n	Exponent	-
$nf(p_r)$	Exponent in Steiner and Taborek (1992) correlation	-
$n(p_r)$	Exponent in Gorenflo (1991) correlation	-
p	Pressure	N/m^2

Symbol	Quantity	SI unit
p_r	Reduced pressure $p_r = p/p_{cr}$	-
$p_{r,o}$	Reduced pressure at normalized conditions	-
p_{cr}	Critical pressure	N/m^2
Δp_{sat}	$= p_{sat}(T_w) - p_{sat}(T_{sat})$	N/m^2
$\dot{Q}_{loss}$	Heat loss per unit length	W/m
$\dot{q}$	Heat flux	W/m^2
$\dot{q_G}$	Internal heat generation	W/m^3
$\dot{q}_o$	Heat flux at normalized conditions	W/m^2
r	radial dimension	m
R	Radius	m
R_a	Roughness parameter	μm
$R_{a,o}$	Roughness parameter at normalized conditions	μ
R_{busbar}	Electrical resistance of bus bars	Ω
$\tilde{R}_g$	Universal gas constant	$J/kmolK$
R_p	Roughness parameter	μm
$\bar{R}_{TC}$	Thermal resistance of wall thermocouple	m^2K/W
S	Suppression factor	-
T	Temperature	K
T_i	Interface temperature	K
ΔT	Wall superheat $= T_w - T_{sat}$	K
ΔT_{eff}	Effective wall superheat	K
ΔT_{bp}	Mixture boiling range	K
ΔT_{NVG}	Subcooling at point of net vapour generation	K
$\Delta T_{sub,d}$	Subcooling at point of bubble detachment	K
U	Voltage	V
v	Velocity	m/s
$\dot{V}$	Flowmeter volume flow rate	$USgal/min$
x_g	Mass quality	-

Symbol	Quantity	SI unit
x'_g	Pseudo-mass vapour quality in subcooled region	-
$x_{g,d}$	Negative mass quality at bubble detachment	-
$X_1, X_2, X_4,$		
X_5, X_{13}	parameters defined in eq. 2.33	-
x	Mass fraction of liquid phase	-
$\tilde{x}$	Mole fraction of liquid phase	-
y	Mass fraction of vapour phase	-
$\tilde{y}$	Mole fraction of vapour phase	-
z	Axial dimension	m

Greek symbols:

Symbol	Quantity	SI unit
α, $\hat{\alpha}$	Heat transfer coefficient	$W/(m^2K)$
$\alpha_{nb,o}$	Nucleate boiling heat transfer coefficient at normalized conditions	$W/(m^2K)$
β	Mass transfer coefficient	m^2/s
β	Contact angle	*degrees*
γ	Coefficient of thermal expansion	$1/K$
δ	Parameter defined in eq. 2.63	-
η	Viscosity	Ns/m^2
κ	Thermal diffusivity $= \lambda/(\rho c_p)$	m^2/s
λ	Thermal conductivity	W/mK
ν	Kinematic viscosity	m^2/s
ρ	Density	kg/m^3
$\bar{\rho}$	Integrated density, eq. 4.12	kg/m^3
σ	Surface tension	N/m
τ_o	Wall shear stress	N/m^2

Nondimensional numbers:

Symbol	Name	Definition
Bo	Boiling number	$\frac{\dot{q}}{\dot{m}h_{LG}}$
Co	Convective number	$(\frac{1-x_g}{x_g})^{0.8}(\frac{\rho_L}{\rho_V})^{0.5}$
Gr^*	Grashof number	$\frac{g\gamma D^4\dot{q}}{\lambda\nu_b^2}$
$\bar{G}r$	Grashof number	$\frac{(\rho_b-\bar{\rho})D^3 g}{\rho_b\nu_b^2}$
Ja	Jacob number	$\frac{c_{p,L}\rho_L\Delta T}{h_{LV}\rho_V}$
Le	Lewis number	$\frac{\kappa}{D_{12}}$
Nu	Nusselt number	$\frac{\alpha D}{\lambda}$
Pe	Peclet number	$\frac{\dot{m}Dc_p}{\lambda}$
Pr	Prandtl number	$\frac{\eta c_p}{\lambda}$
Ra_P	Raleigh number	introduced in eq. 4.16
Re	Reynolds number	$\frac{\dot{m}D}{\eta}$
Re_{2ph}	Two-phase Reynolds number	defined in eq. 2.6
Sc	Schmidt number	$\frac{\eta}{\rho D_{12}}$
Sn	Scriven number	defined in eq. 2.36
St	Stanton number	$\frac{Nu}{RePr}$
X_{tt}	Martinelli parameter	$(\frac{1-x}{x})^{0.9}(\frac{\rho_L}{\rho_V})^{0.5}(\frac{\eta_L}{\eta_V})^{0.1}$

Subscripts:

1, 2	component number
b	bulk
bub	bubble point
calc	calculated
cr	critical
exp	experimental
fc	forced convective
ft	fully turbulent
i	component *i*
i	inner
id	ideal
in	inlet
L	saturated liquid
l	α, *Re* based on liquid fraction flow
lo	α, *Re* based on total flow as liquid
mix	mixture
n	number of components
nb	nucleate boiling
nbi	incipience of nucleate boiling
o	outer
out	outlet
pre	predicted
sat	saturation
sub	subcooling
TC	thermocouple
TS	test section
V	saturated vapour
w	wall

Chapter 1

Introduction

This study is concerned with the experimental investigation of forced convective boiling of pure components and mixtures in a vertical tube. Interest in the study of this phenomenon arises from the need to vaporise fluids used in the chemical and process industries and in steam generation. The accurate design of heat exchangers for these duties is important for the user in terms of size, cost, efficiency, reliability.

Although numerous prediction methods for evaporative heat transfer exist, they still show a high degree of uncertainity, especially for mixtures where additional complicating factors make the prediction more difficult. Evaluation of the research devoted to boiling of binary mixtures shows a lack of experimental data in forced convective flow boiling, where very few experiments have been performed, as previously reported by Stephan (1982) and Shock (1982) and recently reviewed by Steiner (1991). During the last two decades, the refrigeration industry showed interest in the prospects of using mixtures for the enhancement of refrigerating processes and a number of experiments have been conducted (e.g. Jung (1989c), Hihara (1989), Mishra (1981)); however, these studies were carried out only in horizontal tubes and for refrigerants. A relatively new field of application is in the cooling of microelectronic chips.

Experimental data on flow boiling of *organic mixtures* especially of hydrocarbons are very limited; this is due to complexity of the experimental apparatus

required to safely boil flammable and toxic organic liquids. One possibility might be to carry out tests on industrial heat exchangers. However, the use of this approach (for example studying operating reboilers) is of little value for the fundamental study of the effects of flow rate, heat flux, quality, and pressure since local measurements cannot be made in such systems and their range of operating variables is limited.

Although many experimental data and heat transfer correlations exist, prediction of heat transfer for mixtures with a wide-boiling range is still subject to large uncertainities. This is due to a close interaction between mass and heat transfer processes. Additionally, there is a further difficulty in the analysis of the experimental data because two mechanisms of heat transfer exist. The first one is convective evaporation, the heat transfer coefficient depending on the flow variables and not significantly on the heat flux. The second one is nucleate boiling where the coefficient is dependent on the heat flux (wall superheat), the microstructure of the surface, the pressure and the composition of the mixture and less significantly on the flowrate. If the dependent variables are not systematically varied over a sufficiently large range, the different mechanisms cannot be detected. The derived correlations then contain an array of empirical constants and cannot be used for conditions other than the tested ones. There is still a lack of knowledge of the basic phenomena in vaporisation of liquid mixtures; one of the problems is that there is such a variety of mixtures ranging from those which have similar proportions of two or more components (e.g. petroleum fluids) to mixtures with one component in very dilute solution (e.g. dissolved gas, salts in boilers). The first type of mixture is the one studied in the work described here.

The ultimate aim of research on boiling is the ability to predict a priori the boiling characteristics of any combination of solid heater and fluid coolant; this goal is still some way in the future. Forced convective boiling of mixtures is increasingly important in the chemical and petroleum industries, where many, if not most, boiler feeds are mixtures of two or more (and often many more – up to 40 in a typical petroleum feed) substances. It is also increasingly significant

in the cooling of high power-density electronic components by boiling liquids, where the use of mixtures offers a possible advantage in an increase of maximum heat load. Other applications include the evaporation of fuel for engines and the evaporation of spills of liquefied gases.

1.1 Overview of thesis

Chapter 2 presents a review of the literature on forced convective boiling for both single component and multicomponent mixtures. This has necessarily had to be rather selective, concentrating on those aspects which are relevant to the present study. Chapter 3 describes the facility used, the associated measurement devices and the data processing systems; an analysis of experimental error is also presented. Chapter 4 presents an analysis of the experimental data, starting with single phase convection (Section 4.1) and continuing with single component boiling (Section 4.2) and multicomponent boiling (Section 4.3). Finally, Chapter 5 and 6 deal respectively with conclusions and suggestions for further work.

Chapter 2

Literature survey

2.1 Forced convective boiling of pure components

The first research investigations of forced convective boiling date back to the 1940's where examples of the studies are those of Cichelli and Bonilla (1945) and Davidson (1943). In the 1950's and 1960's the research on forced convective boiling was intensified due to the development of nuclear power plants, where large amounts of heat had to be removed reliably and efficiently from the core of the reactor. This led to the improvement of understanding, the generation of experimental data and the development of models for the prediction of the flow boiling heat transfer. However, despite the large amount of work dedicated to the phenomena of forced convective boiling, there is by no means a thorough understanding nor a satisfying general method for predicting the heat transfer in vertical flow boiling. The main problem in dealing with forced convective boiling is that two heat transfer mechanisms of different nature (i.e. convective heat transfer due to the flow of the fluid and nucleate boiling) are occurring at the same time and interact with each other. In addition, the vapour generation causes changes in two-phase flow pattern, the latter evolving from bubble flow to slug, to churn flow and finally to annular flow along the channel. Finally, the

liquid film in the annular flow may be entrained and evaporate away, leading to dryout of the film and a deterioration of heat transfer.

The following Sections give an introduction to the phenomena and describe the problematic nature of this area of research and the models to predict the heat transfer performance. In view of the huge amount of work dedicated to forced convective boiling of pure components, only the fundamentals are presented, with more details on special aspects which are relevant to this present study. More detailed introductory reviews are given in the books by Collier and Thome (1994) and Carey (1992).

2.1.1 The flow boiling process in a vertical tube from single-phase to two-phase

The flow in a vertical heated tube may be visualised and explained with the help of Figure 2.1 from Steiner and Taborek's (1992) comprehensive paper. This figure shows flow patterns, typical wall and fluid temperature profiles and heat transfer coefficients for different heat fluxes. The schematic picture at the bottom subdivides flow boiling process into regions from A to G, which will be described now in more detail.

Up to point A the heat transfer is single-phase convective heat transfer to the liquid. At point A the required wall superheat for bubble nucleation is reached and bubbles grow near the wall. The bubbles collapse as they reach the core of the stream, which is still subcooled. At point B the generated bubbles penetrate into the flow and condense less rapidly with the result that there is a permanent presence of bubbles in the flow despite the fact that the mean enthalpy of the liquid is less than that for saturation; point B is referred to as the point of net vapour generation. With increasing enthalpy (quality), the flow regime progresses from bubbly to churn flow (point C). With further increasing in quality the flow pattern changes to annular (point D) flow which is characterised by

high velocity vapour flowing in the centre of the tube dragging a liquid film up the wall. Annular flow is prevalent over most of the tube. In this flow regime the high velocities of the vapour cause droplets to be entrained from the tips of waves at the film interface (point E). These droplets subsequently deposit, the entrainment and deposition processes coexisting along the channel. A necessary condition for droplet entrainment is the existence of large interfacial waves known as "disturbance waves" which move along the tube interspersed with smoother patches covered by smaller ripples. With further increase of vapour fraction the liquid film thins and eventually dries out leading to a deterioration of heat transfer at the dryout point F. The heat transfer coefficient decreases dramatically as the dry wall condition is reached and the tube wall temperature rises accordingly for a constant heat flux condition. The entrained drops may persist over substantial tube lengths in the post-dryout region but gradually evaporate in the superheating vapour. Finally, the evaporation is completed and the heat transfer coefficient drops to the value for vapour only (point G).

2.1.2 Observations in flow boiling

Several fundamental characteristics of flow boiling can be noted, which not only must be respected in the development of predictive methods, but which also suggest the most suitable model. Here the presently accepted dependencies are mentioned; later, some controversial findings will be discussed.

Effect of mass flux

Since forced convective heat transfer is associated with the flow of the vapour-liquid mixture a direct and strong effect of mass flux on the heat transfer is evident. For fully nucleate boiling dominant heat transfer, virtually no effect on the heat transfer can be observed.

Effect of heat flux

The heat flux has a strong influence on nucleate boiling, which creates the required superheat at the wall for bubble growth and activation of more cavities. No effect can be seen for purely convective heat transfer.

Effect of quality

For convective heat transfer, increase in quality has a similar effect as the increase in mass flux, because both increase the effective velocity. Nucleate boiling decreases with increase in quality, because the wall superheat decreases with increasing convective heat transfer coefficient and is able to sustain nucleation from a decreasing range of sites. Eventually, all the nucleation sites are suppressed.

Effect of pressure

An increase in pressure changes considerably the saturated fluid properties, which has different effects on the two heat transfer mechanisms. If nucleate boiling is dominant, the nucleate boiling heat transfer increases with increasing pressure. This is due to the reduction in the slope of the pressure-saturation curve, which reduces the superheat required to generate the same over-pressure in the bubble to sustain growth. The surface tension of the fluid reduces with increasing pressure and this also eases the bubble growth. On the other hand, for the forced convective dominant region, the ratio of liquid to vapour density, which reduces with increasing pressure, has a considerable influence on the convective heat transfer. When vapourisation is occurring a larger volume of vapour is generated at low pressure for a given amount of liquid vapourised. This means that the flow has to accelerate accordingly to meet the continuity criterion, which in turn increases the heat transfer coefficient.

Figure 2.2 shows on the left a typical graph with quality at the x-axis and heat transfer coefficient as the y-axis. The convective envelope is shown, when nucleate boiling is fully supressed. It can be noted that there is a strong heat flux dependence in the nucleate boiling dominant region, where higher qualities are

required to suppress nucleate boiling fully with increasing heat flux. Figure 2.2 on the right shows a plot of heat flux versus superheat, showing the effect of mass flux. At low superheats the slope of the lines is unity, signifying constant heat transfer coefficient and the existence of convection. The onset of nucleate boiling is characterised by the point where the straight lines begin to curve. The straight lines for the different mass fluxes converge into a single line for higher superheats which indicate a fully developed nucleate boiling region. The mechanism of the transition between the two regimes can be abrupt or more gradual; mass velocity, dissolved gases, and especially the distribution of the nucleation cavity sizes play a significant role.

2.1.3 Concepts modelling the interaction of nucleate boiling and convective heat transfer. Classification of boiling models

The models developed to date are all phenomenological in nature and no fully analytical model has been developed so far. In the literature, three different types of models can be found, the superposition model, the enhancement model and the asymptotic model. These models are not limited to a specific flow geometry or fluids; however different empirical constants may be required in different circumstances.

Superposition model (nucleation suppression)

The superposition model assumes that the total heat flux, $\dot{q}$, is the sum of the "nucleate boiling" component and the "convective evaporation" component. Thus, the basic equation for the superposition model is $\dot{q} = \dot{q}_{nb} + \dot{q}_{fc}$. Since $\dot{q}_{nb}$ and $\dot{q}_{fc}$ are calculated at the value of wall superheat $\Delta T = (T_w - T_{sat})$ the superposition model can also be written in terms of the component heat transfer coefficients $\alpha = \alpha_{nb} + \alpha_{fc}$. This model was initially proposed by Rohsenow (1952) for application to subcooled convective vaporization and was later slightly modified by

Bergles and Rohsenow (1964). Chen (1966) employed the superposition model in his well-known forced convective boiling correlation. The convective and nucleate boiling heat transfer mechanisms were clearly separated and Chen found that the simple addition of the two coefficients overpredicts the data. He derived a correlation to account for the suppression of nucleate boiling heat transfer.

Enhancement model

The "enhancement model" was proposed by Shah (1976) for flow in tubes with a correction for gravitational effects (partial wetting) in horizontal tubes. The correlations are based on two non-dimensional parameters, the Martinelli parameter (X_{tt}) and the Boiling Number (Bo). The former accounts for the enhancement of the heat transfer due to the flow, the latter is a measure of the nucleate boiling contribution. The correlations have the form: $\alpha/\alpha_l = f(X_{tt}, Bo)$ where α_l is the heat transfer coefficient for the flow of the liquid fraction flowing alone in the channel. Typically, several constants have to be fitted. These types of correlations have no particular physical basis, but often give reasonable data fits to the studied systems and are easy to use. The use of the Boiling Number (Bo) to solely account for the nucleate boiling restricts the range of applicability and accuracy, especially with respect to pressure effects.

Asymptotic model

The method of asymptotic addition was introduced by Kutateladze (1961) for subcooled convective boiling of water in tubes. The form of the equation is

$$\alpha = (\alpha_{nb}^n + \alpha_{fc}^n)^{1/n} \tag{2.1}$$

where α_{nb} is the nucleate boiling coefficient and α_{fc} the forced convective coefficient. Kutadeladze suggested a value of 2 for the exponent n. The choice of the exponent is derived by a best fit to data and has no theoretical basis. The same approach was used for single-phase convection, and has been formalized by Churchill and Usagi (1972) for modelling the transition between two different

heat transfer regimes, namely forced and natural convection. A smooth transition occurs as the system progresses from a situation in which one of the mechanisms is dominant to one in which the other is dominant. When n increases, the curved region between the asympotes contracts.

2.1.4 Suppression of nucleate boiling

The classical understanding of forced convective boiling is that, when nucleate boiling is dominant, the heat transfer coefficient is only a weak function of quality or rises slightly. From recent literature there is a strong indication that the suppression of nucleate boiling due to the flow can be so strong as to reduce the heat transfer coefficient with increasing quality. This phenomenon was either attributed to a real effect or to entrance effects.

Kenning and Cooper (1989) found in their experiments with water in vertical tubes that the heat transfer coefficient, α decreased with increasing quality at lower qualities, followed by an increase in α at higher qualities. Jensen and Bensler (1986) found the same behaviour for R-113 in a 8.1 mm diameter, 1.2 m long stainless steel tube and they attributed this to a thermal entry length effect. Also Jallouk (1974) shows a decreasing trend of α vs. x_g for R-114 in the entire saturated boiling region (x_g up to 35%). Jung et al. (1989 a,b) found that, in the nucleate boiling region α was almost independent of x_g at lower values of $\dot{q}$. At higher $\dot{q}$ values, α decreases with increasing quality. In the region where α decreases with increasing quality, both the forced convective evaporation and nucleate boiling mechanisms are significant. Similar regions were observed by Radermacher et al. (1983), Ross and Radermacher (1987a), Toral et al. (1982) and Chaddock and Noerager (1966).

Reid et al. (1987) showed some data with dropping heat transfer coefficient with increasing quality. Figure 2.3 shows a temperature profile for a typical boiling run. The tube wall temperatures are much lower than would be expected in a fully developed single-phase flow. Therefore, subcooled boiling was probably occurring in the vicinity of the first thermocouple position. The profiles of heat

transfer coefficient against equilibrium quality can be seen in Figure 2.4 showing first a decrease and then an increase with increasing quality. Two test section diameters were examined (D = 10.92 and 8.71 mm). All the trends could be found for both diameters, being more pronounced with the the larger tube at low qualities.

2.1.5 Nucleate boiling during forced convection

As can be seen from the previous section, nucleate boiling appears to be suppressed during forced convection and the suppression can be such as to make the sum of the convective and nucleate boiling components approximately constant (the classical picture) or to decrease with increasing qualities (as experimental data cited in Section 2.1.4 demonstrates). There is no reason in principle why the sum of the coefficients should actually increase or decrease in the region where both nucleate boiling and forced convection are significant. The result depends on the nature of the boiling surface. The classical mechanism for suppression of nucleate boiling in annular flow (see Collier and Thome, 1994) bears the same characteristics as the onset of nucleate boiling except that it occurs in the opposite direction. As the flow pattern turns into annular flow, the main heat transfer mechanism becomes conduction across the liquid layer. As the quality is increased, the liquid layer becomes thinner and thinner and hence the heat transfer coefficient increases due to the reduction in thermal resistance. Thus the wall superheat available in the liquid layer for a given heat flux decreases with increasing quality or mass flux. When the wall superheat available falls below that required to form bubbles, nucleate boiling is fully suppressed (no bubble formation on the wall). This interpretation of the mechanisms of forced convective boiling was strongly challenged by Mesler (1976) who, noting that for thin static films the nucleate boiling coefficient increased with decreasing film thickness, suggesting that the increase in heat transfer coefficient at high qualities was due to the presence of *secondary nucleation*, i.e. nuclei formed away from the wall as a result of such processes as droplet impingment or the release of bubbles from

the film surface. Careful studies by Aounallah et al. (1982) showed that, for an equilibrium annular flow, the heat transfer coefficient remained constant, independent of heat flux, which would not be the case for nucleate boiling. However, it could be argued that the secondary nucleation process could also give rise to a constant heat transfer coefficient since it did not depend on heat flux related processes of wall nucleation site activation. Some faith may have been restored in the traditional mechanisms by recent experiments by Sun and Hewitt (1996) who found (again for equilibrium annular flow – see Section 2.1.8) that the heat transfer coefficients were similar for evaporation and condensation respectively. This would imply that nucleation and bubble growth played no significant role after wall nucleation has been suppressed.

2.1.6 Correlations

Numerous correlations have been developed for forced convective boiling. Here, we summarize some of the more prominent ones as a background to their use in analysing the present data.

Chen (1966)

This correlation is of the superposition type (see Section 2.1.3). The nucleate boiling contribution is calculated by the well known correlation by Forster and Zuber (1955) multiplied by a suppression factor S to account for the reduction of effective superheat caused by the coexistence of the forced convective mechanism. For the enhancement of the convective heat transfer coefficient α_l for the liquid phase flowing alone in the channel, a parameter F is introduced which was shown by Chen through a Reynolds analogy to be represented as a function of the Martinelli parameter

$$X_{tt} = \left[\frac{(dp_F/dz)_L}{(dp_F/dz)_V}\right]^{1/2} \approx \left(\frac{1-x_g}{x_g}\right)^{0.9} \left(\frac{\rho_V}{\rho_L}\right)^{0.5} \left(\frac{\eta_L}{\eta_V}\right)^{0.1} \tag{2.2}$$

where $(dp_F/dz)_L$ and $(dp_F/dz)_V$ are the frictional pressure gradients for the liquid and vapour flowing alone in the channel. Chen's graphs for the F and S factor

are displayed in Figure 2.5. The correlation is thus expressed as:

$$\alpha = \alpha_l F + \alpha_{nb} S \tag{2.3}$$

Fits to the curves in the graphs are as follows:

$$F = \begin{cases} 2.35\,[1/X_{tt} + 0.213]^{0.736} & \text{for } 1/X_{tt} > 0.1 \\ 1 & \text{for } 1/X_{tt} \leq 0.1 \end{cases} \tag{2.4}$$

$$S = 1/[1 + 2.53 \cdot 10^{-6} Re_{2ph}^{1.17}] \tag{2.5}$$

with the two phase Reynolds number being defined as

$$Re_{2ph} = F^{1.25} Re_l \tag{2.6}$$

Re_l $(= \frac{\dot{m}(1-x_g)D}{\eta_L})$ is the Reynolds number for the liquid fraction mass flux in the channel. α_l is calculated from the Dittus-Boelter (1930) correlation for the appropriate value of Re_l and α_{nb} is estimated from the Forster–Zuber correlation as follows:

$$\alpha_{nb} = 0.00122 \left(\frac{\lambda_L^{0.79} c_{p,L}^{0.45} \rho_L^{0.49}}{\sigma^{0.5} \eta_L^{0.29} h_{LV}^{0.24} \rho_V^{0.24}} \right) \Delta T^{0.24} \Delta p_{sat}^{0.75} \tag{2.7}$$

with $\Delta p_{sat} = p_{sat}(T_w) - p_{sat}(T_{sat})$ and $\Delta T = T_w - T_{sat}$. The saturation pressure difference corresponding to the temperature difference ΔT can be estimated from the Clapeyron-Clausius equation:

$$ln\left(\frac{p_w}{p_{sat}}\right) = \frac{h_{LV}\,\tilde{M}}{\tilde{R}_g} \left(\frac{1}{T_{sat}} - \frac{1}{T_w}\right) \tag{2.8}$$

where $\tilde{M}$ is the molecular weight and $\tilde{R}_g$ is the universal gas constant (8314.5 J/kmol K). Chen's correlation gives good agreement with data for water but can give considerable errors for boiling of refrigerants.

Bjorge (1982)

Bjorge et al. (1982) used a variant of the superposition model to correlate their in-tube data for saturated water; they subtracted the incipient pool boiling heat flux, $\dot{q}_{nbi}$, using $\dot{q} = \dot{q}_{fc} + \dot{q}_{nb} - \dot{q}_{nbi}$.

Subtraction of $\dot{q}_{nbi}$ makes $\dot{q} = \dot{q}_{fc}$ at the incipient boiling point. The prediction of F is based on an annular flow model of Traviss et al. (1972). $\dot{q}_{nb}$ was predicted by using the Mikic and Rohsenow (1969) correlation and $\dot{q}_{nbi}$ was predicted by using the Bergles and Rohsenow (1964) method.

Kandlikar (1990b)

This correlation was developed on the basis of over 5000 data points from twenty-four experimental investigations for ten fluids and amounts to an extension of the Shah correlation.

$$\frac{\alpha}{\alpha_{lo}} = \text{maximum of} \begin{cases} [\alpha/\alpha_{lo}]_{nb} \\ [\alpha/\alpha_{lo}]_{fc} \end{cases} \tag{2.9}$$

$$\left[\frac{\alpha}{\alpha_{lo}}\right]_{nb} = 0.6683(\rho_L/\rho_V)^{0.1} x_g^{0.16}(1-x_g)^{0.64} f_2(Fr_{lo}) + 1058.0 Bo^{0.7} F_{fl}(1-x_g)^{0.8} F_M \tag{2.10}$$

$$\left[\frac{\alpha}{\alpha_{lo}}\right]_{fc} = 1.1360(\rho_L/\rho_V)^{0.45} x_g^{0.72}(1-x_g)^{0.08} f_2(Fr_{lo}) + 667.2 Bo^{0.7} F_{fl}(1-x_g)^{0.8}/F_M \tag{2.11}$$

where $f_2(Fr_{lo})$ denotes a correction for gravitational effects in horizontal tubes and has, for the vertical case, the value of 1. Bo is the "Boiling number" defined as $Bo = \dot{q}/(\dot{m}\, h_{LV})$. F_{fl} is a fluid dependent parameter which accounts for the differences in the nucleate boiling components of different fluids. α_{lo} is the single phase heat transfer coefficient with the total flow as liquid. The flow boiling chart is shown in Figure 2.6. Kandlikar (1991) extended his (Kandlikar, 1990b) correlation to binary mixtures by accounting for the nucleate boiling mixture effects by using the Calus and Rice (1972) mixture correction which is expressed as the following:

$$F_M = \left[1 + |y-x|\left(\frac{\kappa}{D_{12}}\right)^{0.5}\right]^{0.7} \tag{2.12}$$

where y and x are the mole fractions of the vapour and liquid phase respectively, κ the thermal diffusivity of the liquid phase and D_{12} the binary diffusion coefficient in the liquid.

Shah (1976, 1982)

Shah (1976, 1982) proposed a correlation in which the nucleate boiling component is represented by the boiling number, while a convective number Co (really a two-phase multiplier), $f(x_g, (\rho_L/\rho_V))$, is used for the convective boiling component. The two components are selected from a graphical chart (see Figure 2.7), which was later curve fitted by Shah (1982); the greater of the two components is used. This procedure is similar to the one originally proposed by Chawla (1967). The Shah (1976, 1982) curve fits to the Shah (1976) correlations are as follows:

$$\alpha = E\,\alpha_l \tag{2.13}$$

$$E = max\,(E_{fc}, E_{nb}) \tag{2.14}$$

with E_{fc} and E_{nb} being functions of the boiling number, Bo, and the convective number, Co. The correlation for the convective enhancement factor is

$$E_{fc} = 1.8/Co^{0.8} \tag{2.15}$$

The nucleate boiling enhancement factor being defined for three different regions:

$$If\ \ Co > 1.0:$$

$$E_{nb} = 230\,Bo^{0.5}\ (if\ Bo \geq 0.3 \cdot 10^{-0.4}) \tag{2.16}$$

$$E_{nb} = 1 + 46\,Bo^{0.5}\ (if\ Bo < 0.3 \cdot 10^{-0.4}) \tag{2.17}$$

$$If\ \ 0.1 < Co \leq 1.0:$$

$$E_{nb} = GBo^{0.5} exp(2.47\,Co^{-0.10}) \tag{2.18}$$

$$If\ \ 0.1 \leq Co:$$

$$E_{nb} = G\,Bo^{0.5} exp(2.47\,Co^{-0.15}) \tag{2.19}$$

with G being a constant dependent upon the Boiling number

$$G = 14.7\ (Bo \geq 11 \cdot 10^{-4}) \tag{2.20}$$

$$G = 15.3\ (Bo < 11 \cdot 10^{-4}) \tag{2.21}$$

Gungor and Winterton (1987)

This correlation is a typical enhancement model for both vertical and horizontal orientations and is given as:

$$\alpha = E\,\alpha_l \tag{2.22}$$

$$E = 1 + 3000 Bo^{0.86} + 1.12\,(x_g/(1-x_g))^{0.75}(\rho_L/\rho_V)^{0.41} \tag{2.23}$$

where α_l is the liquid fraction heat transfer coefficient calculated from the Dittus-Boelter correlation. The correlation has been tested against 4200 data points from 30 literature sources.

Steiner and Taborek (1992)

Steiner and Taborek (1992) correlated separately the contributions of nucleate and forced convective boiling and used the asymptotic addition of the two. The correlation was developed from a large data bank of about 20000 data points (all tube orientations).

$$\alpha = [(F\,\alpha_{lo})^3 + (F_{nbf}\,\alpha_{nb,o})^3])^{1/3} \tag{2.24}$$

where F is the forced convective enhancement factor given in equation 2.25 for $x_g \leq 0.6$. α_{lo} is calculated from the Gnielinski (1983) correlation based on the total flow as liquid.

$$F = [(1-x_g)^{1.5} + 1.9\,x_g^{0.6}\,(\rho_L/\rho_V)^{0.35}]^{1.1}|_{x_g \leq 0.6} \tag{2.25}$$

F_{nbf} is the nucleate flow boiling correction factor and is expressed as

$$F_{nbf} = F_{pf}\left(\frac{\dot{q}}{\dot{q}_o}\right)^{nf(pr)} f(D)\,f(R_a)\,f(\tilde{M}) \tag{2.26}$$

where F_{pf} and $nf(pr)$ are functions of reduced pressure, $f(D)$ accounts for diameter effect, $f(R_a)$ for the effect of roughness and $f(\tilde{M})$ is a molecular weight correction. $(\dot{q}/\dot{q}_o)^{nf(pr)}$ is the heat flux correction in relation to the normalized heat flux $\dot{q}_o$. $\alpha_{nb,o}$ is the nucleate pool boiling heat transfer coefficient at normalized values of $\dot{q}_o$ and $p_{r,o}$ determined from the Stephan and Preusser (1978) correlation. Details are given in the original paper of Steiner and Taborek (1992).

2.1.7 Other correlations

As mentioned above, many correlation have been developed so far, and will continue to be developed. Examples of recent correlations are those by Wattelet (1995), which is focused on predicting boiling heat transfer in small diameter tubes using an asymptotic model. Other examples are the correlations of Wadekar (1995), Yagov (1995), Klimenko (1990) and Liu and Winterton (1991).

2.1.8 Flow history

There is fundamental difficulty in designing objective experiments on forced convective boiling because of the effect of flow history. At any given quality in annular flow, the liquid is split between the wall film and droplets entrained in the gas core. However, the split depends on the previous history of the flow. This is illustrated in Figure 2.8 which plots entrained flow rate as a function of local quality with the heat flux increasing successively from point B to D. Curve A is for hydrodynamic equilibrium which is attained in long channels with adiabatic flow. The entrained liquid flow rate decreases for fixed quality with an increase in heat flux. This implies gross changes in the hydrodynamic conditions (film thickness, interfacial wave configuration, interfacial shear stress and pressure gradient) and this provides a very serious challenge to objectivity in interpreting forced convective boiling processes.

The ultimate limit in the departure from the hydrodynamic equilibrium conditions shown in Figure 2.8 is when all the liquid is entrained and dryout occurs. Further information on those processes is given by Hewitt and Hall Taylor (1970) and Hewitt (1982) and models for dryout etc describing the processes are given, for instance, by Govan and Hewitt (1990).

2.1.9 Heat transfer in the intermittent flow regime

Wadekar and Kenning (1990) developed a model to predict the heat transfer characteristics in the slug/churn flow region. This flow regime occurs at low

qualities, low mass and heat fluxes. The analysis is based on the data by Kenning and Cooper (1989) on flow boiling of water. They showed that it was possible to predict the boiling data in the intermittent region using a slug flow heat transfer model. This model combined additively the heat transfer associated with the falling liquid film surrounding the vapour plug with the convective heat transfer within the liquid slug. This model for purely convective heat transfer has been extended by Wadekar (1991) to include nucleate boiling within the slug.

2.1.10 Void fraction and thermodynamic disequilibrium in subcooled boiling

Clearly, if boiling is occurring at the channel wall, and the averaged enthalpy is below that for saturation, then the contents of the channel must be in a state of thermodynamic disequilibrium. When boiling starts, bubbles are formed at the wall and the heat transfer is a mixture of boiling and convection often referred to as "partial boiling".

As the heat flux is increased, convection becomes less significant and the "fully developed" boiling regime is entered. An important transition within the subcooled boiling region is that at which *net vapour generation (NVG)* occurrs, see Figure 2.9. At this condition, vapour enters the core of the flow and flows along with the (still subcooled) liquid, condensing relatively slowly.

The earlier models for subcooled boiling are described in detail by Collier and Thome (1994). Most of the experiments in this region have been carried out with water and the detailed information on other fluids is very limited. Examples of the kind of model which have been developed are as follows:

Bowring (1962): This model is very detailed but was interesting in that it introduced the concept of bubble detachment which was incorporated in subsequent models. Bowring defined a detachment length and gave empirical correlations for its value. Though this model was an important step forward, it was addressed specifically at water and is in dimensional form.

Levy (1967): The basis of the empirical method suggested by Levy (1967) is very similar to that proposed by Kröger and Zuber (1968). It is assumed that the "true" mass fraction vapour $x'_g(z)$ is related to the "thermodynamic" mass fraction of vapour $x_g(z)$ by the relationship

$$x'_g(z) = x_g(z) - x_g(z)_d \, exp\left(\frac{x_g(z)}{x_g(z)_d} - 1\right) \tag{2.27}$$

where $x_g(z)_d$ is the (negative) thermodynamic quality at the point of bubble detachment given by

$$x_g(z)_d = -\left[\frac{c_{p,L}\,\Delta T_{sub}(z)_d}{h_{LV}}\right] \tag{2.28}$$

where $(z)_d$ is the distance from the channel inlet at which detachment occurrs. Once the value of $x'_g(z)$ is established, the local void fraction can be calculated using conventional two phase flow relationships.

Saha and Zuber (1974): Saha and Zuber (1974) argued that the vapour generation must satisfy both the thermal as well as the hydrodynamic restraints. If the situation is such that the bubbles are attached to the surface, but the local subcooling is so high that the bubbles are immediately condensed as they grow into the liquid core, then the void fraction cannot grow. On the other hand, when the local subcooling is low, the bubbles may detach from the surface and condense only slowly in the core of the flow. For high and moderate inlet subcooling the local enthalpy at the point of net vapour generation is almost independent of the inlet subcooling. Therefore it can be argued that the point of net vapour generation is dependent only on local thermal conditions, which determine the rates of vapour condensation and evaporation at the wall. Saha and Zuber developed a model based on this concept. The expression for the point of net vapour generation (NVG) is:

$$\begin{aligned} Nu &= \frac{\dot{q}D}{\lambda \Delta T_{NVG}} = 455 \qquad if\ Pe \leq 70000 \\ St &= \frac{\dot{q}}{\dot{m}\, c_{p,L}\, \Delta T_{NVG}} = 0.0065 \quad if\ Pe > 70000 \end{aligned} \tag{2.29}$$

where St is the Stanton number and Pe the Peclet number defined as $Pe = Re \cdot Pr$. ΔT_{NVG} is the temperature difference between T_{sat} and T_{NVG}, i.e. the temperature

at the onset of net vapour generation.

2.2 Nucleate pool boiling

Though most of the experimental work on boiling has been conducted with pool boiling, the relevance of such work to the forced convective boiling case is often marginal. However, it can be argued that aspects relating to nucleation and fully developed nucleate boiling have some common features between pool boiling and forced convective boiling systems. Indeed, pool boiling based correlations often form the basis for predicting the nucleate boiling component in forced convective boiling. It is for this reason that a brief review of pool boiling is given here. More details can be found in the texts by Collier and Thome (1994), Carey (1992) etc.

Nucleate boiling heat transfer is difficult to predict, because surface characteristics, the fluid properties and the complex dynamic processes involved in bubble growth, departure, boundary layer stripping and interaction of growing bubbles are all involved and prediction methods show a high degree of uncertainity. Many component processes are involved at the microscopic or statistical level and they are interlinked in a very complicated manner (see Figure 2.10). A generalised understanding of the elementary processes and interrelationships is needed to describe an analytical model.

Two different types of nucleation can be distinguished, namely homogeneous and heterogeneous nucleation. The former is the rarer case where a liquid is superheated to a temperature at which statistical fluctuations in the liquid lead to the formation of nuclei which then rapidly grow. However, in real boiling systems the temperature required to initiate boiling is much lower than that for homogeneous nucleation; rather, heterogeneous nucleation occurs in which bubbles begin to grow from cavities on the wall (formed from grooves, asperities, cracks due to mechanical and thermal treatment). Therefore, heterogeneous nucleation is the most common type of nucleation and the phenomena of bubble growth and dynamics relating to this case shall be discussed here.

2.2.1 Bubble dynamics

Assuming a conical cavity of radius R, bubble nucleation may occur if the following equation, which discribes the mechanical equilibrium of the bubble is fulfilled.

$$p_V - p_L = \frac{2\sigma}{R} \tag{2.30}$$

where p_V is the vapour pressure inside the cavity and p_L is the pressure corresponding to a saturation temperature T_{sat}. An expression for the superheat required for bubble growth can be derived as

$$T_w - T_{sat} > \frac{T_{sat}}{\Delta h_{LV}\rho_V}\frac{2\sigma}{R} \tag{2.31}$$

The higher the wall superheat the smaller are the cavities activated for nucleation.

Bubble growth in an infinite superheated liquid

The early stage of bubble growth is controlled hydrodynamically by the liquid inertia, the displacement of liquid by the growth of the bubble, which lasts only over a short period. In the later stage the growth process is thermally controlled, i.e. by the rate at which heat can be transferred through the bubble interface. The diffusion controlled growth was expressed by Forster and Zuber (1955) as a function of Jakob number and thermal diffusivity. A detailed description of bubble growth prediction is given by Carey (1992).

Bubble growth at a heated surface

The formation of bubbles from a heated surface has been widely studied; the work of Bräuer and Mayinger (1992) is a recent example of such studies. The heat is not directly transformed from the surface to the vapour bubble, but it first enters the liquid adjacent to the surface, superheating a thin liquid layer; this creates a thermodynamically metastable situation for a very short period. If the nucleus is big enough or the superheating of the thin liquid layer is high enough, a bubble is formed which grows by evaporation from this superheated liquid layer.

2.2.2 Bubble growth, bubble departure and frequency

The prime forces acting on a vapour bubble during the later phases of its growth are buoyancy and hydrodynamic drag forces attempting to detach it from the surface and surface tension and liquid inertia forces acting to prevent detachment. The liquid inertia force is a dynamic force resulting from the displacement of liquid during bubble growth. The growth rate of a bubble and hence the inertial force is a strong function of the liquid superheat which, in turn, is inversly proportional to the size of the active cavity. A small cavity thus forms a bubble with a faster growth rate than does a large cavity. Hatton and Hall (1966) have considered all the forces acting on a growing bubble and have concluded that for small cavity sizes (i.e. those with diameters less than 10 μm for water at atmospheric pressure) the bubble size at departure is dictated mainly by a balance between buoyancy and liquid inertia forces. For larger cavity sizes, the growth rate decreases, the dynamic forces become small, and the bubble size at departure is set by a balance between buoyancy and surface tension forces (Howell and Siegel, 1966). Fritz (1935) first considered this latter case but more complete treatments including inertia, buoyancy and surface tension forces and the 'pinching' effect of the vapour neck joining the bubble to the surface have been developed (Hatton and Hall, 1966; Han and Griffith, 1965; Keshock and Siegel, 1964). When surface tension forces are dominant, the departing bubbles tend to be spherical. With inertia forces dominant the bubble tends to be hemispherical and when both forces are significant the bubble has an elongated oblate shape (Johnson et al., 1966). Cooper et al. (1978) carried out an experimental study on bubble growth and departure in a stagnant uniformly superheated liquid under both normal gravity and reduced gravity conditions. Contrary to the above results and theories, they concluded that the surface tension force can either assist or resist bubble departure depending on the circumstances.

Individual nucleation sites emit bubbles with a certain mean frequency, which varies from site to site. The bubble departure frequency is equal to the reciprocal of the sum of the bubble growth and waiting periods; the "waiting period" is

BIBL.
LONDIN.
UNIV.

the time taken for reinstatement of the thermal boundary layer following bubble departure. The bubble growth time can be obtained by solving a bubble growth equation coupled with a bubble departure criterion (see for instance van Stralen, 1970).

2.2.3 Heat transfer mechanisms, models

Several mechanistic models have been proposed to explain the enhancement of heat transfer in nucleate boiling. These include:

Vapour – liquid exchange mechanism

In this mechanism, the core liquid flows into the near surface region when the bubble departs. Transient conduction then takes place and the boundary layer heats leading to the formation of another bubble and the repeat of the cycle. Mikic and Rohsenow (1969) developed a model describing this process.

Latent heat transport model

Here, heat is transported from the surface in the form of latent heat in the vapour bubbles. This mechanism is likely to become dominant as the boiling becomes fully developed.

Microlayer evaporation model

Here, a thin layer of liquid (the "microlayer") forms underneath the growing bubble and is evaporated, contributing to bubble growth. This microlayer evaporation process represents a significant proportion of heat transfer at low pressure. The mechanism was proposed by Moore and Mesler (1961) and more extensively developed by van Stralen (1965). To determine the heat transfer coefficient using models based on these mechanisms, the dependence of the bubble frequency, departure diameter and boiling site density must be known. Unfortunatley, no general correlations exist for these variables because of the dependence on the

micro-geometry and condition of the heat transfer surface. Figure 2.11 shows schematically the mechanisms occurring.

2.2.4 Correlations

Despite the fundamental difficulties arising from the unknown nature of the surface microstructure mentioned above, a very wide range of correlation have been developed for nucleate pool boiling. The correlation of Forster and Zuber (1955) was stated in Section 2.1.6 above since it is used as a component of the Chen (1966) forced convective boiling correlation. In what follows, several other well-known correlations are reviewed which exemplify the approaches taken.

Stephan and Abdelsalam (1980)

This correlation was derived from statistical regression techniques with data from many sources covering different fluids (water, hydrocarbons, cryogenic fluids and refrigerants) and surfaces from many sources. The correlation does not contain any surface effect correction. The general (not fluid specific correlation) based on non-dimensional numbers is given as follows.

$$Nu = 0.23\, X_1^{0.674}\, X_5^{0.297}\, X_4^{0.371}\, X_{13}^{-1.73}\, X_2^{0.35} \tag{2.32}$$

$$\begin{aligned} X_1 &= \frac{\dot{q}\, D_d}{\lambda_L\, T_{sat}} & X_2 &= \frac{\kappa_L^2\, \rho_L}{\sigma\, D_d} \\ X_4 &= \frac{h_{LV}\, D_d^2}{\kappa_L^2} & X_5 &= \frac{\rho_V}{\rho_L} \\ X_{13} &= \frac{(\rho_L - \rho_V)}{\rho_L} & D_d &= 0.0146\, \beta\, [2\sigma / g\, (\rho_L - \rho_V)]^{0.5} \end{aligned} \tag{2.33}$$

where D_d is the bubble departure diameter and β the contact angle (35 ° for organics, 1 ° for cryogenics, 45 ° for water).

Cooper (1984)

Cooper (1984) noted that it was possible to represent the relevant physical properties in terms of reduced pressure p_r ($p_r = p/p_{cr}$) where p is the pressure and p_{cr} the critical pressure. Thus, all correlations could be expressed in terms only

of reduced pressure and Cooper developed a correlation on this basis. A further parameter was introduced to account for the surface characteristic of the heating surface. The correlation is

$$\frac{\alpha}{\dot{q}^{0.67}} = 55\, p_r^{0.12-0.2\,log_{10}(R_p)} \left(-log_{10}\left(p_r\right)\right)^{-0.55} \tilde{M}^{-0.5} \tag{2.34}$$

where R_p is the roughness of the tube ("Glättungstiefe" in μm according to the German DIN standard) and $\tilde{M}$ the molecular weight.

Gorenflo (1991)

The Gorenflo (1991) correlation relates the nucleate boiling heat transfer coefficient α_{nb} to that for a standard set of conditions ($\alpha_{nb,o}$) by the expression:

$$\alpha_{nb} = \alpha_{nb,o}\, F_{pn} \left(\frac{\dot{q}}{\dot{q}_o}\right)^{n(p_r)} \left(\frac{R_a}{R_{a,o}}\right)^{0.133} \tag{2.35}$$

where $\dot{q}_o$ and $R_{a,o}$ are the heat flux and surface roughness for the standard conditions and $\dot{q}$ and R_a the values for the conditions being evaluated. F_{pn} and $n(p_r)$ are functions of reduced pressure. Details are given by Gorenflo (1991). The correlation is of interest in the present context since it forms the basis of the nucleate boiling component in the forced convective boiling correlation of Steiner and Taborek (1992).

2.2.5 Transfer of pool boiling methods to forced convective boiling

Though pool nucleate boiling correlations are often used for the nucleate boiling component of forced convective boiling, there are significant differences between the two cases which should be borne in mind. These differences are the following:

1. The temperature gradient at the wall is usually higher in forced convection boiling than in pool boiling (see Figure 2.12). This influences the range of nucleation sites which can be activated for a given wall temperature and is, of course, linked to the nucleation suppression effects referenced in Section 2.1.4.

2. The superimposed forced convection exerts a direct effect on bubble departure as has been demonstrated by Koumoutsos et al. (1968). This will influence the heat transfer in nucleate boiling.

3. The presence of forced convection will influence the growth of the thermal boundary layer following the departure of the bubble. Though transient conduction will still play a part, convection effects will be superimposed. Studies of temperature fields in forced convective nucleate boiling are reported by Bräuer and Mayinger (1992).

In the light of the above observations, it is perhaps even surprising that the pool nucleate boiling correlations are even remotely useful in applications to forced convective boiling. The likely explanation for their relative success is that, in the fully developed boiling region, external effects like the ones mentioned above become less significant and the evaporation process is governed by phenomena occurring near the heated surface. These processes are probably related to the formation of a macrolayer (i.e. a layer of liquid penetrated by vapour stems) near the wall at high heat fluxes. A discussion of this mechanism is presented, for instance, in the review by Dhir (1996).

2.2.6 Dissolved gas effects

It is well known that the incipient superheat for bubble nucleation is reduced in fluids which contain dissolved gas. The actual saturation pressure is reduced by the partial pressure of the gas exerted on the fluid; initiation of bubbles can occur even if the saturation temperature of the fluid without dissolved gas is not exceeded, i.e. at negative superheats. There have been a number of studies both in pool boiling and in forced convective boiling aimed at evaluating the effects of dissolved gases on heat transfer. Complete removal of non-condensible gases may not be feasible. Gas is always present and even a trace amount can have a significant role in the boiling incipience process.

An interesting set of pool boiling experiments on the effect of traces of dis-

solved gases was carried out by Marto and and Lepere (1982) who studied boiling of refrigerants. After preboiling for 1 hour at 30 kW/m^2, they then conducted boiling experiments after different waiting periods at zero heat flux (0 min, 30 min and overnight). The cases in which there was no heating overnight always indicated the highest superheat at boiling incipience. This may be due to diffusion of gas from the bubble in the nucleation sites into the surrounding liquid. A relatively short waiting period (30 min) would not lead to a noticeable change in the superheat required to initiate boiling since the process of diffusion is extremely slow.

You et al. (1991) suggests that dissolved gases exert their influence by two mechanisms, namely by increasing the gas partial pressure in the nucleation site and by slowing the condensation of the gas/vapour mixture in the sites following the bubble departure. He found that in experiments with dielectric fluorinert FC-72 that the dissolved air played a perceptible role only when a very high content ($>$ 0.005 moles/mole) was maintained. The insignificance of the effect of the gas at lower concentrations was attributed due to degassing of the liquid in the vicinity of nucleation sites.

Behar et al. (1966) carried out an experimental investigation of the effect of dissolved gas in flow boiling of water and organic liquids. They found that the wall superheat at the onset of nucleate boiling was reduced with increasing dissolved gas content. The improvement in the heat transfer coefficient was more pronounced with organic liquids where solubility of gases are an order of magnitude greater than those for water. Murphy and Bergles (1972) came to the same conclusion regarding in the partial boiling region; however, at higher heat fluxes in the fully developed boiling region the effect of dissolved gas gradually disappeared. Experiments by Mayinger and Bucher (1972) show the same trend; they observed that dissolved gas ceases to exert an influence on the heat transfer coefficient after initiation of net vapour generation.

2.3 The evaporation of mixtures

2.3.1 The temperature – composition diagram

When for example a binary nonazeotropic mixture undergoes evaporation, the composition of the two phases are different for a given overall composition. This can be illustrated with the temperature composition diagram in Figure 2.13. For a given total composition x_o at state 1 below the bubble point only one phase exists. State 2 at the bubble point the liquid has a composition x_o in equilibrium with the vapour which has the composition y_2. During further evaporation the temperature rises and the compositions of the liquid and vapour shift to x_3 and y_3. At the dew point (state 4) the composition of the vapour is x_o and that of the liquid is x_4. Further heat addition evaporates all the liquid to give superheated vapour alone (state 5).

The composition differences between vapour and liquid cause two additional effects relative to the case of evaporation of pure components. Firstly, when the quality is increased, the more volatile component is depleted from the liquid phase and enriches the vapour phase. Secondly, vaporisation at constant pressure does not occur at the same temperature but over a range called the boiling range ΔT_{bp}.

Reductions in the heat transfer performance occur for all mixtures compared to the pure components unless one of the components is surface active and decreases the surface tension.

2.3.2 Difference in bubble growth dynamics between pure fluids and mixtures

The bubble growth rate for a single component is usually limited by the rate of conduction of heat to the interface where the conducted heat provides the required latent heat for vaporisation. In a binary liquid mixture the preferential vaporisation of the more volatile component from the region close to the bubble interface causes a concentration gradient across the liquid boundary layer. Now

the more volatile component has to diffuse towards the interface which causes, in addition to the heat conduction resistance, also a mass diffusion resistance, which slows down the bubble growth. The mass transfer process is slower than the heat transfer, by about an order of magnitude. The stripping of the more volatile component at the interface increases the interface temperature (see Figure 2.14). The composition at the interface moves from $\tilde{x}_1$ to $\tilde{x}_{1,Ph}$ with an increase in the interface temperature from T_b to T_i. The actual superheat, temperature driving force is reduced from ΔT to $\Delta T_{eff} = T_w - T_i$.

Scriven (1959), van Stralen (1966a,b) and Van Stralen and Zijl (1978) theoretically investigated the mass transfer effect on the growth of a spherical bubble in an uniformly superheated binary liquid. As described above the effective superheat is reduced and the reduction of the superheat can be expressed as

$$Sn = \frac{\Delta T_{eff}}{\Delta T} = \left[1 - (y - x)\left(\frac{\kappa}{D_{12}}\right)^{0.5}\left(\frac{c_{p,L}}{h_{LV}}\right)\left(\frac{\partial T_{bub}}{\partial x}\right)\right]^{-1} \tag{2.36}$$

where $\partial T_{bub}/\partial x$ is the differential of the bubble point temperature with respect to composition at the bulk composition. The ratio of the thermal to mass diffusivity represents the ratio of heat to mass transfer rates in the liquid surrounding a bubble and is termed the Lewis number.

Recognising the significant effects of mass transfer on bubble growth, it is not surprising that the heat transfer coefficient for boiling at a given heat flux passes through a minimum value with increasing concentration. A review of information on nucleate pool boiling of mixtures is given by Collier and Thome (1994). Figure 2.15 exemplifies the type of result obtained. For binary mixtures not forming an azeotrope (Figure 2.15 left), there is a single minimum in the heat transfer coefficient corresponding to the maximum difference between vapour and liquid compositions at the bubble point as shown. For a mixture forming an azeotrope (Figure 2.15 right) there are two minima with the coefficient at the aceotropic composition (where there is no difference between the vapour and liquid compositions) being the value calculated on an ideal mixture basis.

2.3.3 Pool boiling of multicomponent mixtures

A large number of empirical or semi-empirical correction factors for nucleate boiling of mixtures has been published in the literature. A very recent paper by Gorenflo and Köster (1997) lists 21 correlations. The mixture effect is often expressed as the ratio of the mixture heat transfer coefficient and the ideal heat transfer coefficient, which is either based on the molar average of the heat transfer coefficients for the pure components or on the molar average of the superheats . If α_i is the nucleate boiling heat transfer coefficient for the pure i th component at the prescribed heat flux $\dot{q}$, then we may calculate an "ideal" heat transfer coefficient for the mixture as

$$\alpha_{id} = \sum_{i=1}^{n} \tilde{x}_i \alpha_i \tag{2.37}$$

where $\tilde{x}_i$ is the mole fraction of component i and n is the total number of components. We may also define an ideal mean superheat ΔT_{id} from the expression

$$\Delta T_{id} = \sum_{i=1}^{n} \tilde{x}_i \Delta T_i \tag{2.38}$$

where ΔT_i is the wall superheat for boiling of component i at the prescribed heat flux $\dot{q}$ (note that $\Delta T_i = \dot{q}/\alpha_i$). We may then define an alternative value for the "ideal" mixture coefficient as:

$$\hat{\alpha}_{id} = \dot{q}/\Delta T_{id} \tag{2.39}$$

It follows from equation 2.38 and 2.39 that

$$\frac{1}{\hat{\alpha}_{id}} = \sum_{i=1}^{n} \frac{\tilde{x}_i}{\alpha_i} \tag{2.40}$$

$\hat{\alpha}_{id}$ and α_{id} do not differ much, unless the heat transfer coefficients of the pure components are extremely different.

Another basis of comparison for the boiling behaviour of mixtures the so-called "equivalent pure fluid". Thus, mixture boiling data is compared with the expected behaviour of a substance that resembles the mixture in all its physical properties save that the liquid and vapour compositions are identical. Such a pure substance is referred to as an equivalent pure fluid (EPF). Since the thermodynamic and

transport properites of mixtures can be complex functions of the composition, it may be difficult to evaluate the predicted behaviour of the EPF, hence the convenient supposition is often adopted that a parameter such a surface superheat or heat transfer coefficient would be linearly related to the composition in the absence of mixture effects and this has led to the widespread use of α_{id} as a basis for comparisons.

All the correlations implicitly contain data on the phase equilibrium of vapour and liquid, either in terms of differences between the compositions of vapour and liquid or in terms of boiling range. With the use of some empirical fitting parameters, others include saturation parameter or the normalised pressure or the heat flux.

Here it is the aim to mention only a few of the correlations listed by Gorenflo and Köster (1997), basing the selection on those which have been used in forced convective boiling applications and those which are potentially good tools for prediction.

One of the earliest correlation for the effect of mixtures was that of Palen and Small (1964) where the heat transfer coeffficient is given by:

$$\alpha = F_M \, \alpha_{id} \tag{2.41}$$

where F_M is a mixture correction factor whose value was given by Palen and Small as

$$F_M = exp(-0.027 \, \Delta T_{bp}) \tag{2.42}$$

where ΔT_{bp} is the "boiling range" (difference between the dew point and bubble point temperatures). An alternative expression for F_M is given by Palen and Yang (1983) as follows:

$$F_M = \frac{1}{1 + 0.023 \, \dot{q}^{0.15} \, \Delta T_{bp}^{0.75}} \tag{2.43}$$

Stephan and Körner (1969) define a temperature driving force

$$\Delta T = \Delta T_{id} + \Delta T_{eff} \tag{2.44}$$

where ΔT_{id} is given (for a binary mixture) by

$$\Delta T_{id} = \tilde{x}_1 \Delta T_1 + \tilde{x}_2 \Delta T_2 = \tilde{x}_1 \Delta T_1 + (1 - \tilde{x}_1) \Delta T_2 \tag{2.45}$$

where ΔT_1 and ΔT_2 are the temperature diffences for boiling of the pure components at the same heat flux. The additional temperature difference ΔT_{eff} was empirically correlated by the expression:

$$\Delta T_{eff} = A (\tilde{y}_b - \tilde{x}_b) \Delta T_{id} \tag{2.46}$$

where $\tilde{y}_b$ is the vapour composition corresponding to the bulk concentration $\tilde{x}_b$ for component 1 at the equilibrium temperature T_{bub}. The coefficient A is given by:

$$A = A_o (0.88 + 0.12\, p) \tag{2.47}$$

where p is the pressure in bars and A_o varies from binary mixture to binary mixture but has an average value of 1.53.

Thome (1983) suggests that, at a boiling site, all of the liquid approaching the site may be evaporated such that the local value of $\tilde{y}_b$ is equal to $\tilde{x}_b$. Thus, there is an elevation in temperature ΔT_{bp} corresponding to the diffference between the bubble point curve and the dew point curve at the local liquid concentration. Thus:

$$\Delta T = \Delta T_{id} + \Delta T_{bp} \tag{2.48}$$

A semi-theoretical treatment that actually gives results rather close to those of Thome was introduced by Schlünder (1983) who obtained the expression:

$$\frac{\alpha}{\alpha_{id}} = \left[1 + \frac{\alpha_{id}}{\dot{q}} \left[(T_{sat,2} - T_{sat,1})(\tilde{y} - \tilde{x}) \left(1 - exp \left(\frac{-B_o \dot{q}}{\rho_L h_{LV} \beta_L} \right) \right) \right] \right]^{-1} \tag{2.49}$$

where $T_{sat,1}$ and $T_{sat,2}$ are the saturation temperatures for components 1 and 2 respectively and $\tilde{y}$ is the vapour composition in equilibrium with the liquid composition $\tilde{x}$ at T_{bub}. β_L is a liquid phase mass transfer coefficient (having a value of approximately 2×10^{-4} m/s) and B_o is a scaling parameter whose value is around unity. The Schlünder analysis represents the data moderately well, but it must still be considered empirical since the constant B_o has to be manipulated

in order to fit the data. Gorenflo (1991) recommends a value of 10^4 for the ratio B_o/β_L. Fujita et al. (1996) carried out a wide range of experiments with the boiling of binary mixtures and compared the data with existing correlations (including those listed above). They suggest the following improved form of correlations:

$$\frac{\alpha}{\alpha_{id}} = \frac{1}{1 + K_S\,(\Delta T_{bp}/\Delta T_{id})} \tag{2.50}$$

where

$$K_S = [1 - exp(-2.8\,\Delta T_{id}/(T_{sat,2} - T_{sat,1})] \tag{2.51}$$

where $(T_{sat,2} - T_{sat,1})$ is the difference in saturation temperatures between the two components. The correlation predicted the data to within $\pm 20\%$ and, overall, performed better than the other correlations tested.

2.4 Forced convective boiling of mixtures

2.4.1 Experiments

Tables 2.1 and 2.2 list some of the main experimental studies of mixture flow boiling. Most of the research conducted on forced convective boiling of mixtures was with refrigerants; using mixed refrigerants has the potential of giving higher performances in refrigerating machines. These refrigerant experiments were mainly conducted in horizontal tubes and are summarised in Table 2.1 and the results are briefely discussed below. Zizyukin and Aerov (1975) calculated average heat transfer coefficients and correlated the data without any mixture correction. The correlation developed contained the Martinelli parameter and a further non-dimensional constant consisting of pressure, surface tension and liquid density.

Mishra et al. (1981) discovered large wall temperature fluctuations and attributed them to unstable behaviour of the flow boiling. The heat transfer coefficients of the binary mixture were found to be lower than the linear interpolation of the pure components. The correlation suggested in form of $f(X_{tt}, Bo)$ is strictly

Author, Date	Fluids	Tube D/L [mm]	Pressure [MPa]	Mass flux [kg/m^{2}s]	Heat flux [kW/m^2]	Quality [ ]
Zizyukin and Aerov (1975)	pentane/hexane propane/pentane iso-butane/hexane propane/pent./hex.	10/2000	0.13 - 0.86	90 - 258		< 0.5
Mishra et al. (1981)	R12/R22	12.5/2600	0.1	125 - 310	3 - 15	< 0.8
Singal et al. (1983)	R13/R12	9.52/2350		235 - 454	5 - 17	< 0.8
Radermacher et al. (1983)	R13B1/R152a	9/700	0.12 - 0.8	100 - 600	10 - 95	< 1.0
Jung (1989c)	R22/R114 R12/R152a	9/2*4000	$p_r = 0.08$	250 - 720	10 - 45	< 0.8
Hihara and Saito (1988)	R12/R22 R114/R22	8/4000	0.23 - 0.83	100 - 350	5.8 - 28.5	< 0.95
Murata and Hashizume (1991)	R123/R134a R11/R114	10.7/734	0.2 - 0.24	100 - 300	0 - 30	0.1 - 0.9
Niederkrüger et al. (1992)	SF2/CF2Cl2	14/200	1.5 - 3.2	80 - 400	7 - 80	0.05 - 0.9
Kattan and Thome (1995a,b)	R125/R290/R22 R125/R143a/R134a R22/R115	12/3013	0.6 - 0.9	100 - 320	3.5 - 30	< 0.99

Table 2.1: Experiments on forced convective boiling of mixtures in horizontal tubes: Authors and range of operating conditions

Author, Date	Fluids	Tube D/L [mm]	Pressure [MPa]	Mass flux [kg/m^{2}s]	Heat flux [kW/m^2]	Quality [ ]
Calus et al. (1973a,b)	n-propanol/H_2O iso-propanol/H_2O H_2O/glycerol	12.7/1200			2.5 - 25	< 0.5
Bennett (1976)	H_2O/ethylene glycol	19/76	0.2	320 - 1200	725 - 2900	< 0.3
Shock (1973)	ethanol/water	31.75/3048				< 0.16
Toral (1979)	ethanol/cyclohex.	26.2/3080	0.24 - 0.27	300 - 900	20 - 240	< 0.3
Kusomowardhoyo and Hardianto (1985)	ethanol/gasoline	26/300				
Nakanishi et al. (1987)	R11/R113	7.0/	< 0.36	350 - 750	< 85	< 0.9
Fujita and Tsutsui (1995)	R134a/R123	10/4000	0.6	300	1 - 50	
Celata et al. (1995)	R12/R114	7.57/2300	1 - 2.2	500 - 1550	18 - 40	

Table 2.2: Experiments on forced convective boiling of mixtures in vertical tubes: Authors and range of operating conditions

applicable only for the fluids used and conditions, because the constants were fitted for each pure fluid and composition of the mixture. The correlation showed a mean deviation of 30% for the data.

Singal et al. (1983) studied the boiling of mixtures of R12 and R13 and found that the effect of mass velocity, heat flux and quality on boiling heat transfer for the investigated mixture was qualitatively the same as in the case of a pure component. The average heat transfer coefficient for the binary mixtures was slightly greater than that of the pure R12; however, no experiments with the pure R13 were performed.

Radermacher et al. (1983) observed that both the local and average heat transfer coefficients were much lower than those for either pure component in the nucleate boiling dominated regime.

Jung and Didion (1989c) conducted flow boiling experiments where the majority of data was in the convection dominant regime. A large suppression of

the heat transfer coefficient is observed relative to the pure components with a reduction in the heat transfer coefficient with increasing quality. The measured mixture heat transfer coefficients for R22/R114 were lower than the ideal values. 80% of the degradation is associated with the physical property variation of the mixture, the remaining 20% (less than 10% of the total heat transfer coefficient) is believed to be due to mass transfer resistance in evaporation with mixtures.

Hihara and Saito (1988) investigated two binary mixtures with two different boiling ranges ((a) $< 3°C$, (b) large). For the low boiling range mixture (see Figure 2.16 left) no heat transfer deterioration was observed, whereas for the wider boiling mixture the mixture heat transfer coefficients are lower (see Figure 2.16 right). The data was correlated with an $f(X_{tt}, Bo)$ type of correlation fitting the parameters for each composition.

Murata and Hashizume (1990, 1991) presents a comparison of results for pure R11 , R114 and a 0.5 mass fraction mixture of R11/R114 for two different heat fluxes and three mass fluxes (see Figure 2.17). The convective and the nucleate boiling regions can be distinguished. In the nucleate boiling dominant region, a considerable reduction in the heat transfer coefficient can be seen. However, for the convective dominant region a nearly linear variation in the mixture heat transfer coefficient between the pure fluids occurred. The Stephan and Körner (1969) mixture correction was used to predict the mixture effects in the nucleate boiling region. More recently Murata and Hashizume (1993) continued work with pure R123 and a mixture of R123 and R134a (boiling range about 54 K) for a smooth and for a spirally grooved tube. They found that the heat transfer coefficients were reduced relative to the equivalent pure fluid not only in the nucleate boiling dominant region but also in the forced convective dominant region. A correlation was developed to account for mixture effects for both heat transfer mechanisms; this include the effect on nucleate boiling and also the effect of sensible heating of the vapour phase accompanying a rise of saturation temperature in the flow direction. The correlation developed is described in Section 2.4.2.

Niederkrüger et al. (1992) presents data for the heat transfer coefficient at

the (completely wetted) bottom of the tube. The results are nucleate boiling dominated because of the high pressures. A systematic investigation was made of the effect of composition and the results are shown in Figure 2.18. The effect of mass flux was small. A reduction of the heat transfer coefficient is observed for qualities greater than 50% (Figure 2.18 bottom). This is due to the depletion of the more volatile component in the liquid phase and it was stated that the higher the quality, the higher is the change of composition in the liquid. The maximum amount of reduction in heat transfer for the mixture depends on heat flux and the minimum heat transfer coefficient does not always correspond to the maximum of the difference in vapour-liquid composition (this feature was also observed by Celata et al. (1993).

Kattan and Thome (1995a,b) studied boiling of two mixtures with low boiling ranges (< 1 °C) and one azeotropic mixture. They found monotonically decreasing heat transfer coefficients with increasing quality. Maximas for the heat transfer coefficients occurred at low qualities and it was suggested that these were caused by a change of flow pattern. The Gungor and Winterton (1986) correlation with the Thome (1989) mixture correction predicted the data well; however, the mixture effect is minimal (1 – 2 % reduction in the heat transfer coefficient).

Table 2.2 gives an overview of the experiments conducted with vertical tubes: all of the experiments were done with upwards flow. The results of these investigations are briefly summarised below.

Calus et al. (1973a,b) conducted experiments in a single tube natural circulation reboiler using non-azeotropic and azeotropic mixtures. The data was correlated by using their single component correlation after two modifications. One modification was the adoption of an effective temperature difference. The other was the use of surface tension evaluated at the interfacial composition.

Toral (1979) carried out experiments on the boiling of cyclohexane/ethanol mixtures and noticed secondary effects like the influence of dissolved gas, hysteresis, and local variations in wall superheat. The wall temperature for higher heat fuxes showed a wavy pattern, which according to the author is due to significant

nucleate boiling contribution and the local variation in nucleation site density. Unfortunately all the Toral data is in nucleate boiling dominant region. Toral found also that the boiling curves for mixtures had a gentler slope than for the single component. The Chen (1966) and Shah (1976) correlations considerably underpredicted the heat transfer coefficient for the pure components.

Kusomowardhoyo and Hardianto (1985) examined forced convective boiling in the bubbly and slug flow regime. The fluid studied was an ethanol/gasoline mixture at various compositions. Their approach to correlation was purely a data fit without any mechanistic basis; they used a correlation of the form $f(Re, Pr, Bo)$.

Nakanishi et al. (1987) investigated forced convective boiling up to high qualities and also found a deterioration of the heat transfer at high quality. Since nucleation was considerably suppressed in an annular liquid film at higher quality , the observed deterioration could not be attributable to the mass transfer resistance in forming bubbles.

Fujita and Tsutsui (1995) compared data for single components and mixtures with the correlations proposed by Gungor and Winterton (1986), Kandlikar(1990b), Stephan and Auracher (1981) and Wadekar (1990). Figure 2.19 shows a comparison of experimental results plotted as reciprocal Martinelli parameter against the ratio of the experimental to the all-liquid heat transfer coefficient. Results for the pure components are nucleate boiling dominated (Figure 2.19 top left and bottom right) and do not cover the convective region. For the mixtures with a composition of 0.5 and 0.75, the data lie below the pure convective F factor, which indicates some mixture effects also in the convective region.

Celata et al. (1995) studied the boiling of R12/R114 mixtures. He compared his data with the correlations of Chen (1966), Bennett and Chen (1980) and Mishra (1981). In the *convective boiling* region the Chen (1966) and Bennett and Chen (1980) show good performance, but the Mishra (1981) correlation seems to be less accurate. Data from this investigation are plotted against equilibrium quality in Figure 2.20. The top figure shows comparisons between pure

components and mixtures in the subcooled boiling region. The single-phase heat transfer regime persists longer for mixtures than it does for the pure components. The other two graphs show the reduction of heat transfer for the mixtures at different heat and mass fluxes.

2.4.2 Correlations:

Few predictive methods for mixture boiling inside tubes have been developed, and those available are usually based on modifying pure fluid methods to account for the mixture effect.

Bennett and Chen (1980):

The Bennett and Chen (1980) correlation is no doubt the most disputed and most frequently tested and discussed. Bennett and Chen (1980) conducted experiments in a very short test section (L/D = 3) with one thermocouple on the test section outer wall and one in the centreline of the tube. It was shown that these sets of data (1000 points) were not predicted well by the original Chen (1966) correlation. A Prandtl number correction was introduced for the convective heat transfer and for the mixture effects and a correction to the convective term was introduced to account for the reduction of the temperature driving force. Also the nucleate boiling term was modified to account for mass transfer effects; the expression by Scriven (1959)(see Equation 2.36) was applied. However, the data base used for the derivation of the correlation consists mainly of data in the convective heat transfer region. The Bennett and Chen correlation is summarised as follows:

$$\alpha = \alpha_l F_{mix} + \alpha_{nb} S_{mix} \tag{2.52}$$

with the enhancement factor F_{mix} being:

$$F_{mix} = F\, f(Pr_L) \left[\frac{\Delta T_{eff}}{\Delta T}\right] \tag{2.53}$$

and the Prandtl correction factor:

$$f(Pr_L) = \left(\frac{Pr_L + 1}{2}\right)^{0.444} \tag{2.54}$$

The reduced superheat is expressed as:

$$\left[\frac{\Delta T_{eff}}{\Delta T}\right] = 1 - \frac{(1-y)\dot{q}}{\rho_L \Delta h_{LV} \beta_L \Delta T} \frac{\partial T_{bub}}{\partial x} \tag{2.55}$$

The mass transfer coefficient β_L is calculated from

$$\beta_L = 0.023 \frac{D_{12}}{D} Re_{tp}^{0.8} Sc^{0.4} \tag{2.56}$$

and the Chen suppression factor S was multiplied by the Scriven number, Sn.

$$S_{mix} = Sn\, S \tag{2.57}$$

α_{nb}, F, S and Re_{2ph} are as in the Chen correlation (see Section 2.1.6). An additional Prandtl correction $f(Pr_L)$ is applied to the convective term and a correction for the actual temperature driving force $\left[\frac{\Delta T_{eff}}{\Delta T}\right]$ for binary mixtures. The Scriven number, Sn, accounts for mass transfer effects in nucleate boiling heat transfer. β is the mass transfer coefficient and Sc is the Schmidt number $(= \eta/(\rho D_{12}))$.

Palen (1983)

Palen (1983) suggests the use of a modified form of the Chen (1966) correlation for boiling of mixtures. The heat transfer coefficient is given by:

$$\alpha = \alpha_l\, F + \alpha_{nb}\, F_M\, S \tag{2.58}$$

where F and S are as in the Chen (1966) correlation (i.e. are identical to those for pure components). F_M is given by Equation 2.42.

Kandlikar (1991)

Kandlikar simply added the Calus and Rice (1972) mixture correction to the nucleate boiling term in his correlation (see Section 2.1.6).

Murata (1993)

The correlation developed by Murata and Hashizume (1993) is based on the model by Sardesai et al. (1982). The nucleate boiling reduction in the nucleate boiling heat transfer is accounted for in a form of the Stephan and Körner (1969) mixture correction factor. Furthermore, a correction for the sensible heating of the vapour phase (single-phase forced convective heat transfer to the vapour phase) accompaning the rise in T_{sat} along the flow direction was included. This approach is taken from the case of condensation of mixtures and called the Silver /Bell and Ghaly method (Silver, 1947; Bell and Ghaly, 1973). The equations are as follows:

$$\alpha = \frac{F\alpha_l + S\,\alpha_{nb,mix}}{1 + x_g\, c_{p,V}(\partial T_{sat}/\partial h)_p(F\alpha_l/\alpha_V)} \tag{2.59}$$

$$F = 2.44\,(1/X_{tt})^{0.863} \tag{2.60}$$

$$\alpha_{nb,mix} = \frac{\alpha_{nb,1}\,\tilde{x_1} + \alpha_{nb,2}(1-\tilde{x_1})}{1 + A_1(\tilde{y_1} - \tilde{x_1})} \tag{2.61}$$

α_l is calculated from the Dittus-Boelter correlation with the liquid fraction as flow. $\alpha_{nb,1}$ and $\alpha_{nb,2}$ are the pure component nucleate pool boiling heat transfer coefficients calculated from the Nishikawa et al. (1982) correlation. A_1 was taken to be 15, with the nucleate pool boiling correlation for a smooth tube being:

$$\begin{aligned} \alpha_{nb} &= 31.4\,[p_{cr}^{0.2}\,F_p/(\tilde{M}^{0.1}\,T_{cr}^{0.9})]\,\dot{q}^{0.8} \\ F_p &= (p/p_{cr})^{0.23}/[1 - 0.99\,(p/p_{cr})]^{0.9} \end{aligned} \tag{2.62}$$

The S suppression factor by Bennett et al. (1980) was used and is given as:

$$\begin{aligned} S &= [1 - exp(-F\,\alpha_l\,\delta/\lambda_L)]/(F\alpha_l\,\delta/\lambda_L) \\ \delta &= C_d[\sigma/g(\rho_L - \rho_V)]^{1/2} \end{aligned} \tag{2.63}$$

where C_d is an empirical constant with a value of 0.08. α_V was determined from the analogy between heat transfer and shear stress at the liquid-vapour interface (see Murata, 1993 for equations).

Jung (1989a)

Jung (1989a) utilises the superposition model with a Chen-type forced convective enhancement factor and a suppression factor S which is a function of X_{tt} and Bo.

Mixture corrections are applied for both the convective and nucleate boiling term. For the nucleate boiling, term the Ünal (1986) nucleate boiling mixture correction was applied. The reduction in the forced convective heat transfer due to mixture effects was found to be small (<10%) and was expressed in terms of the phase equilibrium data ($\tilde{y} - \tilde{x}$).

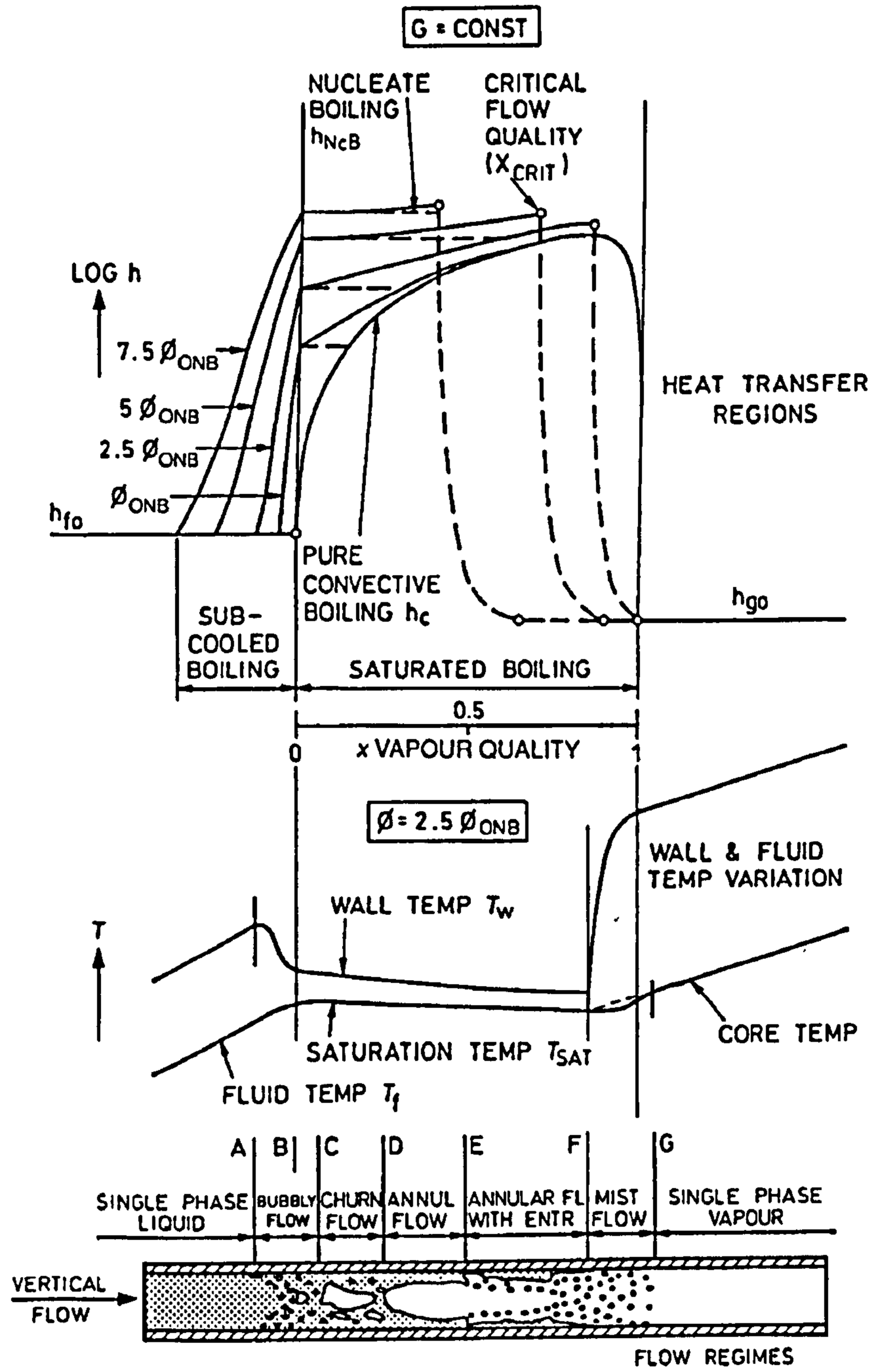


Figure 2.1: Flow boiling map with flow patterns, adapted from Steiner and Taborek (1992)

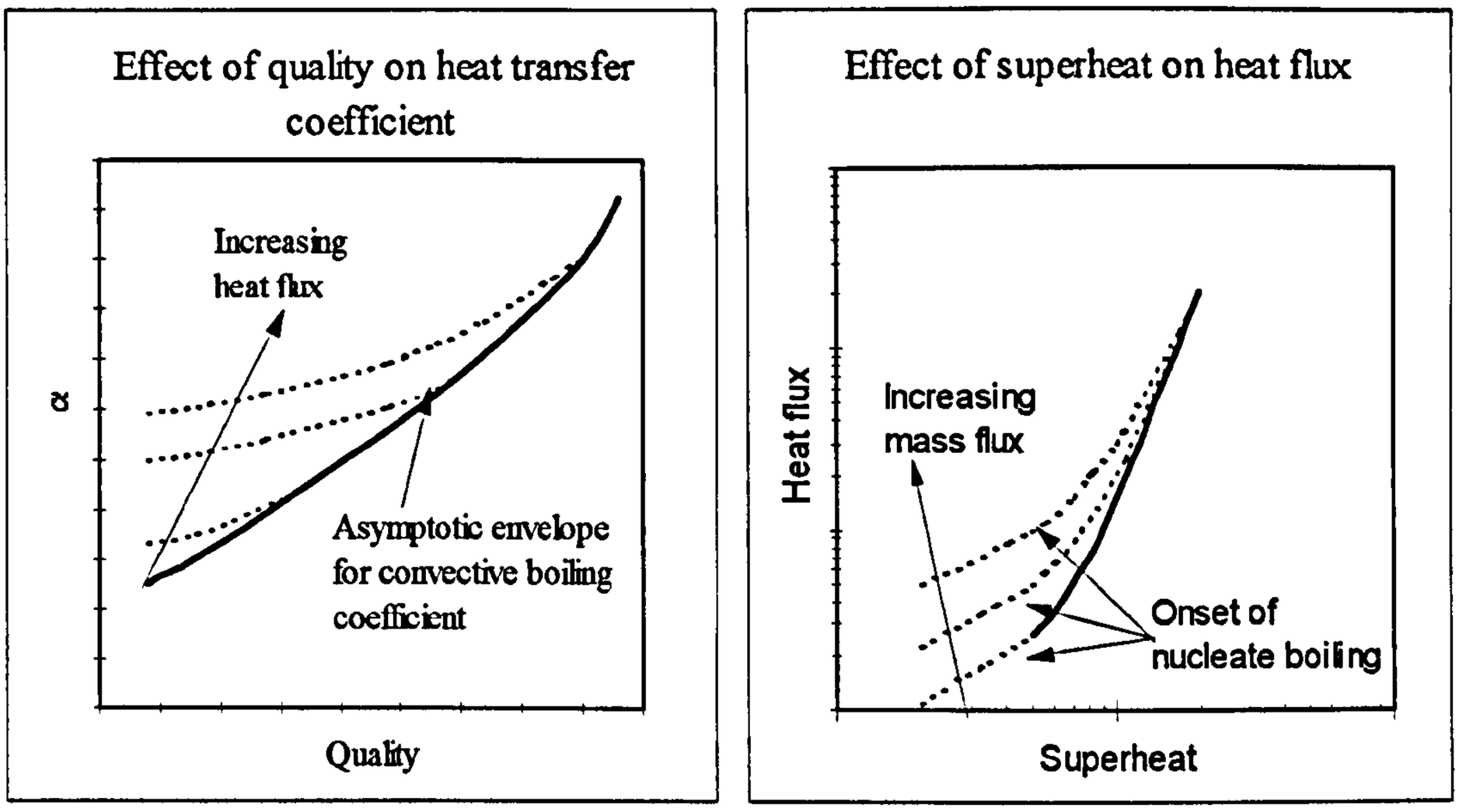


Figure 2.2: The effect of quality (left) on the heat transfer coefficient and (right) the effect of superheat on the heat flux.

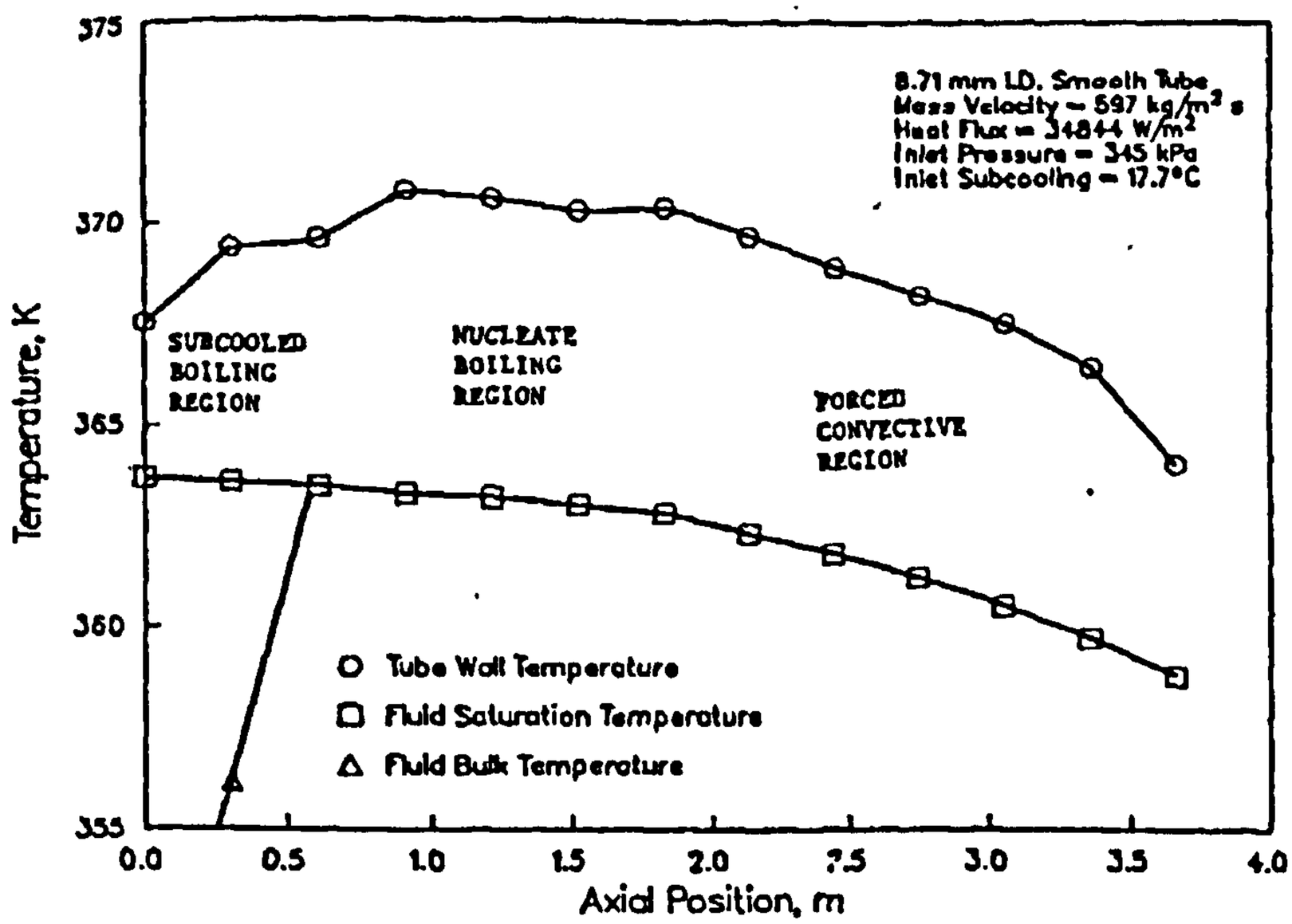
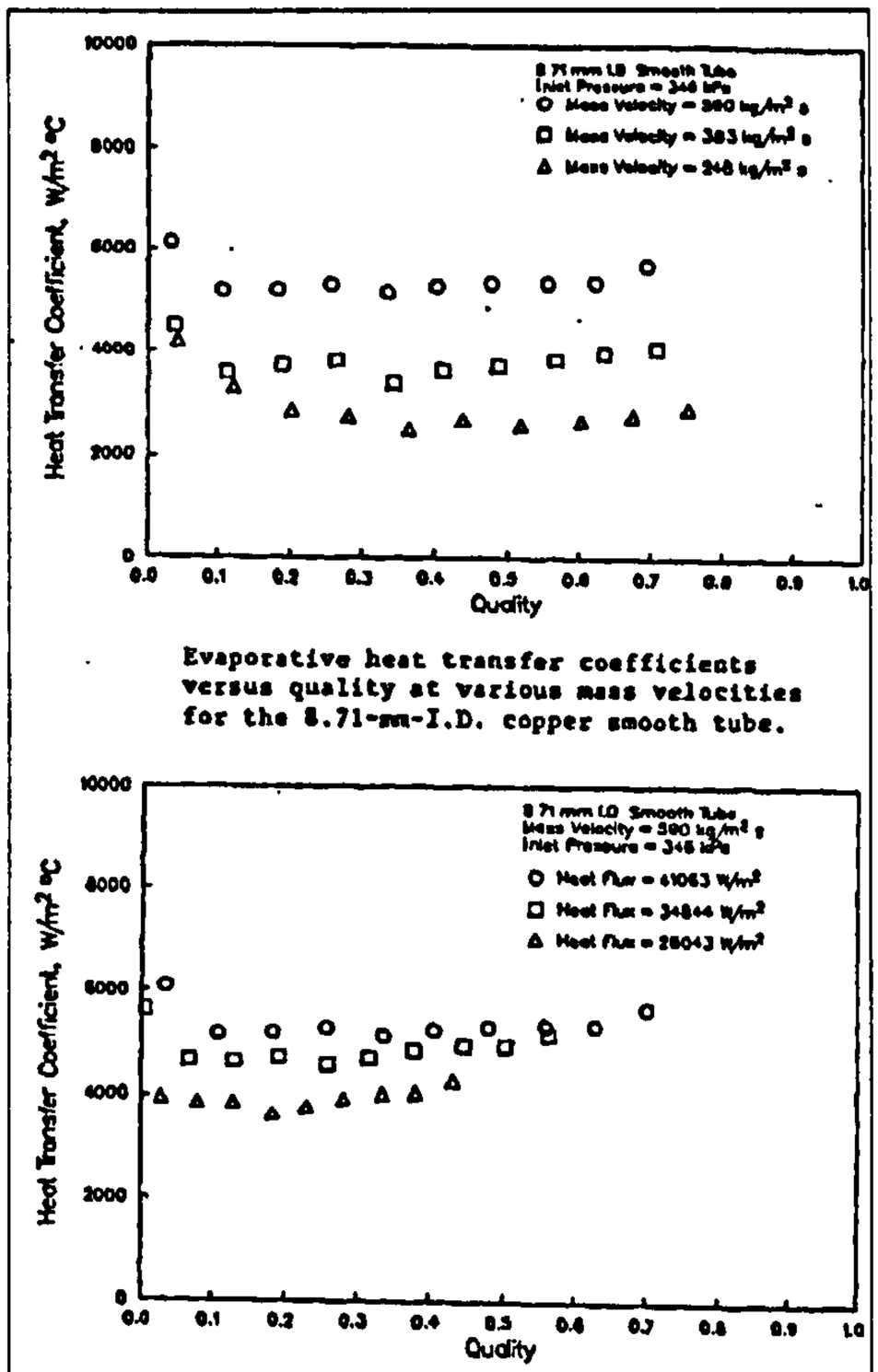
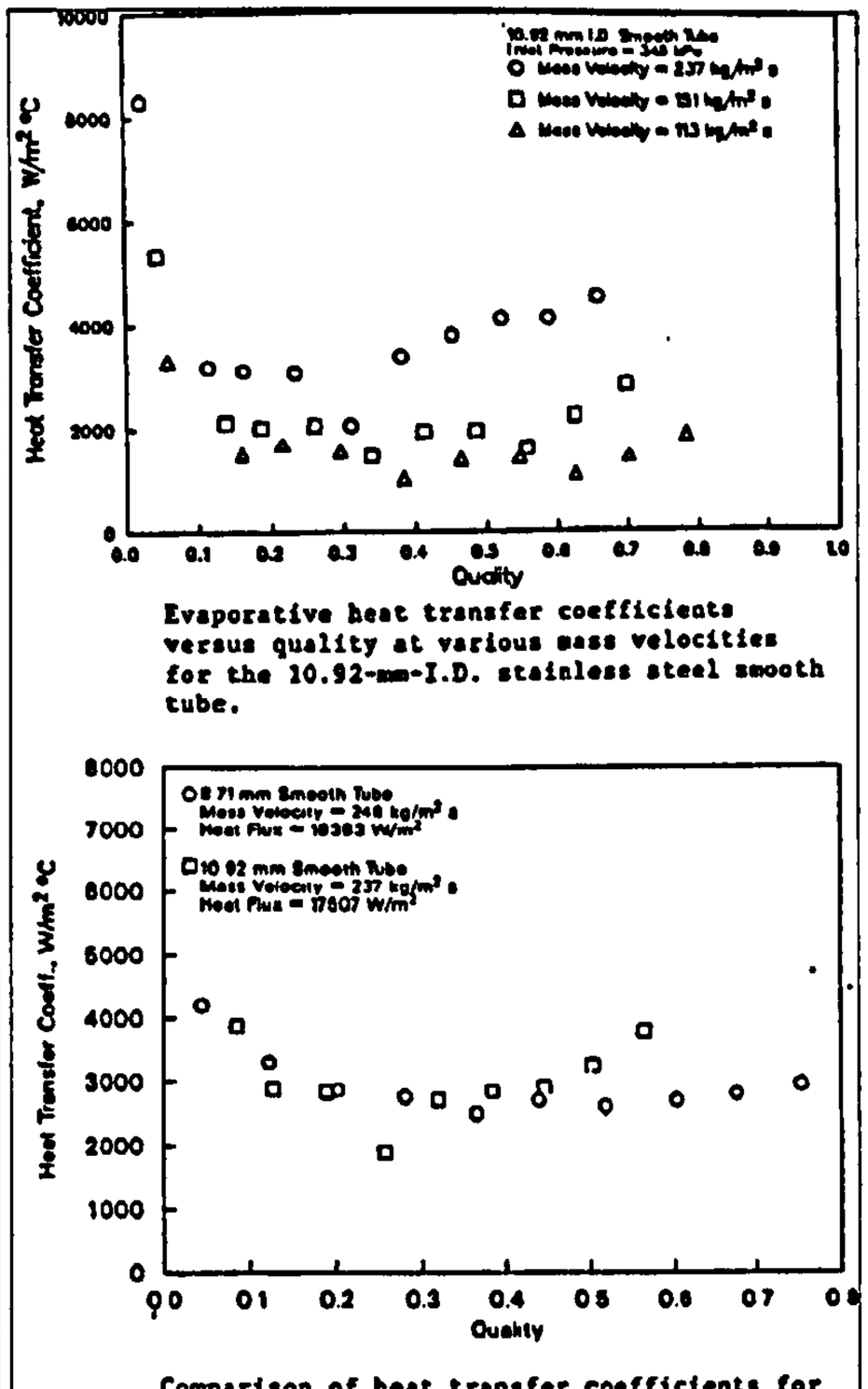


Figure 2.3: Typical temperature profile for flow boiling in a horizontal tube, adapted from Reid et al. (1987).



Evaporative heat transfer coefficients versus quality at various mass velocities for the 8.71-mm-I.D. copper smooth tube.

Evaporative heat transfer coefficients versus quality at various heat fluxes for the 8.71-mm-I.D. copper smooth tube.



Evaporative heat transfer coefficients versus quality at various mass velocities for the 10.92-mm-I.D. stainless steel smooth tube.

Comparison of heat transfer coefficients for the 8.71-mm-I.D. copper smooth tube and for the 10.92-mm-I.D. stainless steel smooth tube.

Figure 2.4: Experimental heat transfer coefficient from Reid et al. (1987) on the effect of tube diameter, mass flux and heat flux.

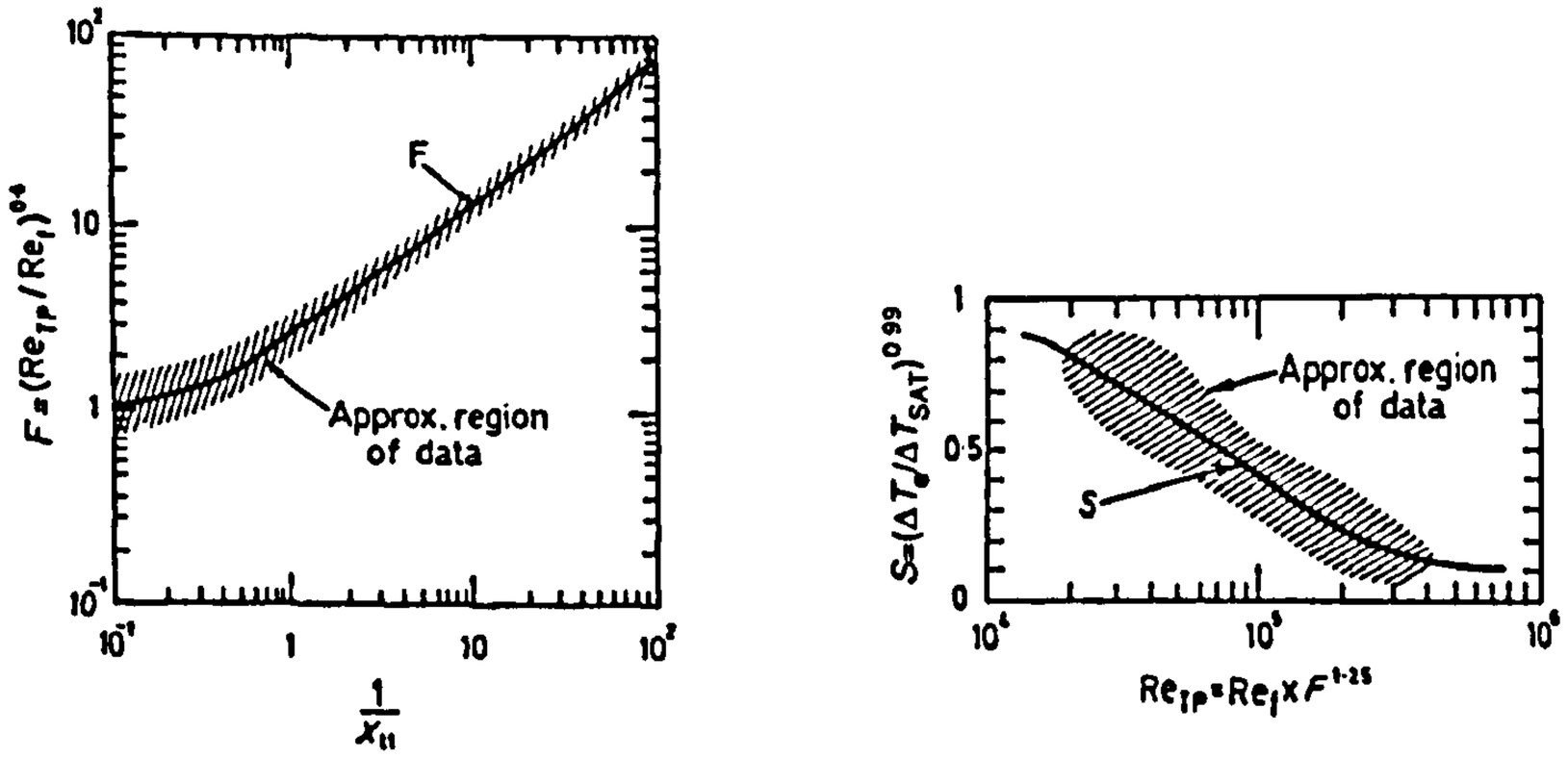


Figure 2.5: Forced convection enhancement factor (F) and nucleate boiling suppression factor (S) as used in the Chen (1966) correlation.

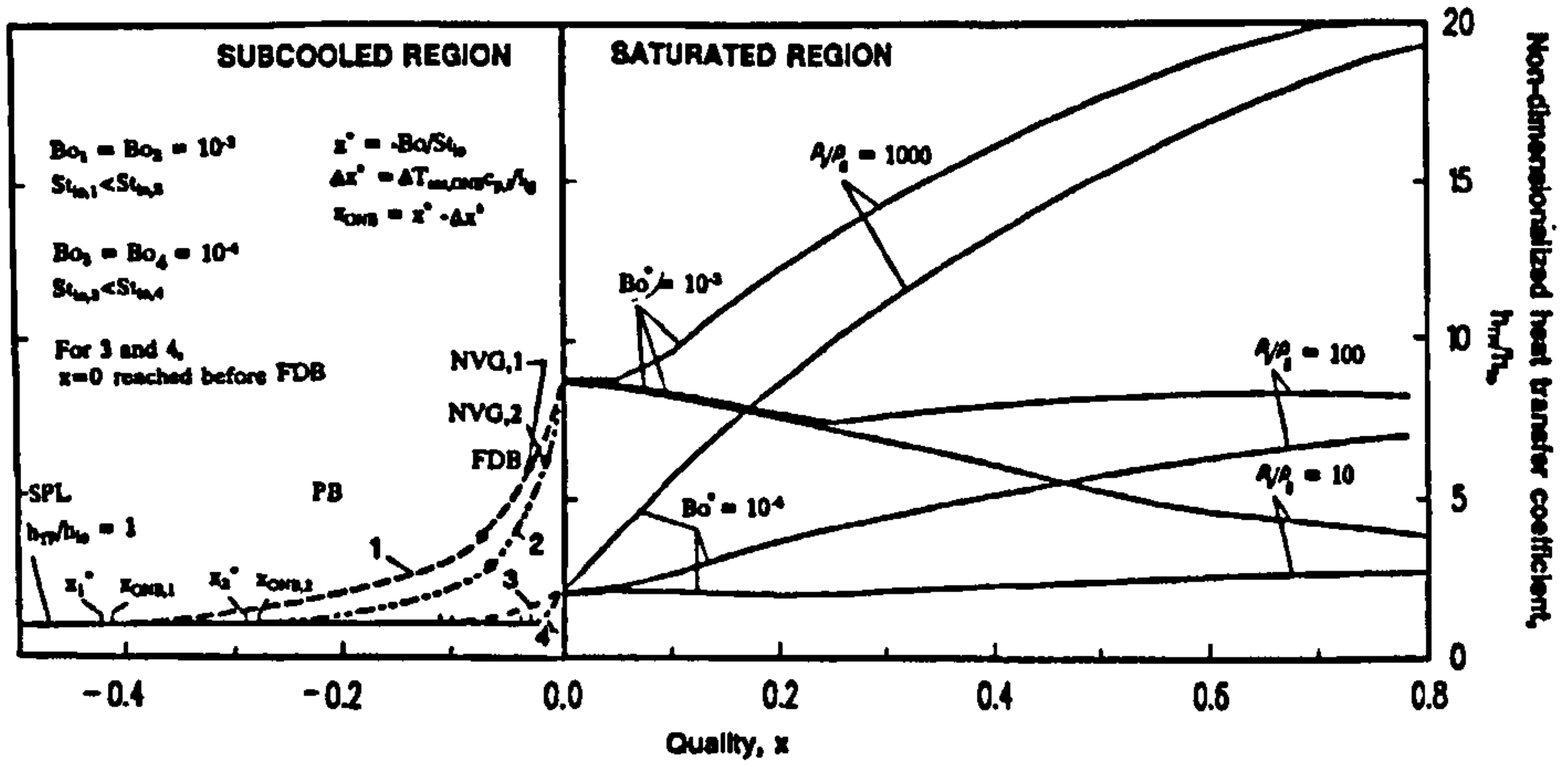


Figure 2.6: Kandlikar (1990a) flow boiling map for different liquid/vapour density ratios and Bo numbers.

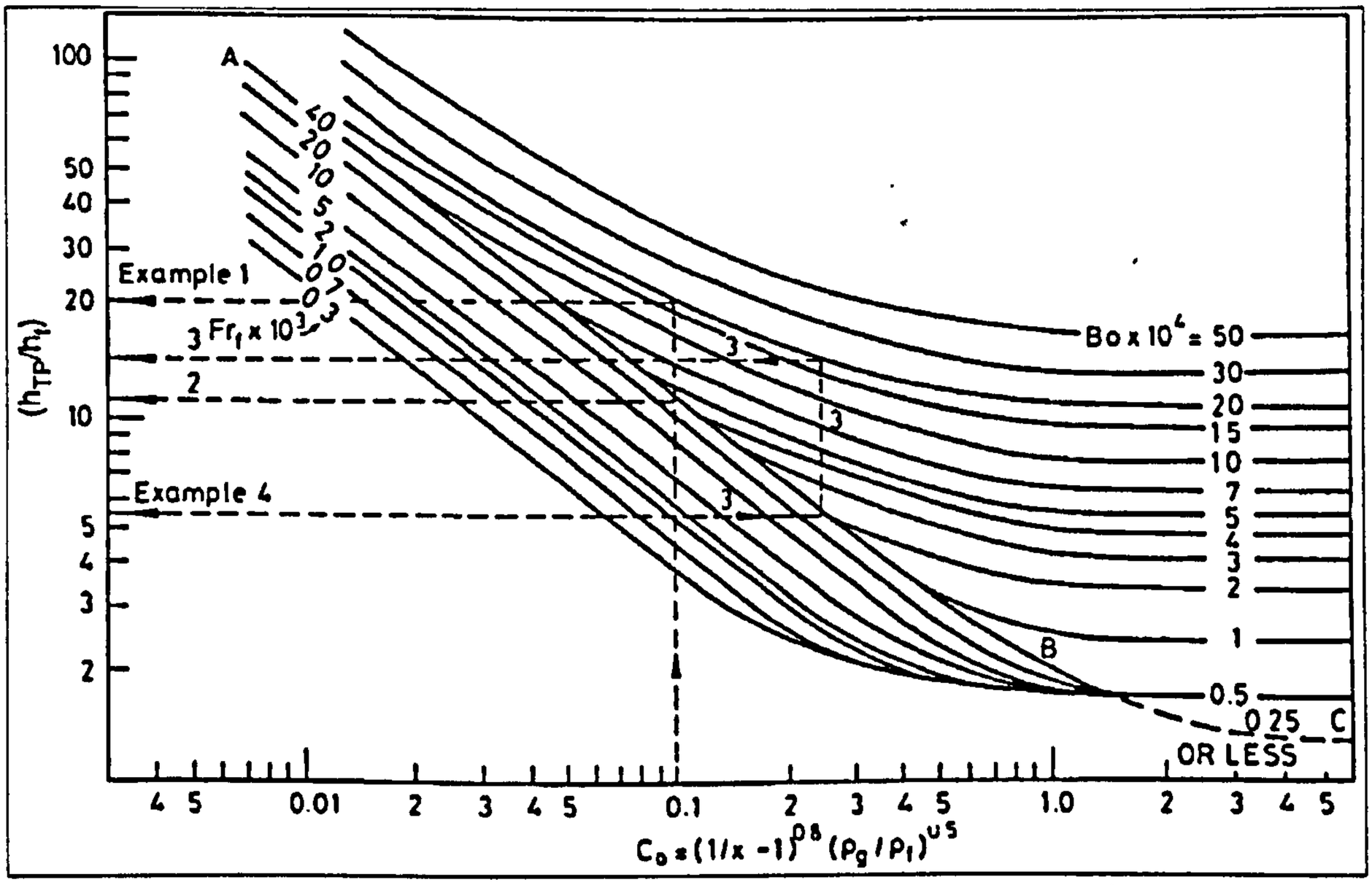


Figure 2.7: Correlation chart of Shah (1976).

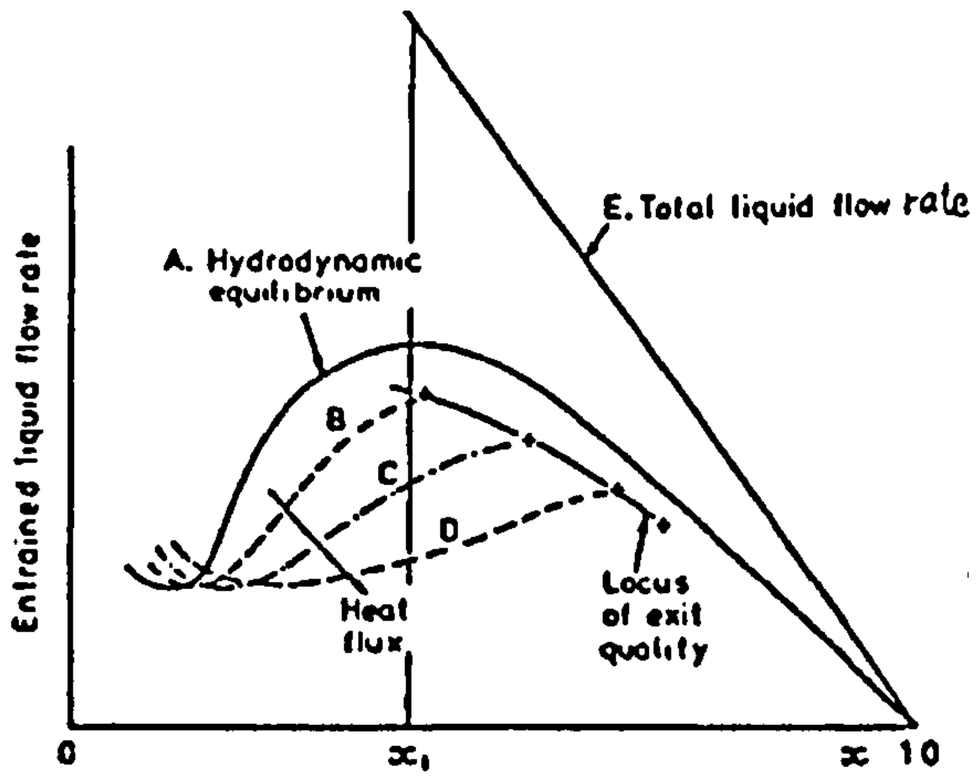


Figure 2.8: Effect of heat flux on relation between entrained liquid flow rate and quality for fixed mass flux and tube length (Sun and Hewitt, 1996).

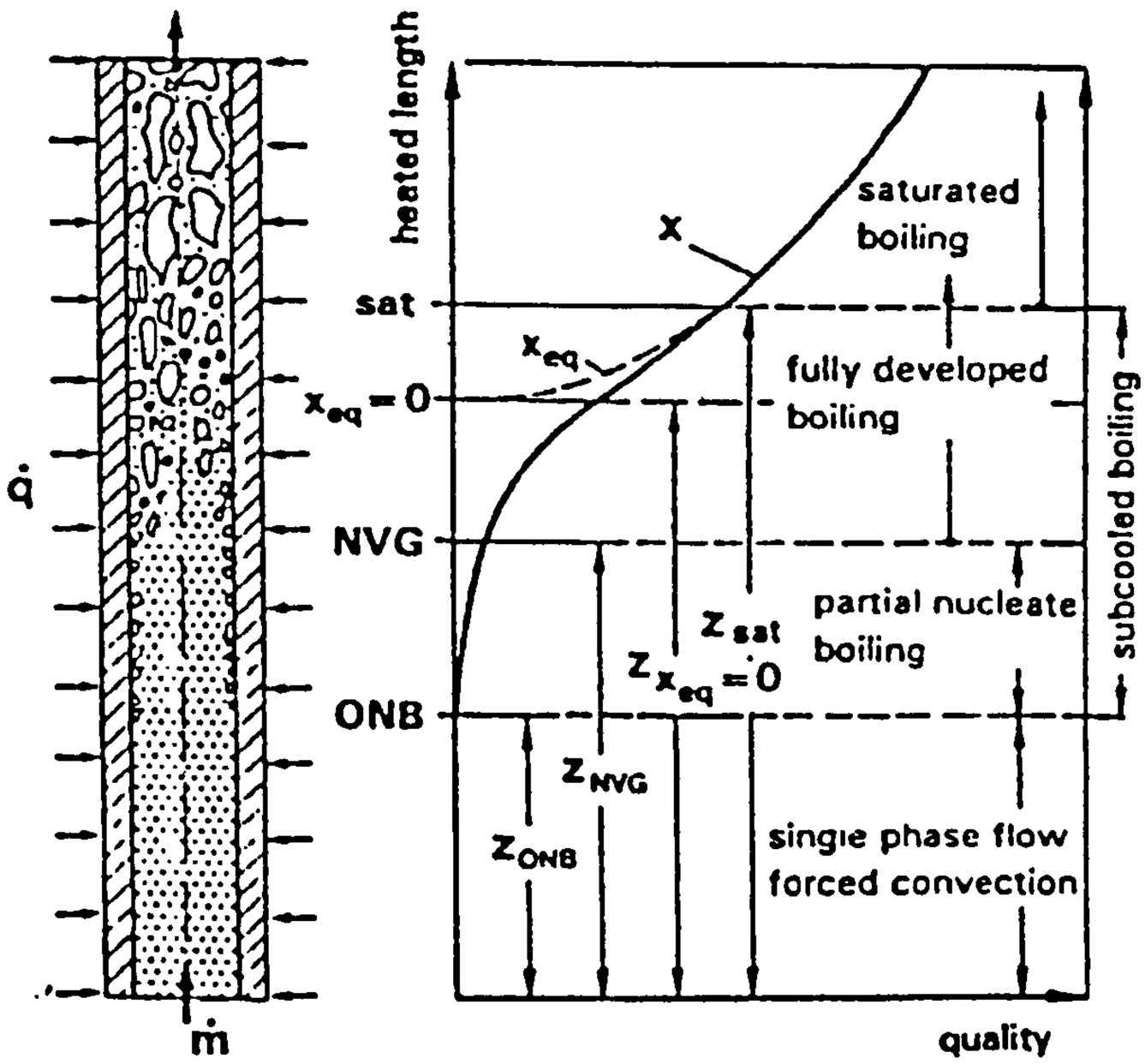


Figure 2.9: Flow pattern and heat transfer regimes for flow boiling in a vertical tube, adapted from Spindler (1994).

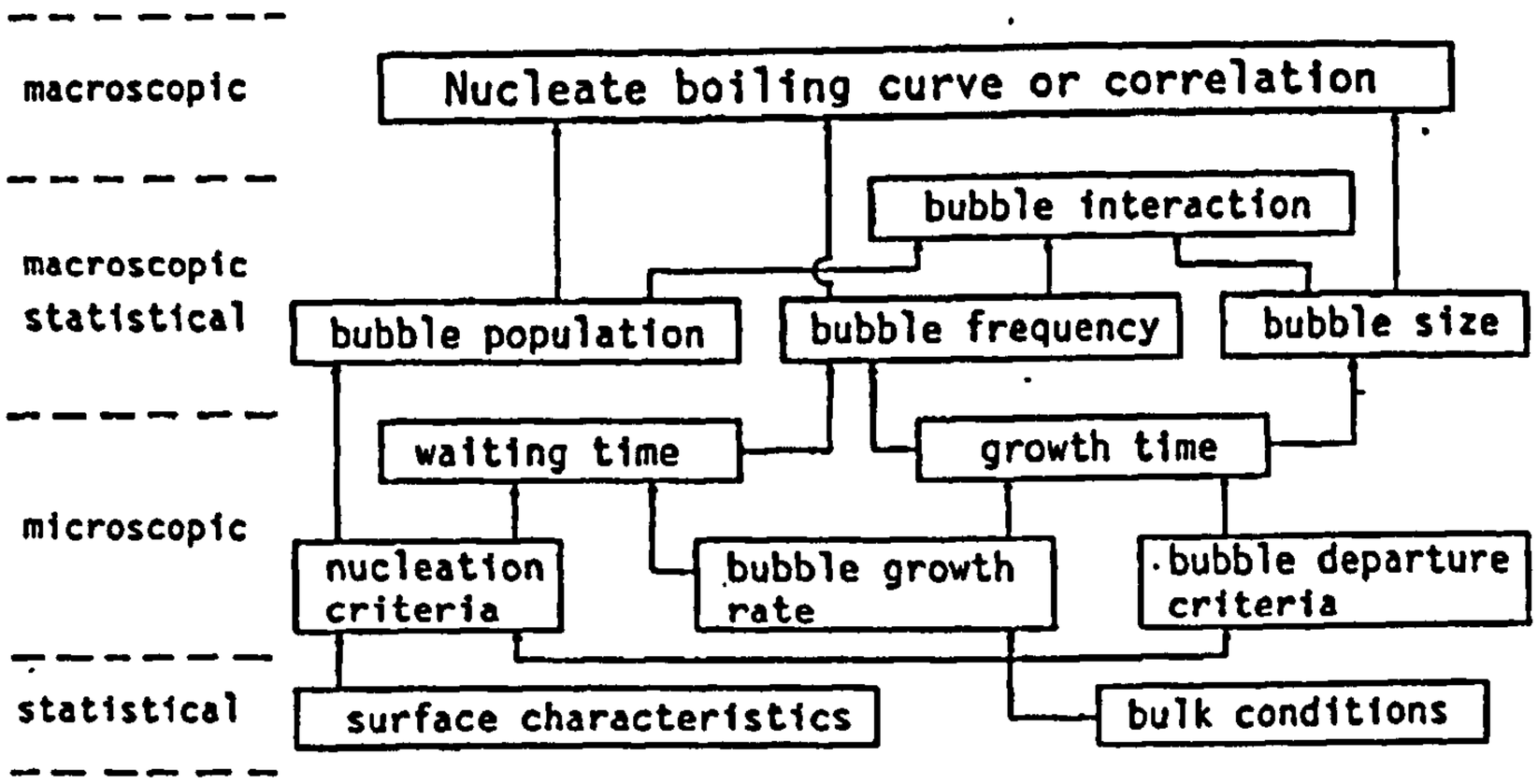
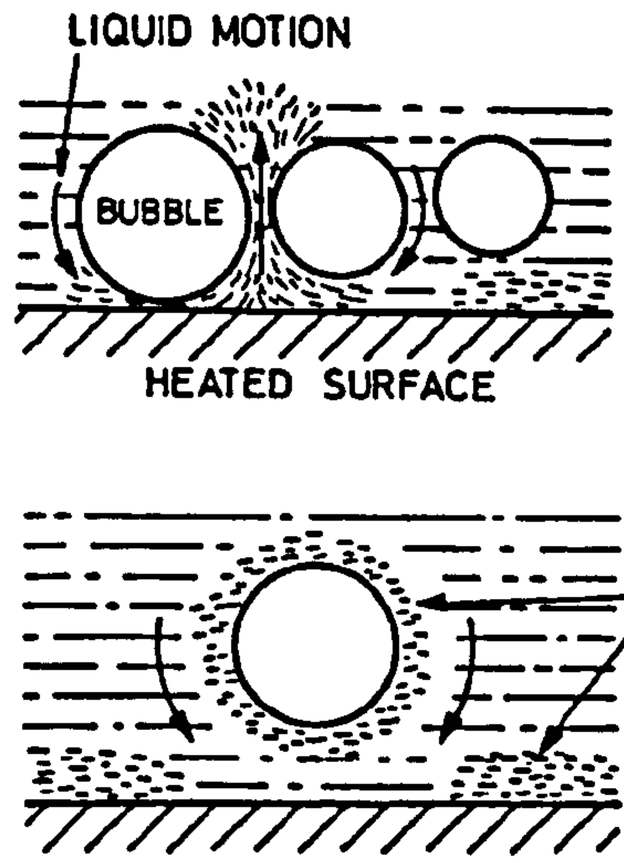


Figure 2.10: Nucleate pool boiling process, Hsu and Graham (1986).



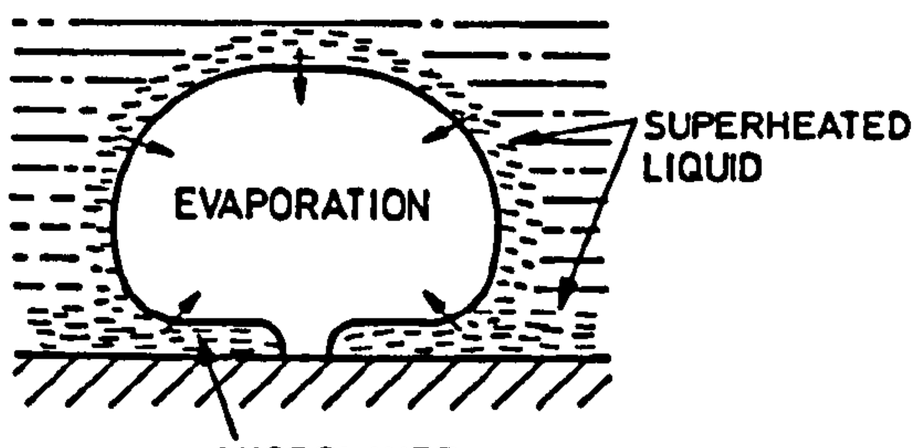


Figure 2.11: The nucleate boiling heat transfer mechanisms: bubble agitation (top), liquid exchange mechanism (middle) and micro layer evaporation (bottom). Adapted from Collier and Thome (1994).

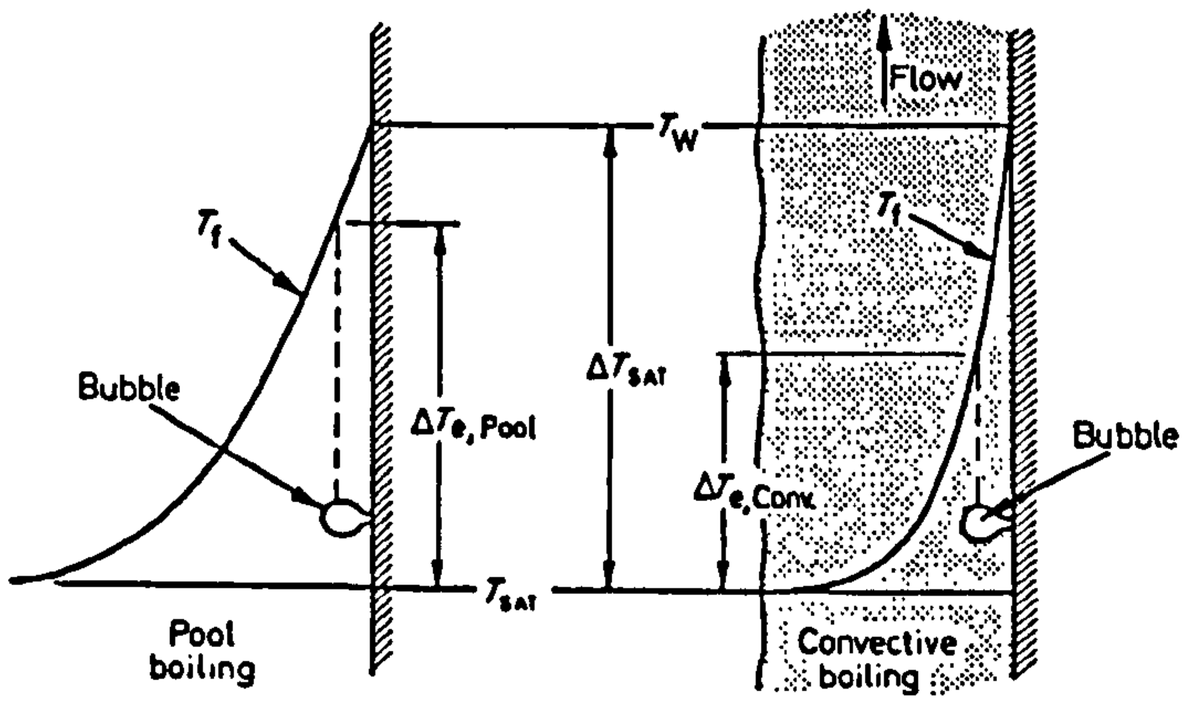


Figure 2.12: Temperature gradient at the wall for nucleate pool boiling (left) and for forced convection (right).

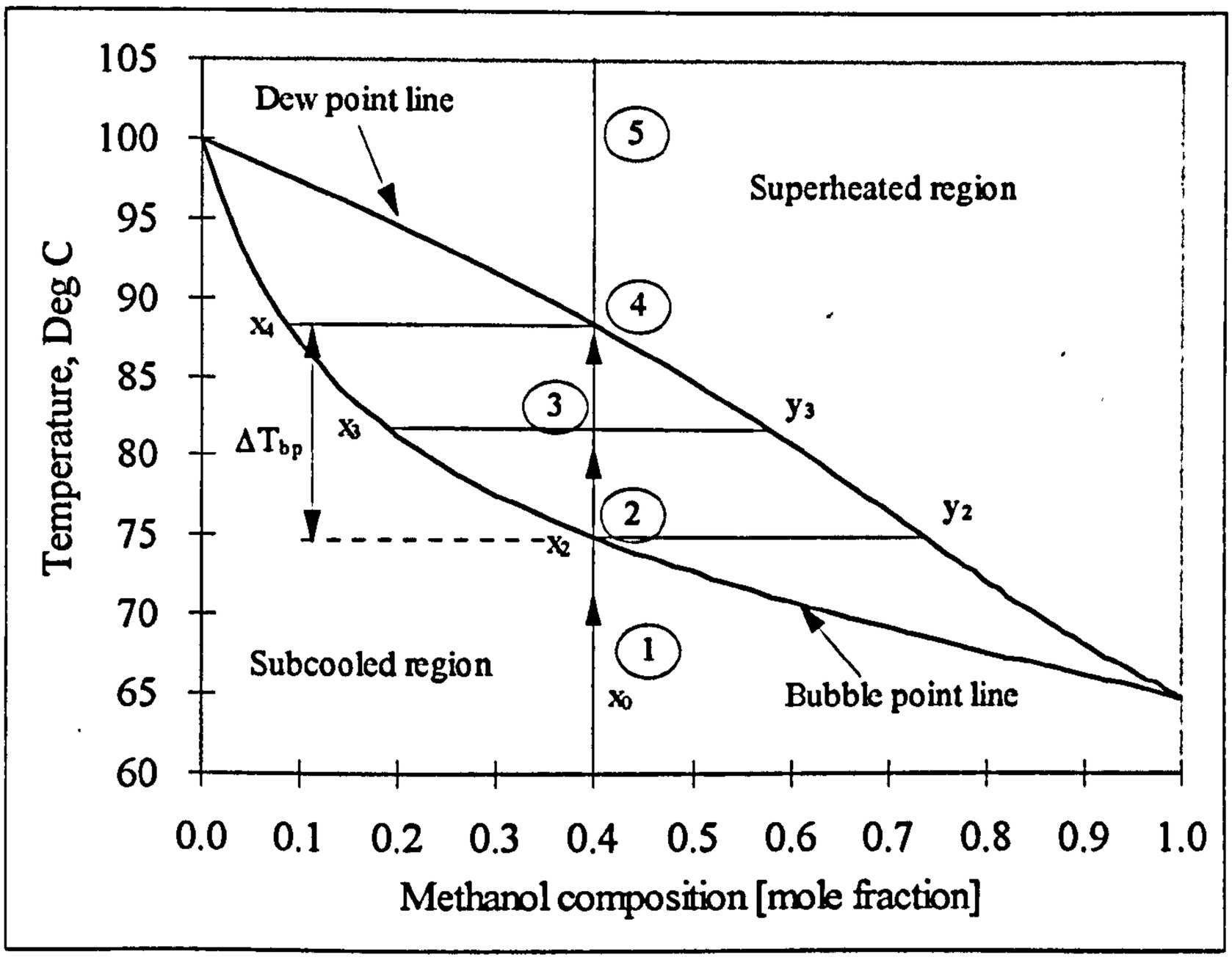


Figure 2.13: Temperature – Composition diagram for a nonazeotropic mixture, (water–methanol).

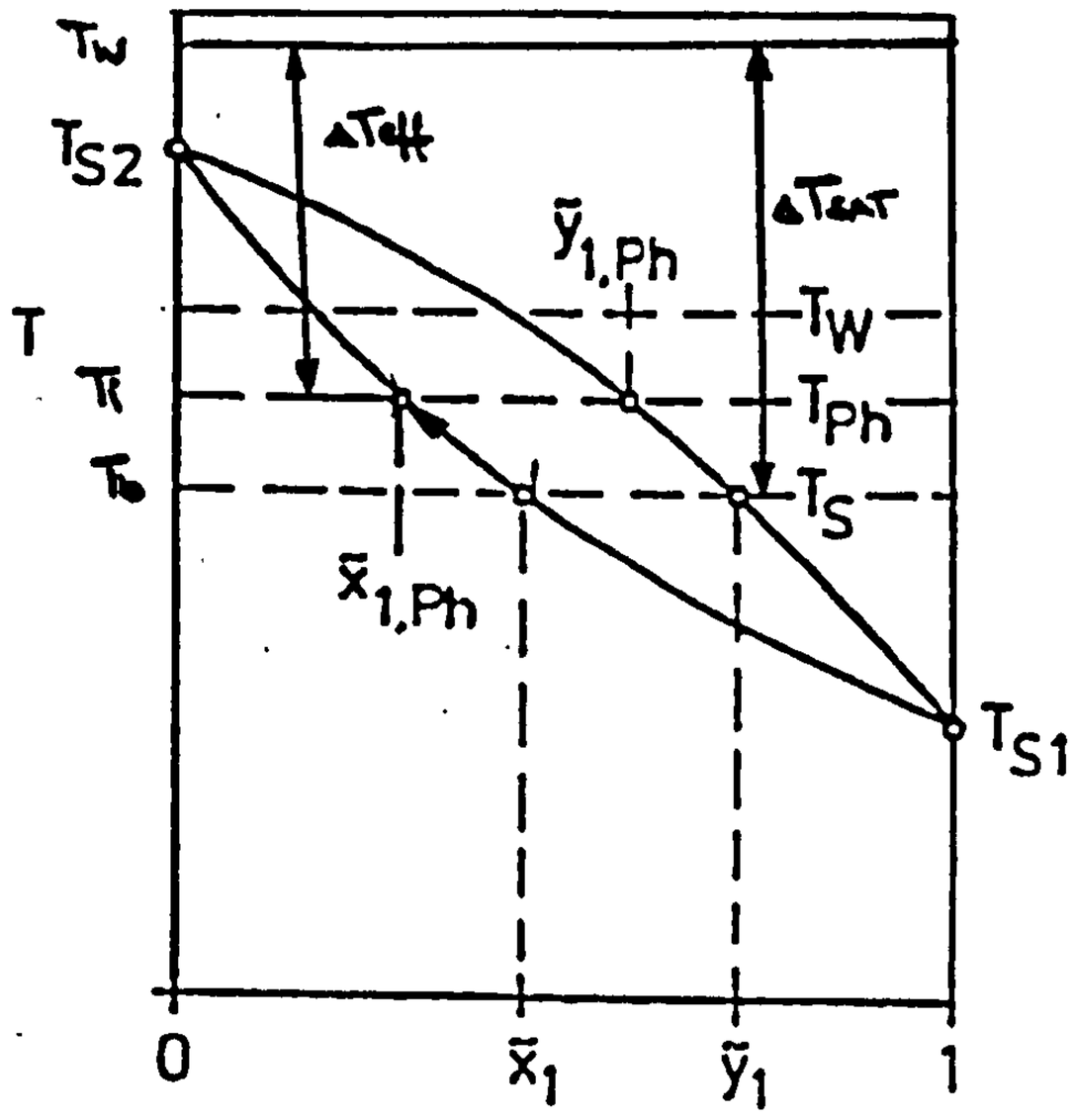


Figure 2.14: Temperature – Composition diagram, reduction in effective wall superheat due to mixture effects.

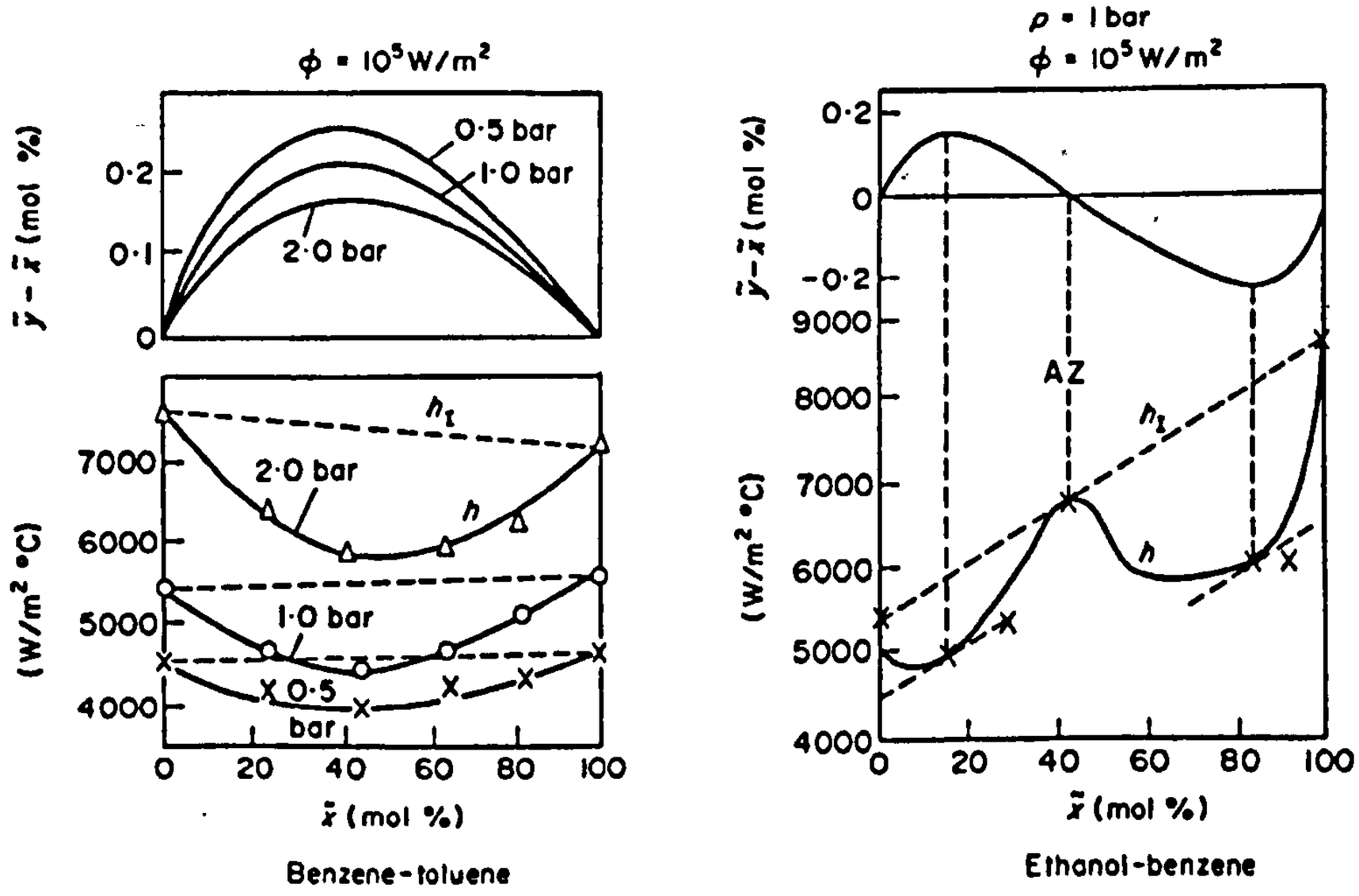


Figure 2.15: Variation of heat transfer coefficient with composition for binary mixture (Happel and Stephan, 1974).

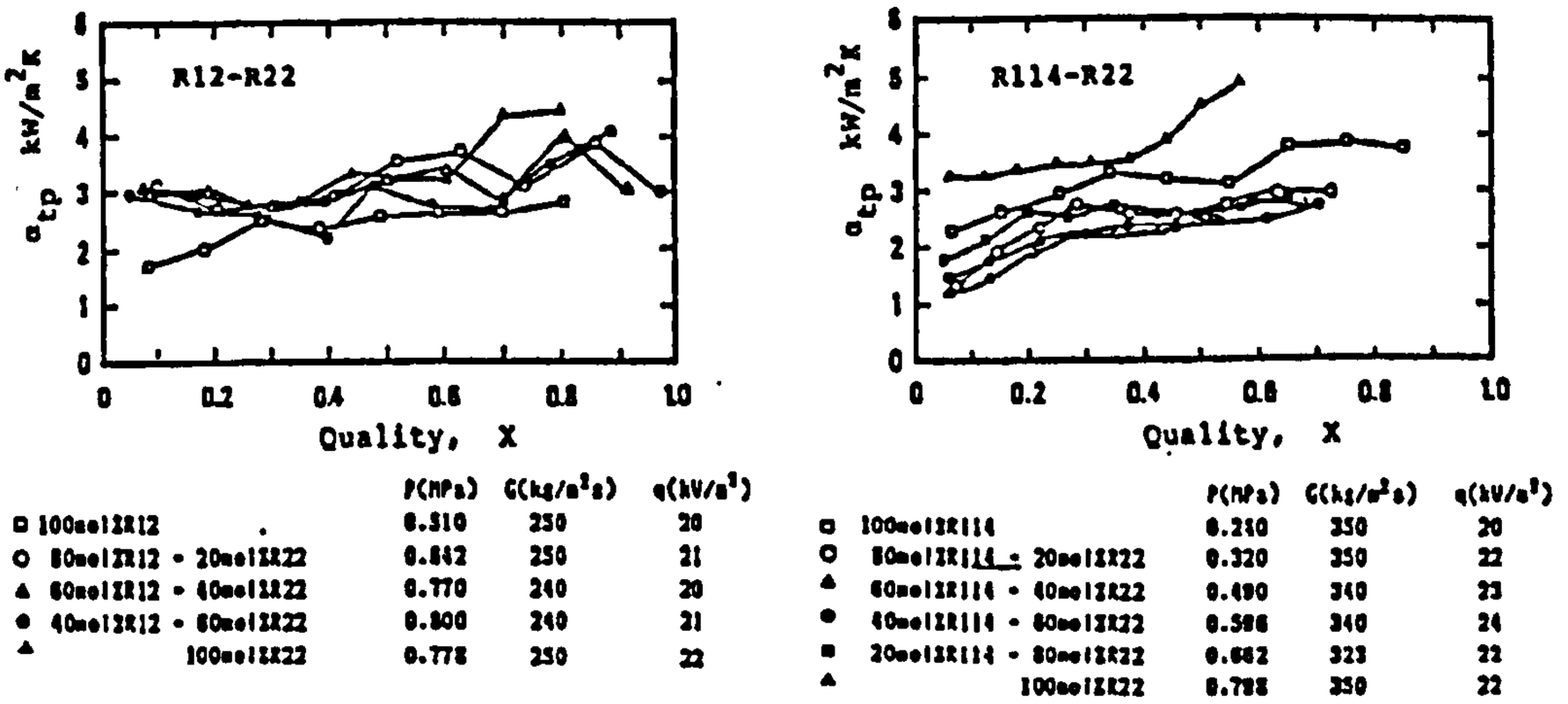


Figure 2.16: Hihara and Saito (1988) data for the two different mixtures with different boiling ranges: low boiling range (left) and large boiling range (right).

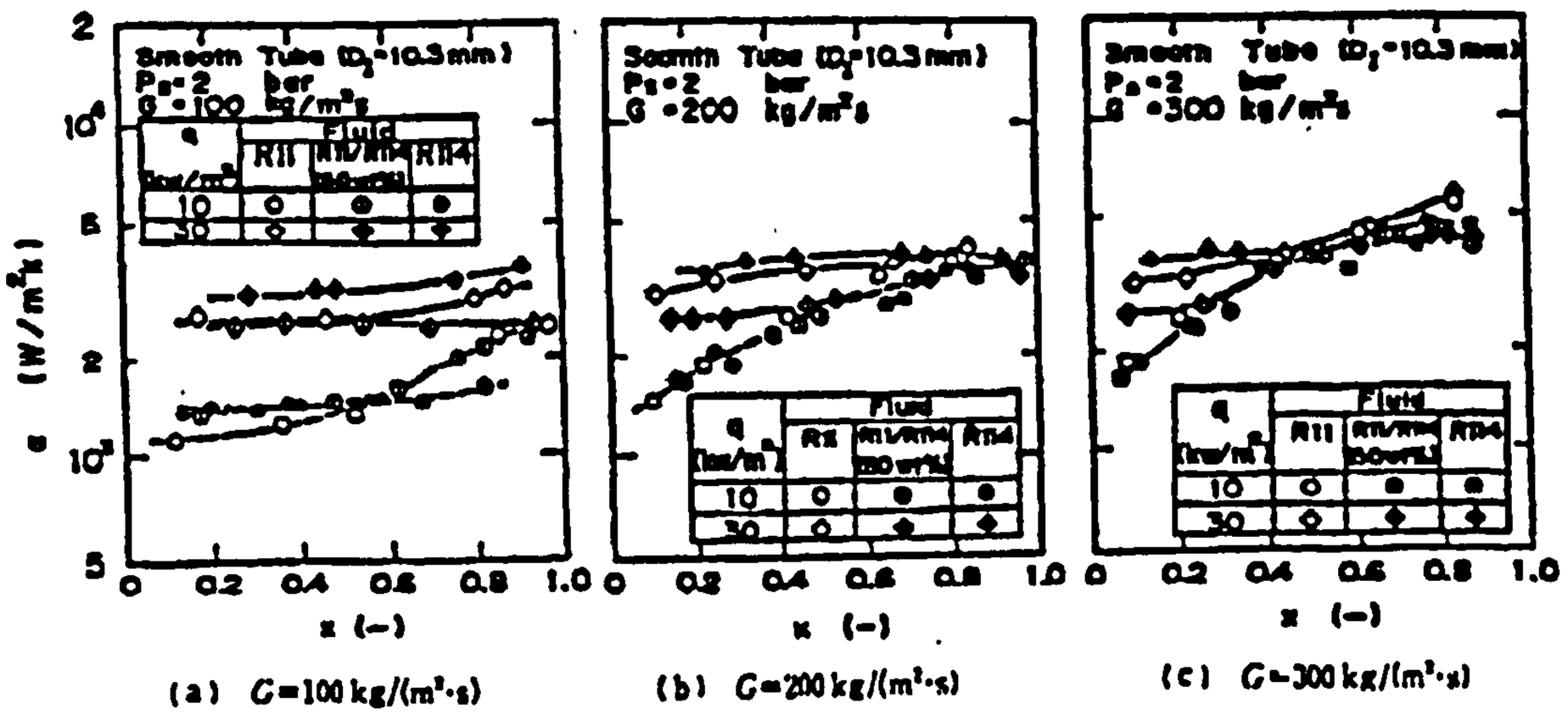
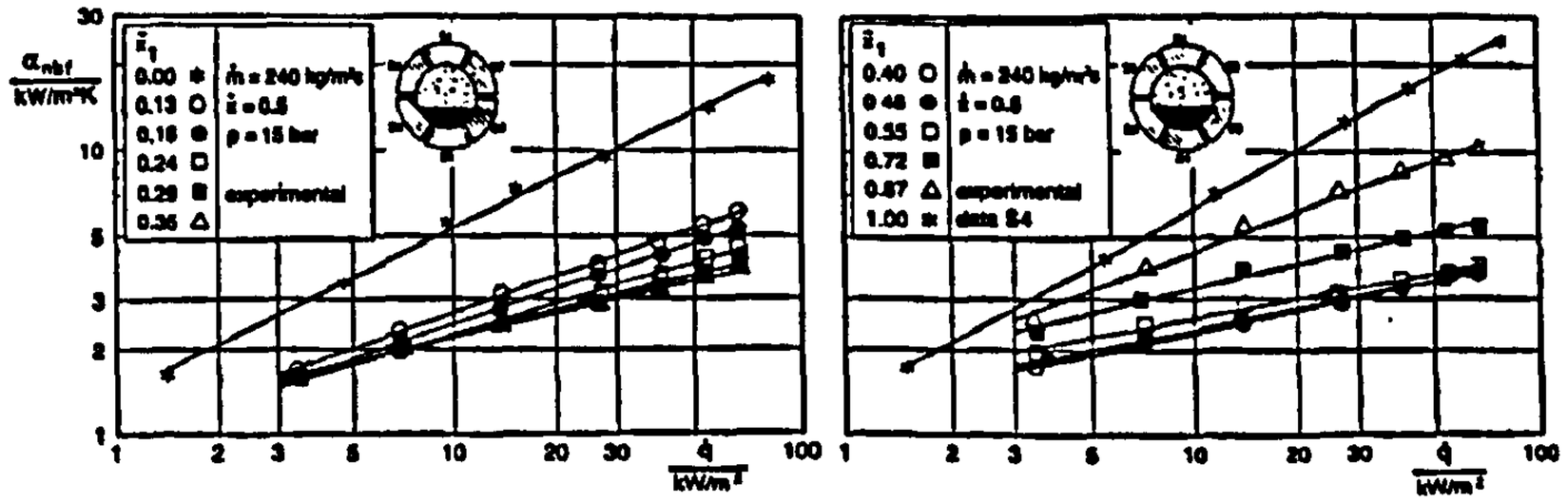
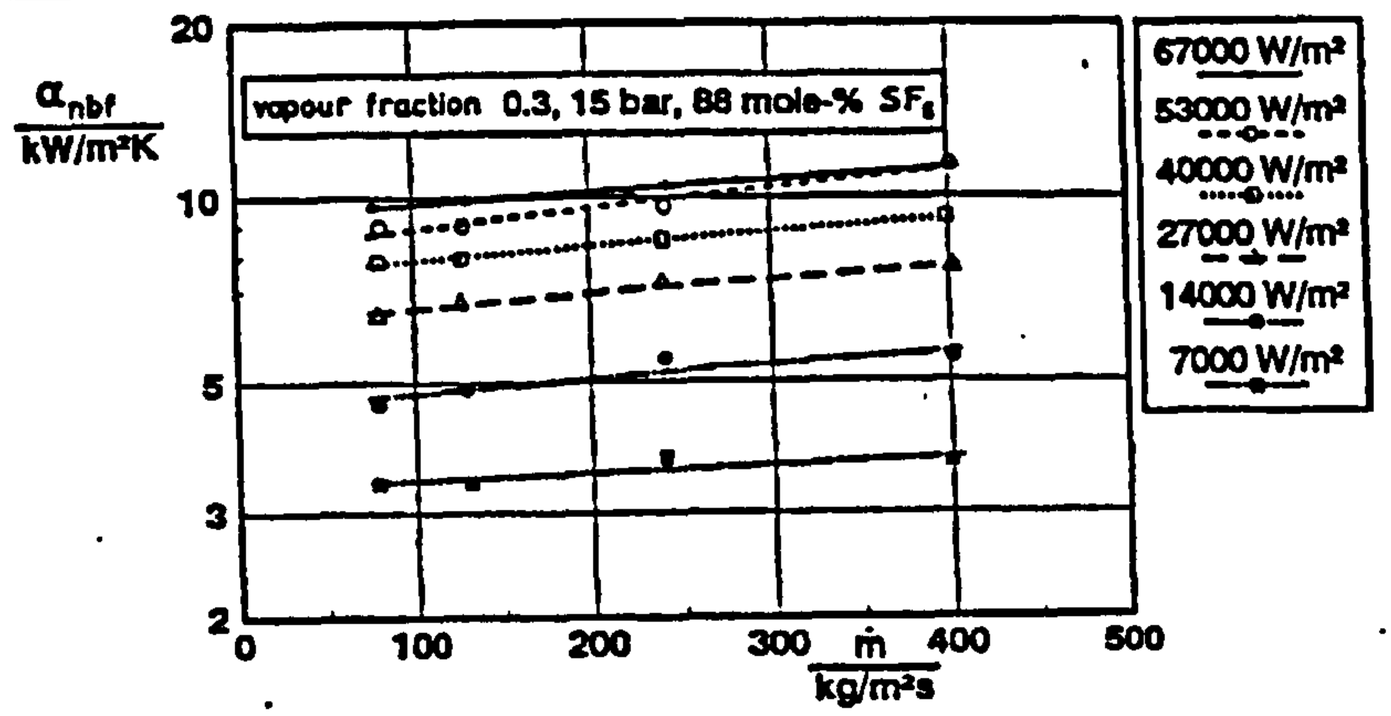


Figure 2.17: Murata and Hashizume (1991) experimental data for pure component and binary mixtures at different mass fluxes and two heat fluxes.





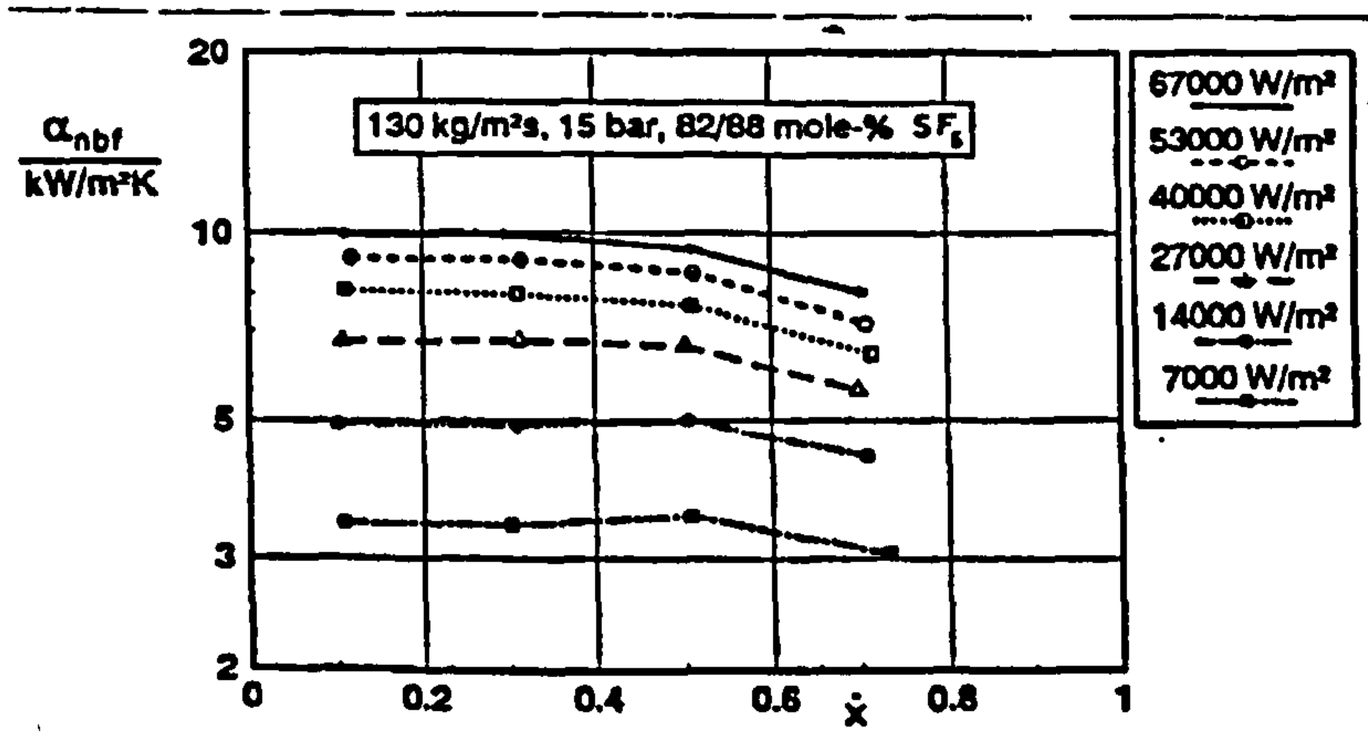


Figure 2.18: Niederkrüger et al. (1992) horizontal tube flow boiling data (D = 14 mm) for a SF2/CF2Cl2 mixture.

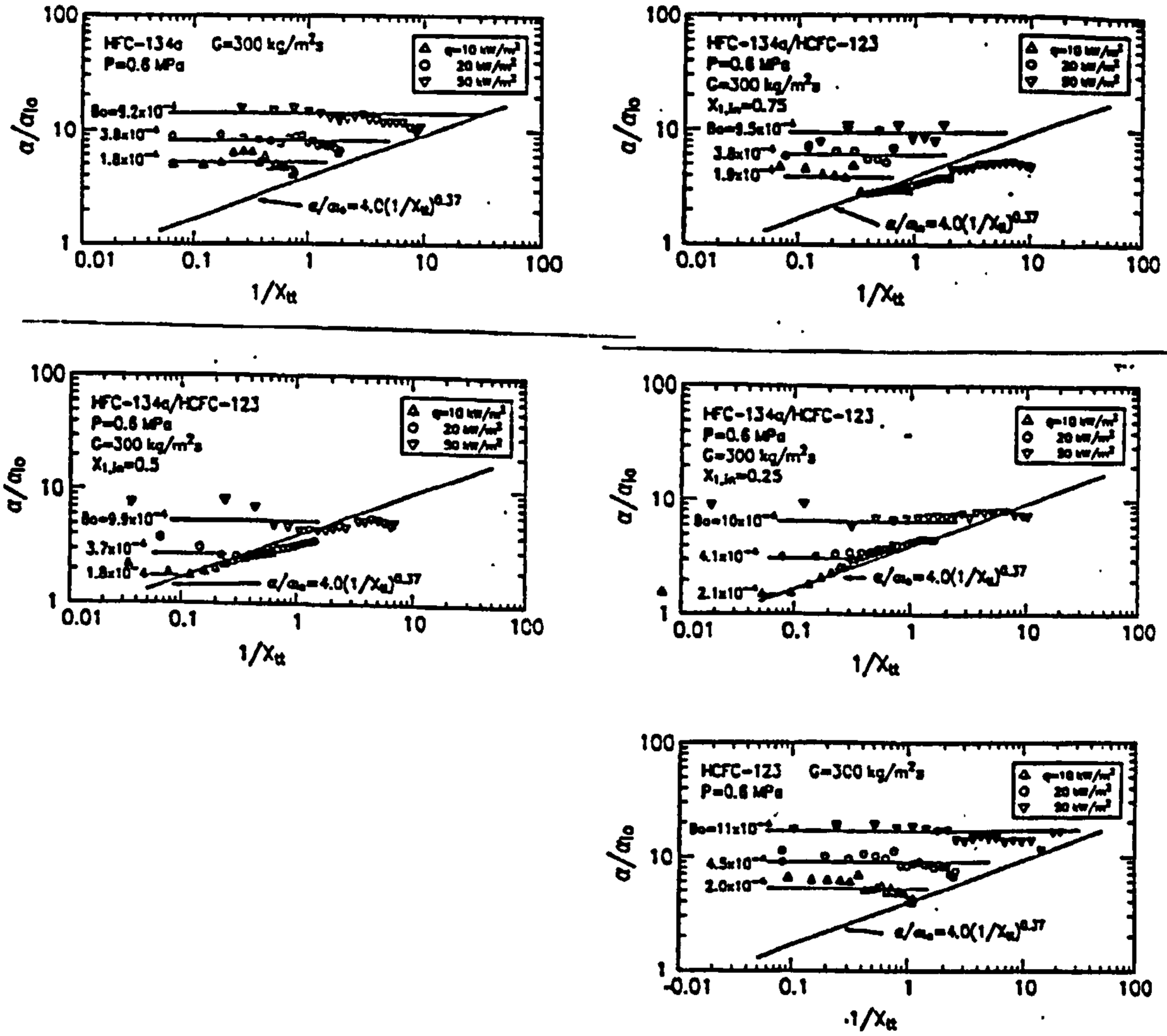


Figure 2.19: Fujita and Tsutsui's (1995) results for the binary mixture R134a/ R123 and the pure components of R134a and R123 at a pressure of 0.6 MPa and mass flux of 300 kg/m^{2}s.

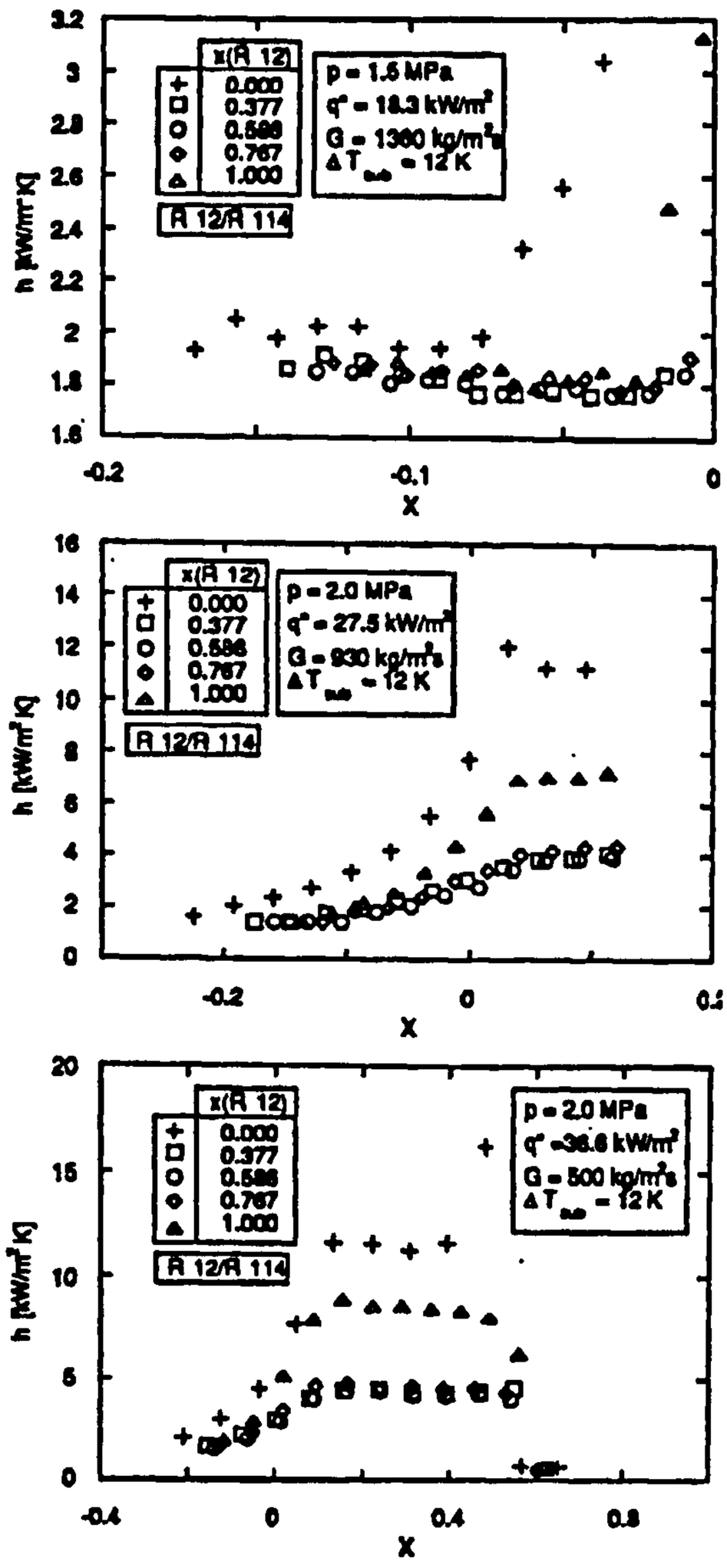


Figure 2.20: Comparison of pure component and binary mixture results from Celata et al. (1995): (top) subcooled boiling region and (middle and bottom) two-phase region.

Chapter 3

Description of experimental apparatus, measuring devices and error analysis

The experiments presented in this thesis were carried out on a large rig (the High Pressure Boiling Rig, HPBR) at the Harwell Science and Technology Centre of AEA Technology plc. The HPBR was completed in 1990 and a preliminary series of experiments was conducted by Frankum (1996). For the current work, extensive modifications to the rig were carried out, mainly to allow a much larger range of flow qualities. In what follows, Section 3.1 describes the HPBR and the modification made to it. Section 3.2 describes the test section and the instrumentation and Section 3.3 describes the operation of the rig and the data reduction methods.

3.1 The apparatus

A detailed description of the experimental apparatus, the High Pressure Boiling Rig, is given by Frankum (1996); Frankum also presents a detailed safety analysis. In what follows here, a schematic flowsheet, short description of the circuits and procedure for the conduction of experiments will be given. The test section and

the associated instrumentation is then described in more detail.

The rig consists of three circuits, the primary circuit, the pressurising circuit and the degassing circuit (see Figure 3.1) and is rated for a working pressure of 3 MPa. The primary circuit contains the test section through which the test fluid can be circulated at a fixed flow rate, temperature and pressure. Included in this circuit are the circulating pump, the flowmeter, the preheater, the density meter, a sampling device and a condenser. A new preheater was added as part of the present work. The pressurising circuit generates a constant pressure by two pressurising pumps (P1, P9) in series, generating the pressure in the primary circuit by pumping against a partially open valve (V14). Adjustment of the pressure was controlled by the speed of the pump and by the throttling applied at the partly open control valve.

3.1.1 History of rig

Construction of the HPBR began 1988, and in August 1990, the first experimental program started with the commissioning of the rig with water and was continued with the data collection using hydrocarbons. The hydrocarbons used is this first programme of work were mainly the same as in the present project (namely n-pentane, iso-octane and n-hexane either as single components or as mixtures). The exploitation of the whole operating range was limited in this earlier programme due to the lack of preheating capabilities; the most important change in the new programme described here was the installation of a much more powerful preheater which allowed the generation of a much wider range of qualities, thus allowing a more systematic analysis of the heat transfer characteristics of pure components and a direct comparison with the corresponding mixtures.

3.1.2 Modifications to the rig

The present project on forced convective boiling using the HPBR started in September 1994. The first series of experiments (Frankum, 1996), had revealed a

number of problems concerning the construction and operation of the apparatus, and these had to be resolved. The main problem was that the existing preheater system could only be operated at low power levels. This restricted the inlet temperature to the test section, and thus restricted the range of conditions which could be studied. To achieve high qualities in the test section, it was necessary to have high heat fluxes. Thus, the range of heat fluxes which could be studied at a given quality was restricted to a higher range of values. This made it difficult to study the full range of heat transfer mechanisms. The ability to control the inlet temperature to the test section up to values close to the saturation temperature allows a much more systematic investigation of the effect of pressure, mass flux and heat flux on the heat transfer. A new preheater was purchased from Chemtec B. V.. It was essentially in the form of a horizontal shell-and-tube heat exchanger with the tubes containing electrical heating elements. The fluid passed over the rods in two shell-side passes. The unit had a maximum power of 75 kW.

A significant operational problem during the earlier work was that, during degassing, the losses of hydrocarbons were very high, since the vacuum pump drew out the vapour very quickly. To prevent this from happening in the present work an adjustable valve was installed before the vacuum pump.

Due to cavitation problems, operation of the pressurising pumps was only possible when a gas pressure of 0.12 - 0.16 MPa was applied to the main storage tank. This results in a certain amount of gas being dissolved in the hydrocarbons. It is known that dissolved gas may affect the heat transfer especially in the subcooled boiling region (Müller-Steinhagen et al., 1988). The nitrogen pressure was needed to enable a flow, generated by the seal pumps (gear pumps), to lubricate the bearings of the pressurising pumps. The design of the pressurising system needed a 4 metre liquid head, according to the supplier, at the inlet to the first pressurising and seal pump, to operate reliably without cavitation. Such a liquid head could not be achieved by gravity since both the tank and the pumps are at ground level, so the liquid head was only 0.3 to 1.2 metre, so the need to apply gas pressure onto the tank was unavoidable. One option to

solve this problem was to install a smaller tank on the ceiling of the building (10 metres above the pressurising pumps), which if connected to the suction of the pressurising pump would generate the required liquid head at the pumps. This option was not pursued because it was too costly and because major pipe work modifications would have been involved causing considerable delays.

The seal pumps are gear pumps with the gears made of graphite. This type of pump only works efficiently in the presence of "lubricating" fluids to reduce wear. The fluids used must have viscosities equal to or higher than that of water to avoid high slippage losses. The hydrocarbons used in the present work are non-lubricating and have viscosities of around a quarter to a third of that of water. This means that the seal pumps are not operating under optimum conditions. It was found that an increase in the pump speed gave a better performance in terms of slippage losses, which was just enough to operate at lower nitrogen pressures in the tank. This gave a short term resolution to the problem and an important set of boiling experiments with different amounts of dissolved gas under identical operating conditions could be conducted (see Section 4.2.3). However, such high pump speeds could not be used for long periods and nitrogen pressure had to be applied to the tank for the main series of experiments.

It was found that the test section liquid mass flux in the earlier experiments had been restricted to around 400 kg/m^{2}s as a result of a partially blocked fine-mesh strainer in the main loop. Unblocking the strainer allowed an increase of mass flux up to 600 kg/m^{2}s for single phase flow in the test section (530 kg/m^{2}s for two phase flow).

3.2 The test section and its instrumentation

The test section is a 8.68 m long, vertical 321 stainless steel tube with an inner diameter of 25.4 mm and an outer diameter of 38.0 mm, which is heated electrically by passing a large DC current (0–30 V, 0–4000 A) through its wall. Further information on the test section (i.e. thermal conductivity, electrial resistivity,

wall thickness and tube roughness) can be found in Appendix B.

At the ends of the test section, flanges were welded to allow installation; to achieve electrical insulation, non-conducting gaskets were employed. The electrical power is transmitted via copper busses and clamps attached to the test section. The distance between the two clamps is 8.509 m, which determines the heated length. The test section was lagged with a 50 mm thick mineral insulation. The tube is equipped with pressure and temperature measuring devices along its length.

Along the test section, both bulk fluid and wall temperatures were measured. The bulk temperature (i.e. the temperature of the fluid at the centerline of the tube) was measured by welding thermocouple pockets into the tube. These pockets were made from a 2 mm outside diameter stainless steel tube, bent at a right angle at the centerline of the tube with the tip, sealed by welding, facing the flow. (See Figure 4.11). Sheathed thermocouples, with an outside diameter of 0.5 mm, could be fed into these pockets. Twelve pockets are located along the test section at a spacing of 750 mm, allowing a fairly good resolution in measuring the bulk temperature profile. It was not technically feasible to measure directly the inner wall temperature. During the earlier development of the test facility, several options for the determination of inner wall temperature were examined. The first option, drilling holes into the tube along the test section and putting thermocouples in was discarded. The reason was that the temperature drop through the wall can be up to 20 °C for high heat fluxes and the accuracy with which the thermocouples could be positioned would cause an high uncertainity in the temperature measurement (see Frankum, 1991). The option which was finally chosen, was to attach to the wall outside special self-adhesive film thermocouples (see Figure 3.2). 74 of these thermocouples were positioned axially along the tube wall. The methodology for calculating the inner wall temperature from readings of these thermocouples is described in Section 3.2.3.

3.2.1 Pressure measurement

The absolute pressures within the test section are measured at distances of 0.106 m, 3.865 m and 8.356 m from the bottom current clamp using Druck PDCR60 transducers. The pressure tappings are welded into the tube wall with a 0.5 mm diameter hole drilled through the test section wall to sense the pressure (See Figure 4.11). The pressure tappings are connected to the transducer via a cooler to ensure that only liquid is in contact with the transducer. This avoids ambiguity in the density of the fluid in the lines. In addition, eight differential pressure transducers (Druck PDCR 120/75/WL/IS type) are evenly spaced between the absolute pressure transducers (Spacing 0.75 m). During operation it became clear that the absolute pressure transducers developed zero offset over a fairly short time (within days), which could be up to 30 kPa. Comparing the measured bulk temperatures under saturated conditions with the calculated saturation temperature at the measured pressure revealed a discrepancy of several $°C$. Because of this, a new absolute pressure transmitter (Druck PTX620, Range 0 – 2 MPa) was installed at the bottom of the test section, thus providing a datum from which the absolute pressure profiles could be determined from the differential pressure transducer outputs. This reduced the discrepancy between measured and calculated saturation temperatures but this discrepancy was still significant. This point will be returned to in Chapter 4.

3.2.2 Temperature measurement

The wiring of the thermocouples can be seen in Figure 3.3. The cold junctions of the rig and test section thermocouples are inserted into a copper block surrounded by hard foam insulation and covered by a lid. The temperatures of the two isothermal boxes were measured with 1 mm Type T sheathed thermocouples which passed from the (hazardous) test section area to the control room via Zener barriers where they terminated in a 0 °C reference unit (accuracy ±0.1 °C). The output from the rig and test section thermocouples could therefore be adjusted

to take account of the readings of these reference thermocouples. The emf signals from the rig and test section thermocouples were transmitted through copper wires and Zener barriers to the data logger. Temperature profiles of experiments conducted previously gave rise to some doubt in the accuracy of the thermocouples. This was evident from the fact that the twelve measured temperatures of the isothermal box had a fairly wide scatter of 1 °C at ambient temperatures of 15 to 20 °C. Furthermore, readings of the bulk and the wall thermocouples at ambient, equilibrium conditions (10 °C ambient temperature, no heating on) showed that wall temperature readings had a scatter of 0.7 °C and the bulk temperature readings had a scatter of 2 to 3 °C. Examination of the temperature measurement lead to the following observations:

1. The thermocouple cold junction ends of the reference thermocouples were only twisted and not welded, which can affect the accuracy. Furthermore, the thermocouples were in poor thermal contact with the reference unit, being mounted in air rather than a liquid phase. The cold junction wire ends were replaced with sheathed thermocouples of the same batch as the reference thermocouples. The ends were immersed in silicone oil to ensure a constant reference temperature of 0 °C.

2. Two isothermal boxes were used in the previous work. One held the cold junctions of the bulk thermocouples and the rig thermocouples, and in the other, cold junctions of the wall thermocouples were inserted. Here again, the thermocouple ends were in air and the lid of the reference box was not protected adequately against draft. Since a forced ventilation system is running during rig operation, the draft caused by it creates a non-isothermal condition. These problems were cured by immersing the thermocouples in silicone oil, by putting all the test section thermocouples in one box and by insulating the isothermal box so that drafts could not reach the copper block holding the thermocouples. Thus isothermal conditions in the block were ensured. As a result, the outputs of the reference thermocouples are

within 0.2 °C. The bulk thermocouples were removed from the test section and checked against a reference mercury thermometer using a water bath. The scatter in the thermocouple readings was within ± 0.2 °C at about 80 °C and these readings were 0.3 °C lower than that of the reference mercury thermometer. The wall thermocouples could not be checked for accuracy in the same way because it was not practical to remove the thermocouple from the test section. However, two were removed and checked after the completion of the experiments; the results indicated a similar accuracy to that of the bulk thermocouples. Both the bulk and the removed wall thermocouples were also checked against a calibrated dry block calibrator which had an accuracy of ±0.3 °C up to a temperature of 140 °C. It was found that the thermocouple outputs were within the accuracy of the calibrator.

3.2.3 The calculation of the inner wall temperature

The temperature profile across the test section wall with internal homogeneous heat generation is shown schematically in Figure 3.4 right. The major part of the heat generated is transferred to the fluid via convection. However good the lagging is, some heat will be lost to the surroundings. This causes a temperature drop through the (very thin) polymide carrier of the film thermocouple, which also has to be considered in the determination of the outer wall temperature, $T_{w,o}$; we shall return to this point below. The required temperature is the inner wall temperature $T_{w,i}$ and this can be obtained using the equations for one-dimensional heat conduction with heat generation. In cylindrical coordinates the differential equation for one-dimensional radial conduction is

$$\frac{1}{r}\frac{d}{dr}\left(r\frac{dT}{dr}\right)+\frac{\dot{q}_G}{\lambda_{TS}}=0 \tag{3.1}$$

This equation can be solved with the boundary conditions:

1. $T = T_{w,o}$ at $R = R_o$. $T_{w,o}$ is estimated from the reading of the wall thermocouples, taking account of the temperature drop through the polymide coating (see below).

2. $dT/dr = -\dot{Q}_{loss}/(2\pi\,\lambda_{TS}\,R_o)$ at $R = R_o$. Here, $\dot{Q}_{loss}$ is the heat loss per unit length of channel (W/m).

Solving the differential equation with the two boundary conditions gives the following final equation for the inner wall temperature.

$$T_{w,i} = T_{w,o} + \frac{\dot{q_G}}{4\lambda_{TS}}(R_o^2 - R_i^2) + R_o\left[\frac{\dot{q_G}}{2\lambda}R_o - \frac{\dot{Q}_{loss}}{2\pi\lambda_{TS}R_o}\right]\ln\frac{R_i}{R_o} \qquad (3.2)$$

$\dot{q_G}$ is the internal heat generation (W/m^3) calculated from the total heat input (W) devided by the volume of the heated test section. $\dot{Q}_{loss}$ was determined experimentally as a function of the temperature of the fluid in the test section by passing liquid at different temperatures through the non-heated test section (see Figure 3.4 left for temperature profile without heating). The heat loss per unit length for the test section could be determined using the following equation:

$$\dot{Q}_{loss}[W/m] = \frac{c_{p,L}\,\dot{M}\,(T_{in} - T_{out})}{(z_{out} - z_{in})} \qquad (3.3)$$

where $\dot{M}$ is the flow rate of the liquid (kg/s), T_{in} and T_{out} the inlet and outlet temperatures measured at distances z_{in} and z_{out} and $c_{p,L}$ the liquid specific heat capacity. The results obtained for $\dot{Q}_{loss}$ are shown in Figure 3.5 where the heat loss of the whole test section $\dot{Q}_{loss}(z_{out}-z_{in})$ is displayed against the inlet temperature. It can be seen that the curve can be approximated as being linear.

To use Equation 3.2 to calculate $T_{w,i}$, a value of $T_{w,o}$ is required. This is related to the temperature T_{TC} measured by the thermocouple by the expression:

$$T_{TC} = T_{w,o} + \frac{\dot{Q}_{loss}}{2\pi\lambda_{TC}}\ln\frac{R_o}{R_{TC}} \qquad (3.4)$$

where λ_{TC} is the thermal conductivity of the thermocouple coating and R_{TC} is the radial position of the thermocouple junction. The problem in applying Equation 3.4 is that neither λ_{TC} nor R_{TC} are known. Thus, a method is used which is adapted from Sivaniah (1992) who derived correction factors for the film thermocouples based on the results of heat loss (without heating) experiments at different inlet temperatures. A theoretical outside wall temperature was calculated applying the following equation

$$T_{w,o,calc} = T_b + \dot{Q}_{loss}\left[\frac{1}{\alpha\pi D_i} + \frac{ln(D_o/D_i)}{2\pi\lambda_{TS}}\right] \qquad (3.5)$$

where λ_{TS} is the thermal conductivity of the test section wall material. The first term in brackets accounts for the temperature increase through the boundary layer and the second term for the conduction through the tube wall. α, the fluid-to-wall heat transfer coefficient, was calculated using the well known Dittus-Boelter (1930) equation for single phase heat transfer in turbulent flow in tubes. Calibrations of the thermocouples also reveal that they have a small offset, C_{offset} (typically a fraction of degree). Thus, Sivaniah (1992) included both the offset and also the temperature gradient due to heat losses in his experiments for the correction of the T_{TC} reading to obtain the tube outside wall temperature. The expression is as follows:

$$T_{w,o} = T_{TC} + C_{offset} + \frac{\bar{R}_{TC}\,\dot{Q}_{loss}}{2\,\pi\,D_o} \tag{3.6}$$

where $\bar{R}_{TC}$ is the thermal resistance of the film thermocouple. The values of C_{offset} and $\bar{R}_{TC}$ can be determined from the results of two heat loss experiments, carried out at different temperatures, for which the outside wall temperature ($T_{w,o} = T_{w,o,calc}$) is calculated from Equation 3.5. The remaining heat loss data sets were used to check the corrections. The correction factors calculated are given in Table 3.1.

3.2.4 Flow measurement

The liquid flowmeter used is a drag disk device (Ramapo Mark V-3/4-F02), in which a disk of accurate dimensions is supported perpendicular to the flow. The force by the fluid on the disk is transmitted via a lever to a strain gauge bridge, where a voltage output is generated. The flowrate was displayed with a Hersey indicator in USgal/min. The actual flowrate needs to be corrected for the specific gravity, $\rho_{process}/\rho_{water}$ of the process fluid as compared to the specific gravity of the fluid stated by the supplier for calibration, $\rho_{calibration}$, of the flowmeter (see Equation 3.7). The supplier uses water for calibration and corrects electronically for the specific gravity of the fluid chosen by the user of the unit (normally close to the value of the process fluid used, in this case 0.68). This electronic correction

apparently has not been implemented, which could be found out by setting the specific gravity at unity and at 0.68 for single phase experiments and comparing heat balances of water with that of hydrocarbons.

$$\dot{V}_{corrected} = \sqrt{\frac{\rho_{calibration}/\rho_{water}}{\rho_{process}/\rho_{water}}} \cdot \dot{V}_{display} \tag{3.7}$$

Good agreement with heat balances was found when the specific gravity at calibration was set to 1 for both types of fluids, water and hydrocarbons, respectively. Furthermore, calibration conducted both in the present and previous work were carried out with iso-octane and water, which confirmed this interpretation.

The heat balances for single phase runs showed an increasing discrepancy when the flow rate fell below 3 USgal/min. Examining this effect showed that this was caused by the electrical interference of the seal pump (P10) inverter (which had been installed to increase the speed of pump P10) which affected the flow meter signal. The amount of interference in the flow rate reading could be expressed as an exponential decay function which reduces to the actual reading at higher flow rates. The correction could be derived with the help of the single-phase heat balances and allowed recalculation of the actual flow rate.

3.2.5 Heat balances for single phase experiments

Heat balances could be performed over the test section in single phase flow. Taking account of the heat losses measured in the adiabatic experiments, heat balances were within ±5%.

3.2.6 Density measurement

A density meter (Paar DPR 4/22 XEI) was installed in the HPBR. The density meter is positioned after the preheater and was installed not only to measure the density of the pure fluids but mainly to derive the composition of the binary mixture from the measured density and the corresponding densities of the two components. Originally, this density meter was installed after the preheater and,

since it could only withstand fluid temperatures less than 125 °C, this led to a limit for the inlet temperature to the test section. As a consequence, boiling experiments were restricted to pressures of less than 0.5 MPa for iso-octane. To resolve this problem, the density meter was moved to a location upstream of the preheater.

3.2.7 Test section heating

The test section is directly heated by a low voltage high current DC supply (Westinghouse Davenset Type SNA 30/4000) capable of delivering 4000A at 30V. The current was passed through copper busbar clamps to the ends of the test section. The current was measured using a high accuracy shunt (60mV corresponds to 4000A). The voltage, $U_{rectifier}$, was not measured directly across the test section but just after the rectifier. This meant that the resistance of the copper bars had to be accounted for, to calculate the voltage across the test section. The total electrical resistance, R_{busbar} of the cooper bars was calculated to be 0.3085 mOhm and hence the actual test section voltage, U_{TS}, is

$$U_{TS} = U_{rectifier} - R_{busbar} I \tag{3.8}$$

where I is the current. The test section electrical resistance is 9.6475 mOhm at 20 $°C$. The DC supply showed a characteristic ripple as shown in Figure 3.6. The supplied heat to the test section would only be precisely uniform, if the temperture of the test section is constant, i.e. electrical resistance constant. Knowing the electrical resistivity as a function of temperature allows a calculation of the local heat flux. It was found that for the boiling experiments the temperature differences along the tube were in such a range that constant heat flux could be assumed; the variation was of the order of 0.5%.

3.2.8 Overall uncertainity in the heat transfer coefficient

The heat transfer coefficient is calculated from 9 measured values each of which has an uncertainity. Table 3.2 gives a summary of the variables and their esti-

mated uncertainities. A function for the heat transfer coefficient consisting only of the measured values was derived and the Gaussian method for error estimation (propagation) was applied. The equation for estimating errors by this method is:

$$\Delta f_{err} = \sqrt{\left(\frac{\partial f_{err}}{\partial x_1}\Delta x_1\right)^2 + \left(\frac{\partial f_{err}}{\partial x_2}\Delta x_2\right)^2 + \ldots + \left(\frac{\partial f_{err}}{\partial x_n}\Delta x_n\right)^2} \qquad (3.9)$$

Here, f_{err} is the function evaluated (i.e. the heat transfer coefficient) and Δf_{err} is the error arising in f_{err} from errors Δx_i in each of the (nine) quantities involved. This involves estimating a partial derivative for each variable, which involves a large amount of calculation effort. Therefore, the software package (Mathcad 6) was used to deal with the error analysis. This made it possible to calculate the relative mean error for every single data point and this was valuable for the further analysis and interpretation of the data. The average error was typically in the region of 5 to 10% for boiling experiments and between 3 and 4% for single phase experiments.

An error occurring due to the discrepancy between measured and calculated saturation temperature results in an uncertainity in at the point of zero quality. The discrepancy between the measured bulk temperature and the calculated saturation temperature in the two phase region ($T_{sat}(p_{abs}) < T_{b,sat}$) could not be resolved. An error in calculated qualities of between 0.00 and 0.03 occurs for the points where the equilibrium quality is near to zero. The calculated quality is lower than the actual quality.

3.2.9 Stability of operating conditions during experiments

Steady state heat transfer experiments can only lead to reproducible andaccurate results when the working conditions of the rig are steady over the period of one test run (up to 10 – 40 min). Fortunately, very steady conditions were observed in the test section of the HPBR. For example, the inlet pressure fluctuates only in the region of ±2 kPa and the flow rate by ±0.01 USgal/min. Also, the preheater delivers a very steady inlet temperature with fluctuations less than ±0.1 °C.

3.3 Operation of rig and conduction of experiments

Experiments on both single phase and on boiling liquid heat transfer were carried out. The data collection procedure is described in Section 3.3.1 and the procedure for the boiling experiments is described in Section 3.3.2.

3.3.1 Data collection

All tests were run at steady state conditions. Data aquisition and control of the system were carried out by a data logger and a microcomputer. The data aquisition system continuously scanned and the temperatures, flow rate, etc. of the system were displayed while the conditions in the test section were approaching to steady state. Each scan took 20 seconds to read about 150 channels. When the conditions were believed to be steady 5 scans were recorded and the average over these 5 scans was used for further analysis. The data were processed using a specially written data reduction program which calculated the relevant variables (wall, bulk temperatures, heat flux, heat transfer coefficient etc).

For the final stage of the data analysis which includes the calculation of physical properties for mixtures and pure components, quality and different boiling correlations a FORTRAN computer code was written. For the calculation of the physical properties the PPDS (Physical Property Data Service) software package was linked to this code. The VLE method used was that of Soave-Redlich-Kwong (Redlich and Kwong (1949), Soave (1972)).

3.3.2 Procedure for boiling experiments

The two-phase experiments were started at low heat flux, generally 10 kW/m^2 with inlet temperature close to saturation, making sure that no vapour was generated in the preheater. This could be checked with the density meter by comparing measured density with calculated density. In the main series of experiments, the

heat flux was increased further in steps of 10 kW/m^2; to avoid dryout, the inlet temperature had often to be reduced with increasing heat flux. Further to the above mentioned sets of experiments other series were carried out where the heat flux, mass flux and pressure were kept constant and only the inlet temperature was increased up to the maximum inlet temperature, typically 5 to 15 °C below saturation. In addition, runs with reduction in the inlet temperature were performed to allow the examination of hysteresis effects. In this context, experiments were also conducted by increasing and decreasing the heat flux. An additional set of experiments only with n-pentane has been conducted to investigate the effect of pressure. These different types of experiments are described in Chapter 4.

Position m	C_{offset} °C	R_{TC} m^2K/W	Position m	C_{offset} °C	R_{TC} m^2K/W
0.106	-0.2289	0.00736	4.956	-0.474	0.01123
0.306	-0.7586	0.01352	5.056	0.0116	0.00324
0.456	-0.0459	0.00182	5.156	-0.0039	0.00202
0.756	-0.0577	0.00245	5.256	-0.0275	0.00098
0.856	-0.031	0.00239	5.356	-0.0097	0.00101
1.306	-0.7835	0.01833	5.456	-0.0062	0.002
1.456	-0.0703	0.00158	5.556	0.0357	0.00248
1.606	0.0248	0.00241	5.656	-0.0024	0.00143
1.706	0.0071	0.00179	5.756	0.0277	0.00152
1.806	-0.035	0.00281	5.856	0.0624	0.0038
1.906	-0.0203	0.00301	5.956	0.0232	0.00234
2.006	0.0073	0.00095	6.106	-0.0071	0.00122
2.206	0.0222	0.00201	6.206	-0.0142	0.00267
2.356	-0.0149	0.004	6.306	-0.0165	0.00138
2.456	-0.0356	0.00289	6.406	-0.0774	0.00457
2.556	0.0176	0.00192	6.556	-0.1828	0.00488
2.856	0.0236	0.00227	6.656	0.0599	0.00214
2.956	0.012	0.0014	6.756	-0.1175	0.00328
3.106	-0.0658	0.00243	6.856	-0.0078	0.00183
3.256	-0.4717	0.00794	6.956	-0.0022	0.00113
3.456	0.1163	0.0003	7.056	-0.0243	0.00182
3.556	0.0223	0.0017	7.156	-0.0237	0.00047
3.656	0.0437	0.00175	7.256	-0.0596	0.00288
3.756	-0.0878	0.00331	7.356	-0.0209	0.00244
3.856	0.0139	0.00126	7.456	0.0187	0.00133
3.956	0.0337	0.00267	7.606	-0.0386	0.00212
4.056	0.0061	0.00117	7.706	0.0181	0.00293
4.156	0.023	0.00209	7.806	0.0227	0.00193
4.256	0.0021	0.0022	7.906	0.0225	0.00246
4.356	0.0082	0.00117	8.006	-0.0006	0.00152
4.606	0.0096	0.0024	8.106	0.0041	0.00216
4.706	0.0696	0.00358	8.206	-0.0709	0.00215
4.806	-0.0421	0.00206	8.356	-0.1028	0.00172

Table 3.1: Correction factors for the wall thermocouples

Uncertainity of measured values:	
Temperature at wall thermocouple	$\pm$ 0.3 $°C$
T bulk temperature	$\pm$ 0.3 $°C$
Voltage across testsection	$\pm$ 1.0 %
Current through test section	$\pm$ 1.0 %
Thermal conductivity of test section	$\pm$ 4.0 %
Heat loss	$\pm$ 20 %
Length of the heated test section	$\pm$ 10 mm
Inner diameter of test section	$\pm$ 0.1 mm
Test section wall thickness	$\pm$ 0.15 mm

Table 3.2: Estimated uncertainities of the measured values needed for the calculation of the heat transfer coefficient

Conditions	Unit	Range
Pressure	[MPa]	0.23, 0.3, 0.6, 1.0
Mass fluxes	[kg/m^{2}s	100, 200, 300, 500
Heat fluxes	[kW/m^2]	10, 20, 30, 40, 50, 60, 70
Inlet subcooling	[oC]	minimum of 5 to 15
Exit quality	[ ]	< 0.8

Table 3.3: Test matrix for two-phase experiments

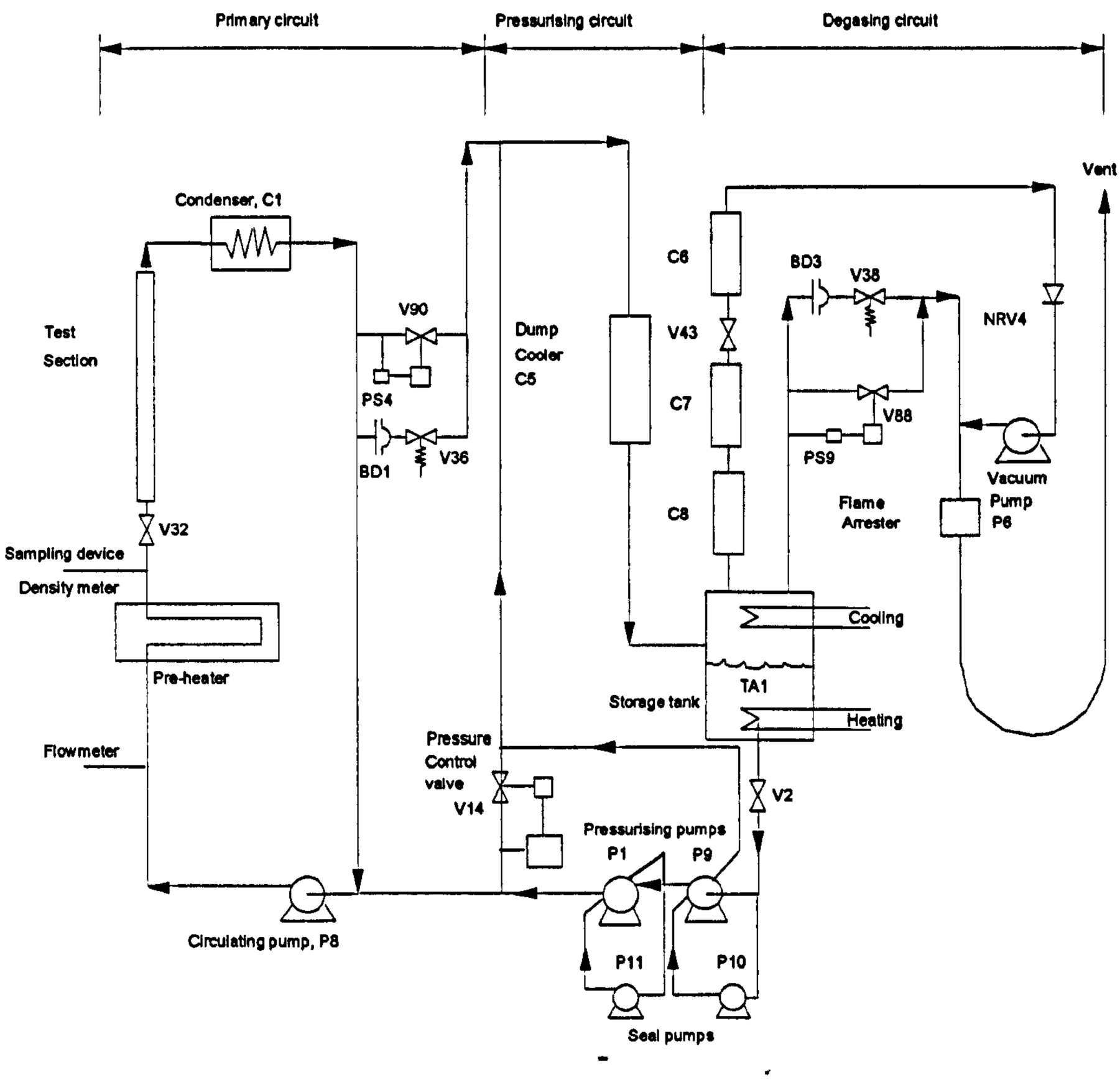


Figure 3.1: Schematic diagram of the HPBR facility.

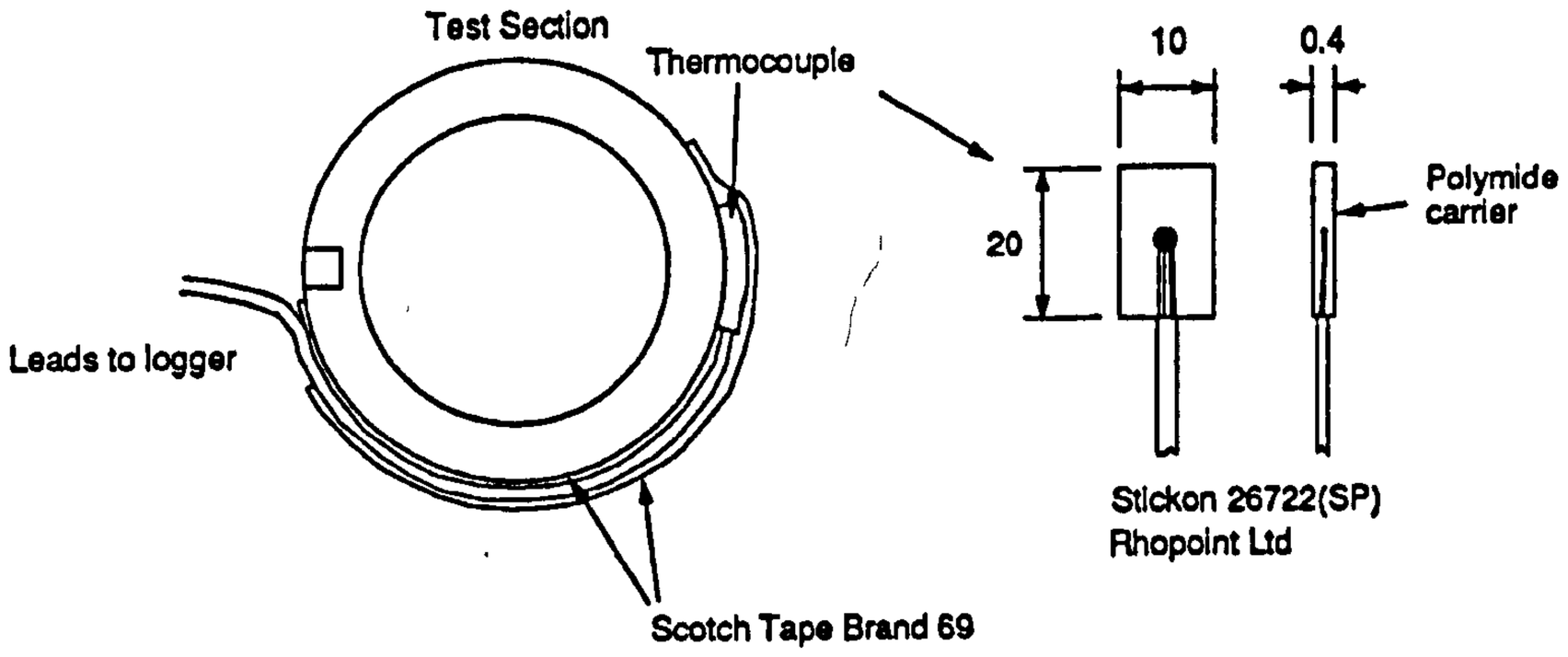


Figure 3.2: Installation of the wall thermocouples.

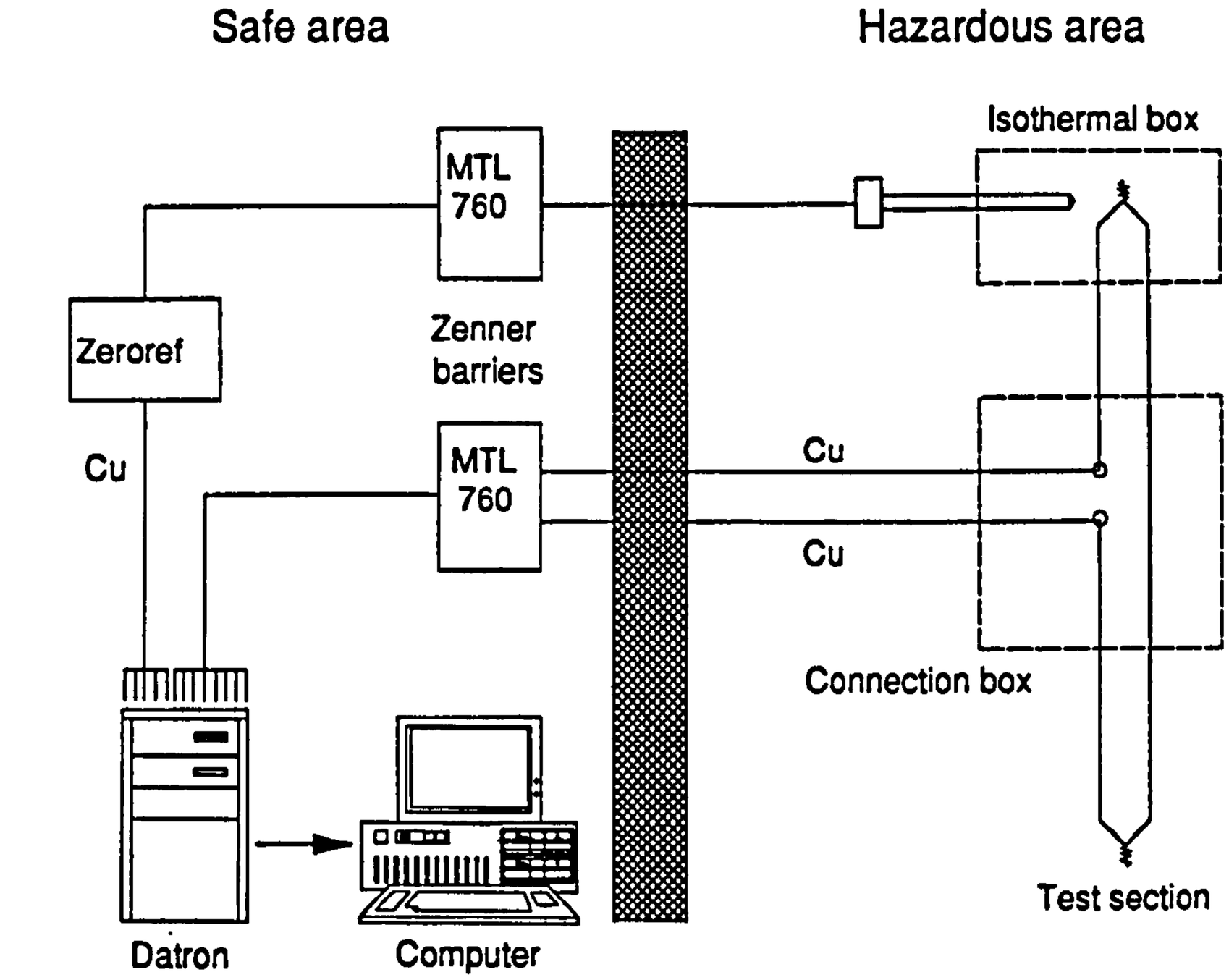


Figure 3.3: Installation of the test section thermocouples.

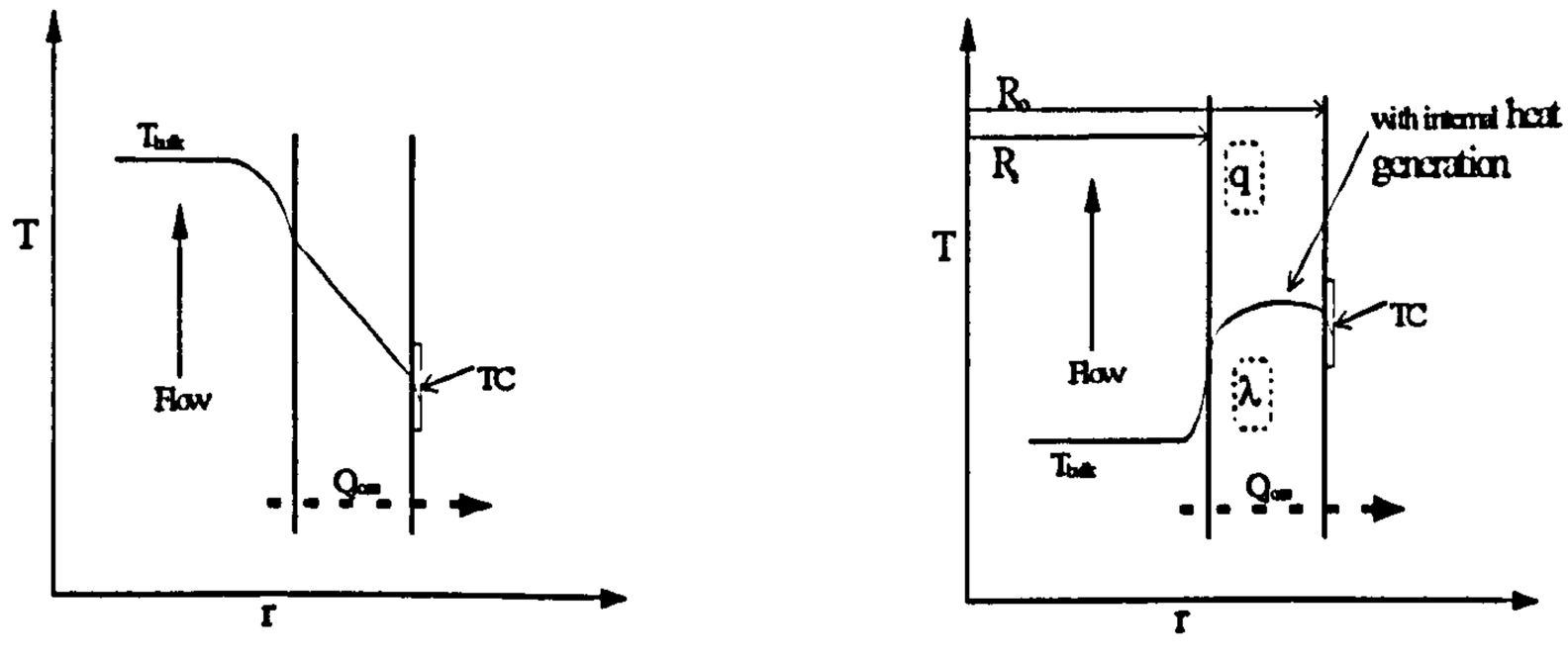


Figure 3.4: Temperature profile across the test section wall: without heat generation but with heat loss to the surroundings (left); with internal heat generation and heat losses (right).

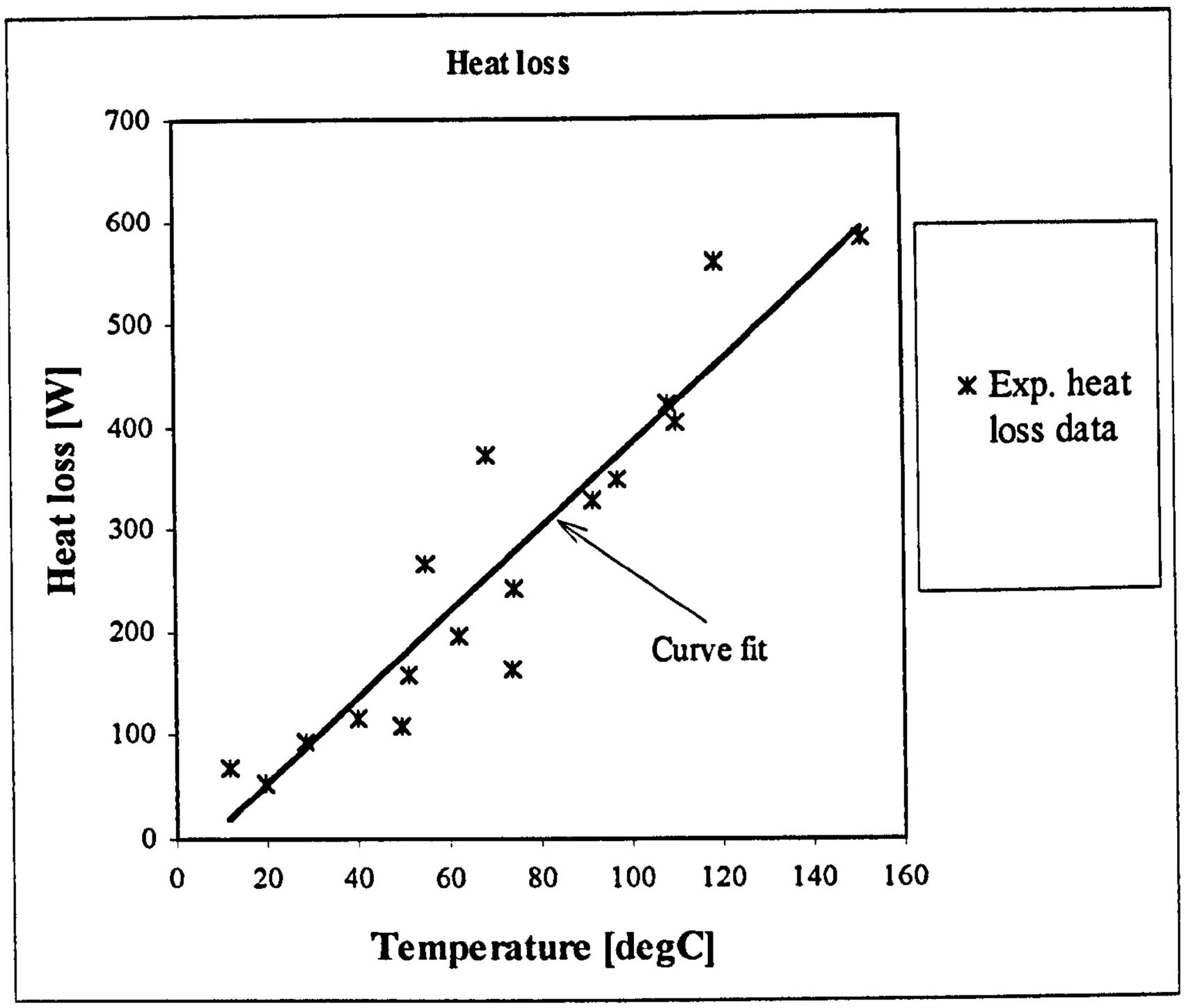
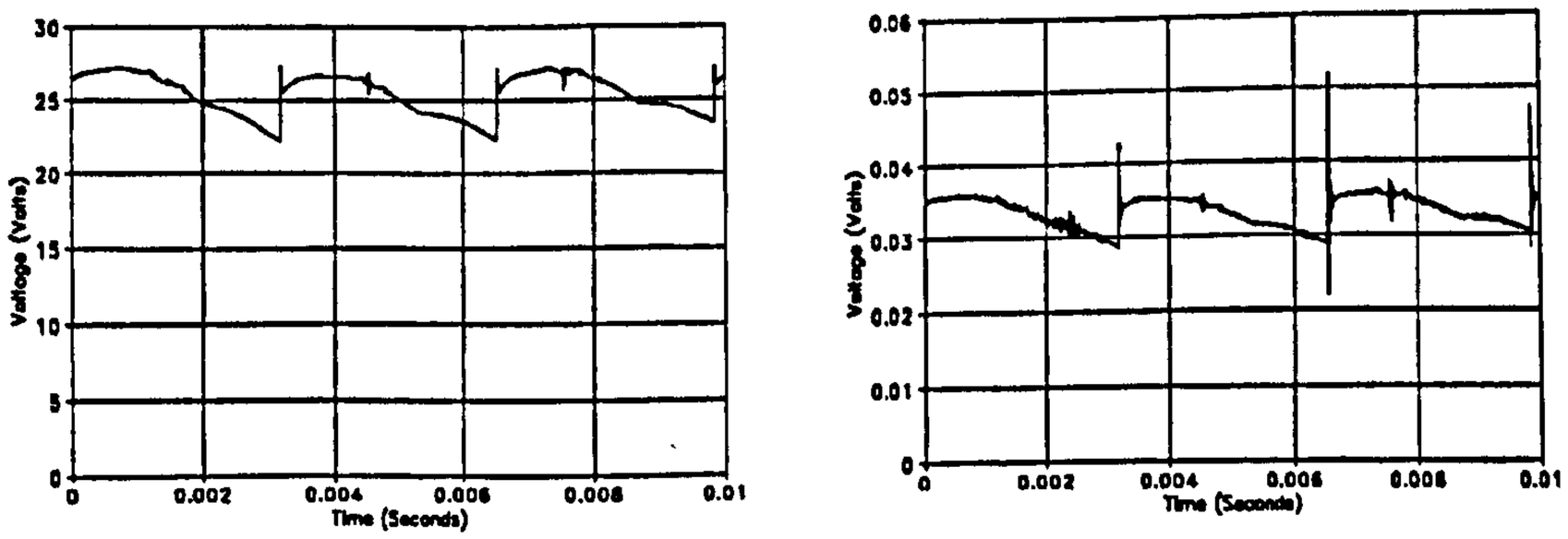


Figure 3.5: Heat loss experiments.



(a) Voltage (b) Shunt

Figure 3.6: Stability of DC supply.

Chapter 4

Analysis of experimental results

4.1 Single phase heat transfer in vertical heated upflow

In this project single phase heat transfer experiments were conducted in addition to the two-phase experiments for two main reasons: Firstly, those experiments give a good means of testing the performance of the measuring devices such as the flow meter, the thermocouples and the electrical power instrumentation, by allowing a comparison between the sensible heating of the fluid and the electrical power input. Secondly, the measured heat transfer coefficient may be compared with correlations for single phase flow. Since single phase heat transfer correlations are used as a basis for many boiling correlations it is advantageous to further assess their performance.

Furthermore, as noticed already in the previous work by Frankum (1996), for mass fluxes of 100 - 280 kg/m^{2}s a phenomenon occurs, which causes a reduction in the heat transfer coefficient compared to fully turbulent heat transfer. This phenomenon is due to buoyancy effects (relaminarisation effects) and was investigated more systematically in the present work by performing experiments with n-pentane and iso-octane.

4.1.1 Effect of bulk thermocouples on the wall temperature profile

The test section is equipped with 12 thermocouple pockets to measure the bulk temperature along the test section (see Section 3.2.2). These pockets are protruding into the tube, which means that those can have an effect on the fluid flow. The small disk where the tube is welded into the tube does not have the same curvature as the tube, so there is a recess there between the disk and the inner tube, which could also contribute to disturbance of the flow (see Figure 4.1). In any apparatus, where direct measurements in the field of fluid dynamics have to be conducted, there is always the possibility that the measuring probe is causing a disturbance. Figure 4.3 displays the bulk and wall temperature profile for a typical single phase run. Here, just after a bulk thermocouple pocket, the wall temperature drops slightly this drop probably being caused by the additional turbulence generated by the pockets leading to a better heat transfer. Thus, in the following analysis, data points taken just before the disturbance are used as being the most representative of the tube. It is believed that the gross effect of the disturbance has died down by this position. The distance from disturbance to measurement point is 750 mm i.e. 30 pipe diameters.

4.1.2 Fully turbulent heat transfer

The general approach for the determination of the heat transfer coefficient in a pipe is to apply the analogy between heat transfer and friction. It has been shown experimentally that for a limited range of these parameters, relations between friction, heat transfer, and mass transfer of the following form can be applied.

$$Nu\, Pr^{-1/3} = (f_o/2)Re \tag{4.1}$$

Nu is the Nusselt number ($= \alpha\, D/\lambda$), Pr the Prandtl number ($c_p\eta/\lambda$) and Re the Reynolds number ($v\, D\, \rho/\eta$). f_o is the Fanning friction factor (defined as $\tau_o/(1/2\,\rho v^2)$ where τ_o is the wall shear stress, ρ the fluid density and v the fluid velocity).

Numerous correlations have been derived from Equation 4.1 by modifying the friction factor, changing constants and including additional terms for density corrections, entrance effects etc. In the present analysis only the most commonly used correlations are discussed, namely those of Dittus-Boelter (1930), Petukhov (1963), ESDU (1967) and Gnielinski (1976). Only experiments where no laminarisation is noticeable are used for this analysis of the fully turbulent region (see Section 4.1.5).

Correlations for fully turbulent region

The equations for the correlations tested are given for completeness.

Petukhov (1963)

$$Nu = \frac{(f_o/8)\,Re\,Pr}{K + 12.7\sqrt{f_o/8}(Pr^{2/3} - 1)} \tag{4.2}$$

$$f_o = (1.82\,\log_{10}(Re) - 1.64)^{-2} \tag{4.3}$$

$$K = 1 + 900/Re \tag{4.4}$$

Dittus-Boelter (1930)

$$Nu = 0.023\,Re^{0.8}\,Pr^{0.4} \tag{4.5}$$

Gnielinski (1976)

$$Nu = \frac{(Re - 1000)Pr(f_o/8)}{1 + 12.7(Pr^{2/3} - 1)\sqrt{f_o/8}} \tag{4.6}$$

ESDU (1967)

$$Nu = Re\,Pr\,exp[-3.796 - 0.205\,lnRe - 0.505\,lnPr - 0.0225\,(lnPr)^2] \tag{4.7}$$

Results

Comparisons of the present data with the four correlations tested are shown in Figures 4.5 and 4.6 where the ratio of the experimental to predicted heat transfer coefficient is plotted against Re and Pr. For Re less than 25000 the Dittus-Boelter, Pethukov and ESDU correlations, overpredict the heat transfer.

Gnielinski's correlation which was derived by modifying Petukhov's equation to represent correctly the experimental values in the range of $2300 < Re < 10000$ gave the best results at low Reynolds numbers. The Petukhov correlation appears to have the smallest scatter; however, it overpredicts the data by at least 10%. Figure 4.7 shows plots of the predicted versus the experimental values for each correlation.

An analysis of the performance including a statistical analysis of the errors is summarised in Table 4.1. The definitions of average and mean errors given in Appendix C are calculated from Equation C.2 and EquationC.3, respectively.

	n-pentane (471 points)		iso-octane (325 points)	
Correlation:	Average error	Mean error	Average error	Mean error
Dittus-Boelter (1930)	-0.010	0.039	0.015	0.042
Petukhov (1963)	0.133	0.133	0.156	0.156
Gnielinski (1976)	0.110	0.111	0.111	0.111
ESDU (1967)	-0.002	0.037	0.040	0.052

Table 4.1: Comparison of average and mean errors of.the single-phase heat transfer correlations compared with present data for single phase heat transfer

4.1.3 Property correction

The effect of radial variations of the fluid properties will become significant under conditions where the difference between the wall temperature and fluid bulk temperature is large, or when operating near the critical point. Variations of viscosity, thermal conductivity, specific heat capacity and density will affect the prediction of heat transfer. The correction factors presented for physical property variation for liquids and gases which are considered to be the most accurate available, are those developed for use with Petukhov's correlation. For liquids

far from their critical points, the thermal conductivity, specific heat capacity and density are weak functions of temperature, but the dynamic viscosity varies significantly with temperature. The relative change of Nusselt number due to viscosity variations with temperature can be expressed as $(\lambda_b/\lambda_w)^n$ where λ_b is the viscosity at the bulk temperature and λ_w is the viscosity at the wall temperature. Petukhov (1970) suggests a value of $n = 0.11$ for heating and $n = 0.25$ for cooling. The property correction is valid over the range $0.08 \leq (\eta_b/\eta_w) \leq 40$, $10^4 \leq Re \leq 1.25 \cdot 10^5$ and $2 \leq Pr \leq 140$.

The VDI Wärmeatlas suggests a correction for physical properties in the form:

$$Nu/Nu_{ft} = (Pr_b/Pr_w)^{0.11} \tag{4.8}$$

where Pr_b and Pr_w are the liquid Prandtl numbers at the bulk and wall temperatures respectively and Nu_{ft} is the fully developed turbulent flow Nusselt number.

For the conditions in the present tests, the maximum property correction was 1.05, so it is not high.

4.1.4 Entrance effect correction

Entrance effects associated with developing boundary layers are very significant in laminar flow but are also present in turbulent flow. A number of distinct thermal entrance conditions can be identified (ESDU, 1991). The first is that in which the velocity and temperature profiles develop simultaneously along the tube (that is the fluid is heated over the complete length of the tube). This condition is appropriate to most practical applications. A second thermal entrance condition is that in which the temperature profile develops after the velocity profile has been fully established; this condition arises when a long unheated length of tube precedes the start of heating (or cooling). Most experimental work on single phase heat transfer in tubes has employed this entrance arrangement. Clearly a range of possibilities intermediate between the above two conditions can arise. However, in most cases the local heat transfer coefficient decreases from a maximum value

at the point of commencement of heating to a constant value at the point where the temperature and velocity profiles become fully developed. Downstream of this point, under conditions of constant fluid properties, the value of the local heat transfer coefficient is constant.

In most practical applications the flow is fully developed at the beginning of the heated section and only the developing thermal boundary layer needs to be considered. The local heat transfer coefficient is initially very high but decreases to the value for a fully developed flow after a distance equal to approximately 15 pipe diameters (in the HPBR this would correspond to 38 cm). For long pipes the entrance effects may often be disregarded and the fully developed value of the heat transfer coefficient may be used as an overall average. A detailed description of entrance effects is given by Gnielinski (1983).

In addition, any maldistribution of the flow in the entrance region (that is a bend, sharp edge, sudden contraction, orifice, etc.) will give rise to further changes in the heat transfer coefficient in the entrance region. Generally, the length necessary for thermal development to be completed is dependent on Re and Pr numbers. A correction for the development of boundary layers has been introduced by Hausen (1959) and is expressed as

$$Nu/Nu_{ft} = [1 + (D/L)^{2/3}] \tag{4.9}$$

where D is the tube diameter and L is the tube length.

4.1.5 Buoyancy effects on heat transfer: Mixed convection

For high temperature differences between bulk and wall, the change in physical properties across the tube may induce a further effect on heat transfer. The density at the wall is lower than in the bulk which induces buoyancy forces occurring in direction of the flow for upflow. These buoyancy forces cause a distortion in the shear stress distribution giving higher wall shear stress but lower shear stresses in the region outside the laminar wall layer. This leads to a reduction in the rate

of generation of turbulence and therefore impairs the heat transfer. This effect is called relaminarisation.

The relaminarisation phenomenon was first found with experiments at pressures near the critical point, because the density and the viscosity are highly temperature sensitive in this region (see Jackson et al. (1989) for more detailed information). However, Jackson and Hall (1979), Petukhov (1977) and Rouai (1987) found that such buoyancy effects occur also under conditions far from the critical point. They developed correlations which estimate the reduction in heat transfer. Other workers like Alferov et al. (1973), Kenning et al. (1974) give criteria when reduction is expected to occur and where a temperature peak occurs corresponding to the highest buoyancy effects. Here, we shall concentrate on the quantitative heat transfer degradation and to establish which method performs best for the current data.

Figure 4.2 shows a typical peak in wall temperature caused by relaminarisation effects. This peak characterises the minimum turbulence generation; further downstream the level of turbulence increases again. A temperature profile showing buoyancy effects without a distinct wall temperature peak is shown in Figure 4.3 and finally Figure 4.4 shows a fully turbulent temperature profile. The results in Figure 4.3 show that the thermocouple pockets can, under conditions close to those for relaminarisation, trigger turbulence giving a local decrease in temperature.

Correlations accounting for the laminarisation effects

The different correlations (Petukhov, Jackson, Rouai) are very similar in their structure, unfortunately the Grashof numbers (Gr) are defined differently which can cause some confusion. They are thus stated here for completeness.

Jackson and Hall (1979)

$$\frac{Nu}{Nu_{ft}} = \left| 1 \pm \frac{10^4 \, \bar{Gr}_b}{Re_b^{2.7} \, Pr_b^{0.5}} \right|^{0.46} \tag{4.10}$$

$$\bar{Gr}_b = \frac{(\rho_b - \bar{\rho}) \, D^3 \, g}{\rho_b \, \nu_b^2} \tag{4.11}$$

$$\bar{\rho} = \frac{1}{(T_w - T_b)} \int_{T_b}^{T_w} \rho \, dT \tag{4.12}$$

where Nu_{ft} is the fully turbulent heat transfer coefficient in the absence of buoyancy effects and $\bar{\rho}$ is the integrated density.

Rouai (1987)

$$\frac{Nu}{Nu_{ft}} = \left[\left| 1 \pm 8 \cdot 10^4 \frac{Gr_b^*}{Re_b^{3.425} \, Pr_b^{0.8}} \left(\frac{Nu}{Nu_{ft}}\right)^{-2} \right|\right]^{0.46} \tag{4.13}$$

$$Gr_b^* = \frac{g \gamma D^4 \dot{q}}{\lambda \nu_b^2} \tag{4.14}$$

Petukhov (1977)

$$\frac{Nu}{Nu_{ft}} = \begin{cases} [1 + 720\,(Ra_P/Re^2)]^{-1} & if\ (Ra_P/Re^2) \leq 0.0016 \\ 3.97\,(Ra_P/Re^2)^{1/3} & if\ (Ra_P/Re^2) > 0.0016 \end{cases} \tag{4.15}$$

where the Raleigh number, Ra_P, and Grashof number, Gr_P are defined as

$$Ra_P = Gr_P \, Pr \tag{4.16}$$

$$Gr_P = \frac{g \gamma D^4 \frac{dT_b}{dz}}{\nu^2} \tag{4.17}$$

with $\frac{dT_b}{dz}$ being the longitudinal temperature gradient.

Discussion of results

Figures 4.9, 4.8, 4.10 for the Petukhov, Jackson, and Rouai correlations respectively show the ratio of the measured to the predicted fully turbulent heat transfer coefficient (calculated from the Dittus-Boelter correlation) for the present data as a function of the respective buoyancy parameter. The maximum reduction of the heat transfer coefficient due to buoyancy effects α_{exp}/α_{ft} is 0.45. Rouai's and Petukhov's correlations incorporate this maximum reduction, however, Jackson's equation shows an inconsistency without a limit on the heat transfer reduction. Also the location of the maximum buoyancy effects is not predicted very well. The Petukhov correlation predicts this better and Rouai's correlation gives the best fit to the data. The transition from fully turbulent to the region where laminarisation is occuring, i.e. at low values of the correlating parameter is slightly

smoother than predicted. The region from the maximum reduction to lower Re is also correlated very well, with some over prediction.

Table 4.2 shows the range of parameters for the single phase experiments conducted.

	n-pentane 840 data points		iso-octane 970 data points	
	min	max	min	max
Re	9400	111000	2500	112500
Pr	3.3	4.8	5.0	10.5
Gr^*	$6.0 \cdot 10^6$	$1.0 \cdot 10^{11}$	$2.0 \cdot 10^8$	$2.0 \cdot 10^{11}$

Table 4.2: Operating conditions of single phase experiments

4.2 Forced convective boiling results for pure components

This section describes the results for the boiling of pure component hydrocarbons n-pentane and iso-octane. First, an assessment of the validity of the results is given, followed by a description of unexpected trends in the data. Finally, a comparison of the data with the most commonly used correlations for in-tube boiling is presented.

4.2.1 Assessment of the effect of the thermocouple pockets on the flow in the tube and the heat transfer

Fluid temperature measurements were made using the thermocouple arrangement shown in Figure 4.11. Hypodermic tubing, of 2 mm outside diameter, was sealed by welding at one end, bent into an L-shape and passed through a hole in the wall tube such that the sealed end was at the tube axis, pointing into the flow. A

disk was welded to the hypodermic tube and, in turn, this disk was welded to the tube wall as shown in Figure 4.11. A 0.5 mm thermocouple was pushed into the hypodermic tube, reaching the tip pointing into the flow. The tip region occupies only 0.62% of the total cross section area of the flow and may be assumed not to be inducing a significant disturbance in the region of the measurement of the fluid temperature using the thermocouple. It is expected that the thermocouple would give an accurate measurement of fluid temperature near the tube axis provided that thermal equilibrium conditions prevail. However, as was shown in Section 4.1.1, there is a possibility that the thermocouple may disturb the wall region giving small effects on the heat transfer coefficient. This was certainly the case in single phase flow experiments (Section 4.1.1) and, in this section we address the problem of the effect in the boiling case. In the single phase flow, the effect may be magnified if there is relaminarisation of the flow as was discussed in Section 4.1.5. It may be that the thermocouple pocket acts as a boundary layer trip for the turbulence which may spread around the tube to the wall thermocouple position (which is displaced from the entry point of the thermocouple pocket by 90°).

Similar effects to those observed in single phase flow can be seen in subcooled boiling; a very small but discernable discontinuity in wall temperature is observed, synchronised with the position of the bulk thermocouples in the region of high subcooling.

For saturated boiling, a very slight effect can be observed but is hardly significant compared to the small variation in the data observed in any case.

We conclude, therefore, that the effect of the wall penetrations by the thermocouples is minimal in the case of boiling. This conclusion is consistent with that reached by Toral (1979) in his work on multicomponent boiling in a tube; Jung et al. (1989c) argued that such thermocouples should be avoided on the grounds that they may have a significant effect on local behaviour but we conclude that this is only true in a very limited range at high subcooling or in single phase flow.

4.2.2 Calculation of heat transfer coefficient from the measurements

The definition of the heat transfer coefficient α is as follows:

$$\alpha = \dot{q}/(T_w - T_b) \tag{4.18}$$

where $\dot{q}$ is the wall heat flux, T_w the wall temperature and T_b the bulk fluid temperature. The heat flux can be obtained from the electrical parameters, the wall temperature estimated by calculation of the response of the thermocouples on the outside of the wall but the estimation of T_b presents specific difficulties. Basically there are two options:

1. To determine the local *pressure* and to estimate T_b from this pressure value using thermodynamic data (saturation tables and/or vapour-equilibrium data). There are three difficulties with this approach:

   (a) It is not clear how valid it is in all cases to assume that the saturation conditions apply. In other words there may be significant departures from thermodynamic equilibrium, either in the form of superheating of the vapour or of subcooling of the liquid relative to the saturation conditions. In a formal sense, one could argue that the *definition* of heat transfer coefficient took account of this effect and that predictive methods should accommodate to it.

   (b) The temperature differences in boiling heat transfer are extremely small and, thus, a pressure measurement has to be made with great accuracy in order to establish an accurate value for T_b. Pressure gradient measurements are notoriously difficult in this kind of system; there are problems with connections to pressure transducers, with drift in the transducers with time and in establishing clear relationships between measurements of absolute and differential pressures.

   (c) In multiphase flows, there are characteristic and large fluctuations in pressure and there is always a concern as to whether any given instru-

ment measures a correct average of these fluctuations.

2. By using a thermocouple inserted into the fluid in a thermocouple pocket as sketched in Figure 4.11, it is possible to measure a representative temperature at the tube axis. Many experimentalists have used this temperature to characterise T_b. However, there are problems with this since, if thermodynamic disequilibrium exists, then the temperature measured at the centre of the channel may be unrepresentative. In fact, if the liquid phase is present as a continuum or in the form of droplets in the core of the channel, then the thermocouple would tend to measure the liquid phase temperature. This is representative of T_b only if thermodynamic equilibrium is assumed.

In the present work, two forms of pressure measurements were employed. The first was a measurement of absolute pressure at the entrance of the test section and the second was the measurement of a series of differential pressures along the test section. This allowed the nominal calculation of local pressure along the test section and, hence, T_b from the appropriate thermodynamic data. A major difficulty is that the inlet pressure transducer has to be ranged sufficiently to cover the full potential range of pressure in the system. In the early work, a pressure transducer with a range of 6 MPa was employed and had a nominal accuracy of 0.1% full scale. Later, this was replaced by a transducer ranged up to 2 MPa which had an accuracy of 0.1% full scale. Even if the the-oretical accuracy of these transducers were achieved, the uncertainity in T_b corresponding to these inaccuracies is still significant when compared with the temperature differences being measured. On the other hand, the accuracy of the differential pressure transducers was much greater and errors in calulating T_b tended to be of the form of *offsets* from the true temperatures due to potential inaccuracies of the inlet pressure transducer. Also, the inlet pressure transducer had to be placed at only around ten tube diameters from the start of the test tube which was preceded by a slightly smaller diameter tube containing a bend and connecting to a valve as is illustrated in Figure 4.12. This inlet configuration may possibly have induced

another small error in absolute pressure measurement and a consequential error in temperature measurement.

On the other hand, the bulk temperature measurements always gave a consistent set of values which agreed well with the saturation temperatures calculated from the (more accurate) pressure measurements at higher pressures as would be expected. Furthermore, comparisons to various correlations for single phase and boiling heat transfer for pure components indicated that the bulk thermocouples were giving consistent readings. *It was decided, therefore, that the bulk thermocouple values would be used consistently throughout this work for the calculations of heat transfer coefficients.*

4.2.3 Effect of dissolved gas

Previous work (see Section 2.2.6) has shown that dissolved gas can significantly affect boiling heat transfer. In the current experiments, assuming that the nitrogen pressurisation in the main liquid storage tank is around 0.15 MPa, the dissolved nitrogen content was in the range of 0.0014 – 0.002 moles/mole. The solubility of the nitrogen increases when the liquid is pressurised, and when the fluid is heated the solubility also changes. Data from Landolt-Börnstein (1976)(Figure 4.13) show that the solubility of nitrogen increases linearly with increasing pressure and is relatively independent of temperature for temperatures below around 60 °C. Thus, the partial pressure of nitrogen at a free interface in the channel is reduced in proportion to pressure and also with increasing temperatures above around 60 °C. Nevertheless, there will still be significant amounts of nitrogen in the vapour (typically corresponding to 120 kPa partial pressure). This has a negligible effect on the saturation temperature in the quality region.

As was discussed in Section 2.2.6, there are a number of effects of dissolved gases:

1. A reduction in the saturation (equilibrium) temperature relative to the saturation temperature in the absence of dissolved gases. Calculations for the present data indicated that this effect could become significant if the partial

Addition to Section 4.2.2: Calculation of heat transfer coefficient from the measurements

The absolute pressure transducers (old and new) at the inlet to the test section have been calibrated in situ with a reference transducer. It was found that the accuracy of the transducers was within the above stated accuracy of 0.1% full scale. This gives an uncertainty for the new transducer of ±0.02 bar and for the old transducer of ±0.06 bar. The corresponding uncertainty in the saturation temperature for the new transducer in the range of pressures examined is about ±0.35 °C at 2 bar and ±0.1 °C at 10 bar for n-pentane, and about ±0.4 °C at 2 bar and ±0.15 °C at 10 bar for iso-octane.

Measured inconsistencies in the saturation temperature calculated from pressure measurements and the measured bulk temperature measurements in the annular flow region during boiling runs of pure components (where equilibrium can be assumed) were greater than would be expected considering the uncertainties in pressure and temperature measurement together. The discrepancy was about 4 °C ±1 °C at a pressure of 2 bar and reduced gradually to 1.5 °C ±0.5 °C at 10 bar. The saturation temperature calculated from pressure measurements was always higher, than the measured bulk temperature. This reflects the difficulty in measuring pressure in two-phase systems.

Addition to Section 4.2.3: Effect of dissolved gas

The partial pressure of the nitrogen gas in the hydrocarbons was calculated as follows: The mole fraction of dissolved gas in the liquid, x_{N2}, was calculated to be 0.002. The K-value for nitrogen ($K_{N2} = y_{N2}/x_{N2}$) at a pressure, p_{tot}, of 0.15 MPa is 400, see Figure 4.13. The concentration of the gas in the vapour phase, y_{N2}, is therefore, $y_{N2} = 400 \cdot 0.002 = 0.8$, and the partial pressure of nitrogen, p_{N2}, is $p_{N2} = y_{N2} \cdot p_{tot} = 0.8 \cdot 0.15 = 0.12\ MPa$.

pressure of the gas within the vapour-gas mixture was large. Once vapour is formed in significant quantities, then the effect is minimal. This is consistent with the observations of Murphy and Bergles (1972) and Mayinger and Bucher (1976) who showed, that in forced convective boiling, the effect of dissolved gases became small once the boiling became fully developed.

2. Dissolved gases are known to have a significant effect in the nucleation processes. If small amounts of gas are formed or trapped in the nucleation centres then this can aid the initiation of nucleation which continues with vapour generation from the nucleation site and gradual dilution of the inert gas originally in the cavity. If the system is cooled down, then the cavities which were initially activated as a result of the presence of inert gas may be deactivated, and this is a familiar phenomenon to everyone who ever boiled a kettle of previously boiled water.

3. In the subcooled boiling region, the presence of the inert gases may affect the collapse of bubbles in the subcooled boiling region, or at least slow this collapse, affecting the overal boiling process.

To check on the influence of inert gases in the present experiments, three sets of tests were conducted as follows:

1. The main storage tank was pressurised with helium rather than nitrogen. Helium shows a much stronger influence of temperature on solubility, the solubility increasing rapidly with increasing temperature.

2. The main storage tank was pressurised with a lower pressure of nitrogen (0.08 MPa).

3. The pressure in the main storage tank was increased to 0.24 MPa.

For each of these cases a series of these experiments was conducted on the boiling of n-pentane at a pressure of 0.6 MPa, mass flux 300 kg/m^{2}s and heat flux of 40 kW/m^2 for 5 different inlet temperatures. The results are shown in Figures

4.14, 4.15 and 4.16. The first two tests show no significant difference, and also no significant difference to the standard conditions of 0.15 MPa. This lends credence to the idea that dissolved gas effects have been very small in the normal experiments. However, if the tank is pressurised to a much higher pressure (0.24 MPa) then significant effects begin to appear. Firstly, the measured fluid temperatures, in what is clearly a boiling situation, are less than the calculated saturation temperatures for the measured pressures (though this may also reflect uncertainities in pressure measurements as discussed above). Secondly, the wall temperatures are much lower, reflecting the formation of bubbles and increased heat transfer coefficients as a result of the dissolved gases.

We conclude, therefore, that the effect of dissolved gases can potentially be significant in tests like the present ones, but that we have established that this effect is not large over the standard range of conditions covered (namely pressurisation of the tank with nitrogen at a pressure of 0.15 MPa).

4.2.4 Sensible heating profiles

In the subcooled (non-boiling) region, the bulk fluid temperature can be calculated from a heat balance. It is very interesting to compare the values measured by the bulk fluid thermocouples with these calculated values and such comparisons are shown in Figure 4.17. Generally, the measured bulk fluid temperatures agree reasonably well with the values calculated from heat balances. At lower temperatures, the bulk fluid values are very slightly less than the calculated values and this would be consistent with the existence of a temperature gradient in the channel, with the wall temperature being higher than the temperature at the centre of the channel. Further up the channel, the bulk fluid temperature measurements are slightly higher than those calculated from the heat balance. This could be explained by the existence of condensing vapour bubbles in the subcooled boiling region which make contact with the bulk fluid thermocouples yielding a somewhat higher average measured temperature. However, these effects are very small and no attempt is made to correct for them in calculating

heat transfer coefficients.

4.2.5 Results of the main experiments and parametric trends

The main series of experiments was conducted with inlet temperatures as close as possible to saturation temperature; normally the subcooling was of the order of 5 – 15 °C. Where dryout occurred at low subcoolings, several of the tests were then conducted at higher subcoolings to cover the higher heat flux.

The ranges of conditions for this main series of tests were as follows:

1. Pressure: 0.23 – 1.0 MPa
2. Mass flux: 100 – 500 kg/m^{2}s
3. Heat flux: 10 – 70 kW/m^2

This gave rise to maximum exit qualities of the order of 60% (depending , of course, on the heat flux and mass flux). In a separate series of experiments, the effects of much greater subcooling were investigated and are discussed in Section 4.2.6. For the main series of experiments the following fluids were used:

1. n-pentane
2. iso-octane
3. Mixture 1: n-pentane/iso-octane mixture with a mole fraction 0.7 n-pentane
4. Mixture 2: n-pentane/iso-octane mixture with a mole fraction 0.35 n-pentane
5. Mixture 3: n-pentane/n-hexane/iso-octane mixture with respective mole fractions of 0.20/0.22/0.58

All of the results from this main series of experiments are shown in Figures 4.54 to 4.83. The layout of the figures is consistent with the operating condition shown

in Figure 4.53 and the definitions of quantities is given in Table 4.5. Essentially, the three series of graphs are:

1. The measured temperatures (these include the wall temperatures and the fluid temperatures) against the axial position in the tube [m].

2. The heat transfer coefficients plotted as a function of subcooling/quality. The data are plotted against subcooling (°C) for sub-cooled conditions and against quality (%) for the quality region. These coefficients are calculated as explained above on the basis of fluid temperature measurements.

3. The ratio (F) of the heat transfer coefficient to that for the liquid phase flowing alone in the channel is plotted as a function of $1/X_{tt}$. On these plots, the forced convective component of the Chen (1966) correlation is also shown as a reference line.

The main series of experiments comprised over 23000 measurements of heat transfer coefficient in the two-phase region and the complete data set has been stored on a CD-ROM. A key to this CD-ROM is given Appendix D. In what follows below, we will discuss the quantitative analysis of the results but at this stage it is worthwhile remarking on a number of the qualitative features as follows:

1. In the region where nucleate boiling is dominant the wall and bulk temperature profiles are either roughly parallel, diverging or converging as quality is increased. The first two cases are consistent with heat transfer dominated or affected by nucleate boiling and the second type of behaviour is characteristic of forced convective boiling where the heat transfer coefficients increase with increasing quality. The heat transfer coefficient results can, of course, reflect these trends. Thus, the results are reasonably consistent with previous observations.

2. In many cases, the wall temperature remains approximately constant in the region near the entrance, though the bulk temperature is rising, giving an

increase in heat transfer coefficient.

3. Many of the tests show a characteristic increase in wall temperature and a characteristic decrease in heat transfer coefficient towards the end of the channel, signifying the onset of dryout. This behaviour is discussed in more detail in Section 4.2.8 below.

4. In some of the tests, there was a very rapid increase in heat transfer coefficient with quality *just before the onset of dryout.* This type of behaviour has been observed previously in forced convective boiling experiments (see Beattie and Lawther, 1986)

5. Much of the data for pure components shows a characteristic peak in heat transfer coefficient at near-zero quality. This is a most interesting effect which is believed to be a genuine representation of the heat transfer behaviour and it will be discussed in more detail in Section 4.2.6 below.

6. In the case of the mixtures, the peaking at zero quality was not observed and, in a region in which the lack of nucleate boiling was evidenced by the lack of an influence of heat flux, conditions were often such that the heat transfer coefficient *decreased* with increasing quality. This is in contrast to the effects observed with pure components. The information with multicomponent systems will be discussed in more detail in Section 4.3 below.

4.2.6 Peak in heat transfer coefficient at near zero quality

One of the most interesting results from the present set of experiments is the existence, under certain conditions, of a sharp peak in heat transfer coefficient at near zero quality. This is shown clearly in the results for the main series of tests (usually carried out at inlet subcoolings of 15 – 20 °C) which are shown in Figures 4.56, 4.57 and 4.62, 4.63. These peaks occur for the single component fluids, and particularily for the pentane tests. Formation of such peaks is much less significant for the case of multicomponent boiling. This is such an interesting

result that a number of separate investigations (outside the main series of tests) were carried out to explore it further. Specifically, the effects of pressure and of inlet subcooling were investigated more systematically.

Figures 4.18 and 4.19 show the effect of pressure for one of the conditions where inlet peaks were demonstrated (namely for the boiling of n-pentane at a mass flux of around 370 kg/m^{2}s, heat flux of around 50 kW/m^2 and with inlet subcoolings of around 14 °C (Figure 4.18) and around 35 °C (Figure 4.19)). As will be seen, the effects occur over a wide range of pressure (0.23 – 0.87 MPa) with the heat transfer coefficient in the peak zone being relatively unaffected by pressure. There is a systematic effect of pressure at higher qualities which is in line with expectations for forced convective boiling.

In the second series of experiments, the effect of heat flux at two different subcoolings was investigated at a fixed pressure of 0.3 MPa and a mass flux of 500 kg/m^{2}s as shown in Figure 4.20. At a subcooling of 12 °C, the peak amplifies with increasing heat flux. For a subcooling of 22 °C, there is less of a peak (though it is still discernable). In both cases, the heat transfer coefficient becomes independent of heat flux at higher qualities, indicating a convective boiling dominance in this region.

Finally, the effect of subcooling was investigated for fixed heat flux, pressure and mass flux. The results from these tests are exemplified by those shown in Figures 4.21 and 4.22. For the results shown in Figure 4.21, inlet subcooling was varied from 40 to 10 °C for a mass flux of 500 kg/m^{2}s and a heat flux of 40 kW/m^2, at a pressure of 1.0 MPa. As will be seen, the inlet peaking begins to disappear as the subcooling is increased. This trend is also shown in Figure 4.22 (mass flux 500 kg/m^{2}s, heat flux 40 kW/m^2, pressure 0.24 MPa).

In the light of these results, it is suggested that the inlet peaking effect may be due to the effect of thermal boundary development at the entrance of the tube. If the inlet subcooling is low, then nucleate boiling begins *in the presence of a thin developing boundary layer*. This would imply rapid condensation of the bubbles penetrating this thin thermal boundary layer and, it is suggested, this produces

Addition to Section 4.2.6: Peak in heat transfer coefficient at near zero quality

It is noteworthy in some boiling experiments, for example in the main series of experiments, (Figure 4.60 top left hand graph) that the wall temperatures from the entrance to the test section up to about 2.5 m are below the pure component saturation temperature. The corresponding heat transfer profiles, see Figure 4.62, clearly show that in this entrance region bubble nucleation is occurring. The dissolved gas is reducing the actual saturation temperature due to the high partial pressure of the gas, so that bubble formation can be sustained at negative wall superheats.

a feedback effect which enhances the heat transfer coefficient. In some ways, the situation is analogous to the microbubble boiling phenomenon observed by Aziz et al. (1986) in the cooling of spheres falling in a liquid. Highly intense heat transfer was observed due to rapid bubble formation and condensation. Though the range of subcoolings is similar to that used by Aziz et al. (1986), the wall temperatures were very high in their case, so the situations are not strictly comparable. However, the enhancement mechanism may be analogous.

High heat transfer coefficients in the entrance region have also been observed by Radermacher et al. (1983), Jung et al. (1989a,b) and Reid et al. (1987); this work is reviewed in Section 2.1.4. Their results also are consistent with the idea of special boiling phenomena within a developing thermal boundary layer. In fact, this concept could provide a unification of many experimental observations and it is believed that the current data (covering systematically a wide range of conditions) could serve as a basis for the development of improved models.

An interesting aspect of the results obtained in the current work is that the inlet peaking effect was less severe in the case of multicomponent mixtures. This may reflect the fact that condensation of such mixtures is also restricted by mass transfer effects. This may suppress the micro-bubble type boiling seen with pure components. Again, this seems a productive area for further research.

4.2.7 Comparison of single component data with existing empirical and semi-empirical predictive methods

The classical picture of forced convective boiling is one in which, at high mass fluxes and qualities, the heat transfer coefficient is governed by convection and is relatively insensitive to heat flux. At low mass fluxes and qualities, on the other hand, nucleate boiling plays an important, and often dominant role in the heat transfer. The problem in correlating or predicting forced convective boiling heat transfer, therefore, is that of establishing the relative roles of the nucleate boiling and forced convective processes. If one looks at the data from the main series of

experiments (Figures 4.56 and 4.57) we see that the data for n-pentane show two distinct regions as expected, namely a region in which the heat flux influence is small and a region (at lower qualities) where it is significant. This distinction is clearest for the n-pentane results; for the iso-octane data (Figures 4.62 and 4.63), the heat flux effect is present over most of the range. This difference between the two fluids arises because of the greater propensity to nucleate boiling for iso-octane due to its higher reduced pressure.

In what follows, we shall first consider relationships for pure forced convective boiling and then go on to consider correlations which attempt to predict the combined effect of forced convection and nucleate boiling. The correlations used were reviewed in detail in Chapter 2 and will not be restated here.

Forced convective boiling relationships. The data have been compared with a variety of forced convective boiling relationships. These are of two types:

1. Plots of F_l, the ratio between the heat transfer coefficient α and the coefficient α_l for the liquid phase flowing alone in the channel against $1/X_{tt}$ (where X_{tt} is the Martinelli parameter, see equation 2.2). Correlations of this type are those of Chen (1966), Jung (1989c) and Kenning and Cooper (1989). A correlation of somewhat similar form, but not involving X_{tt}, has been proposed by Wadekar (1990) who correlates F with quality x_g, reduced pressure p_r and molecular weight $\tilde{M}$ as follows:

$$F = 3.2 \left(\frac{x_g}{x_g - 1} \right)^{0.75} p_r^{-3/8} \tilde{M}^{1/8} \tag{4.19}$$

   For a given pressure and physical properties, this can also be expressed in terms of a relationsship between F and $1/X_{tt}$.

2. Other correlations use F_{lo}, the ratio of the measured heat transfer coefficient α to the heat transfer coefficient α_{lo}, where α_{lo} is the single phase heat transfer coefficient for a fluid flowing at the total mass flux and with the properties of the liquid phase. Correlations of this type are those of Steiner and Taborek (1992) and Fujita (1995).

Typical comparisons between the data and the first type of correlation are given in Figure 4.23 (left) for n-pentane at a pressure of 0.23 MPa and a mass flux of 300 kg/m^{2}s and in Figure 4.23 (right) the second class of correlations are given. As will be seen, all the correlations deviate strongly at low qualities (low values of $1/X_{tt}$), where nucleate boiling is expected to be significant, particularily in the case of iso-octane. For the F_l correlations, the Chen and Kenning and Cooper correlations tend to underpredict the data in the forced convective region, whereas that of Wadekar overpredicts it. The correlation of Jung seems to give the best fit.

Correlations of the F_{lo} type tend to somewhat overpredict the data; it is noteworthy that the correlations of Steiner and Taborek and Fujita give similar results.

Combined forced convective and nucleate boiling correlations. As was explained in Chapter 2, combined nucleate boiling/forced convection correlations are of three main types, namely superposition models, asymptotic models and enhancement models. Here, we choose the classical Chen (1966) correlation as representative of the first type, the correlation of Steiner and Taborek (1992) as representative of the second and the correlations of Shah (1982) and Kandlikar (1990b) as representative of the third class. Typical comparisons with results for n-pentane are shown in Figures 4.24 to 4.27 and for iso-octane in Figures 4.28 to 4.31. Four sets of data have been chosen to represent the range of pressure and mass flux covered in the experiments. For each set of comparisons, three heat fluxes were chosen. It should be stated that these comparisons typify the enormous range of comparisons possible with the present data bank. In comparing correlations with the present data, it should be born in mind that previous data has been much more limited and many of the correlations are based empirically on this previously limited data set.

The Chen and Kandlikar correlations have the feature that they can predict a *decreasing* heat transfer coefficient with increasing quality in the region affected by nucleate boiling. The Kandlikar correlation appears to perform best in this

respect. The Steiner and Taborek, and Shah correlations are not capable of predicting this decrease in heat transfer coefficient with increasing quality and, not surprisingly, fit the present data much less well. There are regions where the data trends are completely opposite to those predicted by the correlations. Overall, we conclude that the correlation of Kandlikar gives the best fit to our data, though examination of Figures 4.24 to 4.31 shows that considerable deviations exist, particularily at high pressure which is well outside the range covered by the correlations.

Conventionally, it is the practice to state standard deviations and average errors and Table 4.3 continues this practice for the selected correlations. Clearly, the errors are very large, with the Kandlikar correlation performing best with respect to predicting the parametric trends. The definition of average error, mean error and standard deviation can be found in the Appendix C. For this statistical analysis all the data points with equilibrium qualities greater than zero have been used, including all the runs taken during the present work. Although tables of the

	n-pentane (13850 points)			iso-octane (4950 points)		
Correlation:	Average error	Mean error	Standard deviation	Average error	Mean error	Standard deviation
Chen (1966)	-0.042	0.198	0.283	0.000	0.189	0.252
Shah (1982)	0.146	0.252	0.207	0.237	0.282	0.166
Steiner and Tab. (1992)	0.255	0.312	0.238	0.230	0.280	0.228
Kandlikar (1990b)	0.133	0.232	0.261	0.214	0.255	0.218

Table 4.3: Statistical performance of pure component forced convective boiling correlations

above type are often found in the literature, a note of caution must be sounded. If the predicted heat transfer coefficients are plotted against the experimental values (as shown in Figures 4.32 for n-pentane and 4.33 for iso-octane data) for the four correlations tested, one can see features which are not immediately apparent from

mere statistical analysis. There are significant numbers of data points which are grossly underpredicted and a significant number which are overpredicted. The former represent the data for pre-dryout heat transfer enhancement (mentioned above) and the second class of data are where dryout has begun to reduce the heat transfer coefficient.

It would have been possible to reoptimise the existing correlations in terms of the present data or to develop an alternative form of empirical formulation. However, it was decided that this was not a profitable approach; merely adding to the existing correlations is not particularly productive. What is needed is a more analytical and predictive approach, possibly, on the lines of that reported by Sun and Hewitt (1996), but this was beyond the scope of this present mainly experimental project.

Hysteresis effects

Hysteresis is a commonly observed phenomenon in both pool boiling and forced convective boiling and it was important to evaluate whether it was significant in the present work. Hysteresis manifests itself as a difference in the value of the heat transfer coefficient depending on the direction of change of an input variable (subcooling, heat flux etc.). In the present test, hysteresis effects were not large and this was demonstrated by two investigations as follows:

1. Heat flux effects. Figure 4.34 shows a set of experiments at a pressure of 0.6 MPa and with a mass flux of 400 kg/m^{2}s in which the heat flux was increased from 50 to 70 kW/m^2 and reduced back again to 50 kW/m^2. No significant change in the heat transfer coefficients at the lower level of heat flux was observed before and after the elevation of the heat flux.

2. Effect of inlet subcooling. As has been shown, inlet subcooling can be a very important parameter and hysteresis effects associated with this paramter might be significant. Figures 4.35 and 4.36 show data for n-pentane boiling at a nominal pressure of 0.6 MPa, a mass flux of 300 kg/m^{2}s and a heat

flux of 40 kW/m^2 in which the inlet temperature was varied. For the results shown in Figure 4.35 successive tests were performed with the inlet temperature increasing successively from 11.0 °C to 94.8 °C in 5 steps. The peaking in heat transfer coefficient was observed as reported above. The inlet temperature was then reduced to 12.3 °C also in 5 steps and the heat transfer measurements repeated. These results are shown in Figure 4.36. As will be seen, there is no significant difference between the results as a function of the direction in which the inlet temperature is increased.

It is concluded, therefore, that hysteresis effects were minimal in the present experiments provided dryout did not occur. However, once dryout has been encountered, there may be a hysteresis effect in heat transfer coefficient. Once the wall temperature rose due to dryout effects, a reduction in heat flux or inlet temperature does not reduce the wall temperature to its original levels. The wall temperatures in the region affected by dryout are lower with the consequence that the heat transfer coefficients are much higher. The heat flux has to be reduced to zero for some time in order to reset this hysteresis effect.

4.2.8 Dryout

In the description of the results given above, the deterioration of the heat transfer coefficient at the dryout point was mentioned. Often, this point of deterioration is preceded by a region of enhancement of heat transfer. The prediction of dryout has been a matter of considerable interest in the nuclear industry and has been the subject of extensive work. Experimental studies have established that dryout occurs because of the gradual decrease to zero of the liquid film flow rate. When the film flowrate is zero, then there is an excursion in the wall temperature (with a corresponding decrease in heat transfer coefficient) as discussed above. Earlier models for the prediction of dryout are summarised by Hewitt (1982). Within the annular flow region, the change of film flowrate $\dot{M}_{LF}$ along the channel can

be expressed at the steady state by the following equation:

$$\frac{d\dot{M}_{LF}}{dz} = \pi D \left[D_d - E - \frac{\dot{q}}{h_{LV}} \right] \tag{4.20}$$

where D is the tube diameter, D_d and E are the rates of deposition and entrainment of droplets per units peripheral area and $\dot{q}/h_{LV}$ is the rate of evaporation per unit peripheral area. Thus, film flow rate increases along the channel as a result of droplet deposition and decreases as a result of entrainment and evaporation. Equation 4.20 is integrated along the channel and the point of dryout is established as the point at which $\dot{M}_{LF}$ reaches zero. The initial condition for the integration is taken at the point of onset of annular flow, where the value of $\dot{M}_{LF}$ is prescribed.

The earlier relationships for D_d and E used in modelling of dryout (Hewitt, 1982) had a number of inconsistencies and difficulties. Improved relationships were developed by Govan (1990) (see also Govan and Hewitt, 1990). These later relationships were used in the present analogies. The deposition is given by:

$$D_d = k\,C \tag{4.21}$$

where C is the concentration of droplets in the core of the annular flow given by Govan (1990) as:

$$C = \frac{\dot{M}_{LE}}{\dot{M}_V/\rho_V + \dot{M}_{LE}/\rho_L} \tag{4.22}$$

where $\dot{M}_V$ is the vapour flowrate (kg/s).

k is the droplet mass transfer coefficient which was correlated by Govan as follows:

$$\begin{aligned} k &= 0.18 \left(\frac{\sigma}{\rho_V D}\right)^{0.5} && for\ C/\rho_V \leq 0.3 \\ k &= 0.083 \left(\frac{1}{C}\right)^{0.65} \left(\frac{\sigma}{\rho_V D}\right)^{0.5} && for\ C/\rho_V > 0.3 \end{aligned} \tag{4.23}$$

where σ is the surface tension.

Entrainment in annular flow does not occur at very low liquid flow rates. The critical liquid film mass flux for the onset of entrainment is given by Owen and Hewitt (1986):

$$\frac{\dot{m}_{LFC}\,D}{\eta_L} = exp\left(5.8504 + 0.4249\,\frac{\eta_V}{\eta_L}\sqrt{\frac{\rho_L}{\rho_V}}\right) \tag{4.24}$$

where critical film mass flux ($\dot{m}_{LFC}$) is defined as the critical film flow rate ($\dot{M}_{LFC}$) divided by the cross sectional area ($\pi D^2/4$). Govan (1990) correlated the entrainment rate as follows:

$$\begin{aligned} E &= 0 && for\ \dot{M}_{LF} < \dot{M}_{LFC} \\ \frac{E}{\dot{M}_V} &= 5.75 \cdot 10^{-4} \left[(\dot{M}_{LF} - \dot{M}_{LFC})^2 \frac{D \rho_L}{\sigma \rho_V^2} \right]^{0.316} && for\ \dot{M}_{LF} \geq \dot{M}_{LFC} \end{aligned} \tag{4.25}$$

The above equations had been programmed into a user-friendly code by Hawkes (1996) and this code, known as GRAMP (General Runge-Kutta Annular Modelling Program), was used to calculate dryout heat fluxes for the present data.

Examples of the present data for dryout, coupled with the calculations from the GRAMP code, are shown in Figures 4.37 and 4.38, the examples being for pentane and iso-octane respectively. The top left hand corner of the graph shows the calculated heat transfer coefficients as a function of quality and the top right hand corner shows the wall and bulk temperatures as a function of length. As will be seen, the wall temperature rises sharply at the dryout point. In Figure 4.37, there is a pre-dryout heat transfer enhancement showing a rise in heat transfer coefficient immediately before dryout though this is not always observed as is shown in the other example given in Figure 4.38. The left hand bottom graph shows the predicted mass fluxes for the liquid film, vapour and entrained droplets and also the predicted film thickness. The bottom right set of curves shows the same information plotted as a function of tube length.

A total of 50 points were obtained for dryout (31 for n-pentane and 19 for iso-octane). Figure 4.39 shows a comparison of the data with the predictions of the GRAMP code. Though the results were in qualitative agreement, the code generally overpredicted the dryout quality.

The data can be plotted in the form of dryout quality as a function of boiling length (see Hewitt, 1982) where boiling length is the distance between the point where $x_g = 0$ and the point at which dryout occurrs. Plots of this kind are shown in Figure 4.40 for pentane and iso-octane and show the expected trend with the dryout quality decreasing with increasing mass flux at a fixed length.

The annular flow model embodied in GRAMP has been shown to predict

dryout moderately well for water and for refrigerants, though this is the first time that the code has been compared systematically with data for organic fluids. It is not yet established whether the entrainment and deposition relationships given in Equations 4.21 to 4.25 can be applied universally. There may also be some direct effect of heat flux on the entrainment rate; this has been investigated by Milashenko et al. (1989).

A factor which might have contributed to the underprediction is the fact that the default value for entrained droplet flow at the onset of annular flow in the GRAMP code was used in the calculations. This is that the entrained flow rate was zero at the onset of annular flow (see Figures 4.37 and 4.38) and that all of the liquid phase was present in the liquid film. This is almost certainly not true and an alternative assumption might be to assume that, at this point, deposition and entrainment are in equilibrium (with $D_d = E$ at this point). A small computer code was written to calculate the entrainment at the onset of annular flow on this basis and the values were introduced into the GRAMP code as entrained fractions at the onset of annular flow, which gave an alternative starting point to the integration. Results comparing the effect of initial entrainment (zero or equilibrium) are exemplified by those shown in Figure 4.41. Although there are clear differences in the predicted entrained flow rates (and also in the predicted liquid film thickness) near to the onset of annular flow, there is a self-compensating effect between entrainment and deposition which leads almost to the same results being obtained at higher qualities. Thus, the prediction of the dryout condition is relatively insensitive to the initial entrained fraction. It could be argued that this must be so, bearing in mind the reasonable success obtained with the models. There are considerable uncertainities about the extent of entrainment at the onset of annular flow and had these uncertainities been reflected in the predicitons of the model, then the model would have been less successful.

We can conclude that the predictions of dryout are in reasonable qualititative agreement with the experiments, though factors influencing the underprediction need to be addressed in future work.

4.3 Forced convective boiling results for mixtures

Experiments were carried out with the following mixtures:

1. A binary mixture of n-pentane/iso-octane with a mole fraction of n-pentane of 0.7 (Mixture 1).

2. A binary mixture of n-pentane/iso-octane with a mole fraction of n-pentane of 0.35 (Mixture 2).

3. A ternary mixture of n-pentane, n-hexane and iso-octane having mole fractions of 0.20, 0.22 and 0.58 respectively of the three components (Mixture 3).

The first two mixtures were chosen to have approximately the same boiling range, the difference between dew and bubble points. The results are presented in the same format as these for the single components. Thus:

Figures 4.66 and 4.67, 4.72 and 4.73 and 4.78 and 4.79 present the profiles of measured bulk and wall temperatures for Mixtures 1, 2, and 3 respectively.

Figures 4.68 and 4.69, 4.74 and 4.75 and 4.80 and 4.81 present the heat transfer coefficients as functions of local conditions (subcooling for $x_g < 0$) for Mixtures 1, 2, and 3 respectively. These coefficients have been calculated in each case from the ratio of the heat flux to the *measured* difference between the wall and bulk thermocouples.

Figures 4.70 and 4.71, 4.76 and 4.77, and 4.82 and 4.83 show the ratio F of the heat transfer coefficient of that for the liquid phase flowing alone in the channel as a function of $1/X_{tt}$ for Mixtures 1, 2 and 3 respectively. In all of these graphs, the value of F calculated from the Chen (1966) correlation (Equation 2.4) is shown for comparison.

All of the data contained within these graphs has been stored on a CD-ROM which is held by HTFS (AEA Technology plc.).

A detailed analysis of the physics of mixture boiling was beyond the feasible scope of the present work (though it is clearly an important subject for development in the future). Here, we will discuss the parametric trends and explore some physical explanations for these trends (Section 4.3.1) and then go on to present comparisons of the data with some of the principal correlations (Section 4.3.2).

4.3.1 Observations and parametric trends for mixtures

The present experimental results allow direct comparison of the heat transfer characteristics for pure components and mixtures. From the graphs shown in Figures 4.66 to 4.83 (temperature profiles, heat transfer coefficients and plots of $1/X_{tt}$ against F enhancement factor) the following observations can be made:

1. For the mixtures, the heat transfer coefficients depend much less on heat flux than those for the pure components. This trend is as expected because nucleate boiling is degraded by mixture effects. At low pressures and mass fluxes, the heat transfer coefficient at a given quality is virtually independent of heat flux. This may indicate that the degradation of the nucleate boiling heat transfer increases with increasing heat flux which would be consistent with the findings of Palen and Yang (1983) (see Section 2.3.3) who include the effect of heat flux on the mixture correction factor. However, the present data for higher pressures and for low to moderate mass fluxes do show an increase in heat transfer coefficient with heat flux though this is less than that observed with the pure components.

2. For qualities up to 15 to 20% the (convective) heat transfer coefficients are comparable with those of the pure components. This suggests that convective heat transfer is not reduced noticeably by mixture effects (see Figures of F vs. $1/X_{tt}$). For higher qualities the heat transfer coefficient begin to fall below the line of the Chen (1966) correlation, which seems to

indicate a reduction in convective heat transfer.

3. At low pressures and high mass fluxes, and in contrast to the results for pure components, the heat transfer coefficient reaches a maximum and then stays either fairly constant or even reduces with increasing quality. This seems to indicate that convective heat transfer is also suppressed with mixtures.

4. The characteristic peaks in heat transfer coefficient at around zero quality, observed in the case of single component boiling and discussed in Section 4.2.6, were not seen in the case of mixture boiling.

In what follows, the observed mixture effects in the low quality and high quality (annular flow) regions respectively are discussed.

Mixture effects at low quality

In Section 4.2.6, results demonstrating a peak in heat transfer coefficient for the single component fluids at near-zero qualities were presented. The coefficients in this region were strongly dependent on inlet subcooling and it was hypothesised that the effects observed may have been associated with thermal boundary layer growth with rapid condensation of the bubbles occurring for thin boundary layers. It was further hypothesised in Section 4.2.6 that this phenomenon may be analogous to the micro-bubble boiling phenomenon observed in the quenching of hot spheres.

In the case of mixture boiling, the peak in heat transfer coefficient at around zero quality was not observed. This is apparent from the main series of results which are shown in Figures 4.66 to 4.83. However, a clearer indication is given in the results shown in Figure 4.42 which shows, at the top, the temperature measurements and, at the bottom, the heat transfer coefficients, for a series of tests carried out at constant mass flux, heat flux and pressure but with varying inlet subcooling. The heat transfer coefficient is seen to vary principally with local conditions without the effect of inlet subcooling observed with the single component boiling cases.

The dramatic change of behaviour observed with mixtures may actually be consistent with the hypothesis of micro-bubble boiling with single component systems. This mechanism depends on rapid bubble growth and collapse, both of which processes would be inhibited by the interfacial concentration of the heavier phase which occurs in the evaporation of mixtures.

Annular flow region

As was mentioned above, the present results show that at higher qualities heat transfer coefficients for mixtures tend to fall with increasing quality. This decrease does not seem to have the character of that associated with dryout, the latter being much sharper.

Two possible explanations for the effects observed were pursued as part of the present work, namely the effect of mass transfer at the liquid film interface of the annulus and the effect of liquid entrainment.

Mass transfer resistances within the liquid film and the adjacent vapour core are an obvious possible source of the discrepancies observed. Modelling of such mass transfer in multicomponent annular flow systems is reviewed by Carey (1992), and Collier and Thome (1994). Shock (1976) analysed the film and vapour phase resistances in typical binary mixture evaporation systems by applying a turbulence model to both regions. For the binary mixture systems studied, the mass transfer resistance in the liquid film was calculated to be negligible and the mass transfer resistance was, therefore, concentrated in the vapour phase immediately adjacent to the interface. However, according to Shock's calculations, the mass transfer resistance in the vapour was found to be quite small under conditions of annular flow where the core is highly turbulent. It seems unlikely, therefore, that interfacial mass transfer effects could account for the gross reduction in heat transfer coefficient observed in the present experiments.

In annular flow, a significant fraction of the liquid phase can be entrained as droplets in the gas core. Calculations of the entrained flow rate were made in the present work using the GRAMP code in the context of dryout calculations

and are described in Section 4.2.8. The entrained fraction is always significant and, of course, approaches unity (i.e. zero film fraction) as the dryout point is approached. The evaporation takes place from the liquid film only and there is clearly an opportunity for the film to become enriched in the heavier phase as the film proceeds up the channel. The droplets may, therefore, be richer locally in the lighter phase than is the liquid film. This would lead to the film interface having a higher temperature than the value which would be calculated from equilibrium data if the liquid phase is assumed to be well mixed and to have a uniform concentration. This would, therefore, be an explanation for the apparent decrease in heat transfer coefficient as quality increases.

To address the problem of differential concentrations of the heavier phase in the liquid film, it might prove feasible to modify the GRAMP code to include mass balance equations for the individual components in the liquid phase. The concentration effect on the liquid film would be offset to some extent by the processes of droplet entrainment and deposition which will tend to mix the liquid phase. However, these mixing processes could be fairly slow as was shown by the experimental work of Cousins and Hewitt (1968). The development of a complex mixing model was beyond the scope of the present work, though it would obviously be an area for further development. Rather, a simplistic approach was adopted as follows:

1. A fixed entrained fraction was assumed at the onset of annular flow and it was assumed that entrained droplets have no further contact with the liquid film.

2. It was assumed that there was no further droplet entrainment and that the liquid film was depleted by evaporation only, this evaporation process giving rise to the concentration of the heavier phase in the film. The mean film concentration could thus be calculated and (to a first approximation at least) the interface temperature could be estimated from equilibrium data if it is assumed that the bulk turbulent region of the film is well mixed

(consistent with the calculations of Shock, 1976). This is also consistent with the concept that most of the temperature drop is concentrated in the laminar region near the wall. The difference between this interface temperature and the measured wall temperature represents the *real* driving force for heat transfer through the film and can be significantly greater than that calculated assuming a fully mixed liquid phase.

3. New values of heat transfer coefficient were calculated using the *real* driving force derived in (2) and were compared with those calculated using the conventional calculations assuming a uniform liquid composition.

Typical results from calculations carried out using the above methodology are shown in Figures 4.43 to 4.46. The left hand sides of these figures show the measured and calculated temperatures and the right hand sides the respective heat transfer coefficients. The calculations of *real* bulk temperatures (i.e. at the interface temperature) were carried out for initial entrained fractions (at the onset of annular flow) of 0, 0.1, 0.2, 0.4 and 0.6. The measurements of bulk temperature agree with the line calculated for zero initial entrainment which corresponds to the liquid phase being well mixed and at local equilibrium with the vapour phase. This is not surprising since the bulk thermocouples would be wetted by the drops and would therefore record a temperature more characteristic of the drops than of the liquid film which, on the hypothesis being investigated here, would have a higher temperature since it contains more of the heavier phase than do the droplets.

The interface (bulk) temperatures calculated for the liquid film show a characteristic increase with increasing assumed initial entrained fraction. This is because, as the initial amount of liquid in the film decreases, the heavier phase is concentrated increasingly rapidly along the channel. Thus, the difference between the wall and interface temperature decreases with increasing initial entrained fraction.

The heat transfer coefficients calculated from the differences between the wall

and film interface temperatures show the characteristic fall with increasing length (quality) when the initial entrained fraction is assumed to be zero. However, as the assumed entrained fraction increases, then the coefficients begin to increase with quality in a manner which is consistent with normal behaviour in forced convection. There does seem, therefore, to be a *prima facie* case for the occurrence of the suggested film concentration mechanism. This effect should be investigated much more thoroughly, possibly using an extension of the GRAMP code as mentioned above.

4.3.2 Comparison of correlations with mixture data

The various correlations available for mixture boiling data are discussed in Section 2.4.2. The correlations of Kandlikar (1991), Palen (1983) and Murata (1993) were selected for comparison with the present data. Typical comparisons (covering a range of pressures, mass fluxes and heat fluxes) are shown in Figures 4.47, 4.48 and 4.49. The following observations can be made:

1. The performance of the correlations deteriorate as the pressure increases, possibly reflecting the fact that the correlations were based largely on low pressure data.

2. The correlations do not adequately reflect the trends in the data, and in particular the deterioration of the heat transfer coefficient mentioned above.

The present data set significantly extends the amount of information available on multicomponent boiling and it could be worthwile attempting to derive new correlations which would subsume this new data. This was not attempted in the present work and is a possible avenue for future development. However, perhaps the more phenomenological approach suggested in Section 4.3.1 would provide a more fruitful attack towards the prediction problem.

Figures 4.50, 4.51 and 4.52 show the predicted versus the experimental heat transfer coefficients for the Palen (1983), Kandlikar (1991) and Murata (1993) correlations respectively. These figures show on the left hand side the data for

Mixture 1 and on the right hand side that for Mixture 2. These plots include dryout points as well, so some data points are grossly overpredicted. The predicted heat transfer coefficients are generally greater than the experimental with the discrepancy increasing for higher values of the experimental heat transfer coefficient. This is not so pronounced with the Palen (1983) method and this is therefore recommended as being the most suitable. Table 4.4 gives the average and mean errors and standard deviations for the two binary mixtures.

	mixture 1 (6830 points)			mixture 2 (2950 points)		
Correlation:	Average error	Mean error	Standard deviation	Average error	Mean error	Standard deviation
Palen (1983)	0.252	0.255	0.151	0.301	0.305	0.154
Kandlikar (1991)	0.295	0.324	0.208	0.330	0.354	0.216
Murata (1993)	0.318	0.356	0.249	0.318	0.362	0.252

Table 4.4: Statistical performance of mixture forced convective boiling correlations

Temperature profiles against length:	
x-axis	Axial position along test section in metres.
y-axis	Wall and measured bulk temperatures in °C.
Heat transfer coefficients against equilibrium quality:	
x-axis	Negative values give the subcooling in °C, positive values the equilibrium quality in %.
y-axis	Heat transfer coefficient calculated from the measured bulk and wall temperature and the heat flux.
F enhancement factor against $1/X_{tt}$:	
x-axis	Reciprocal Martinelli parameter.
y-axis	The ratio of the experimental heat transfer coefficient to the predicted liquid fraction heat transfer coefficient (Dittus-Boelter correlation). The green line shows the Chen F enhancement factor.
Legend in graphs give operating conditions:*	
KPEN$$$	denotes the run number.
Pr	inlet pressure in 10^5 Pa.
MFlux	mass flux in kg/m^{2}s.
HFlux	heat flux in kW/m^2.
* This type of legend to identify the experimental run is also used in other graphs unless otherwise stated.	

Table 4.5: The description of the displayed items in the graphs of the main series, Figures 4.54 to 4.83

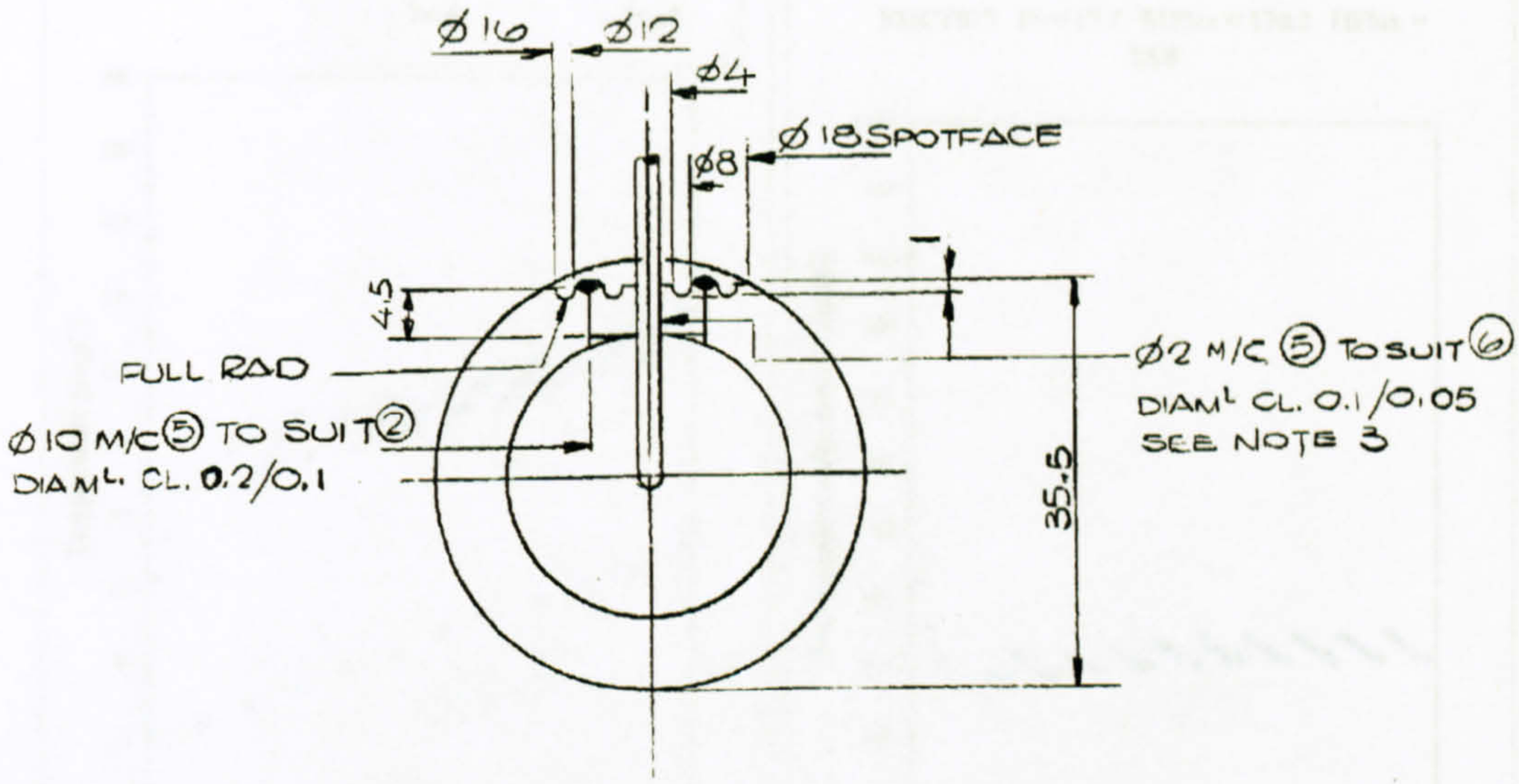


Figure 4.1: Detailed drawing of the bulk thermocouple pocket.

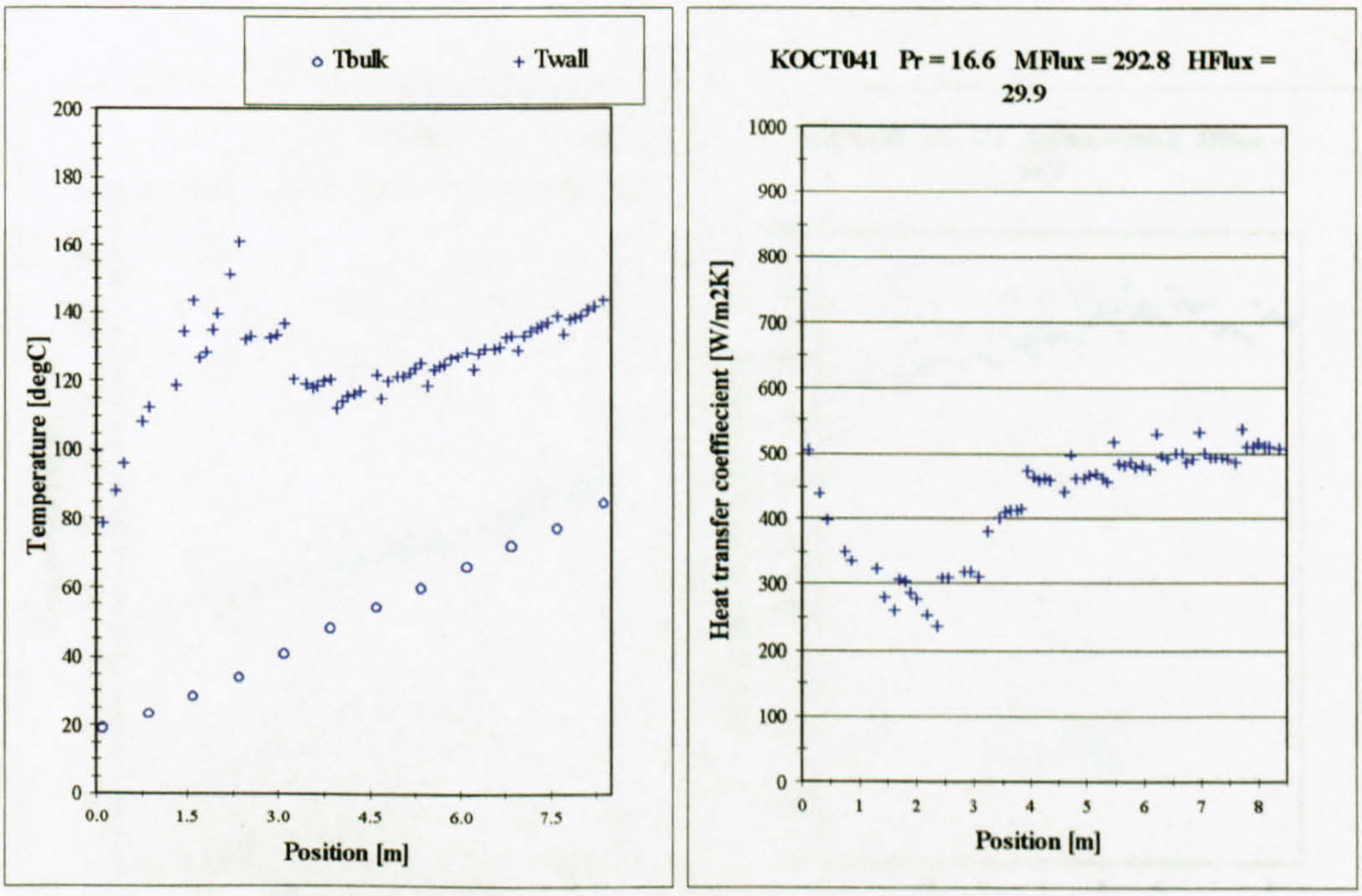


Figure 4.2: Single phase run at a pressure of 1.66 MPa, mass flux of 292.8 kg/m^{2}s and a heat flux of 29.9 kW/m^2 showing a wall temperature peak.

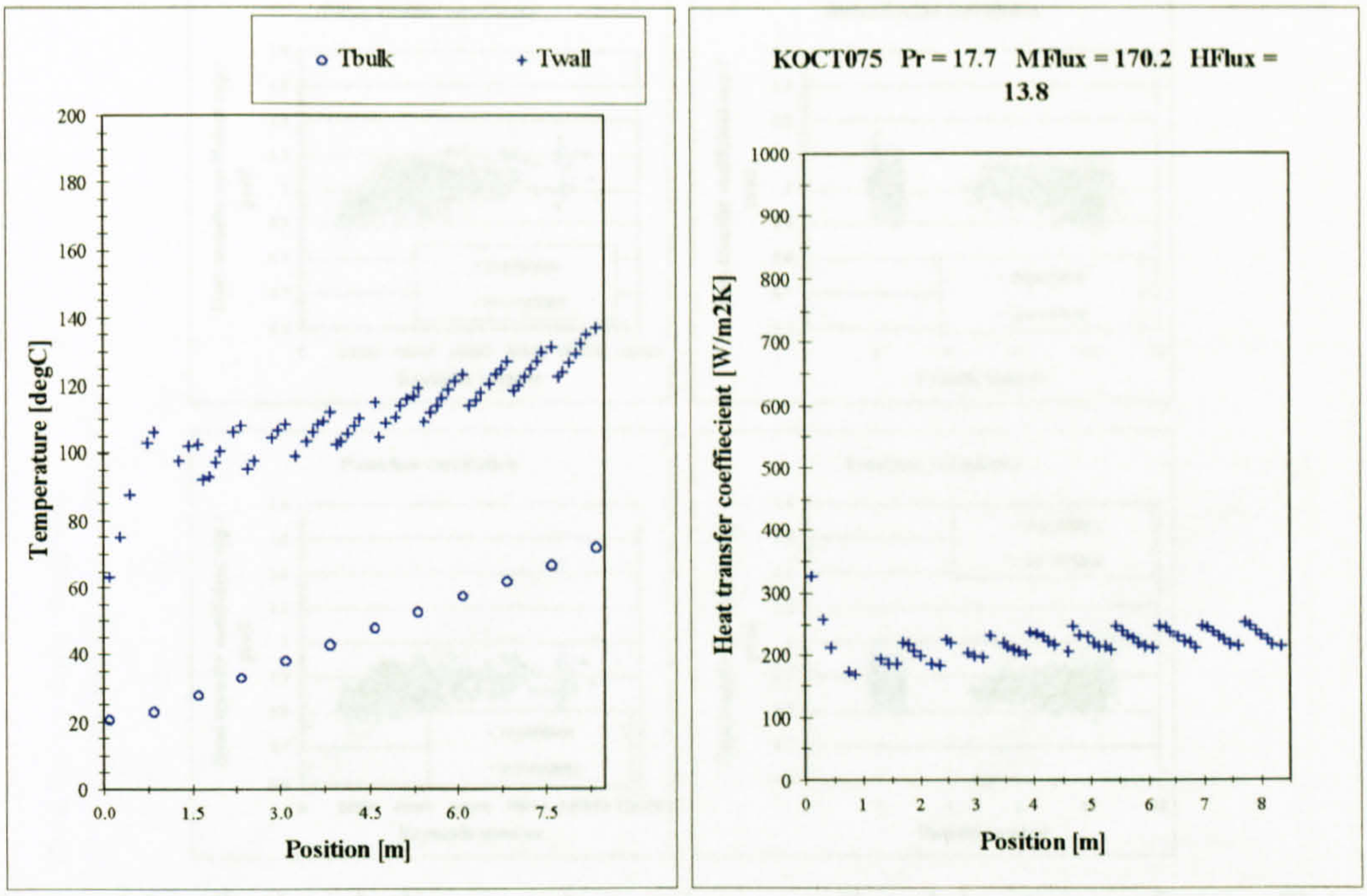


Figure 4.3: Single phase run at a pressure of 1.77 MPa, mass flux of 170.2 kg/m^{2}s and a heat flux of 13.8 kW/m^2 showing the effect of wall thermocouple pockets.

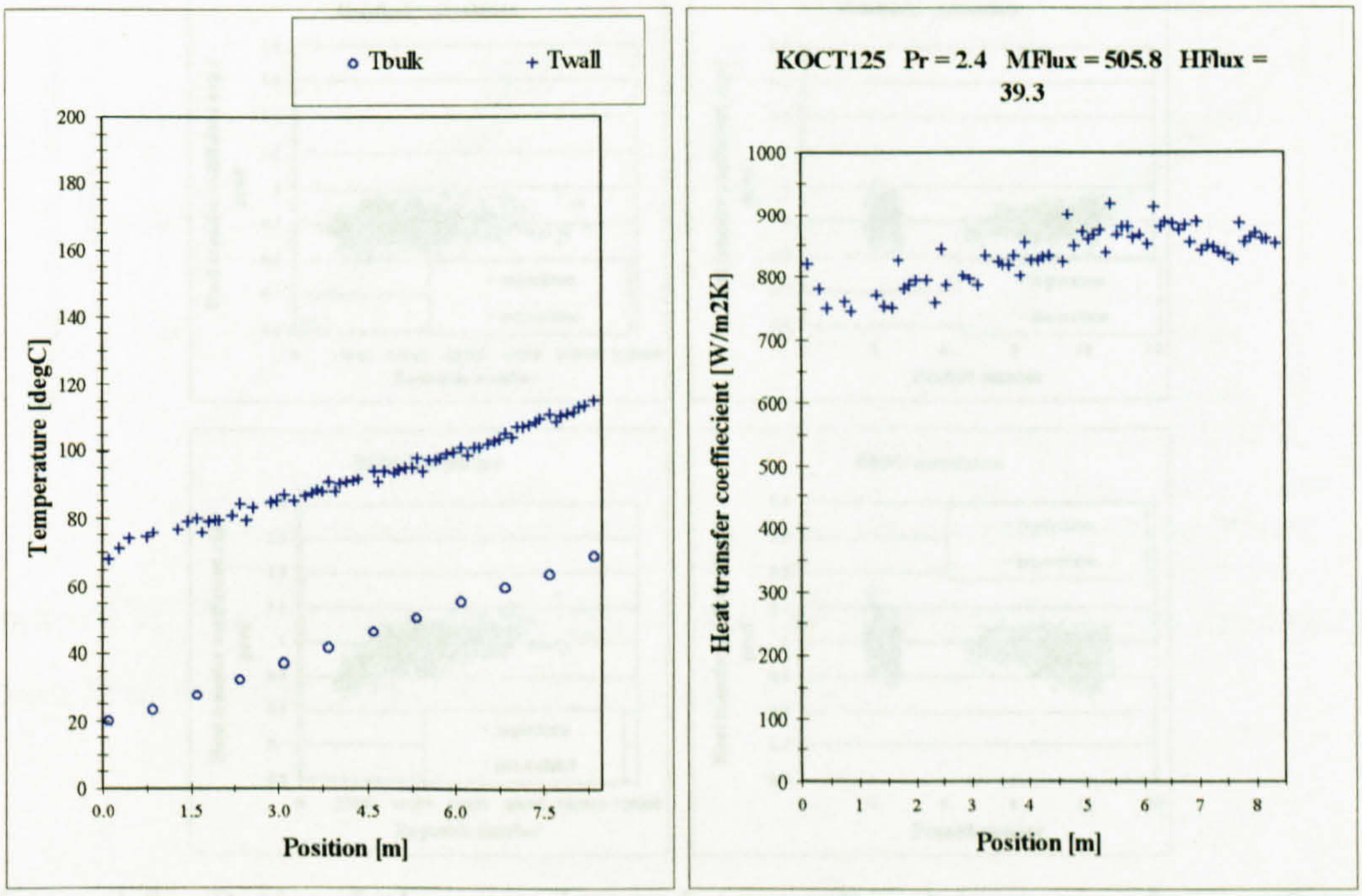
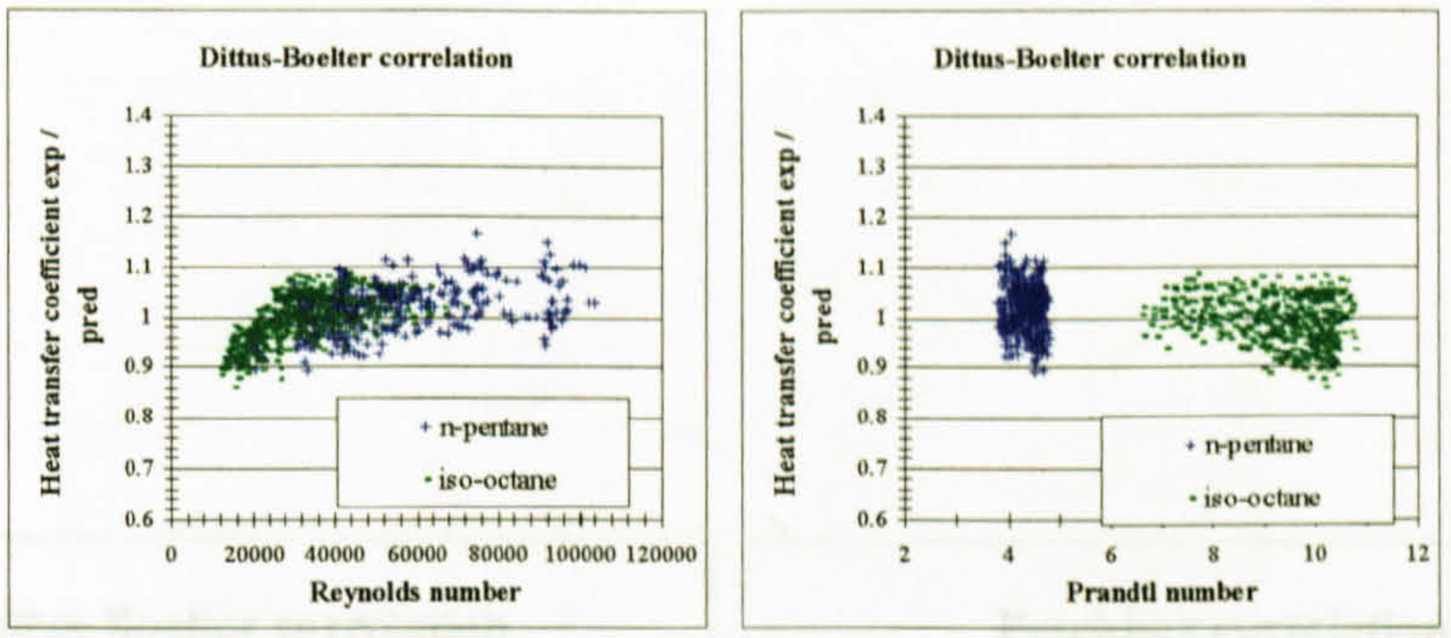


Figure 4.4: Fully turbulent single phase run at a pressure of 0.24 MPa, mass flux of 505.8 kg/m^{2}s and a heat flux of 39.3 kW/m^2.



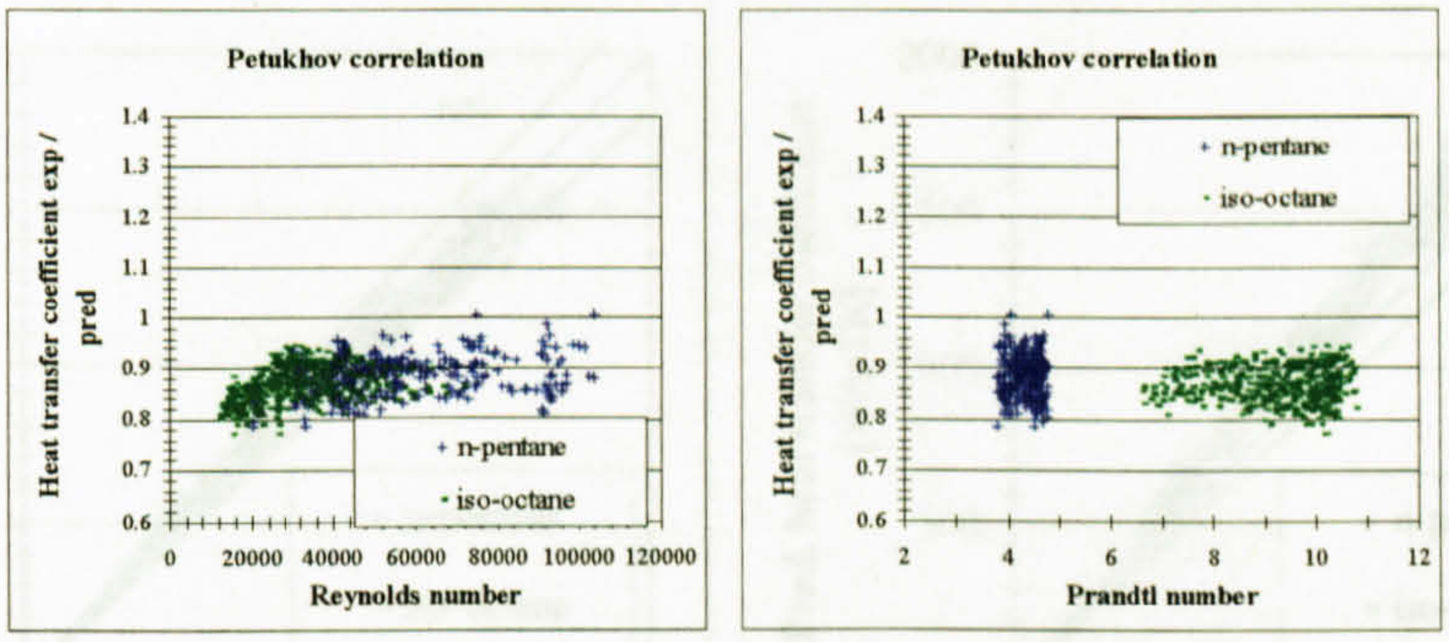


Figure 4.5: Ratio of the experimental to predicted heat transfer coefficient (Dittus-Boelter (1930) and Petukhov (1963)) plotted against the Reynolds and Prandtl number.

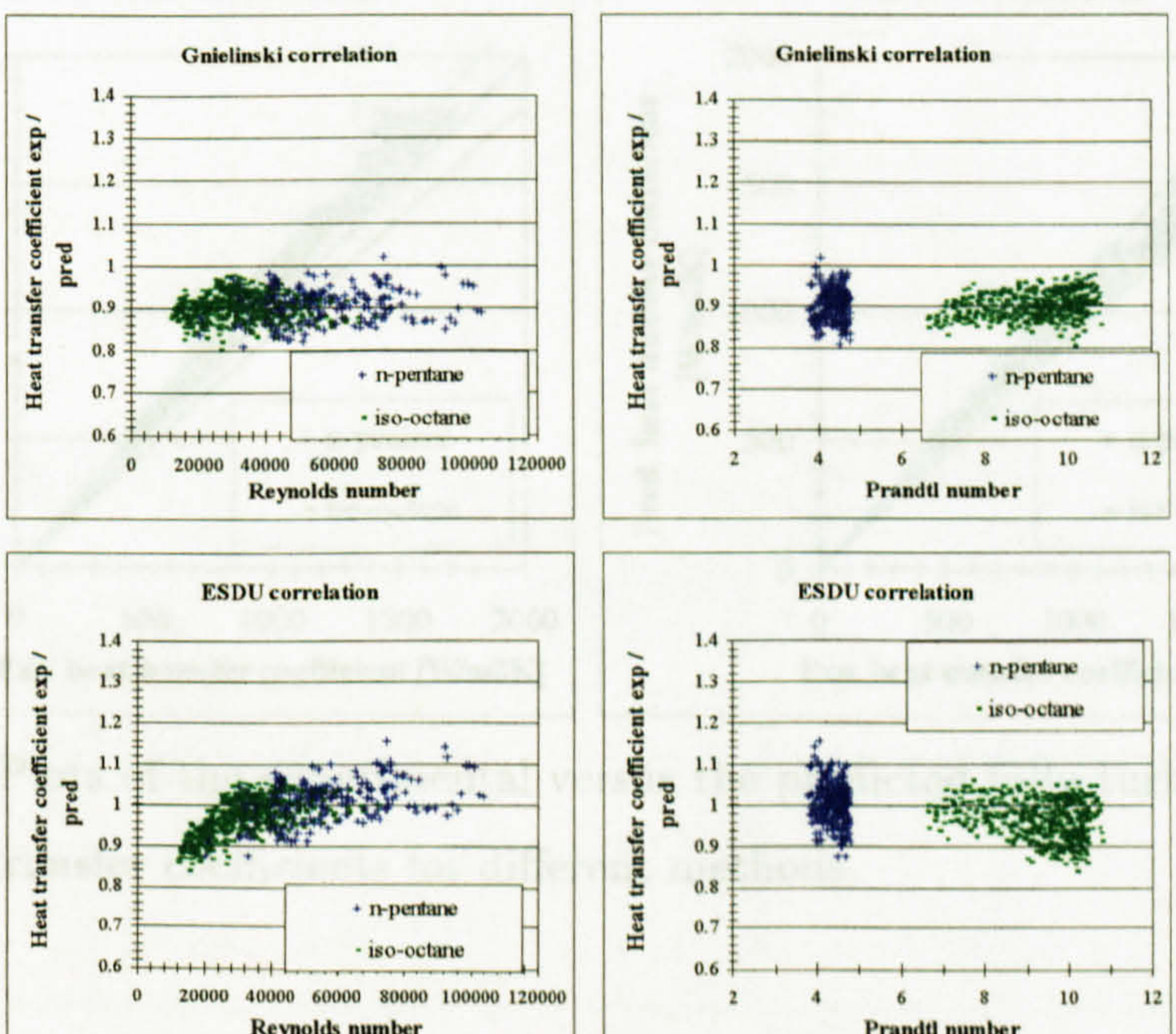


Figure 4.6: Ratio of the experimental to predicted heat transfer coefficient (Gnielinski (1976) and ESDU (1967)) plotted against the Reynolds and Prandtl number.

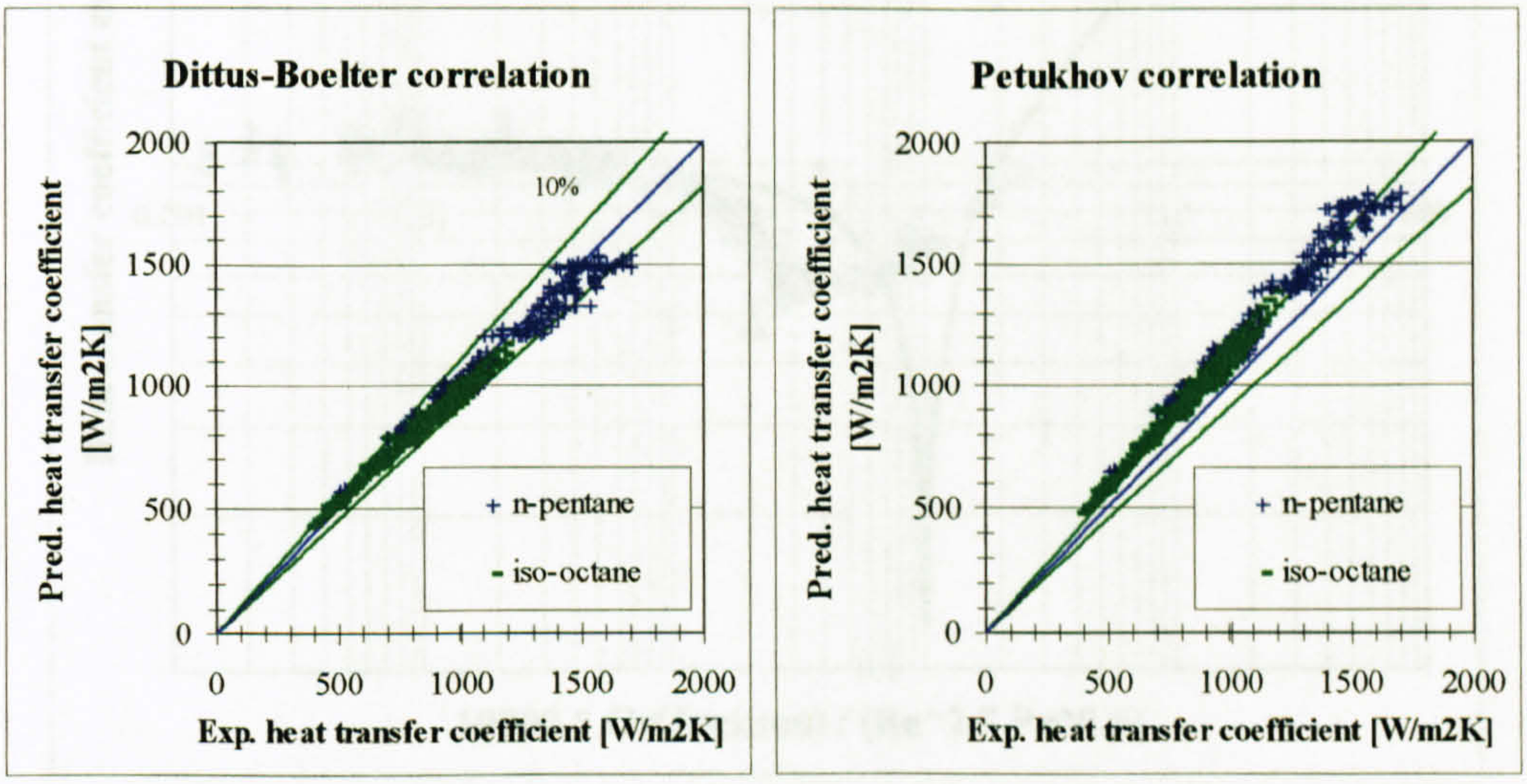


Figure 4.7: Plots of the experimental versus the predicted fully turbulent single phase heat transfer coefficients for different methods.

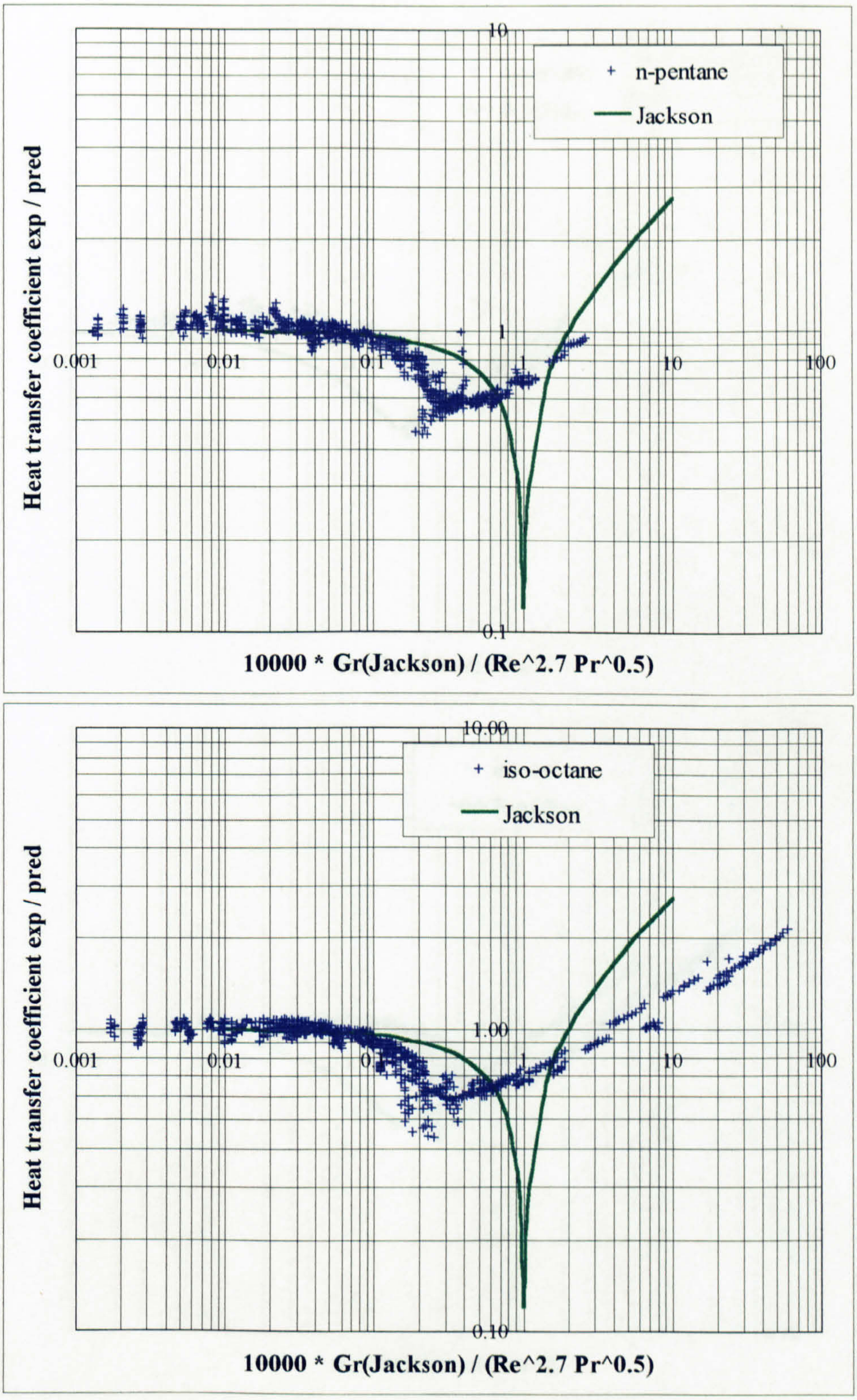


Figure 4.8: Single phase experimental results compared with the correlation of Jackson (1979).

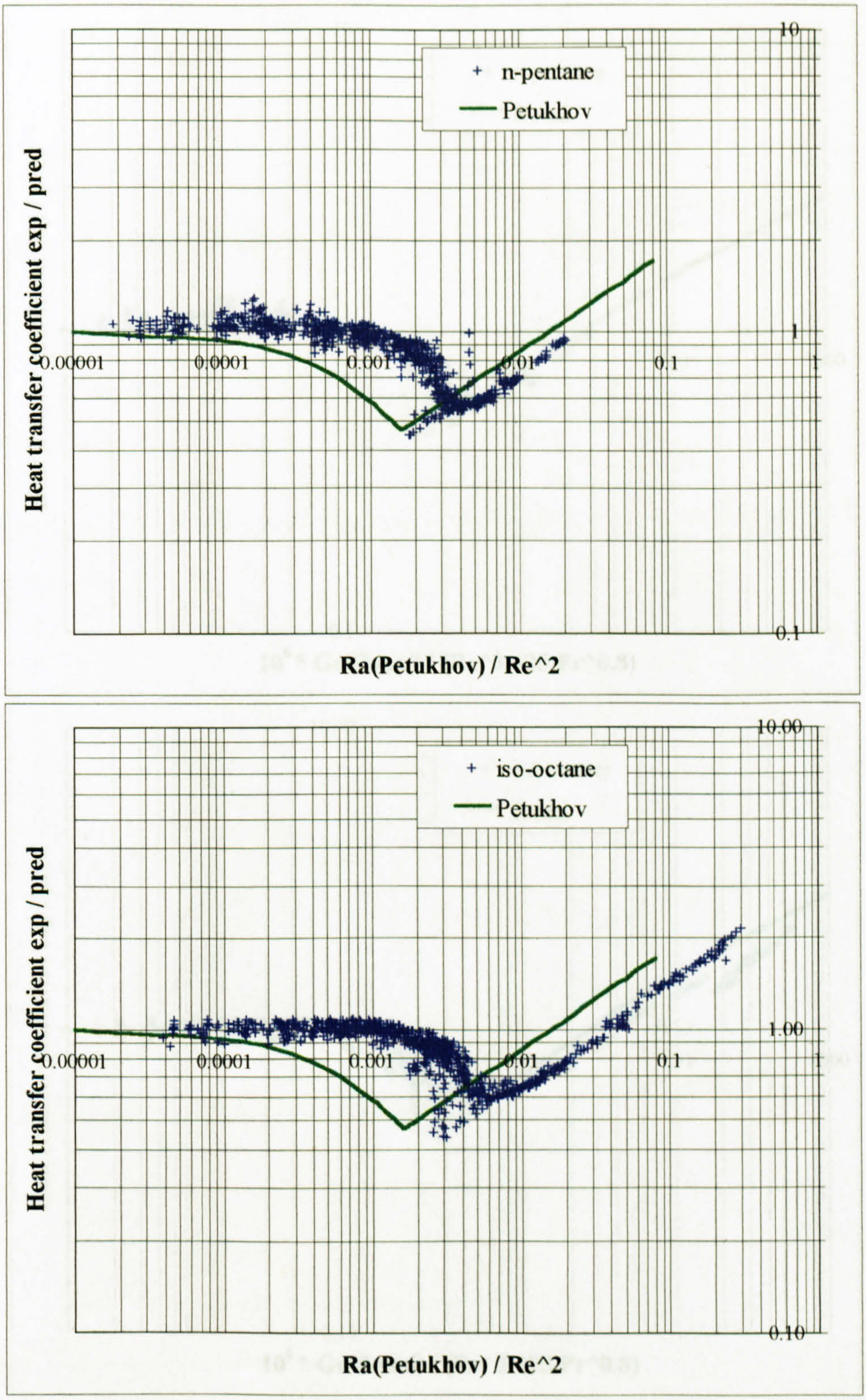


Figure 4.9: Single phase experimental results compared with the correlation of Petukhov (1977)

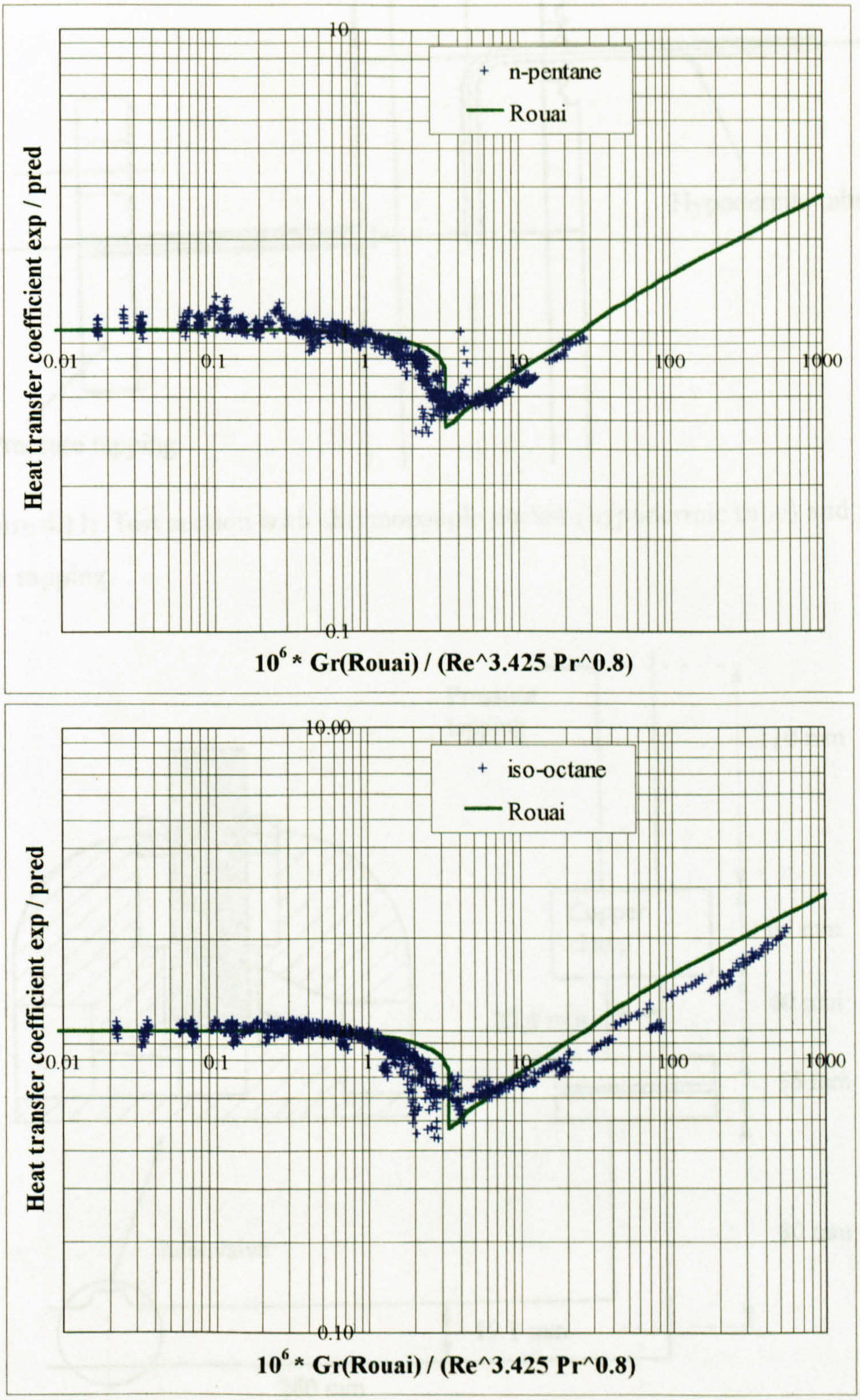


Figure 4.10: Single phase experimental results compared with the correlation of Rouai (1987).

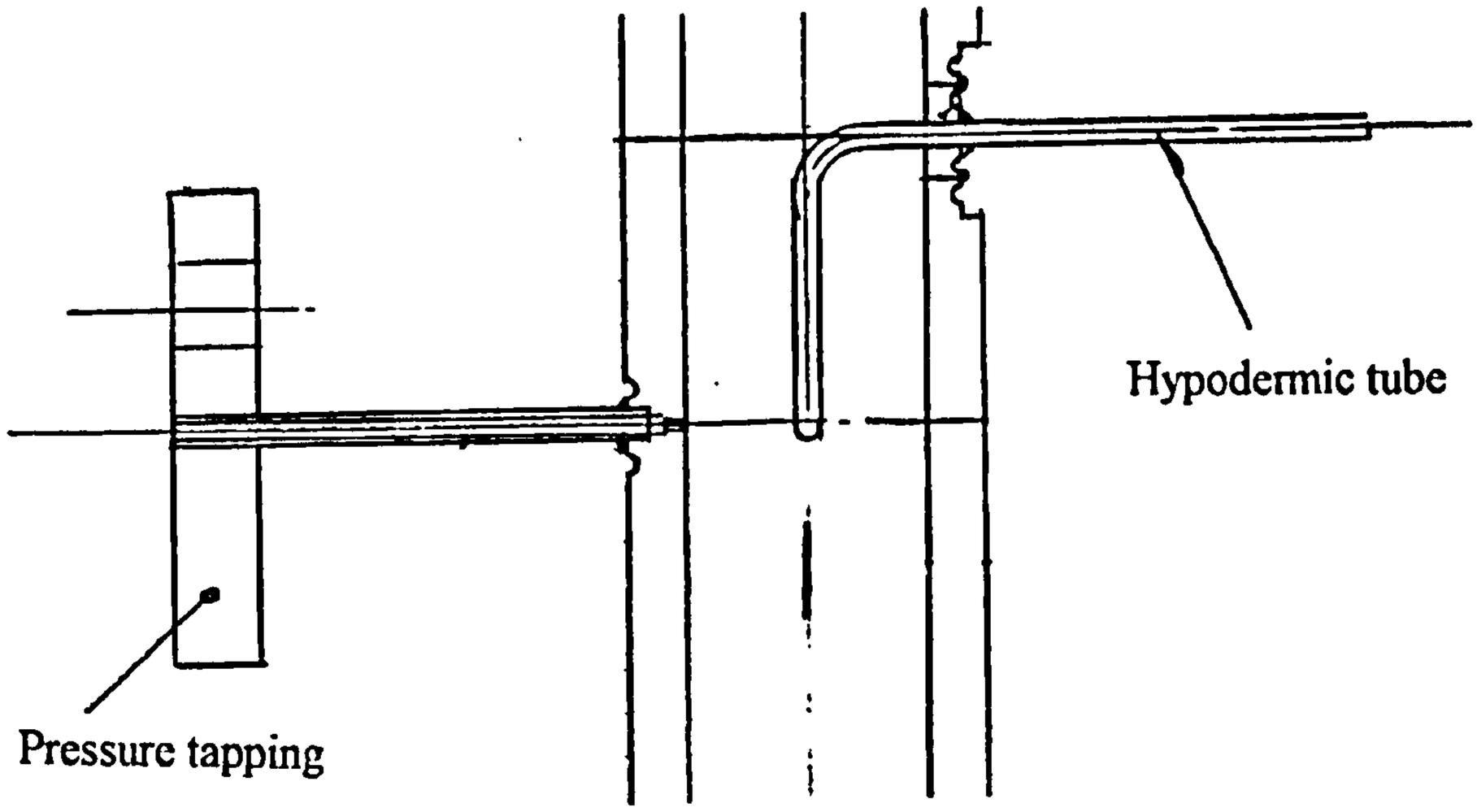


Figure 4.11: Test section with thermocouple pocket (hypodermic tube) and pressure tapping.

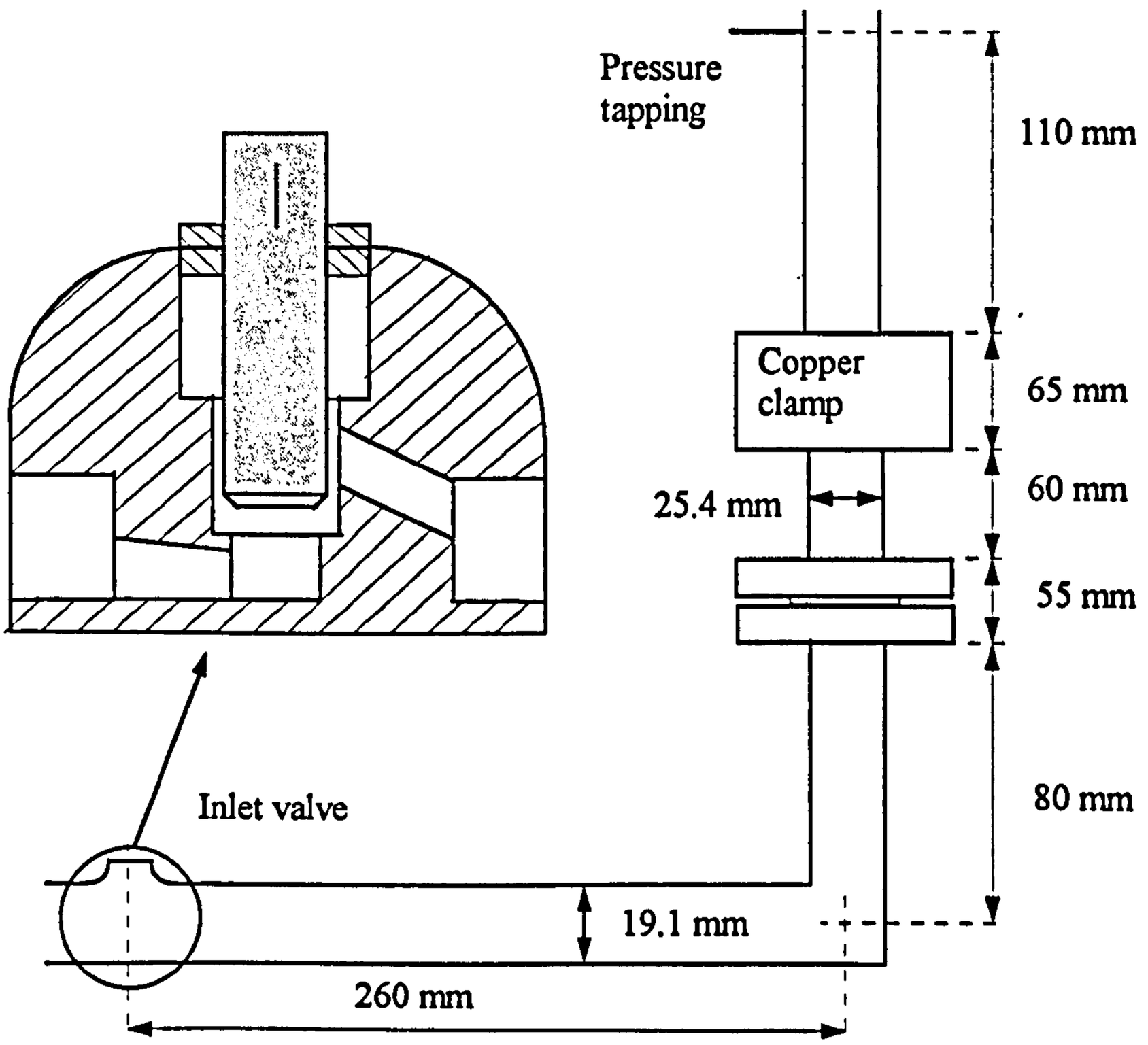


Figure 4.12: Schematic diagram of the entrance to the test section.

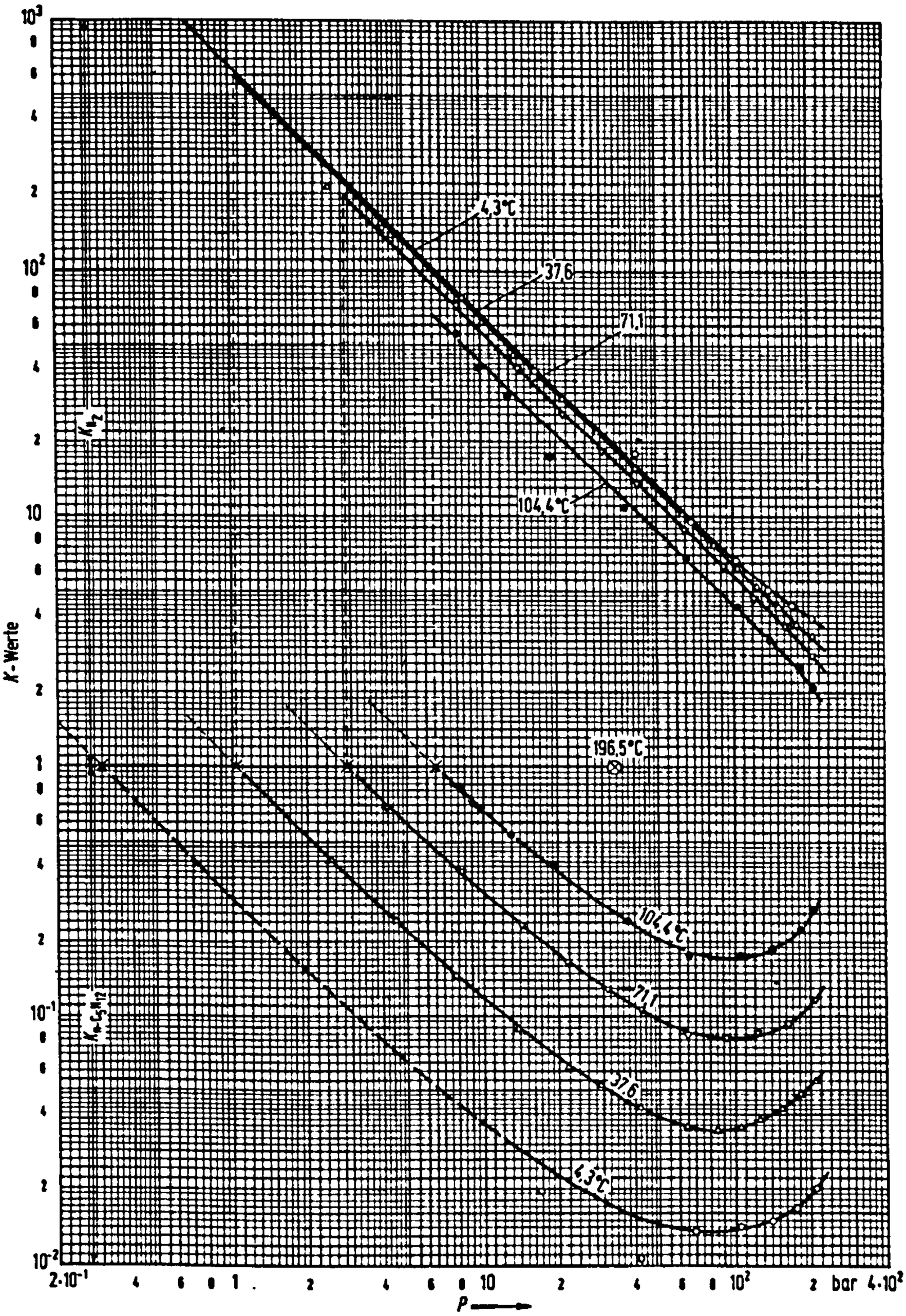


Figure 4.13: Solubility chart of the solubility of N_2 in n-pentane, from Landolt-Börnstein (1976).

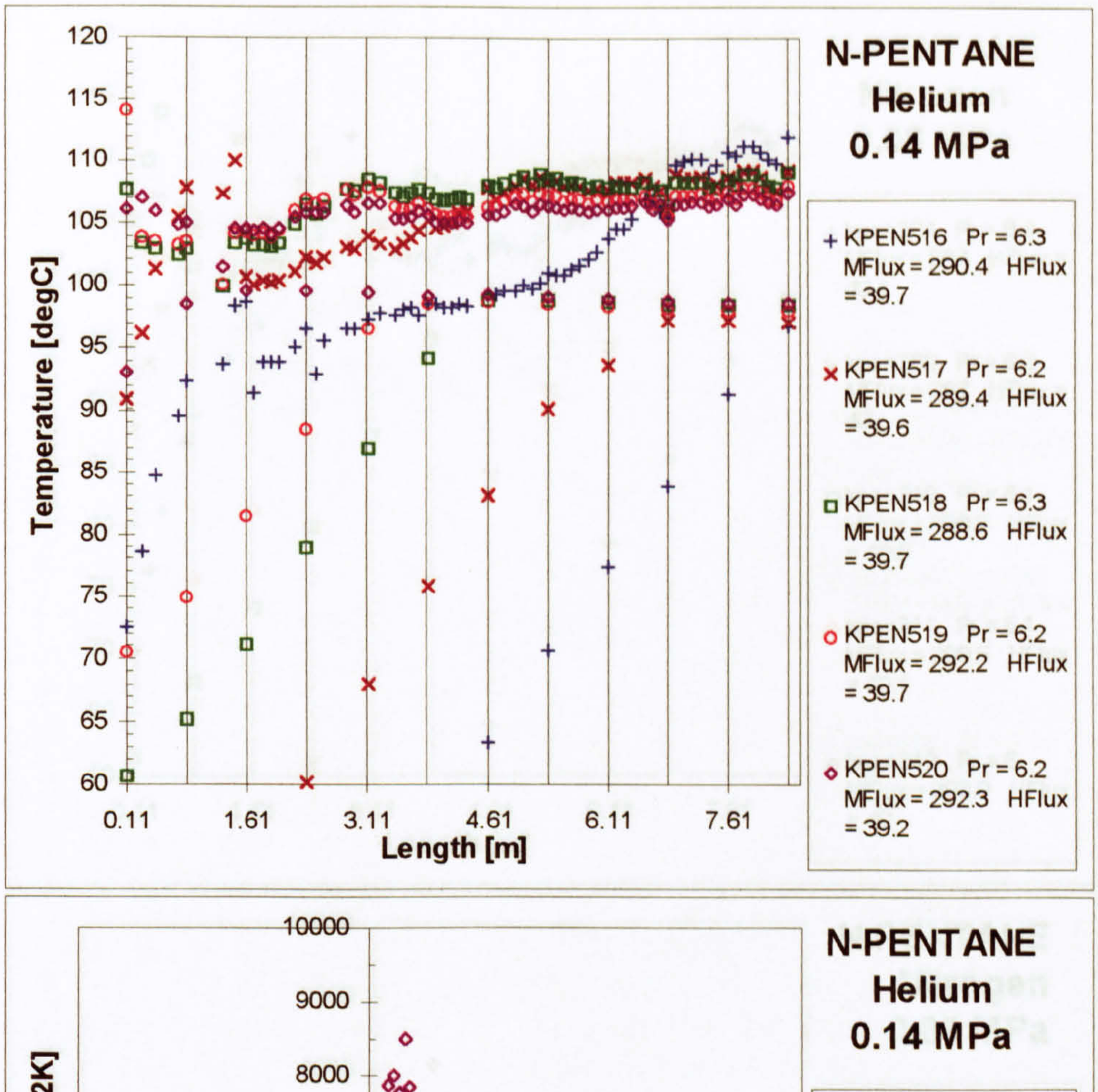


Figure 4.14: n-pentane experiments with a Helium pressure of 0.14 MPa in the main storage tank.

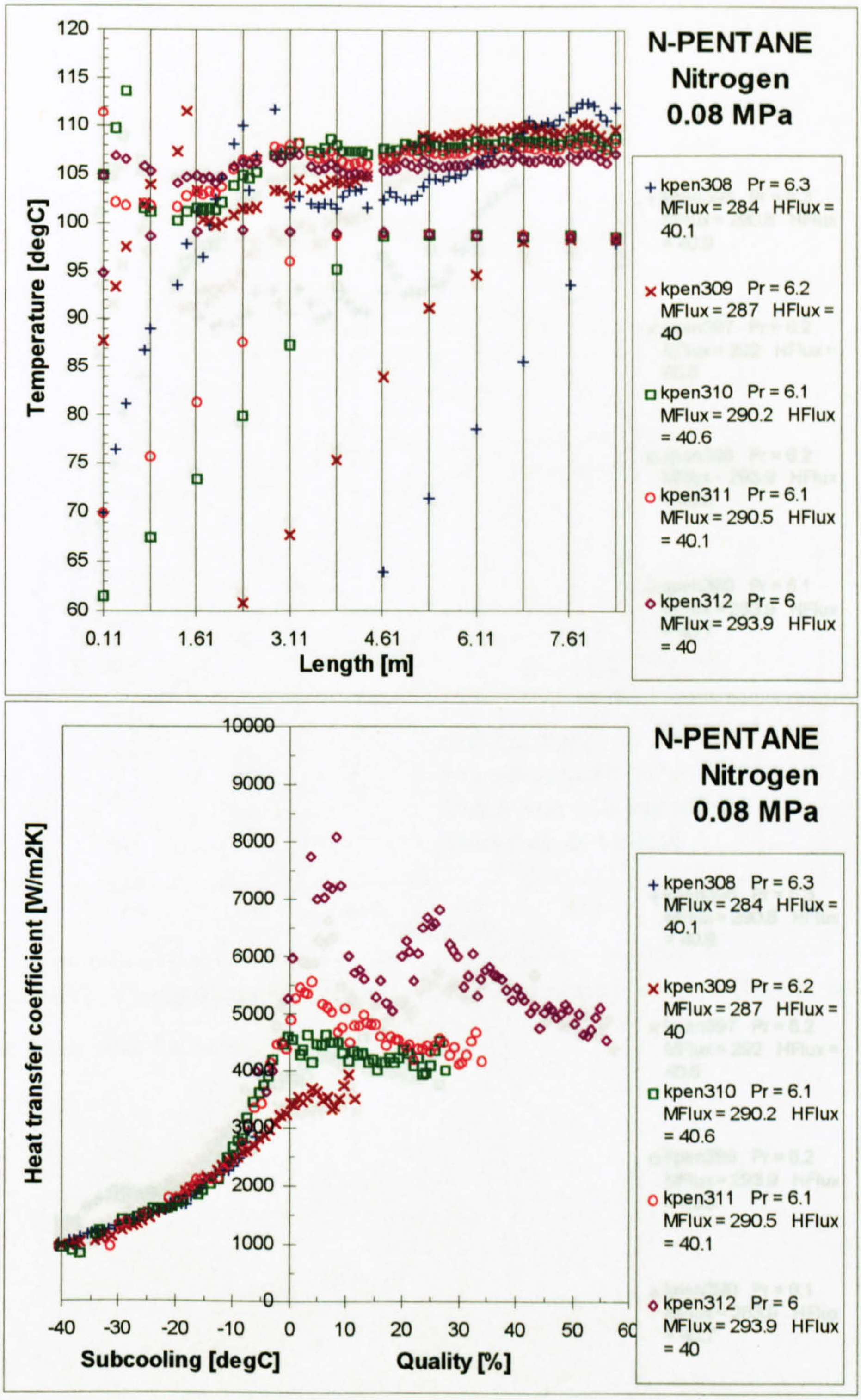


Figure 4.15: n-pentane experiments with a Nitrogen pressure of 0.08 MPa in the main storage tank.

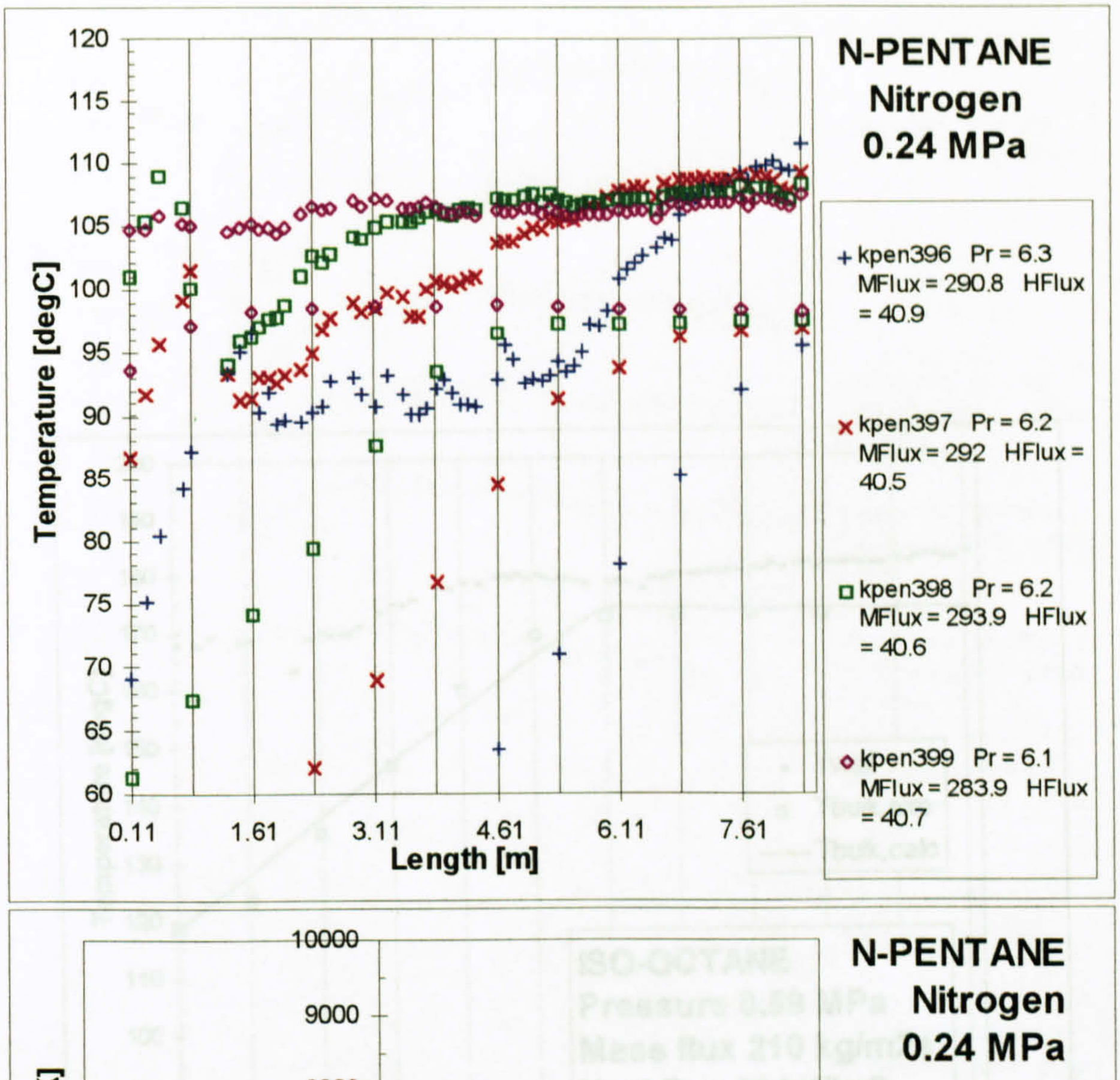


Figure 4.16: n-pentane experiments with a Nitrogen pressure of 0.24 MPa in the main storage tank.

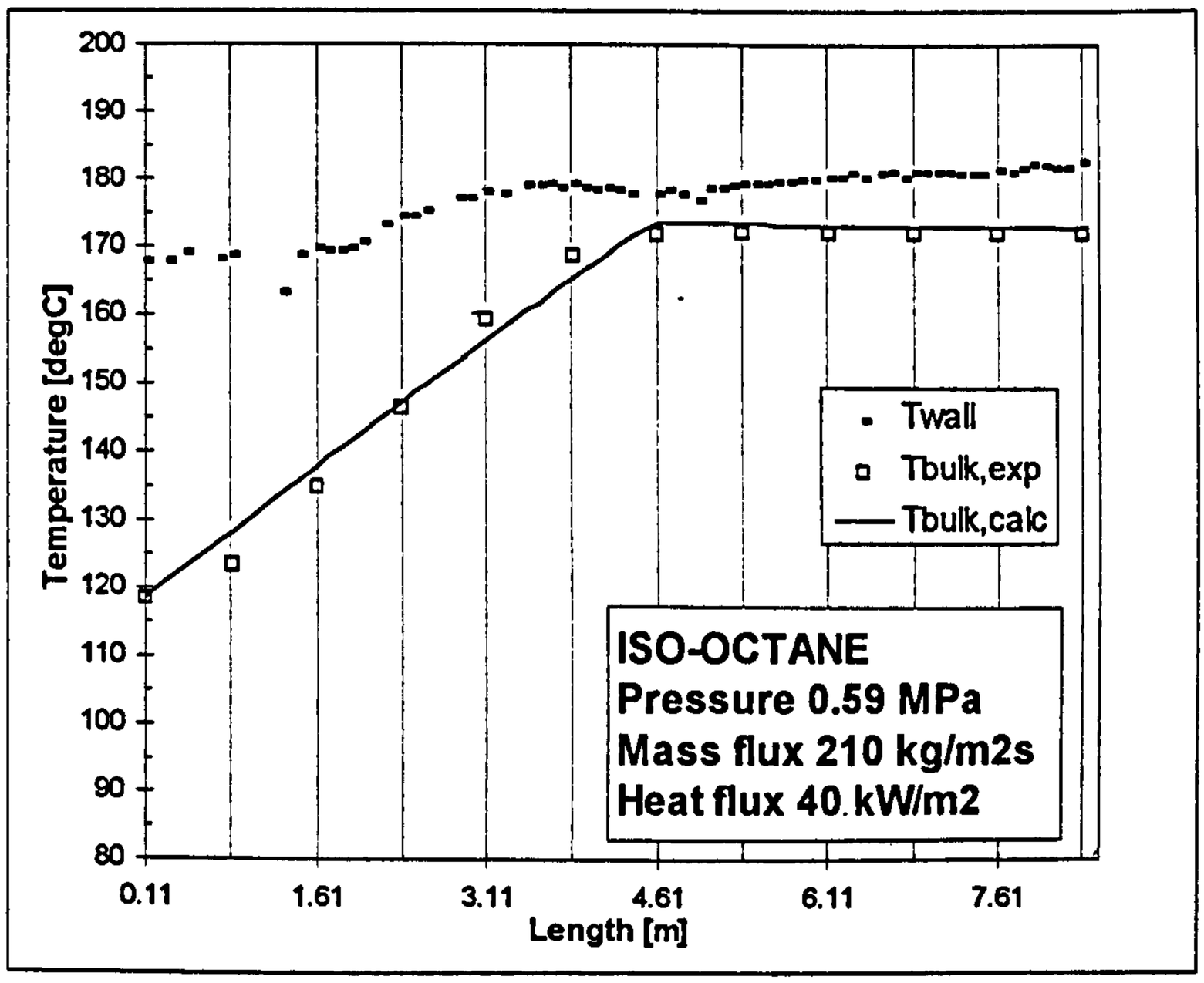


Figure 4.17: Comparison of measured bulk fluid temperatures with the calculations from heat balances.

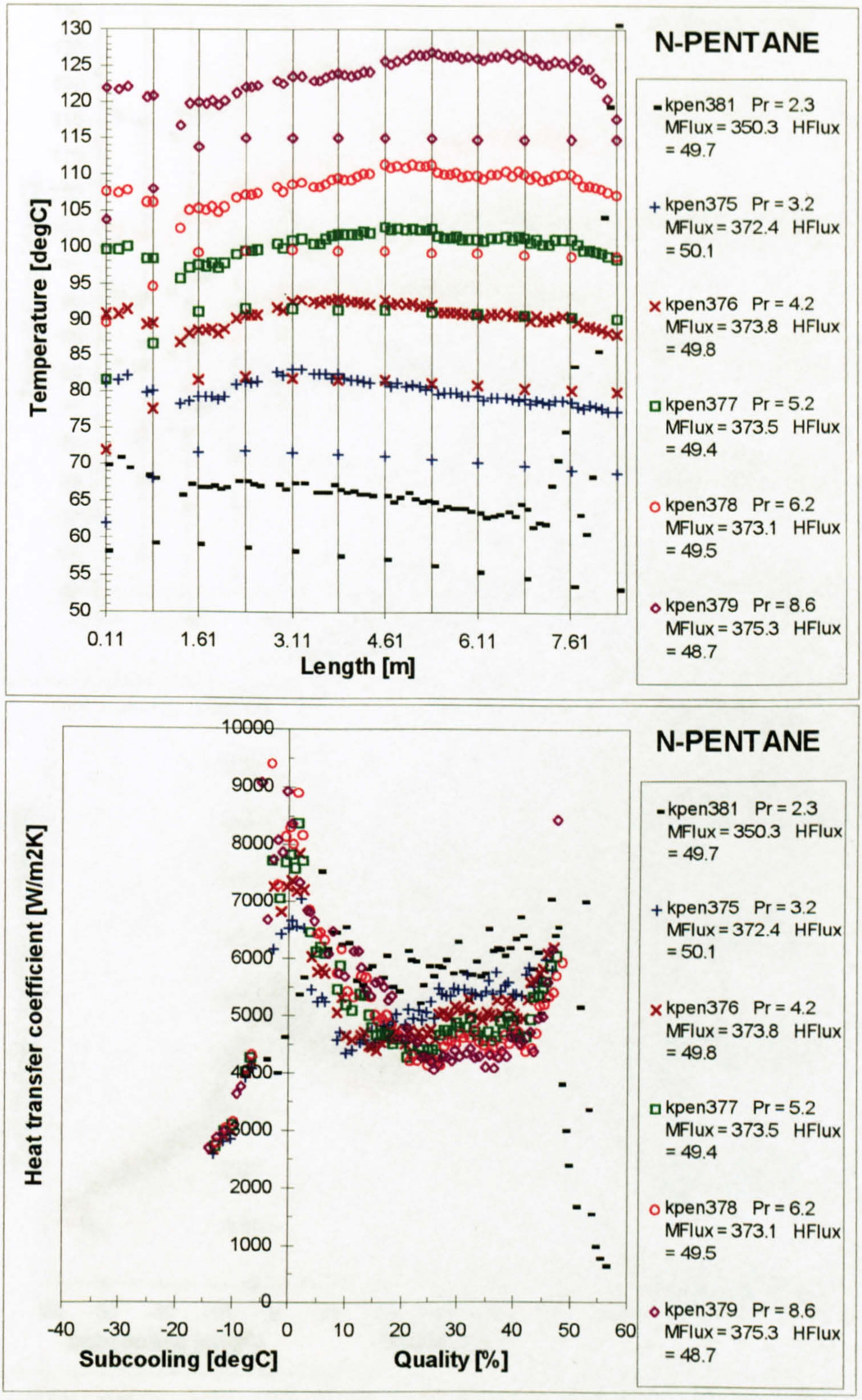


Figure 4.18: Effect of pressure on heat transfer coefficient, subcooling of about 14 °C.

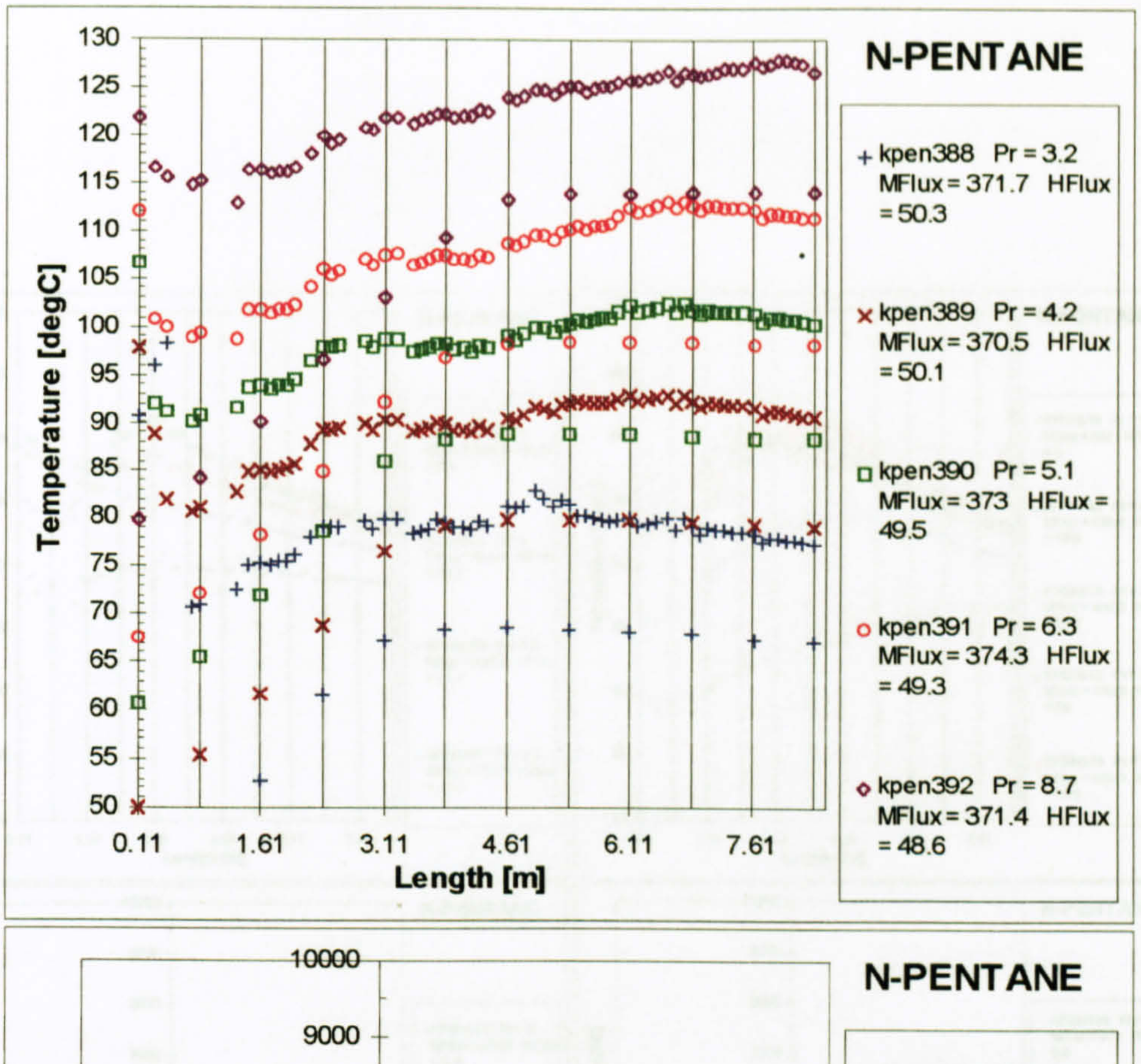


Figure 4.19: Effect of pressure on heat transfer coefficient, subcooling of about 35 °C.

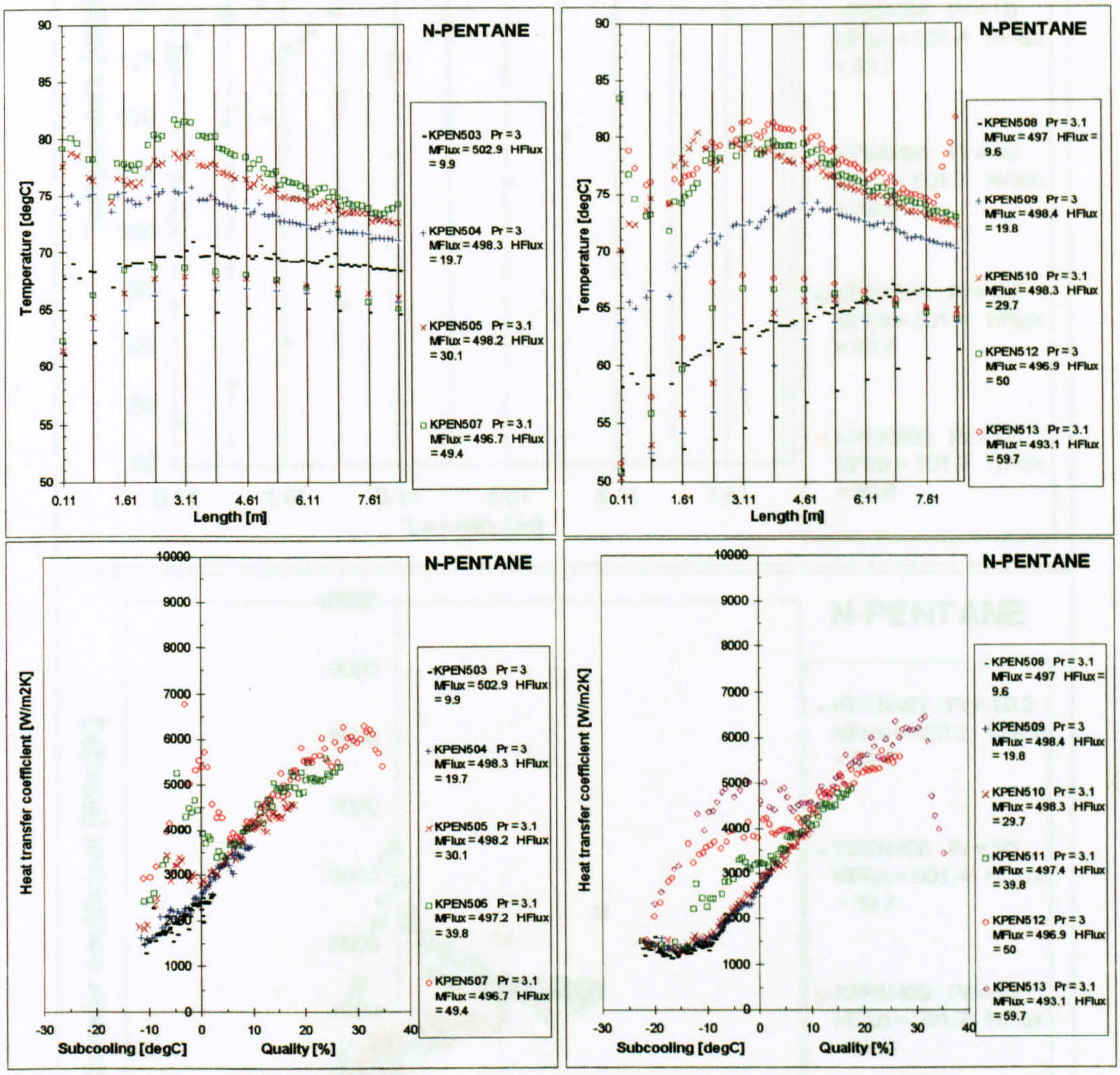


Figure 4.20: The effect of subcooling for two inlet suboolings with variation in heat flux. Subcooling of around 10 °C (left) and subcooling of around 23 °C (right).

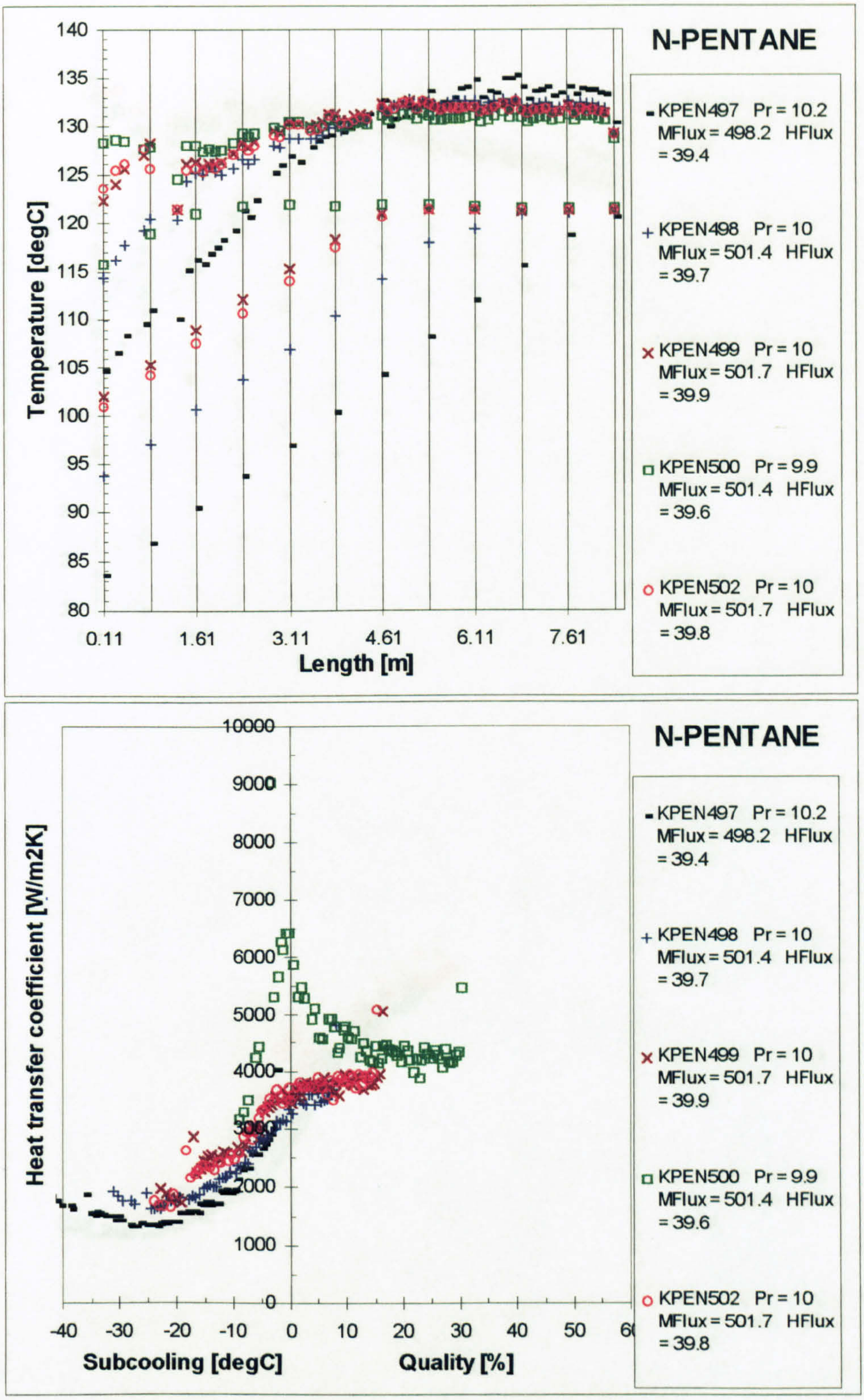


Figure 4.21: The effect of variation in inlet temperature at a pressure of 1.0 MPa, mass flux of 500 kg/m^{2}s and a heat flux of 40 kW/m^2.

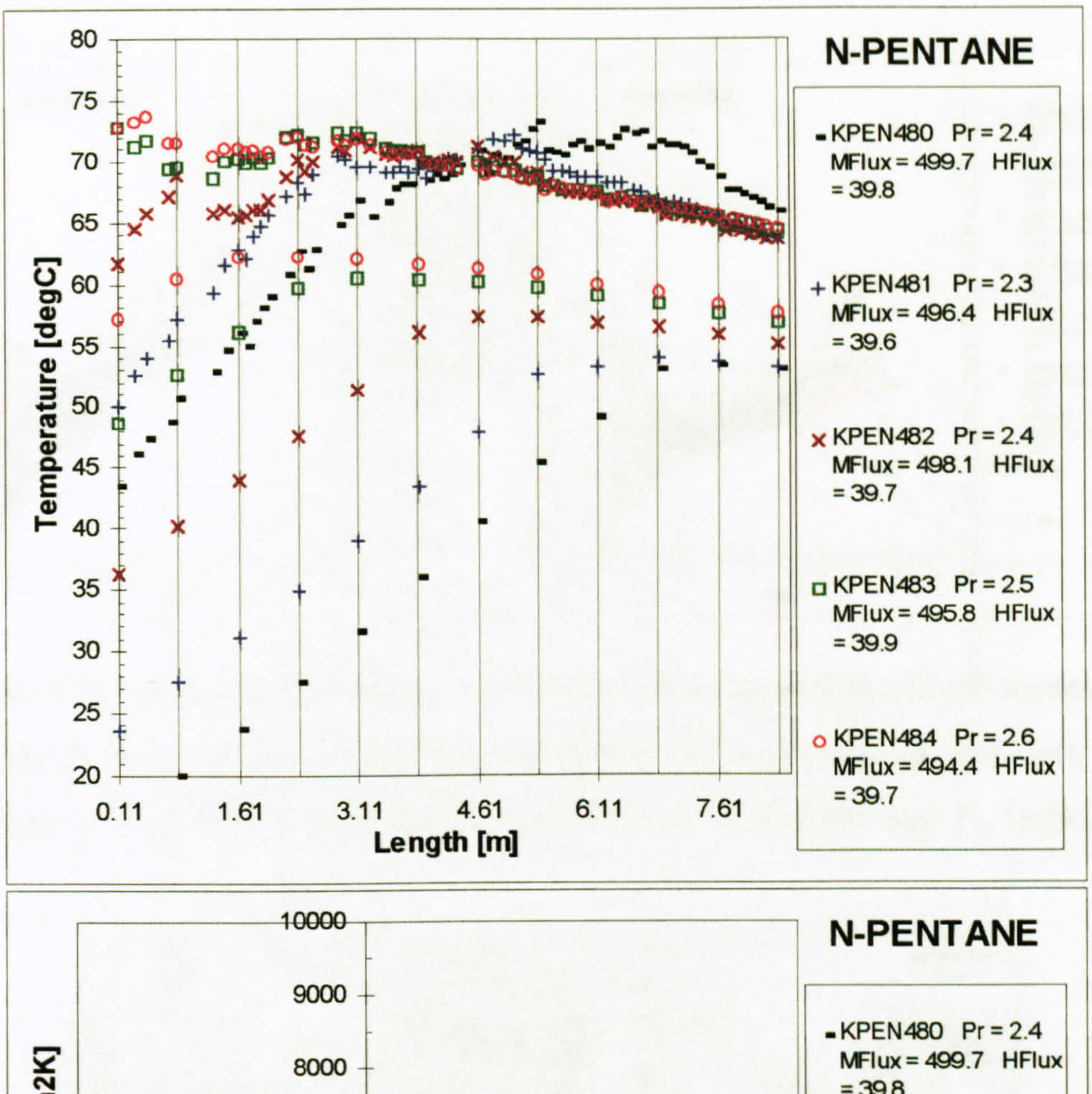


Figure 4.22: The effect of variation in inlet temperature at a pressure of 0.24 MPa, mass flux of 500 kg/m^{2}s and a heat flux of 40 kW/m^2.

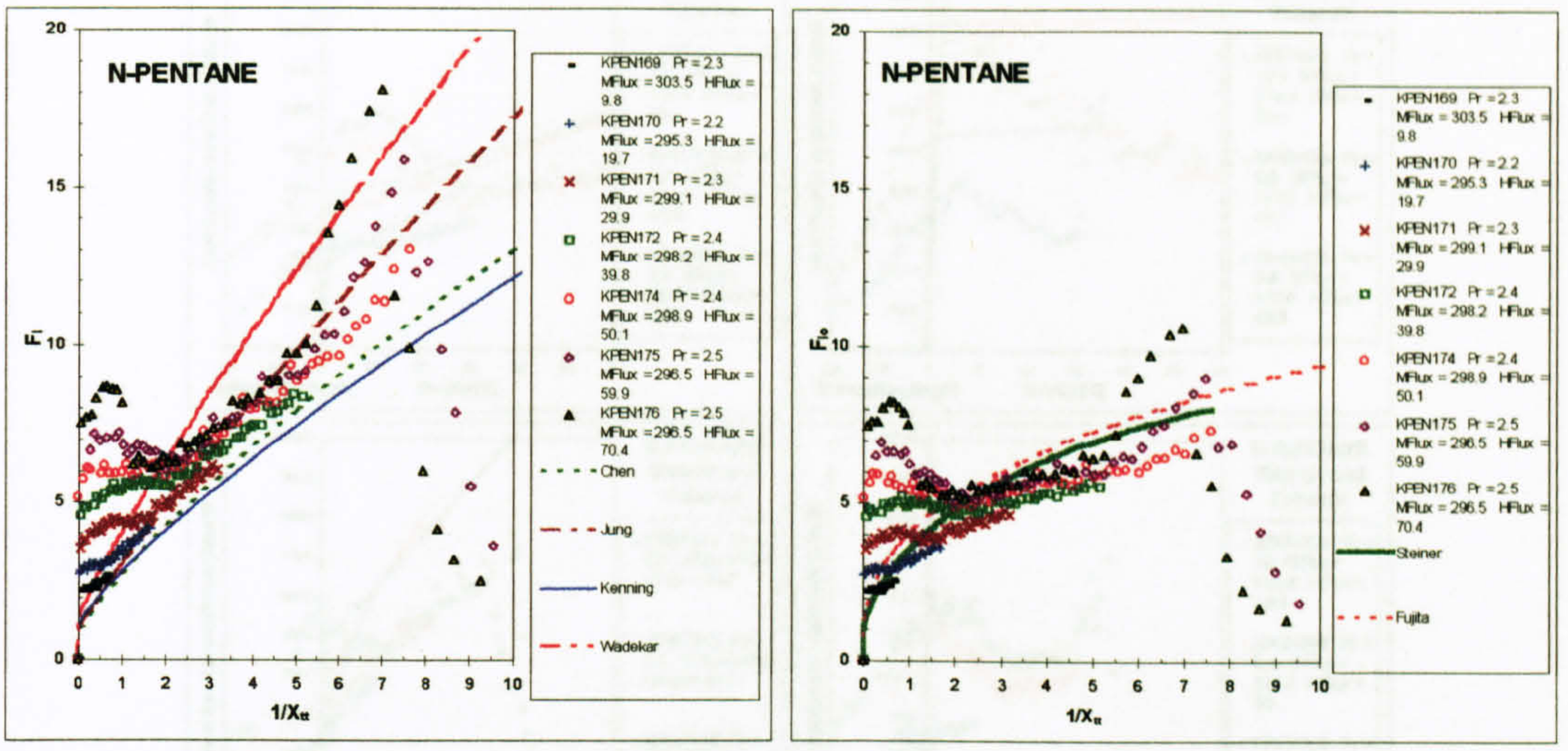


Figure 4.23: Enhancement factor as a function of reciprocal Martinelli parameter calculated from various correlations compared with n-pentane experiments at a pressure of 0.23 MPa and a mass flux of 300 kg/m^{2}s; F_l (left) and F_{lo} (right).

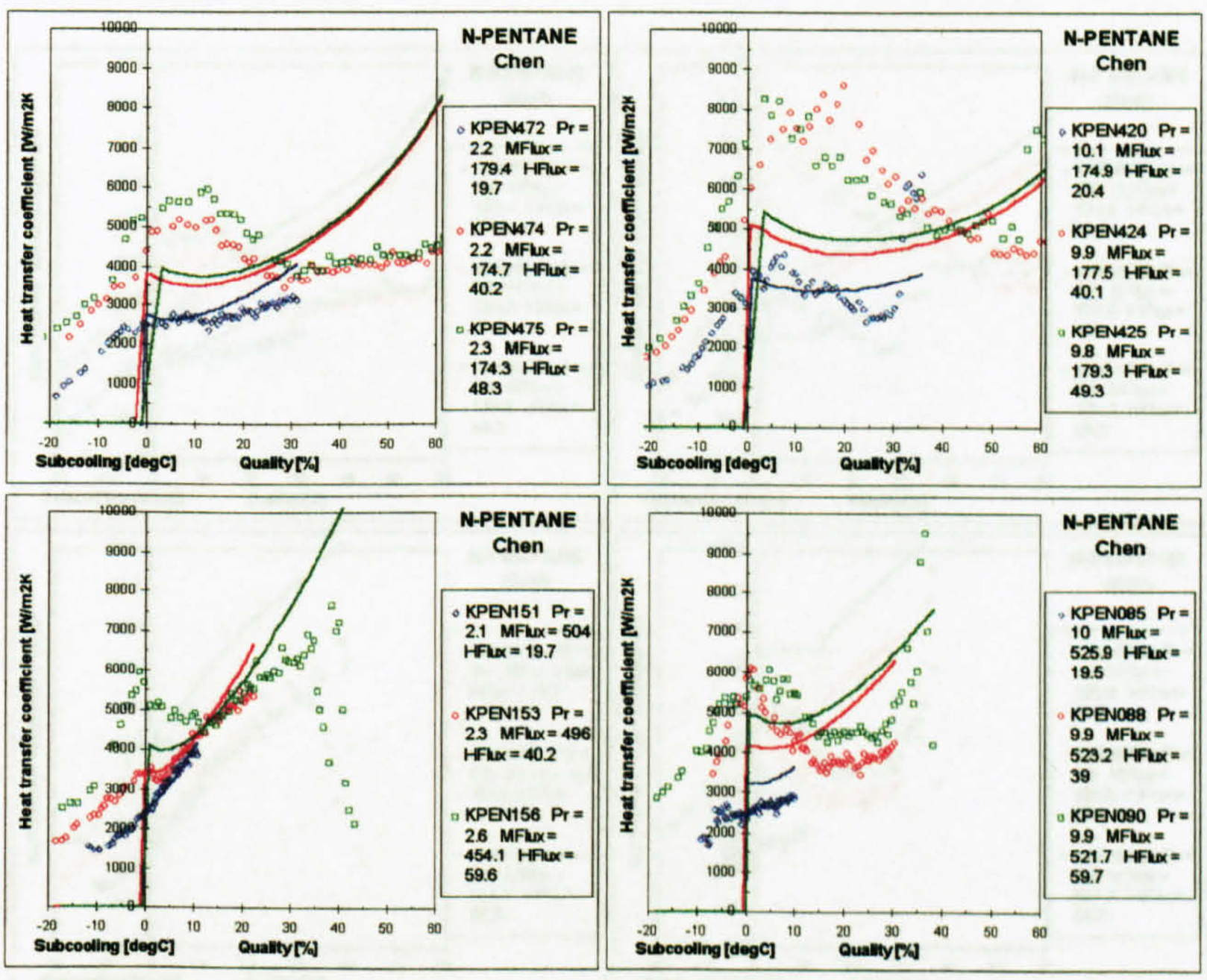
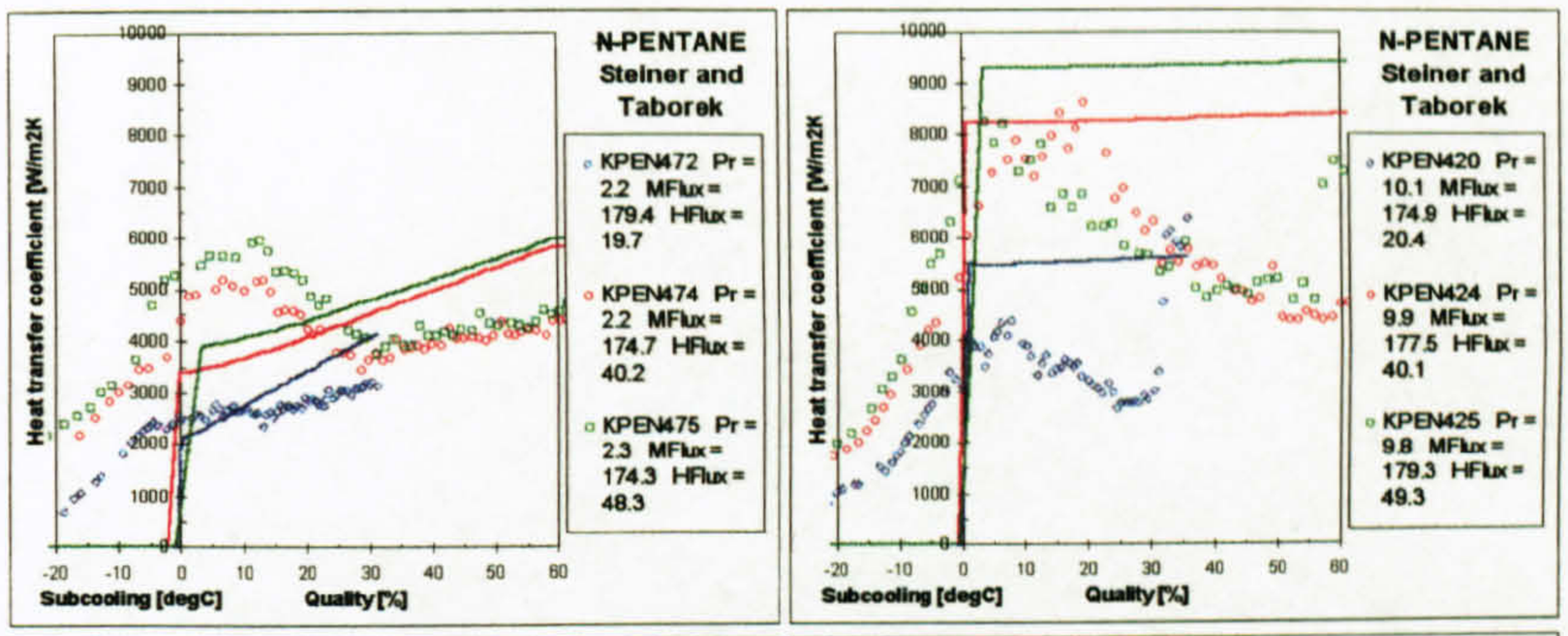


Figure 4.24: Chen (1966) correlation compared with n-pentane data for pressures of 0.23 and 1.0 MPa, mass fluxes of 200 and 500 kg/m^{2}s and for various heat flux levels.



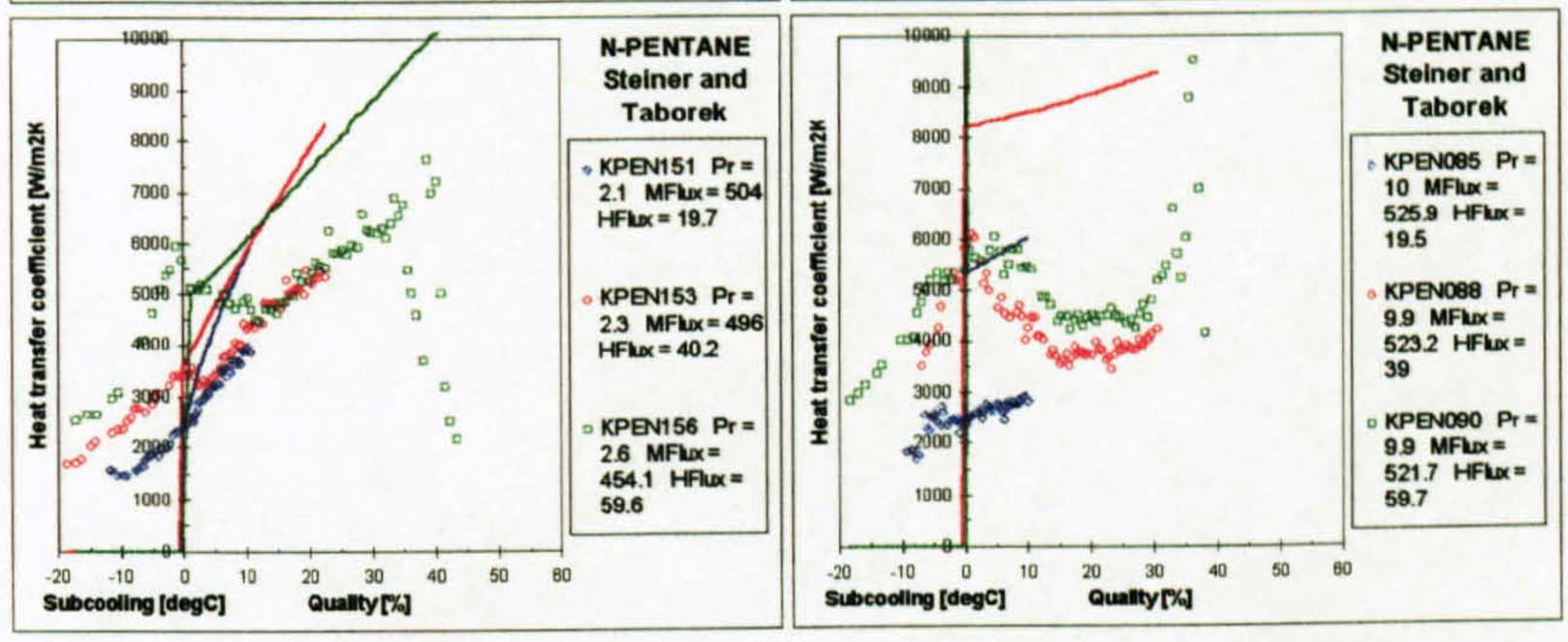


Figure 4.25: Steiner and Taborek (1992) correlation compared with n-pentane data for pressures of 0.23 and 1.0 MPa, mass fluxes of 200 and 500 kg/m^{2}s and for various heat flux levels.

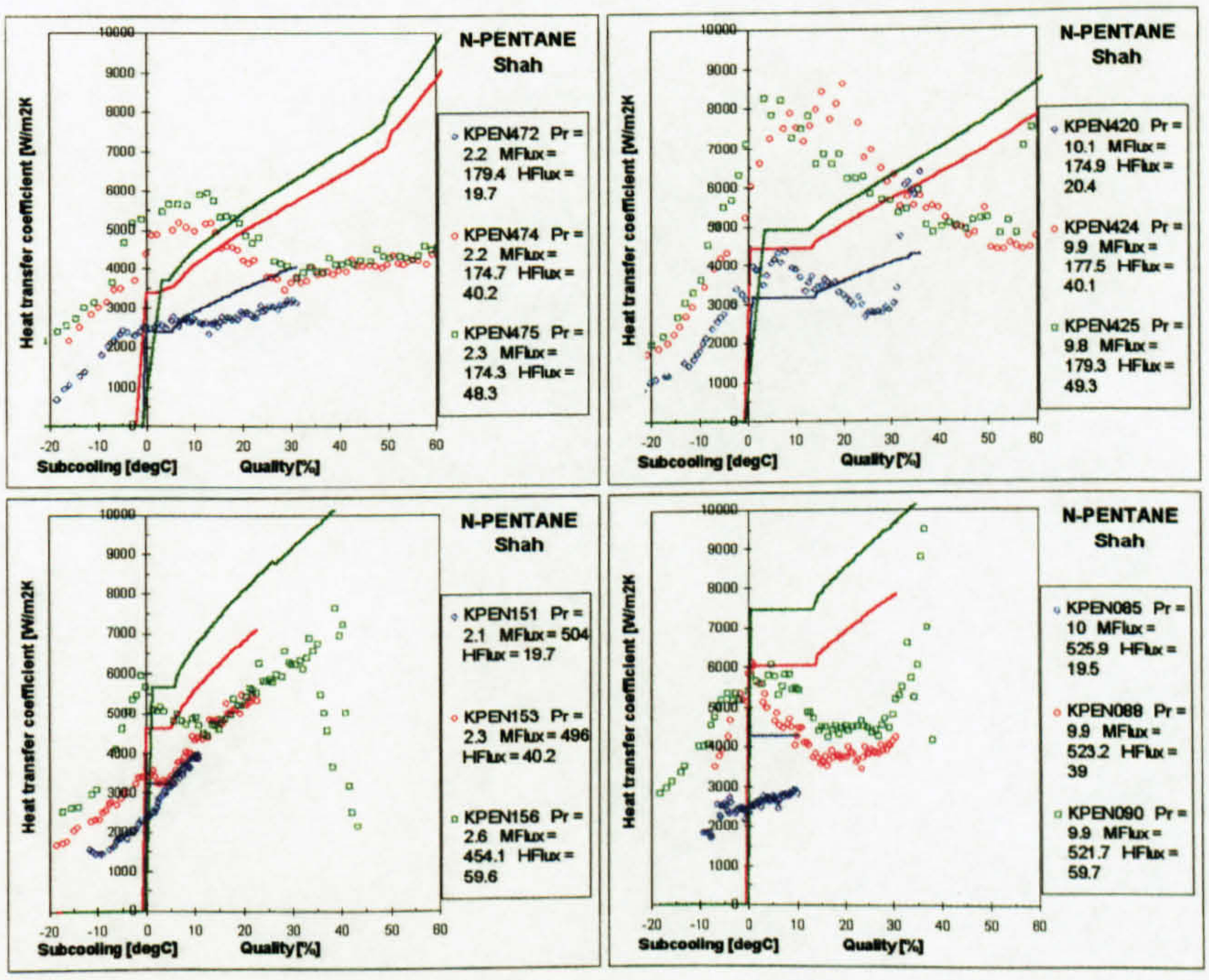
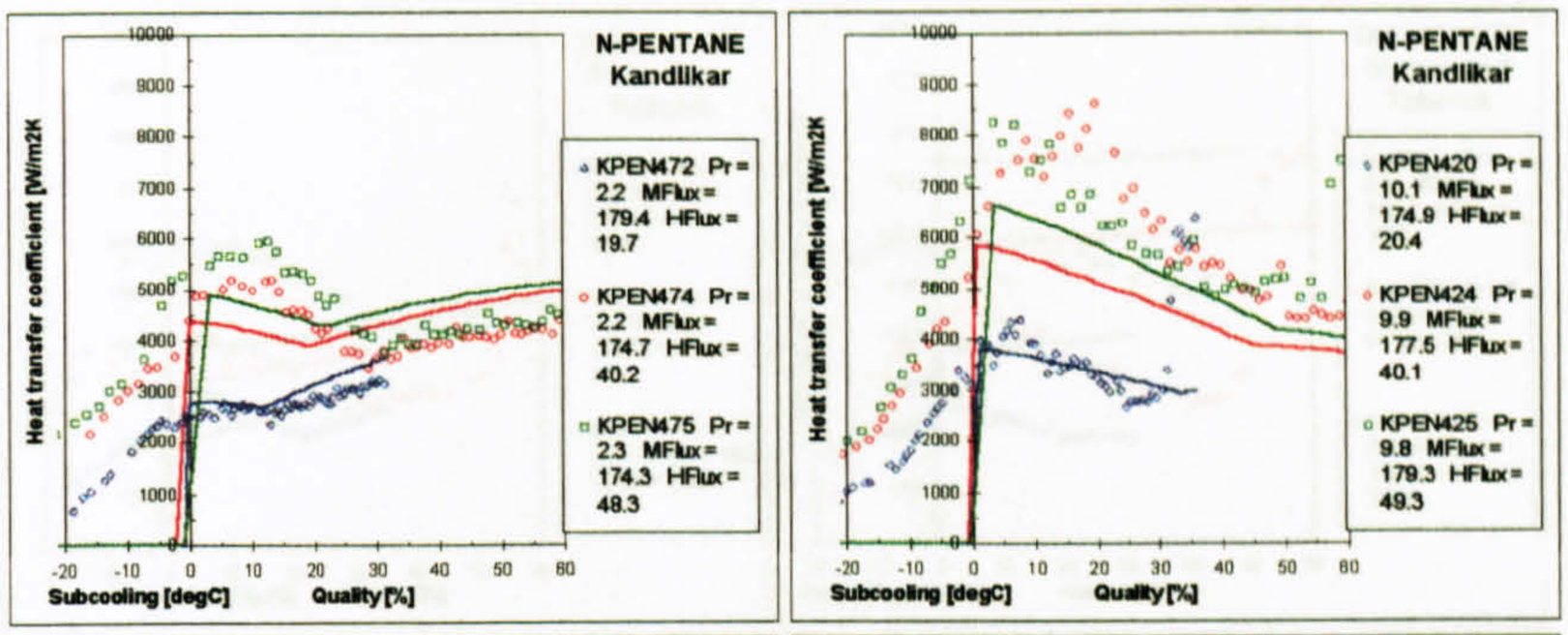


Figure 4.26: Shah (1982) correlation compared with n-pentane data for pressures of 0.23 and 1.0 MPa, mass fluxes of 200 and 500 kg/m^{2}s and for various heat flux levels.



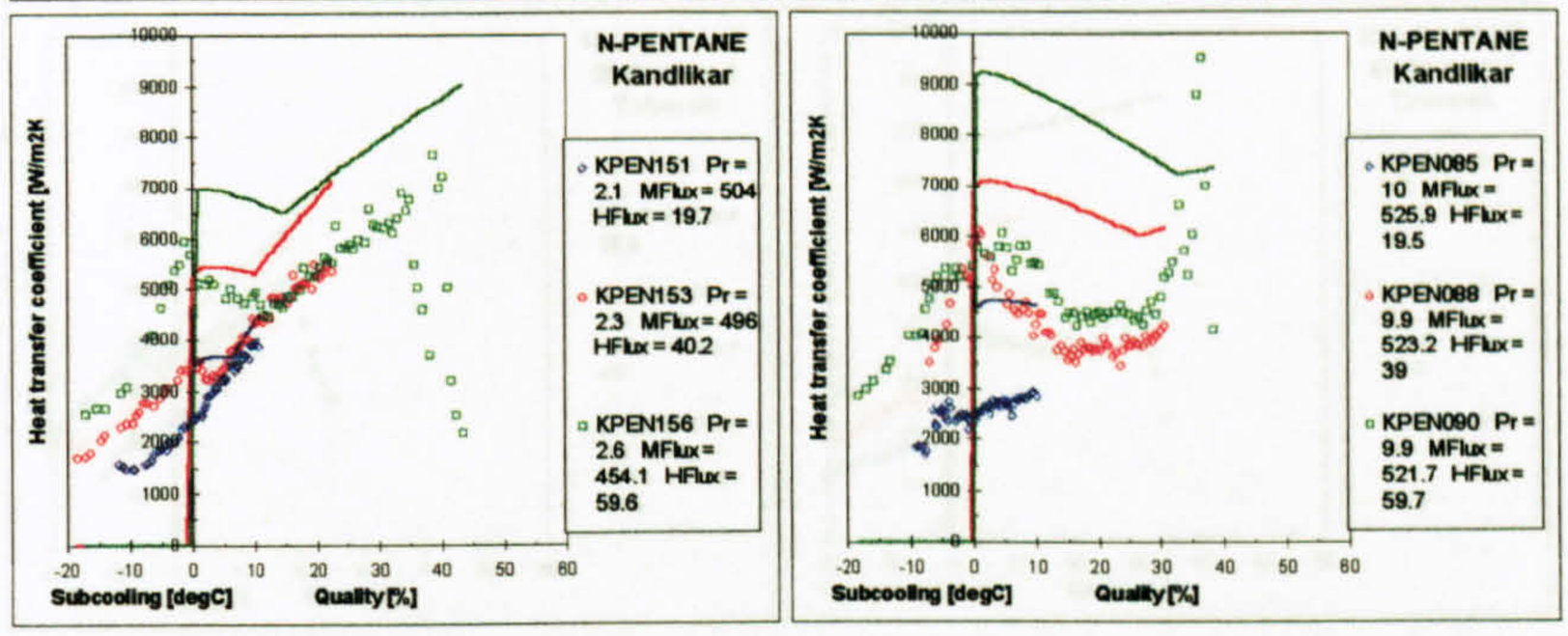


Figure 4.27: Kandlikar (1990b) correlation compared with n-pentane data for pressures of 0.23 and 1.0 MPa, mass fluxes of 200 and 500 kg/m^{2}s and for various heat flux levels.

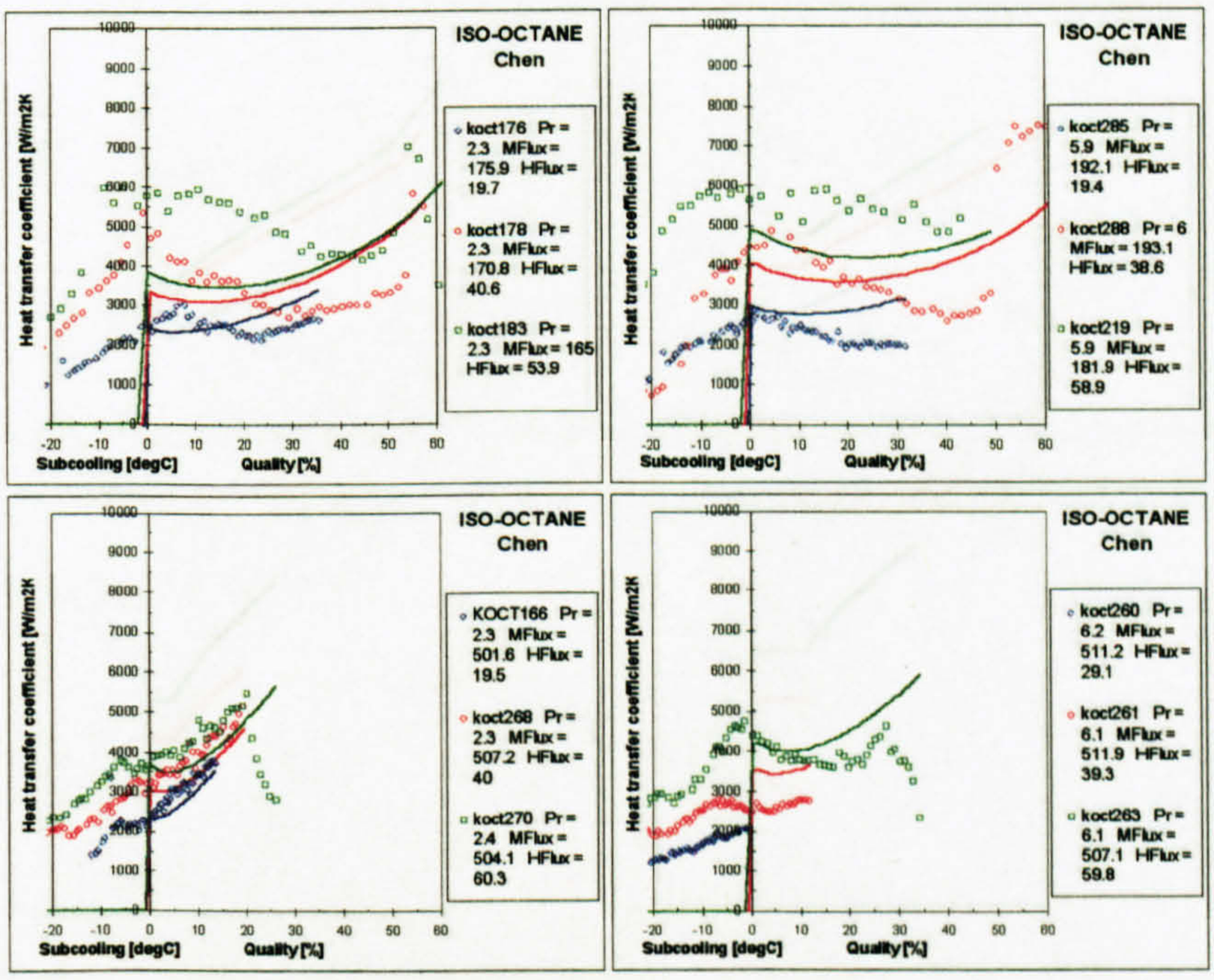


Figure 4.28: Chen (1966) correlation compared with iso-octane data for pressures of 0.23 and 0.3 MPa, mass fluxes of 200 and 500 kg/m^{2}s and for various heat flux levels.

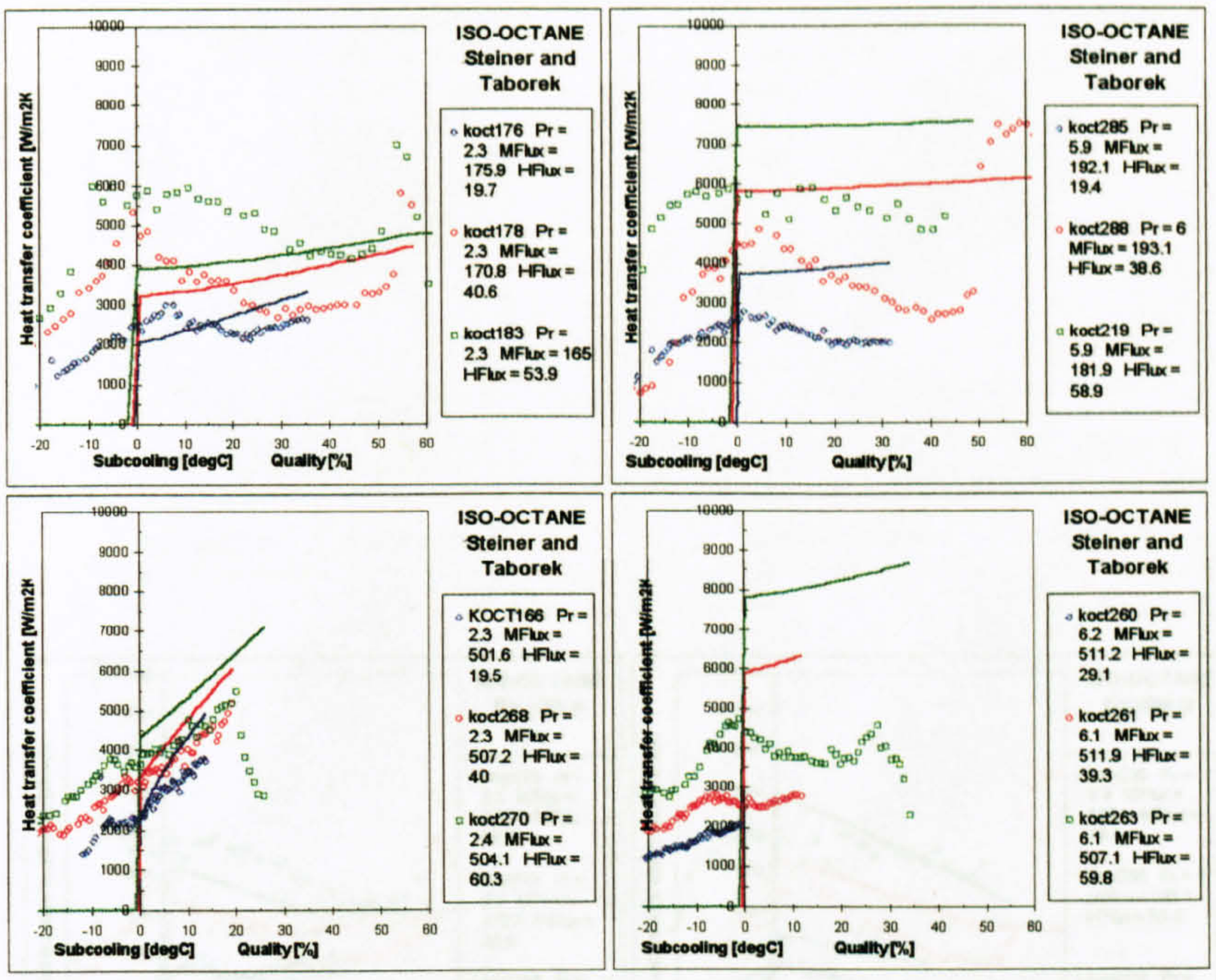


Figure 4.29: Steiner and Taborek (1992) correlation compared with iso-octane data for pressures of 0.23 and 0.6 MPa, mass fluxes of 200 and 500 kg/m^{2}s and for various heat flux levels.

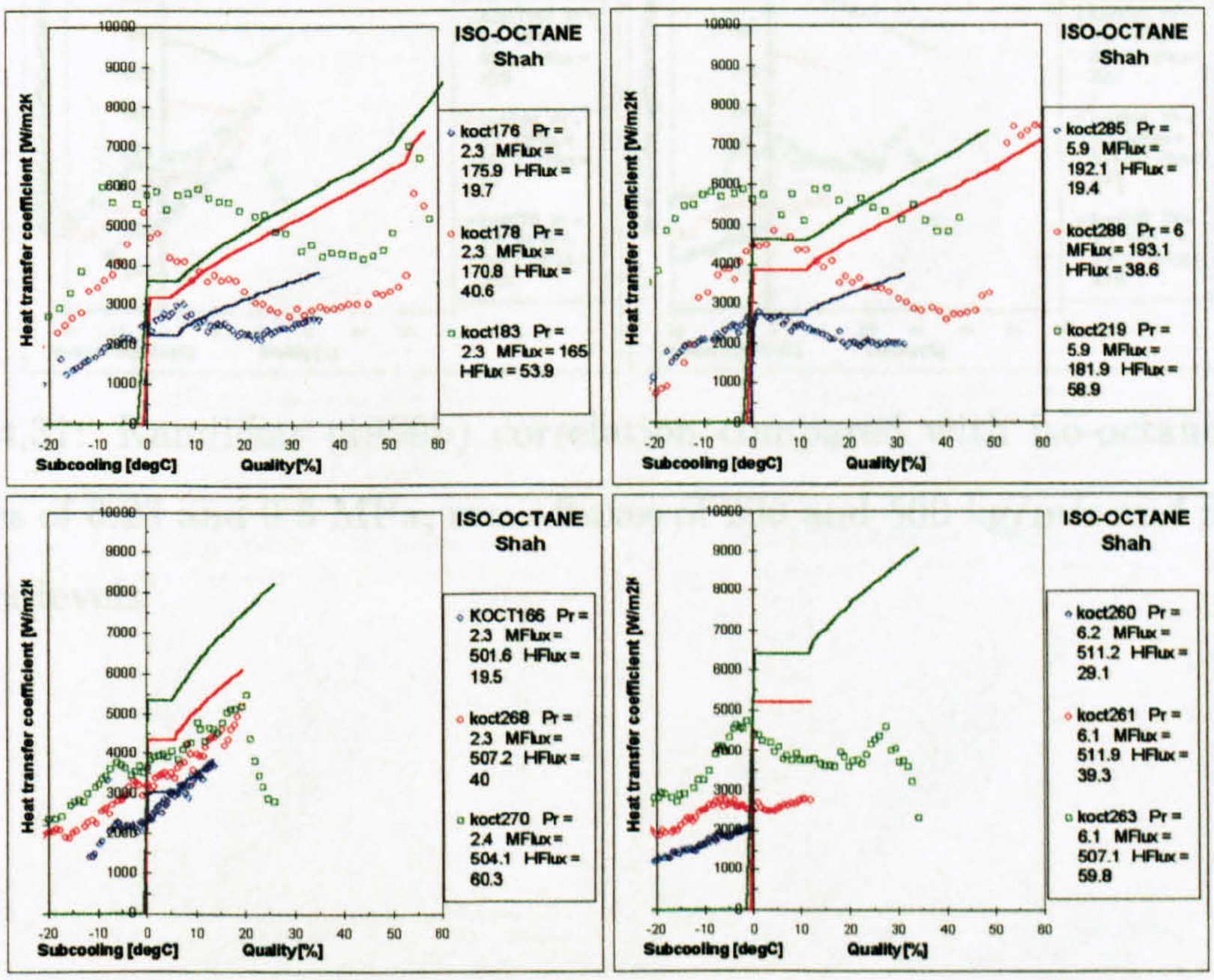


Figure 4.30: Shah (1982) correlation compared with iso-octane data for pressures of 0.23 and 0.6 MPa, mass fluxes of 200 and 500 kg/m^{2}s and for various heat flux levels.

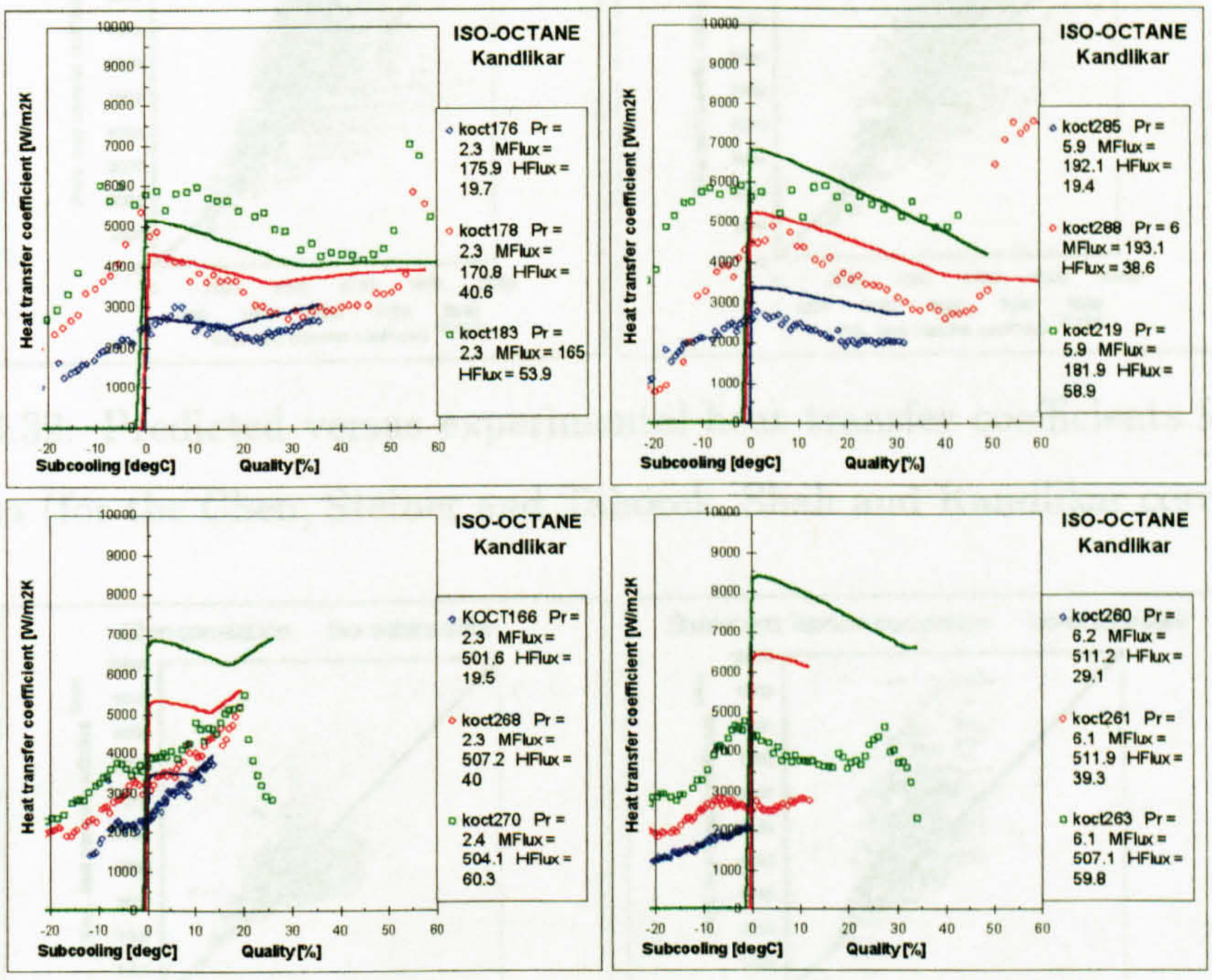


Figure 4.31: Kandlikar (1990b) correlation compared with iso-octane data for pressures of 0.23 and 0.6 MPa, mass fluxes of 200 and 500 kg/m^{2}s and for various heat flux levels.

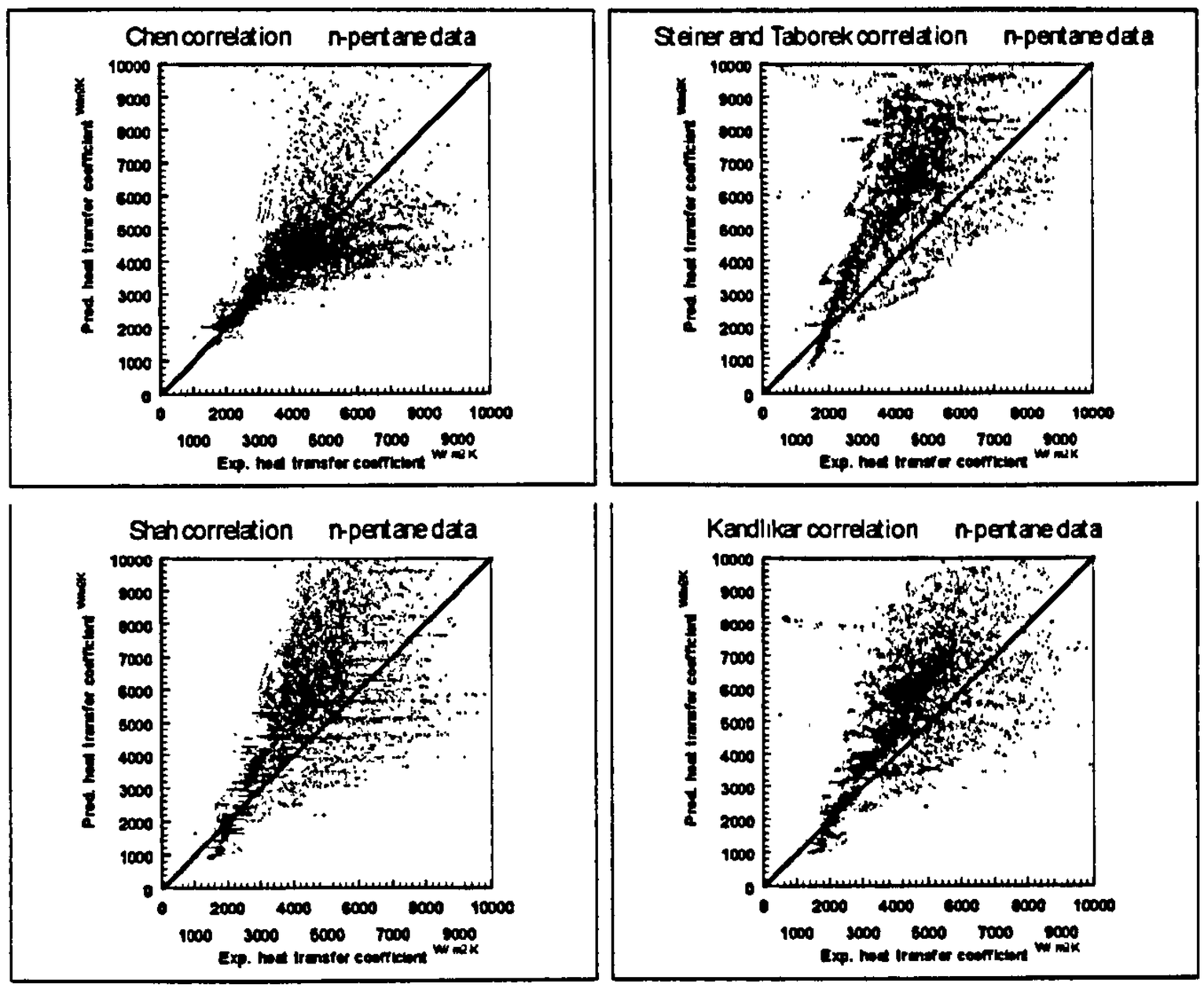


Figure 4.32: Predicted versus experimental heat transfer coefficients for n-pentane data (for the Chen, Steiner and Taborek, Shah and Kandlikar correlations).

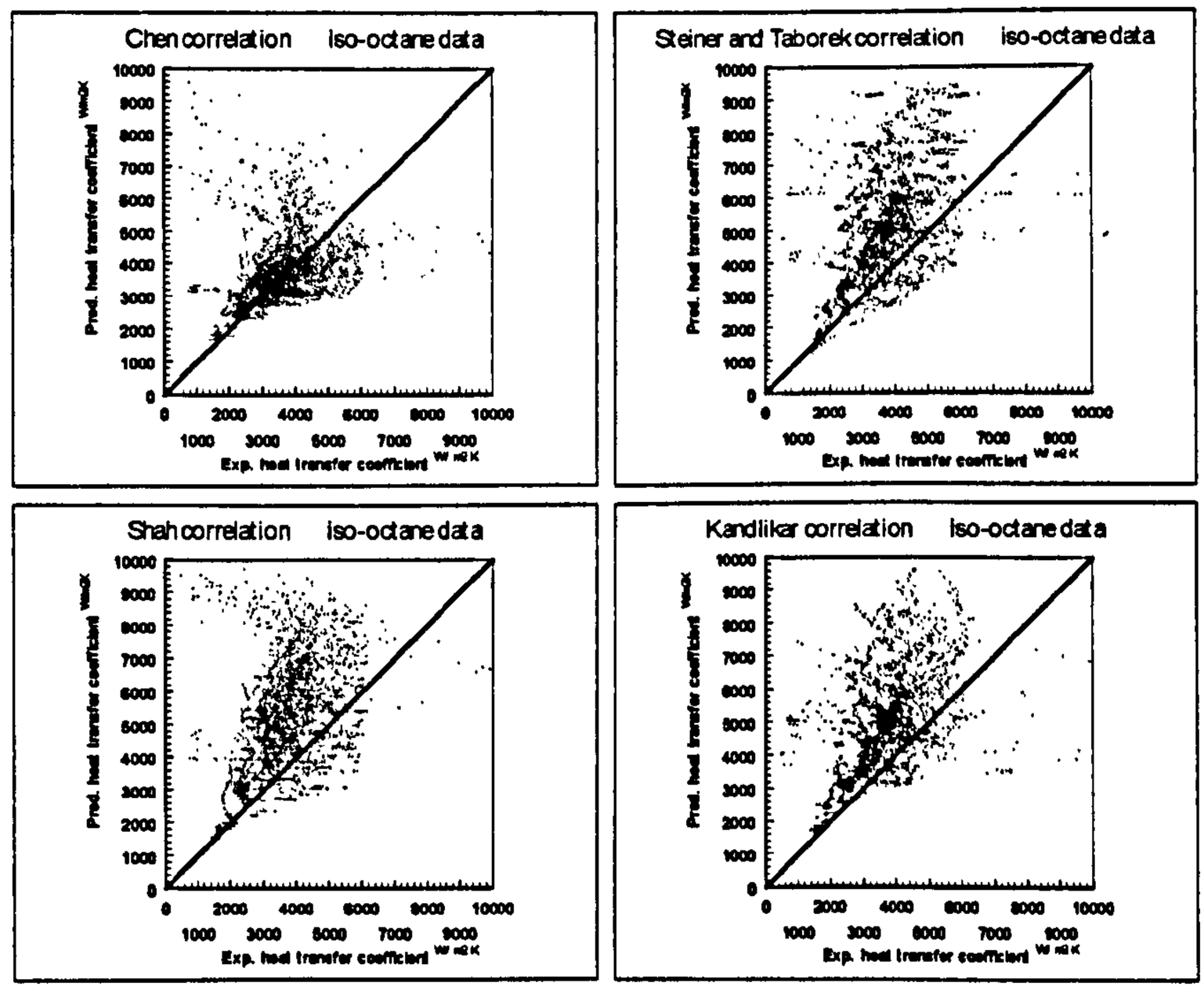


Figure 4.33: Predicted versus experimental heat transfer coefficients for iso-octane data (Chen, Steiner and Taborek, Shah and Kandlikar correlations).

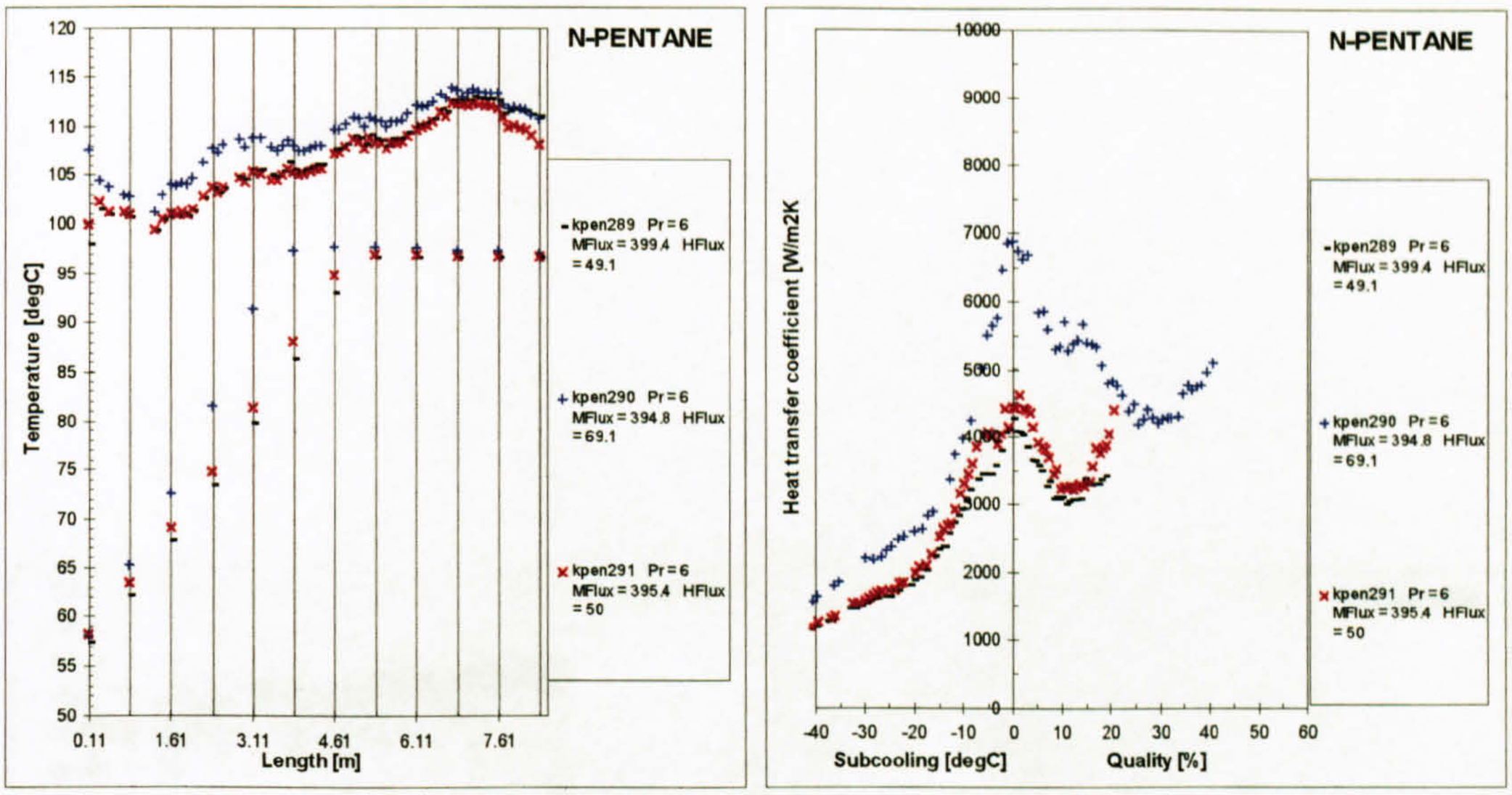


Figure 4.34: Hysteresis effects for change in heat flux.

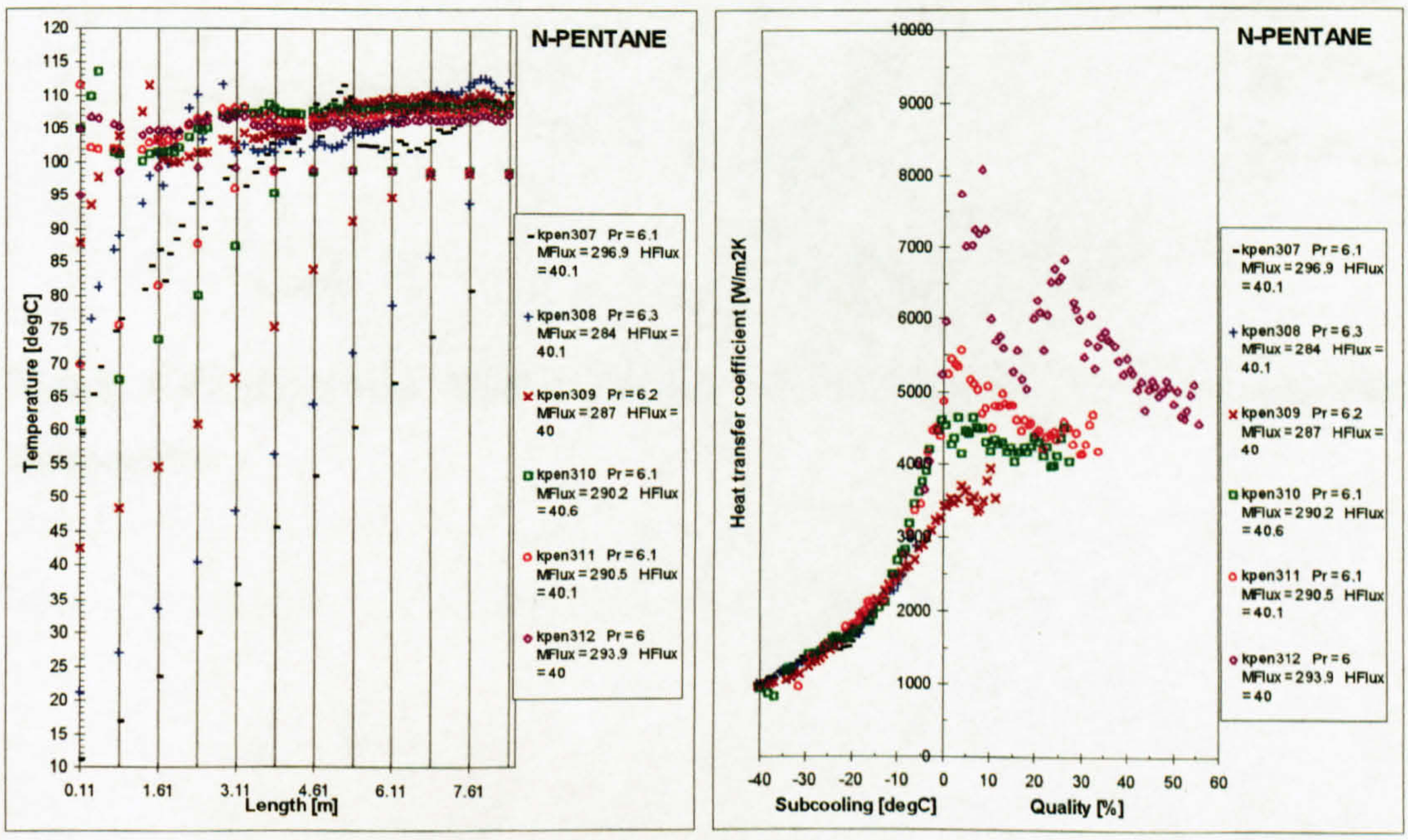


Figure 4.35: Hysteresis effects for change in inlet temperature: Increasing inlet temperature.

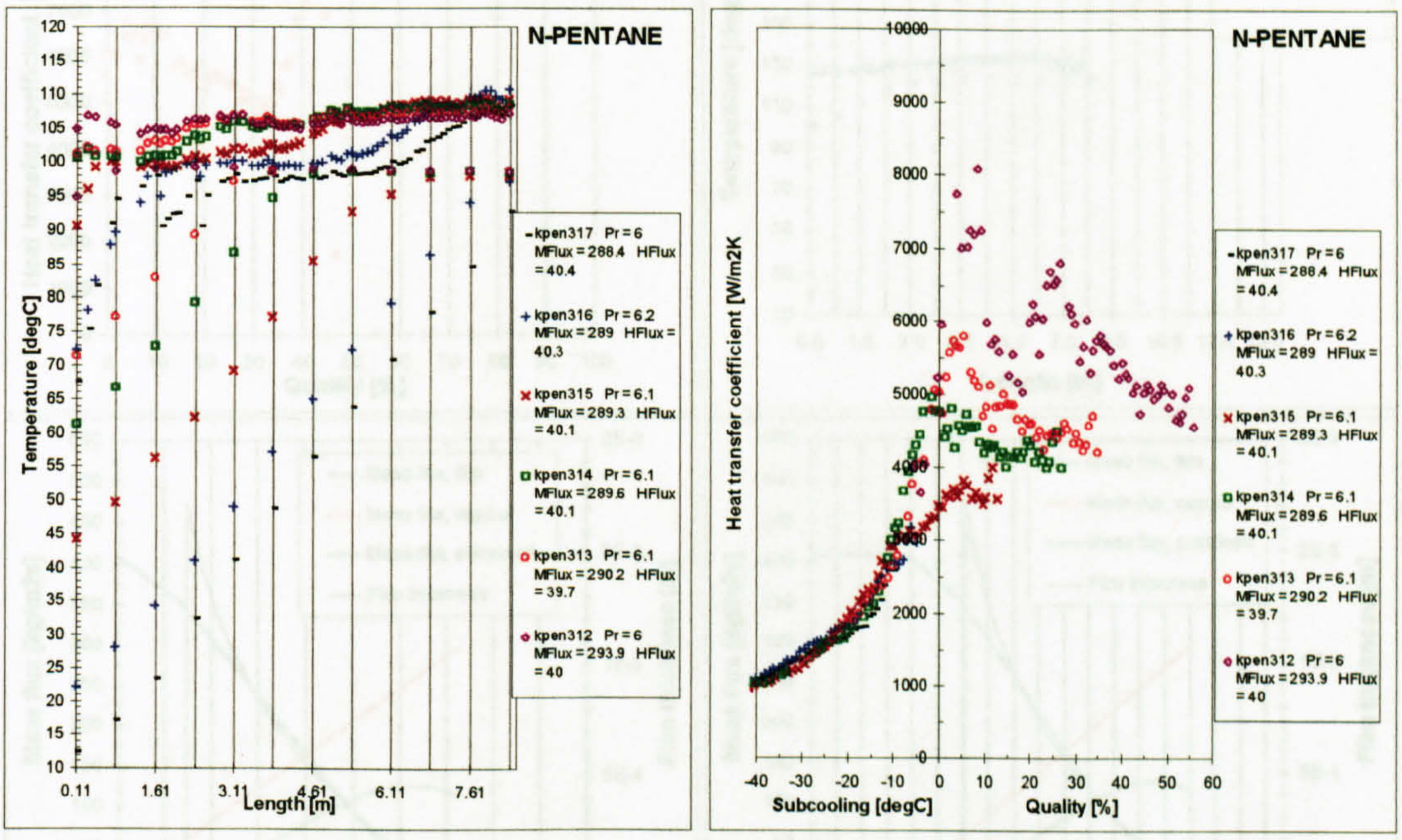


Figure 4.36: Hysteresis effects for change in inlet temperature: Decreasing inlet temperature.

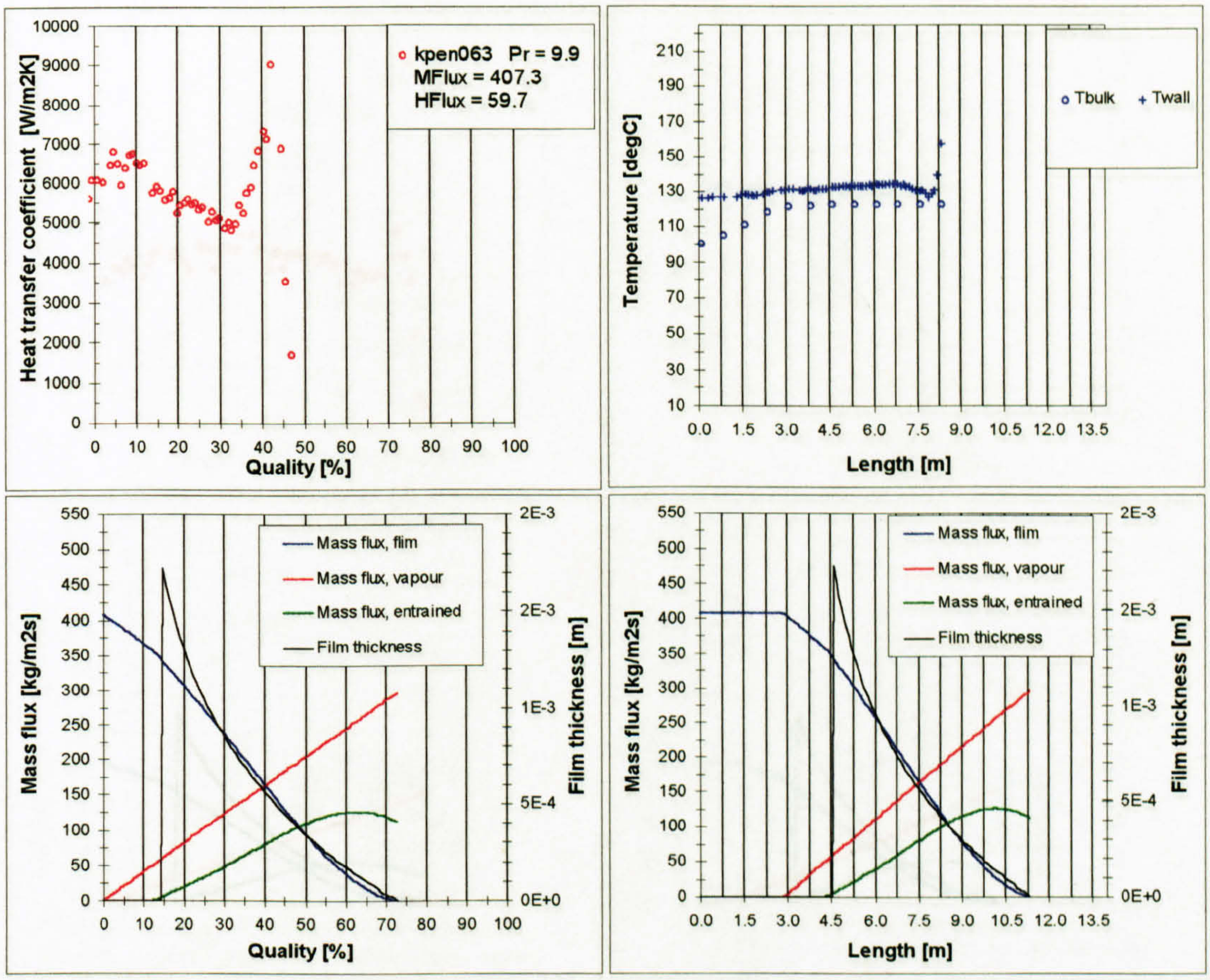


Figure 4.37: Measured heat transfer coefficient and wall temperature and calculated film parameters for a typical n-pentane dryout experiment.

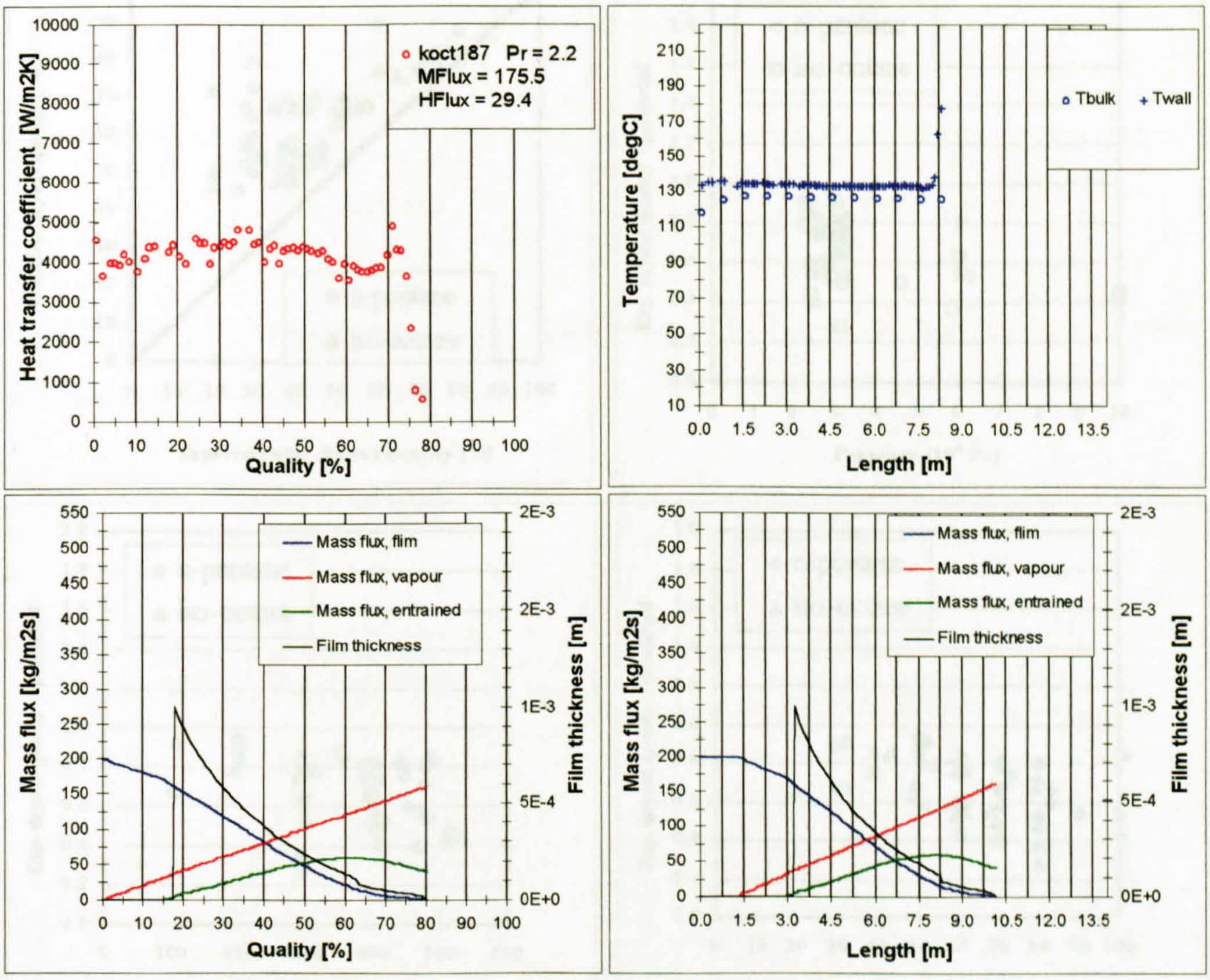


Figure 4.38: Measured heat transfer coefficient and wall temperature and calculated film parameters for a typical iso-octane dryout experiment.

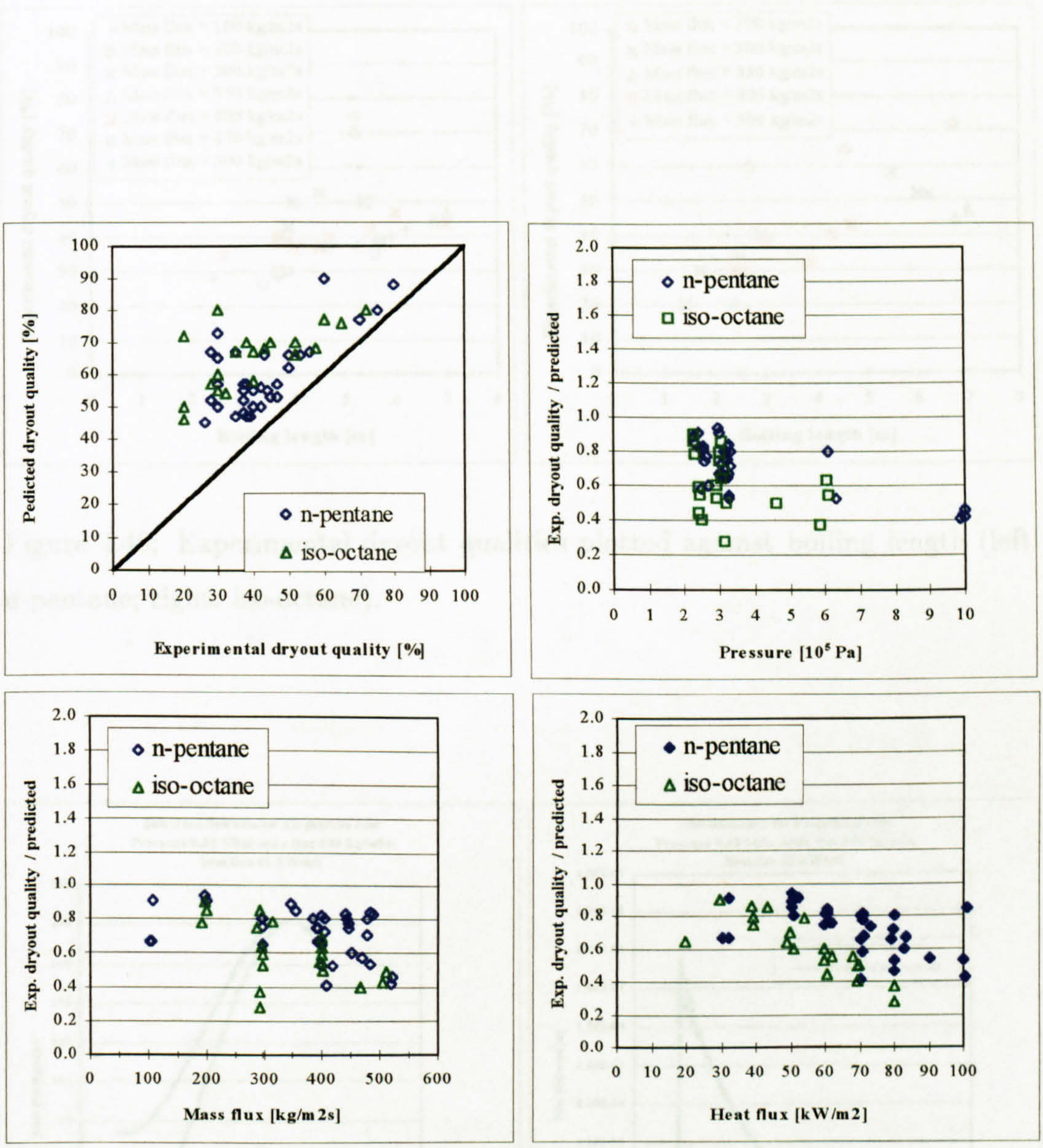


Figure 4.39: Comparisons of experimental dryout results with predictions from the GRAMP code.

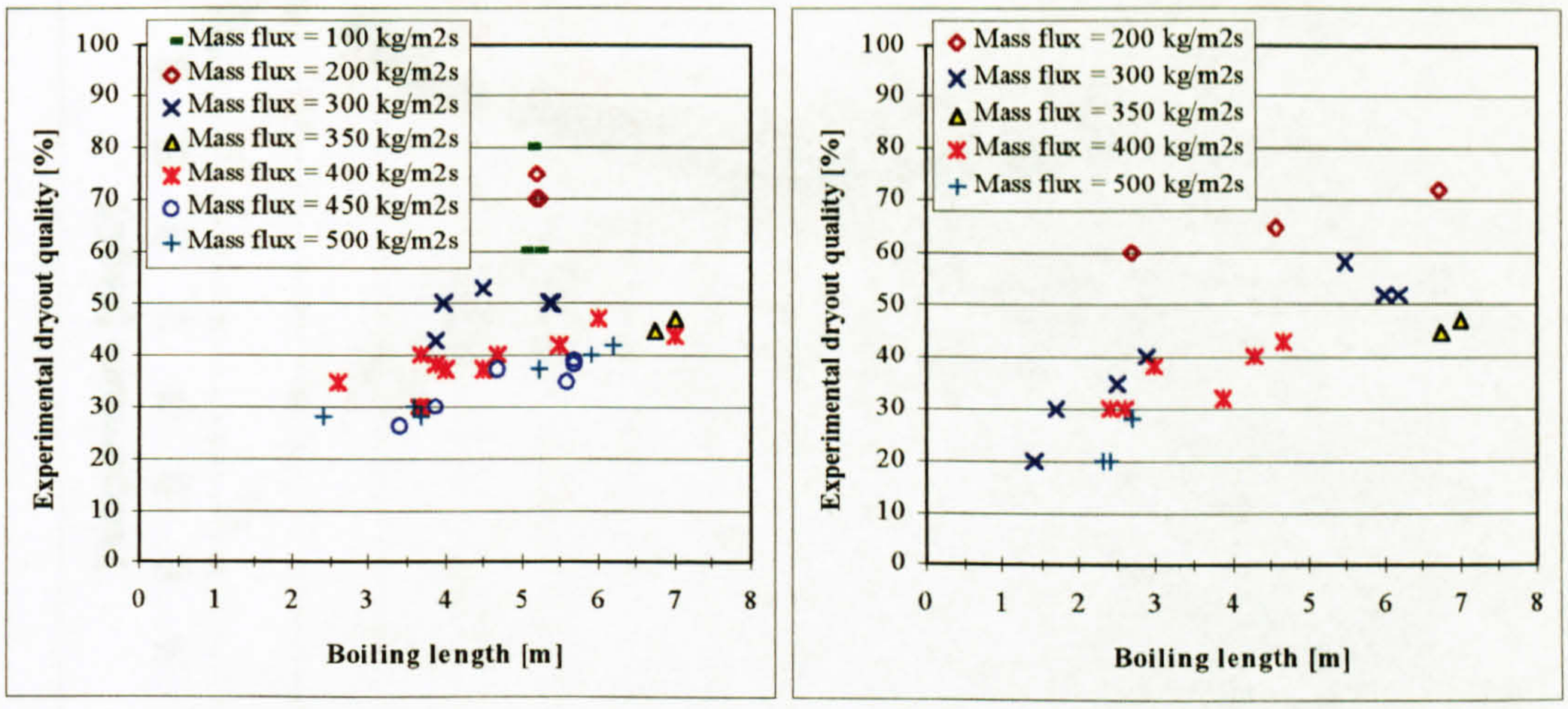


Figure 4.40: Experimental dryout qualities plotted against boiling length (left: n-pentane; right: iso-octane).

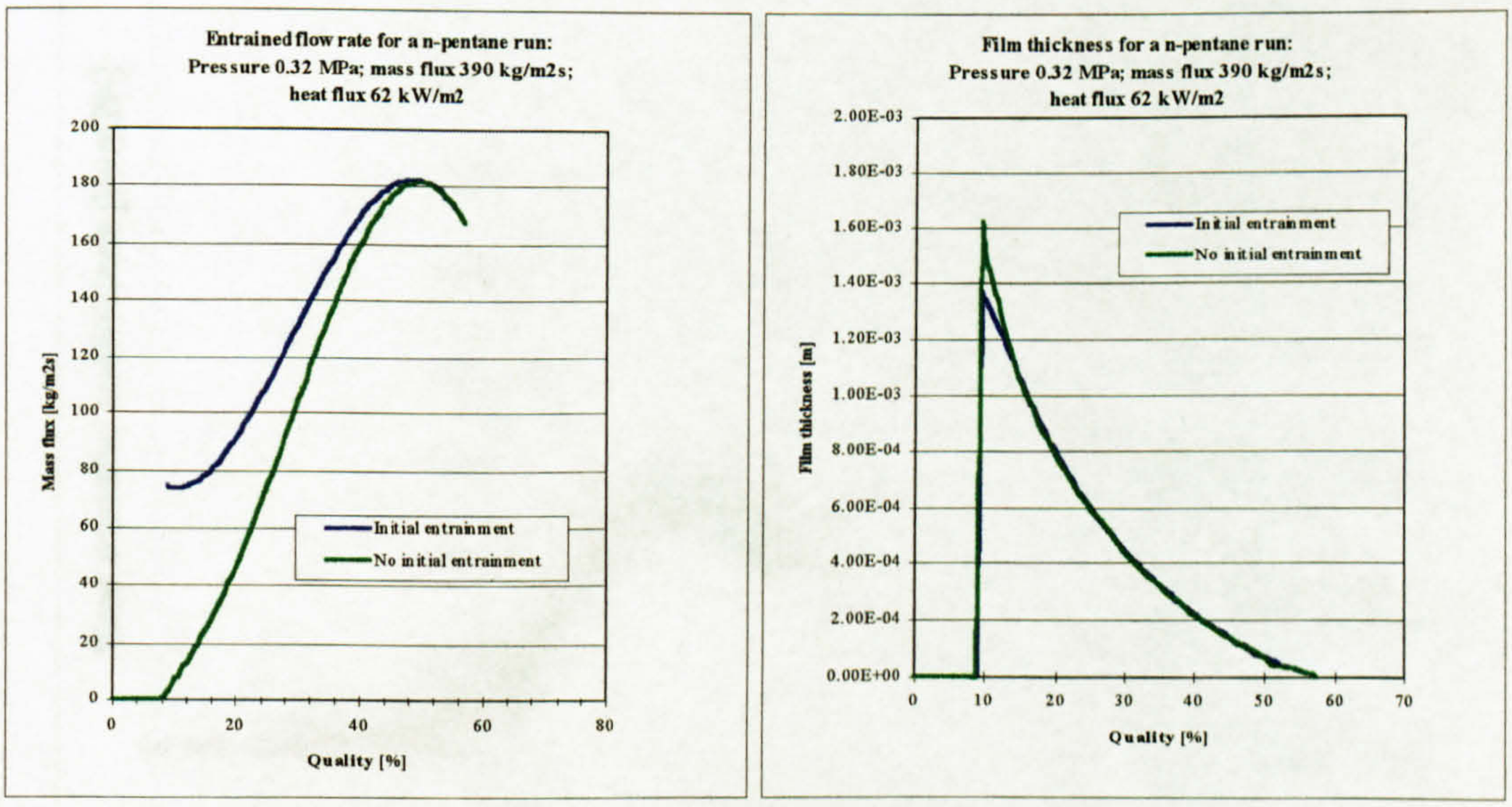
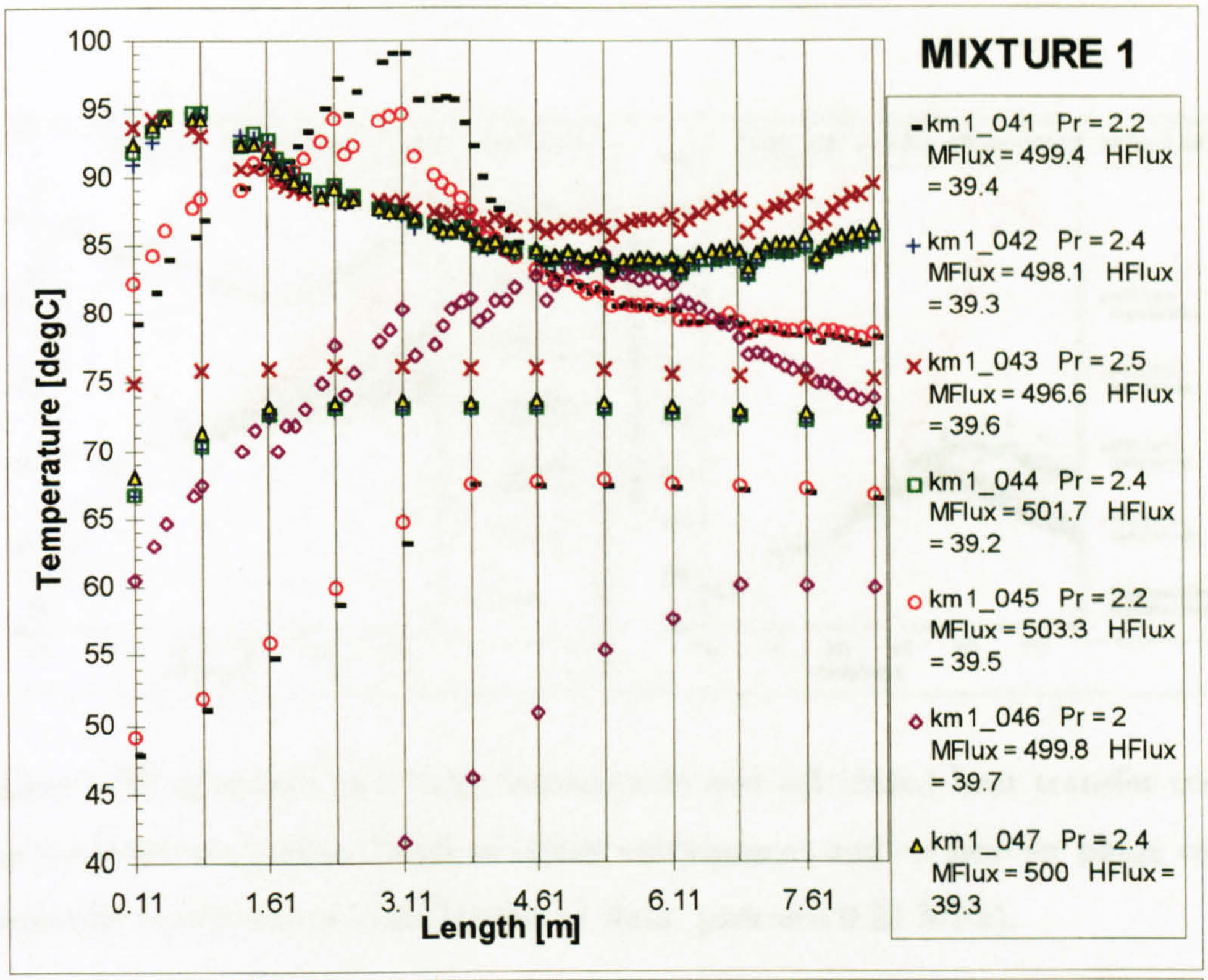


Figure 4.41: Comparison of entrainment and film thickness with and without initial entrainment at the onset of annular flow.



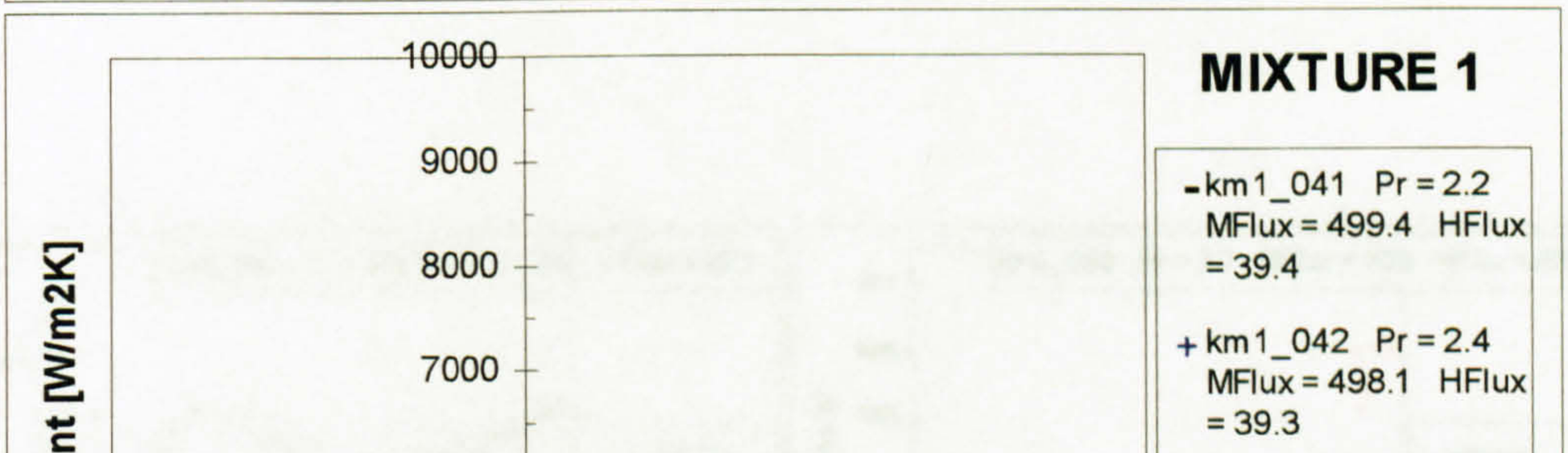


Figure 4.42: The effect of inlet temperature on the heat transfer coefficient for Mixture 1 at a pressure of 0.22 MPa, mass flux of 500 kg/m^{2}s and a heat flux of 40 kW/m^2.

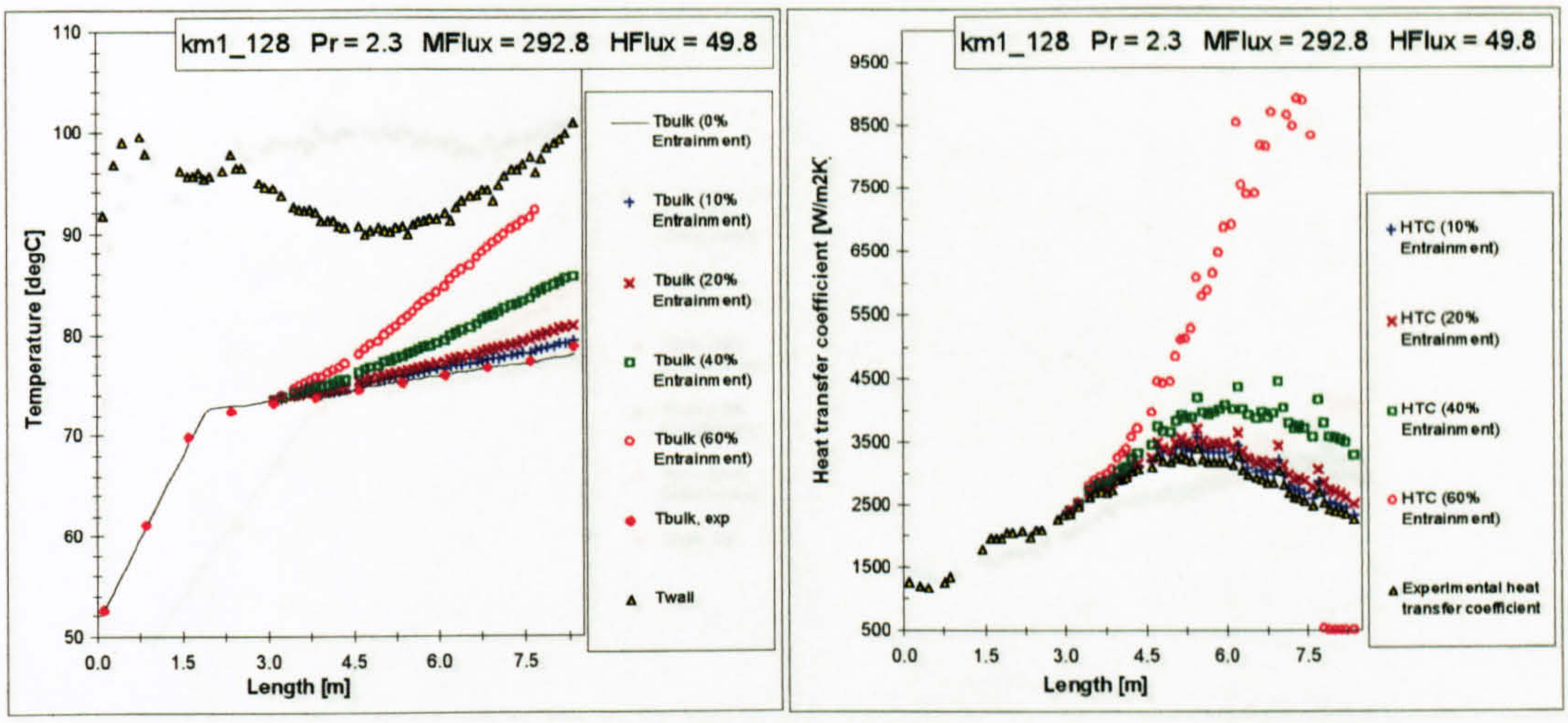


Figure 4.43: Interface and wall temperatures and calculated heat transfer coefficients based on various levels of initial entrainment and on heavier phase concentration in the liquid film (Mixture 1 data, pressure 0.23 MPa).

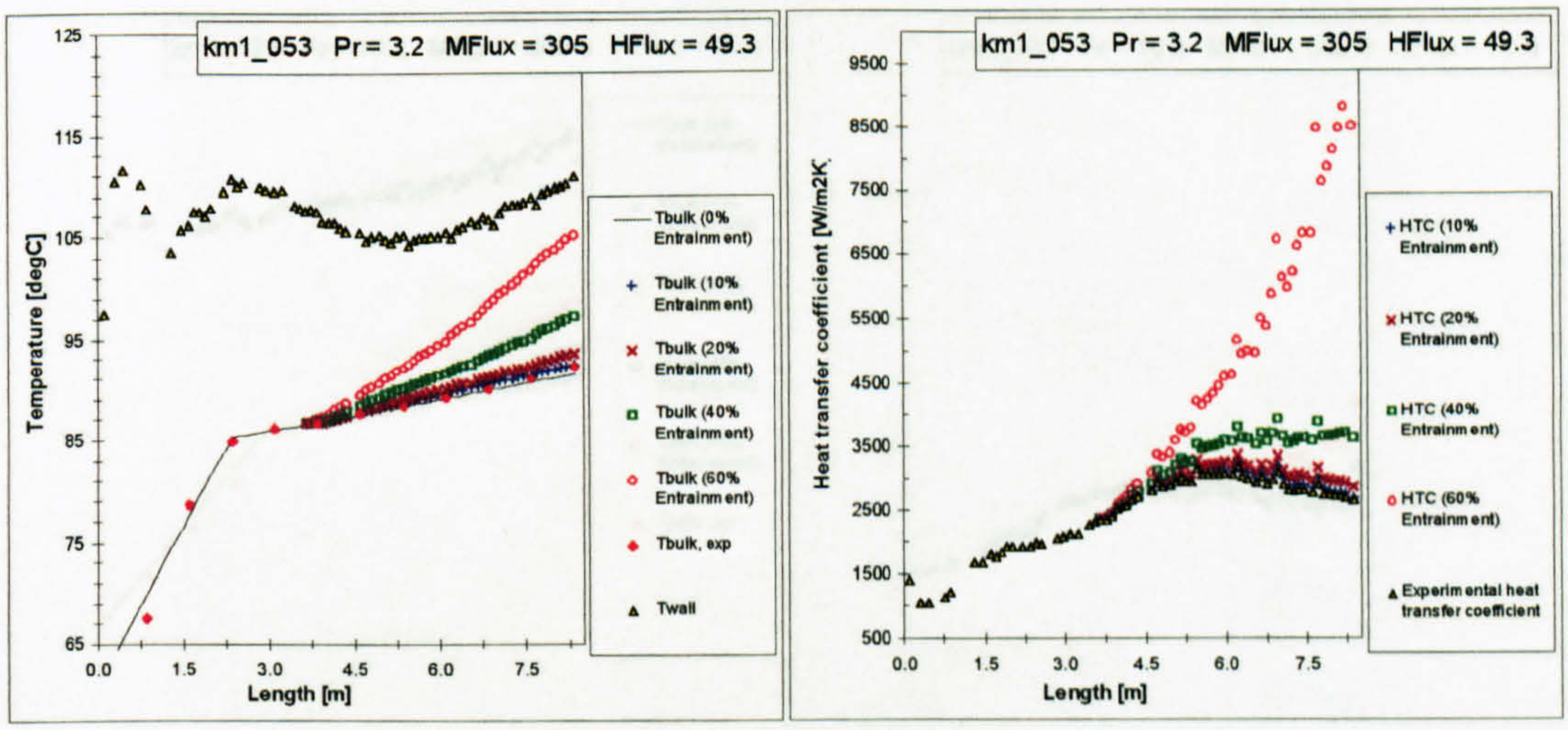


Figure 4.44: Interface and wall temperatures and calculated heat transfer coefficients based on various levels of initial entrainment and on heavier phase concentration in the liquid film (Mixture 1 data, pressure 0.32 MPa).

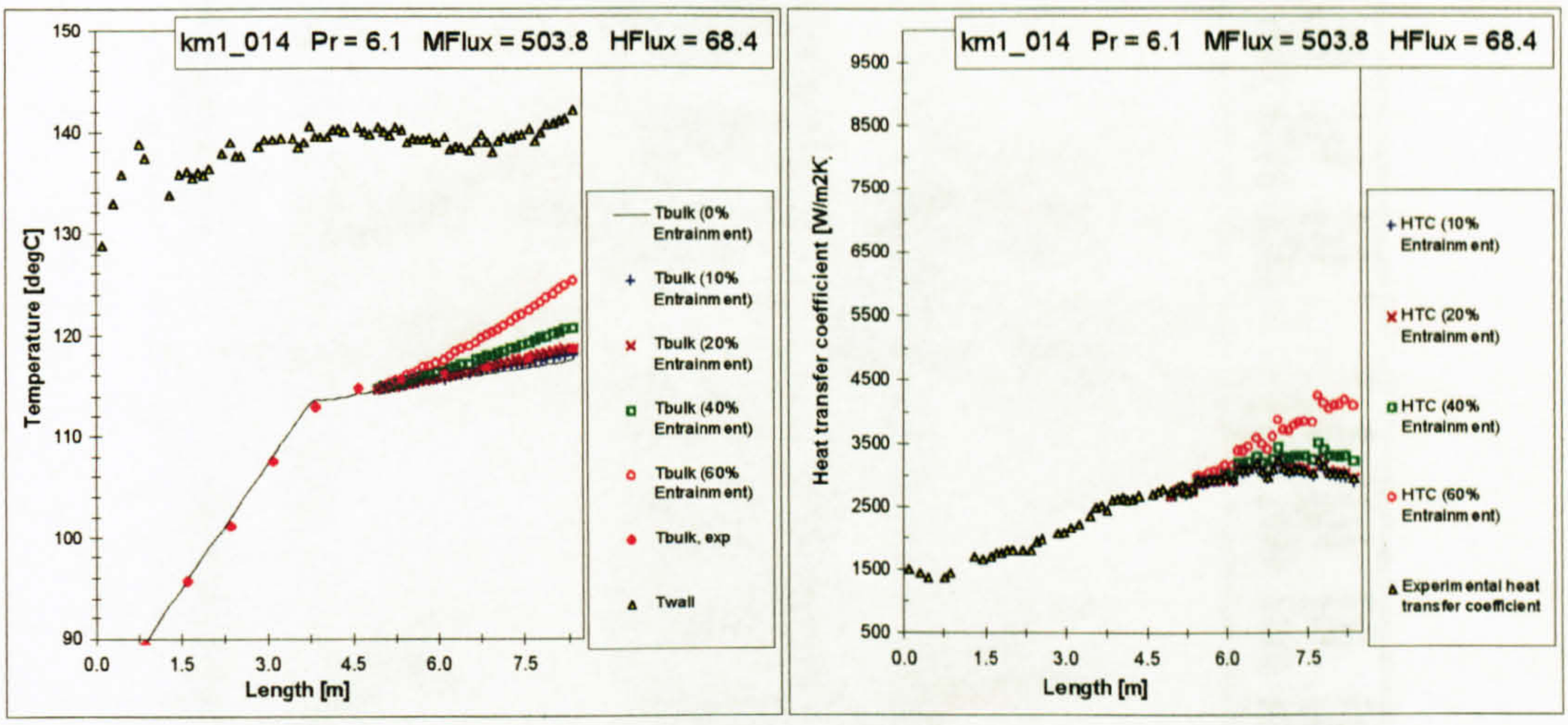


Figure 4.45: Interface and wall temperatures and calculated heat transfer coefficients based on various levels of initial entrainment and on heavier phase concentration in the liquid film (Mixture 1 data, pressure 0.61 MPa).

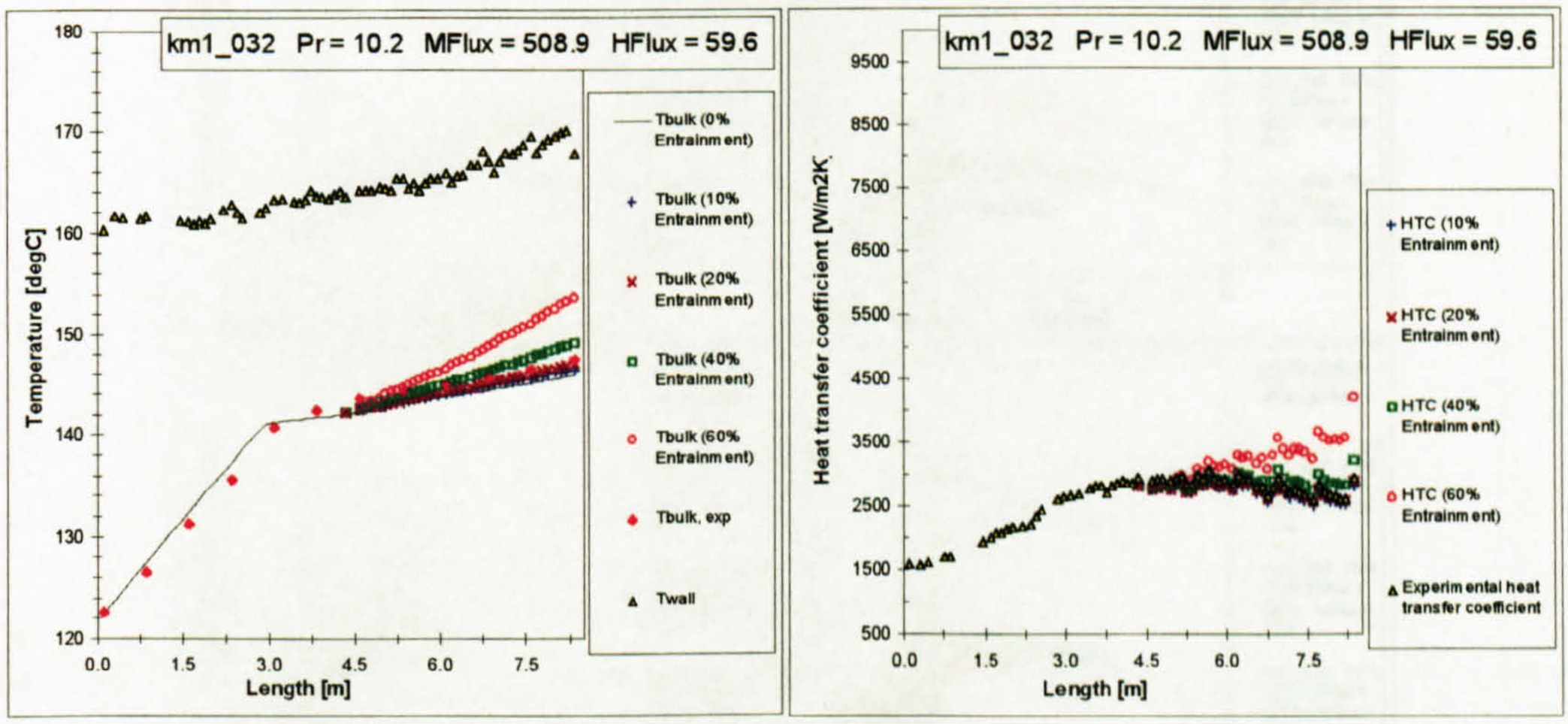


Figure 4.46: Interface and wall temperatures and calculated heat transfer coefficients based on various levels of initial entrainment and on heavier phase concentration in the liquid film (Mixture 1 data, pressure 1.02 MPa).

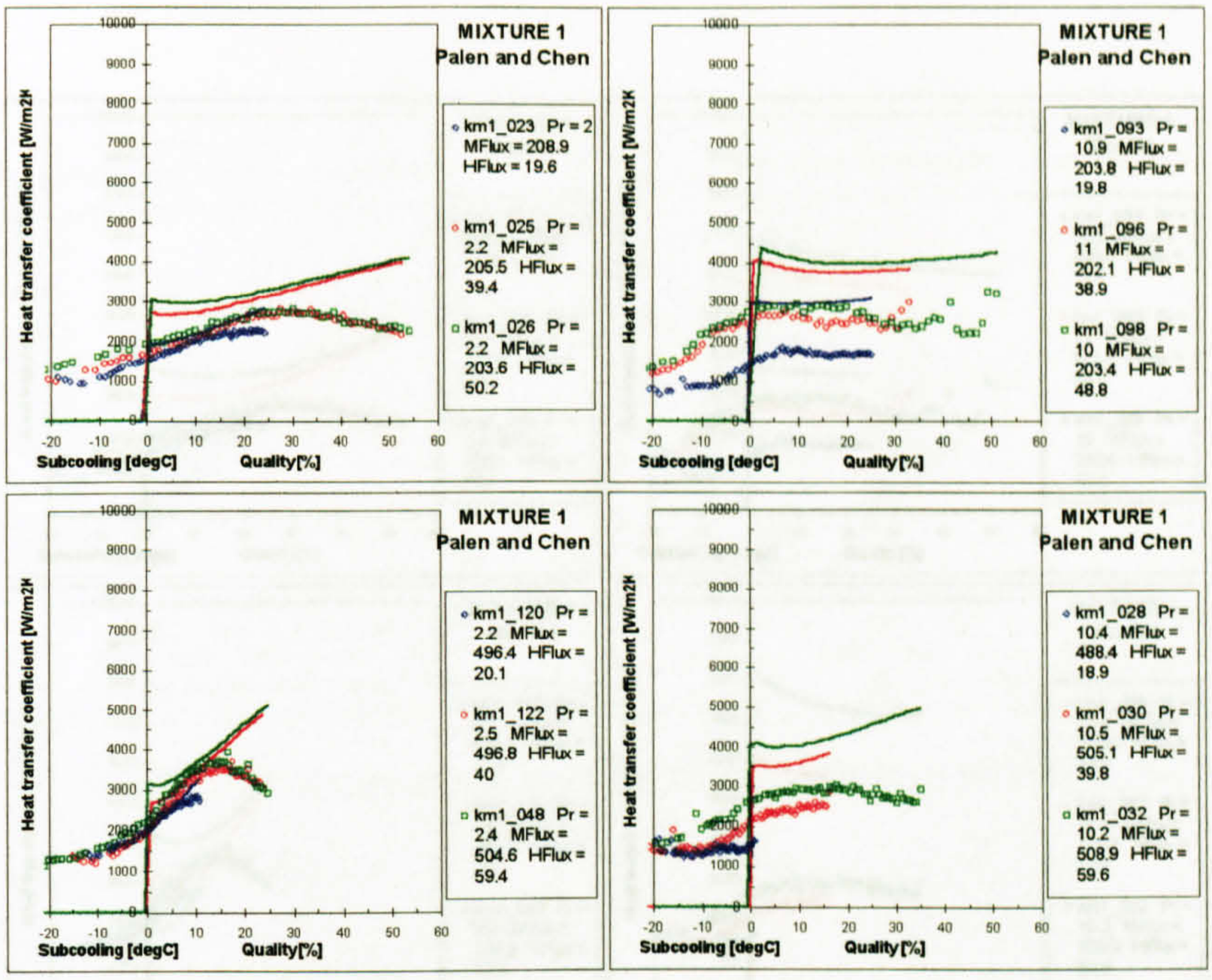


Figure 4.47: Palen (1983) correlation compared with Mixture 1 data for pressures of 0.23 and 1.0 MPa, mass fluxes of 200 and 500 kg/m^{2}s for various heat flux levels.

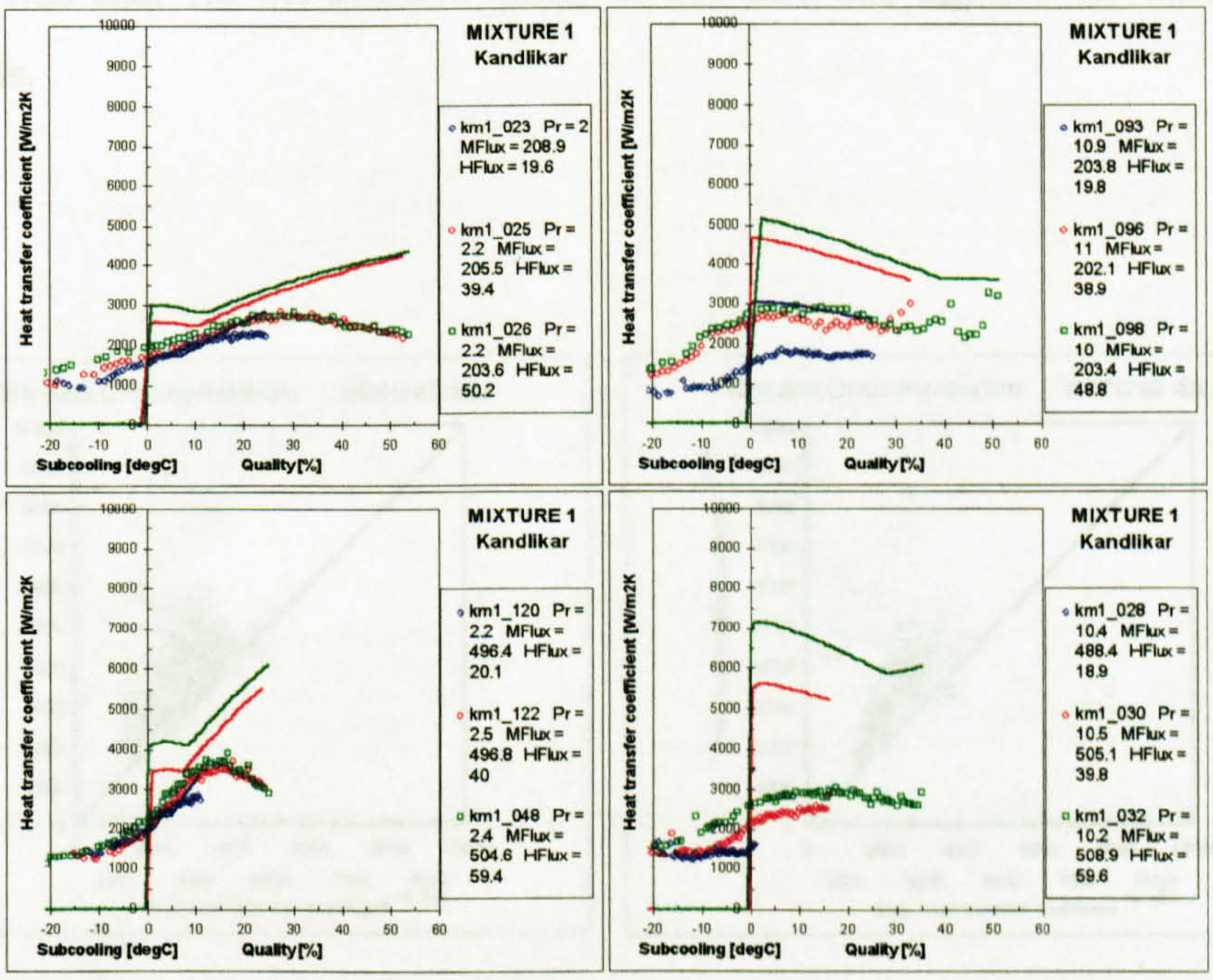


Figure 4.48: Kandlikar (1991) correlation compared with Mixture 1 data for pressures of 0.23 and 1.0 MPa, mass fluxes of 200 and 500 kg/m^{2}s for various heat flux levels.

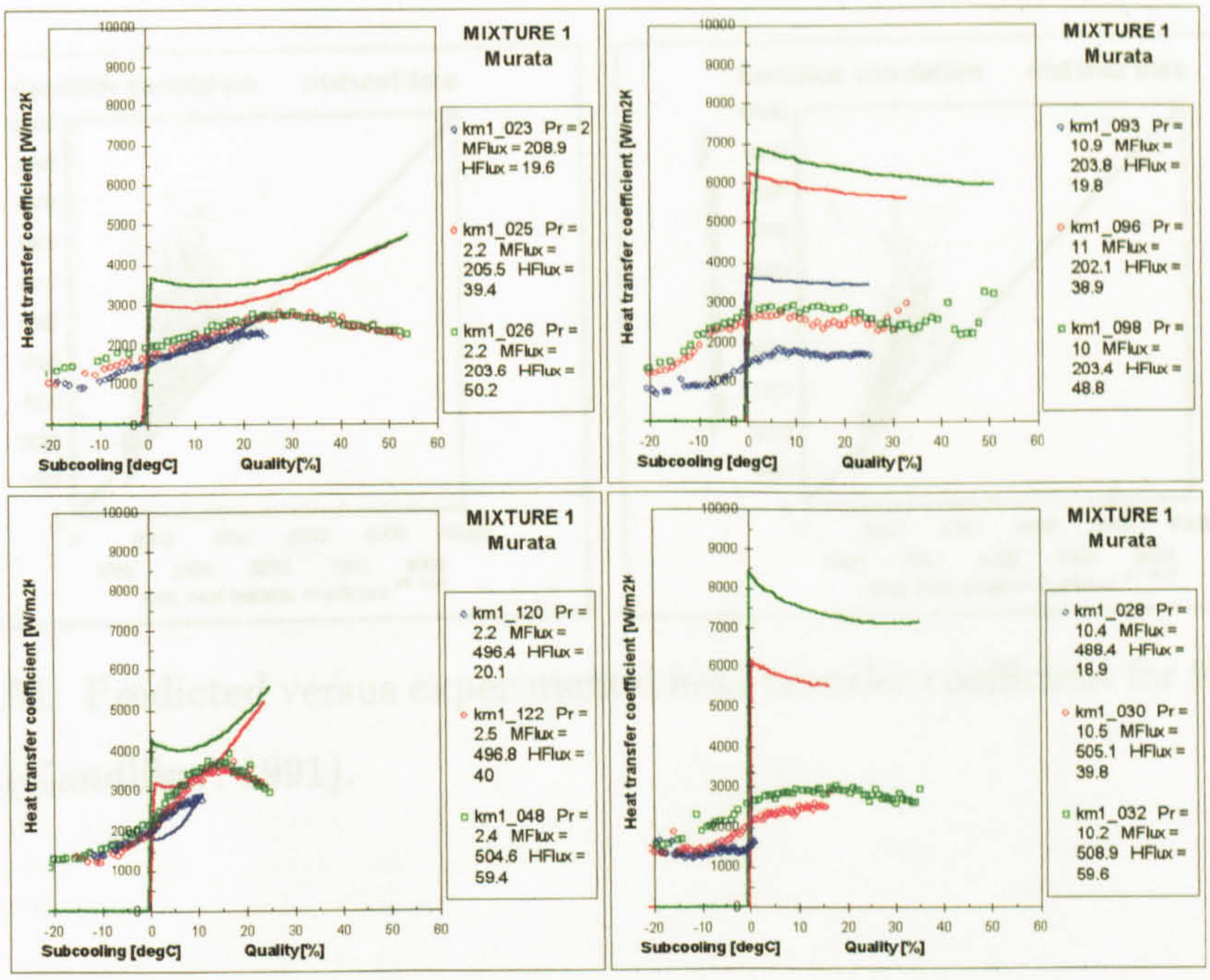


Figure 4.49: Murata (1993) correlation compared with Mixture 1 data for pressures of 0.23 and 1.0 MPa, mass fluxes of 200 and 500 kg/m^{2}s for various heat flux levels.

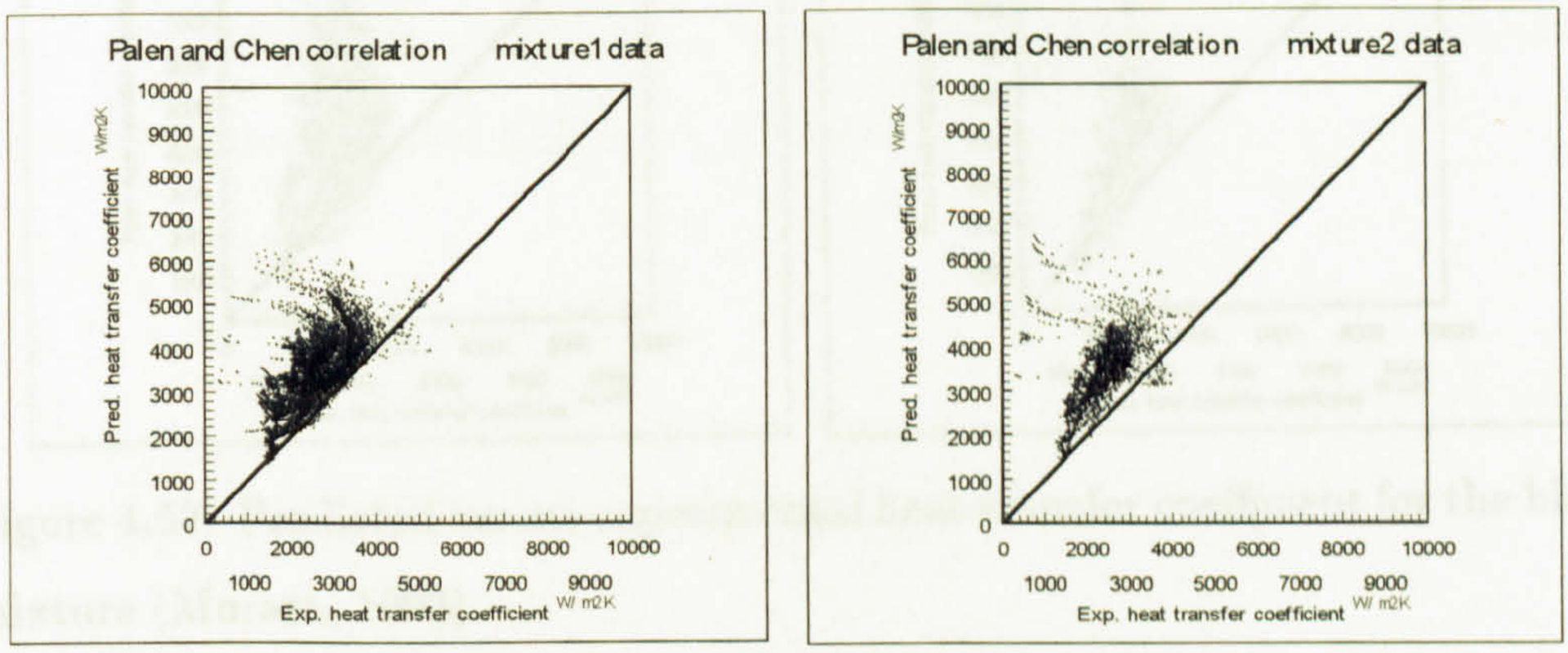


Figure 4.50: Predicted versus experimental heat transfer coefficient for the binary mixture (Palen, 1983).

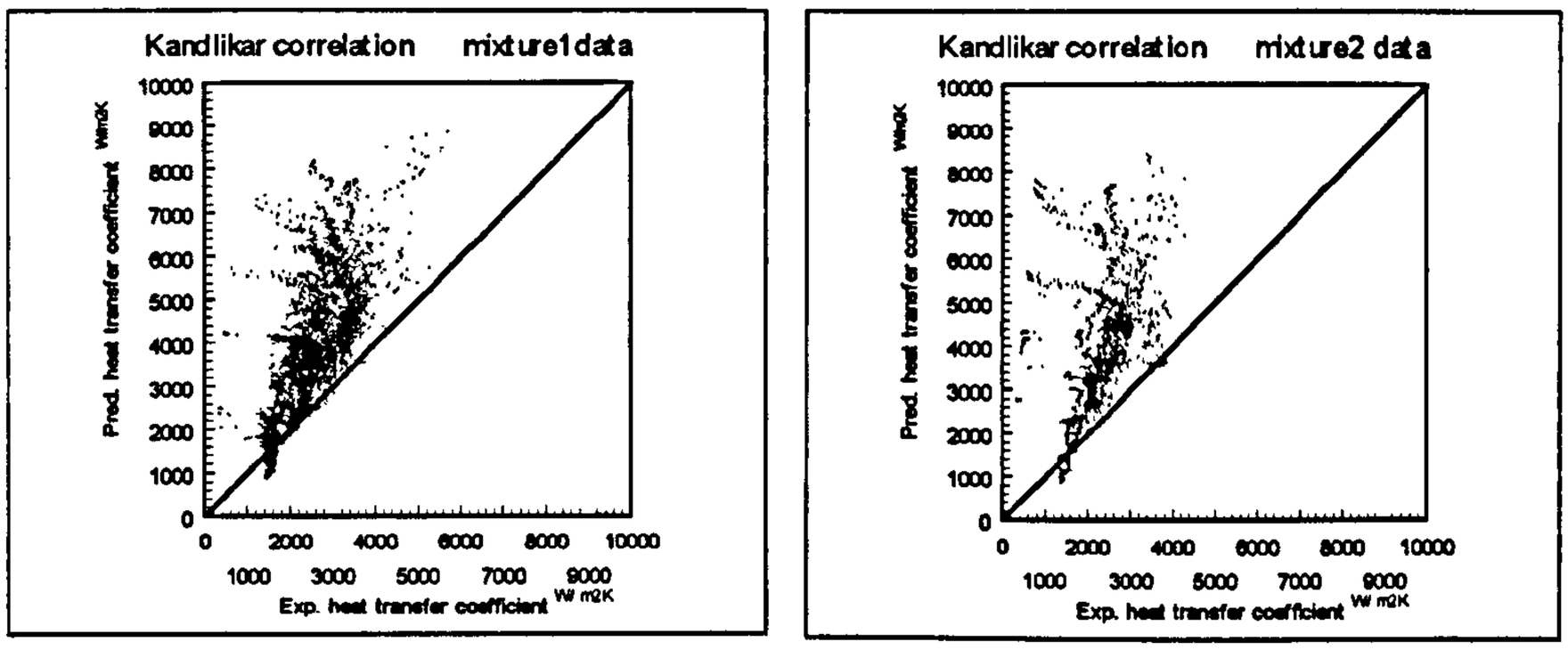


Figure 4.51: Predicted versus experimental heat transfer coefficient for the binary mixture (Kandlikar, 1991).

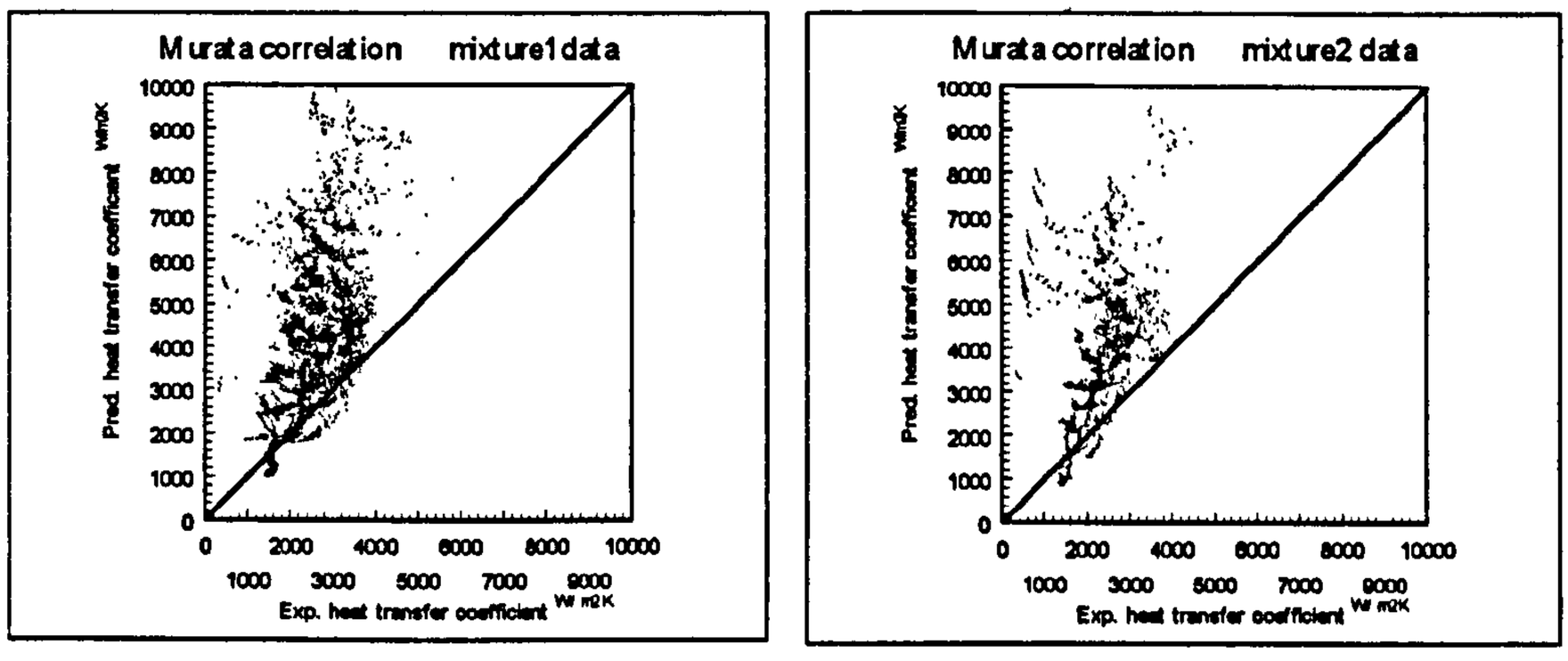


Figure 4.52: Predicted versus experimental heat transfer coefficient for the binary mixture (Murata, 1993).

Pressure: 0.23 [MPa] Mass flux: 100 [kg/m²s]	Pressure: 0.3 [MPa] Mass flux: 100 [kg/m²s]	Pressure: 0.6 [MPa] Mass flux: 100 [kg/m²s]	Pressure: 1.0 [MPa] Mass flux: 100 [kg/m²s]
Pressure: 0.23 [MPa] Mass flux: 200 [kg/m²s]	Pressure: 0.3 [MPa] Mass flux: 200 [kg/m²s]	Pressure: 0.6 [MPa] Mass flux: 200 [kg/m²s]	Pressure: 1.0 [MPa] Mass flux: 200 [kg/m²s]
Pressure: 0.23 [MPa] Mass flux: 300 [kg/m²s]	Pressure: 0.3 [MPa] Mass flux: 300 [kg/m²s]	Pressure: 0.6 [MPa] Mass flux: 300 [kg/m²s]	Pressure: 1.0 [MPa] Mass flux: 300 [kg/m²s]
Pressure: 0.23 [MPa] Mass flux: 500 [kg/m²s]	Pressure: 0.3 [MPa] Mass flux: 500 [kg/m²s]	Pressure: 0.6 [MPa] Mass flux: 500 [kg/m²s]	Pressure: 1.0 [MPa] Mass flux: 500 [kg/m²s]

Figure 4.53: Operating conditions for boiling experiments as used in the following charts of the main series, Figures 4.54 to 4.83.

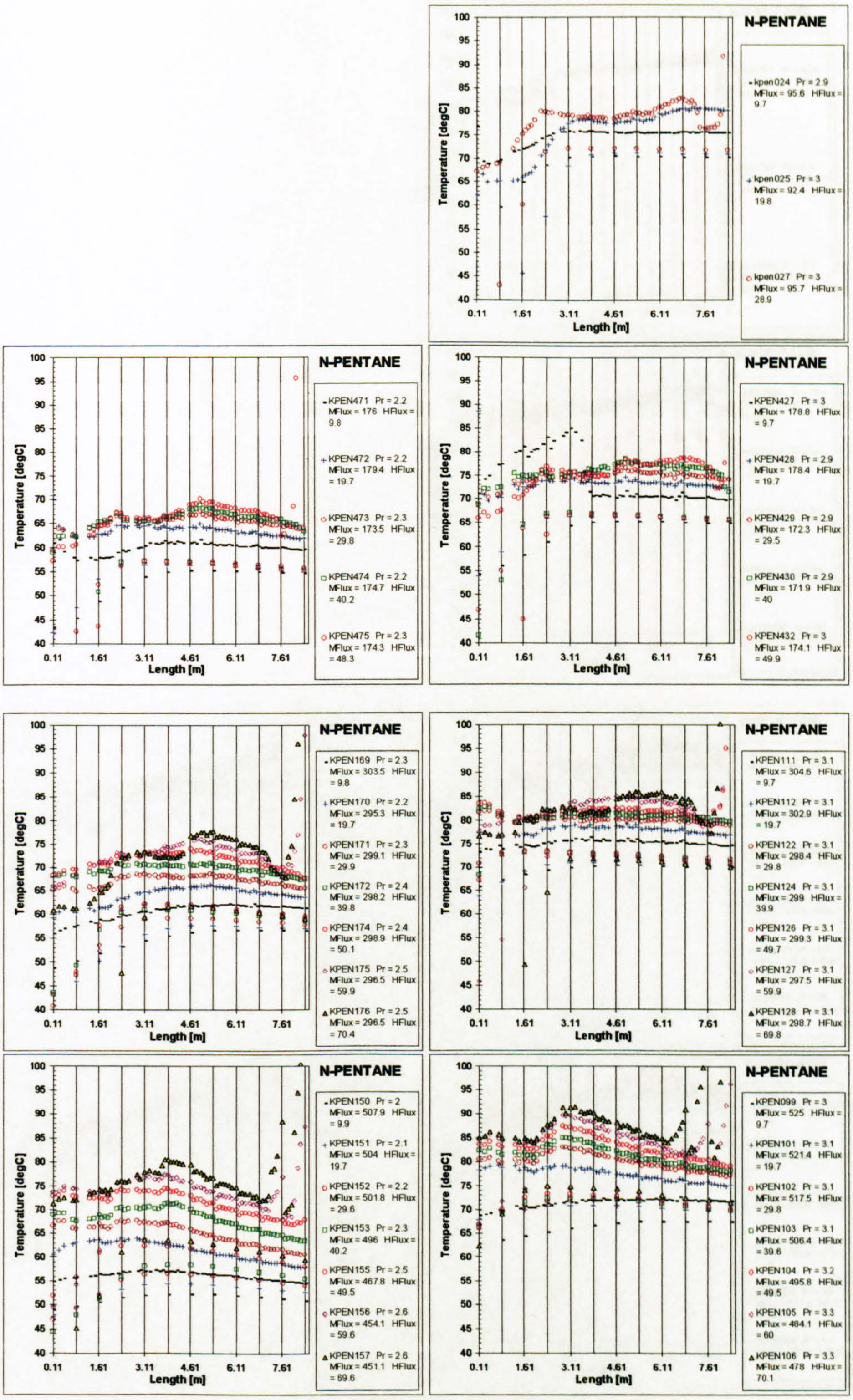


Figure 4.54: Temperature profiles plotted against tube length for the n-pentane boiling experiments at a pressure of 0.23 and 0.3 MPa.

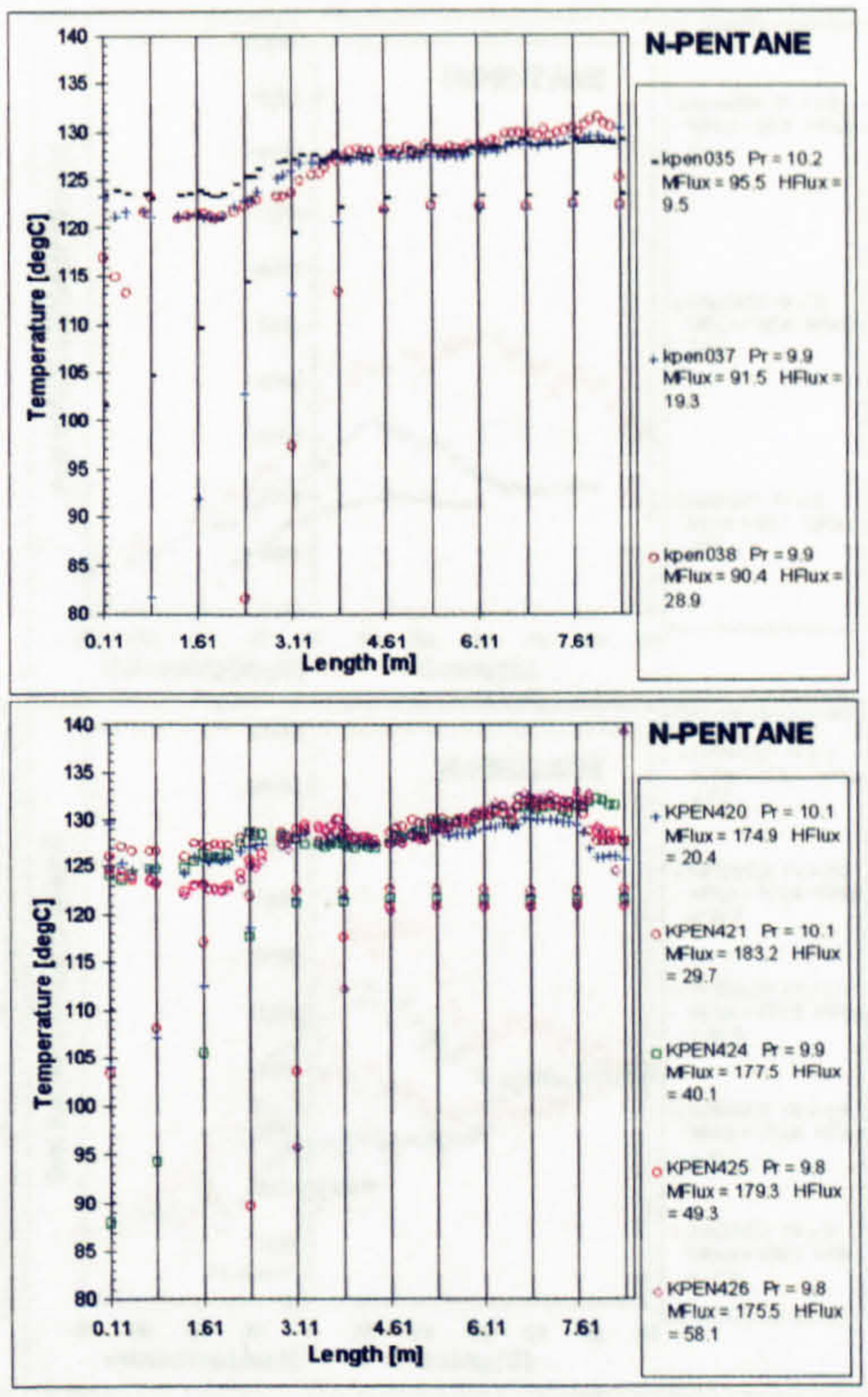


Figure 4.55: Temperature profiles plotted against tube length for the n-pentane boiling experiments at a pressure of 0.6 and 1 MPa.

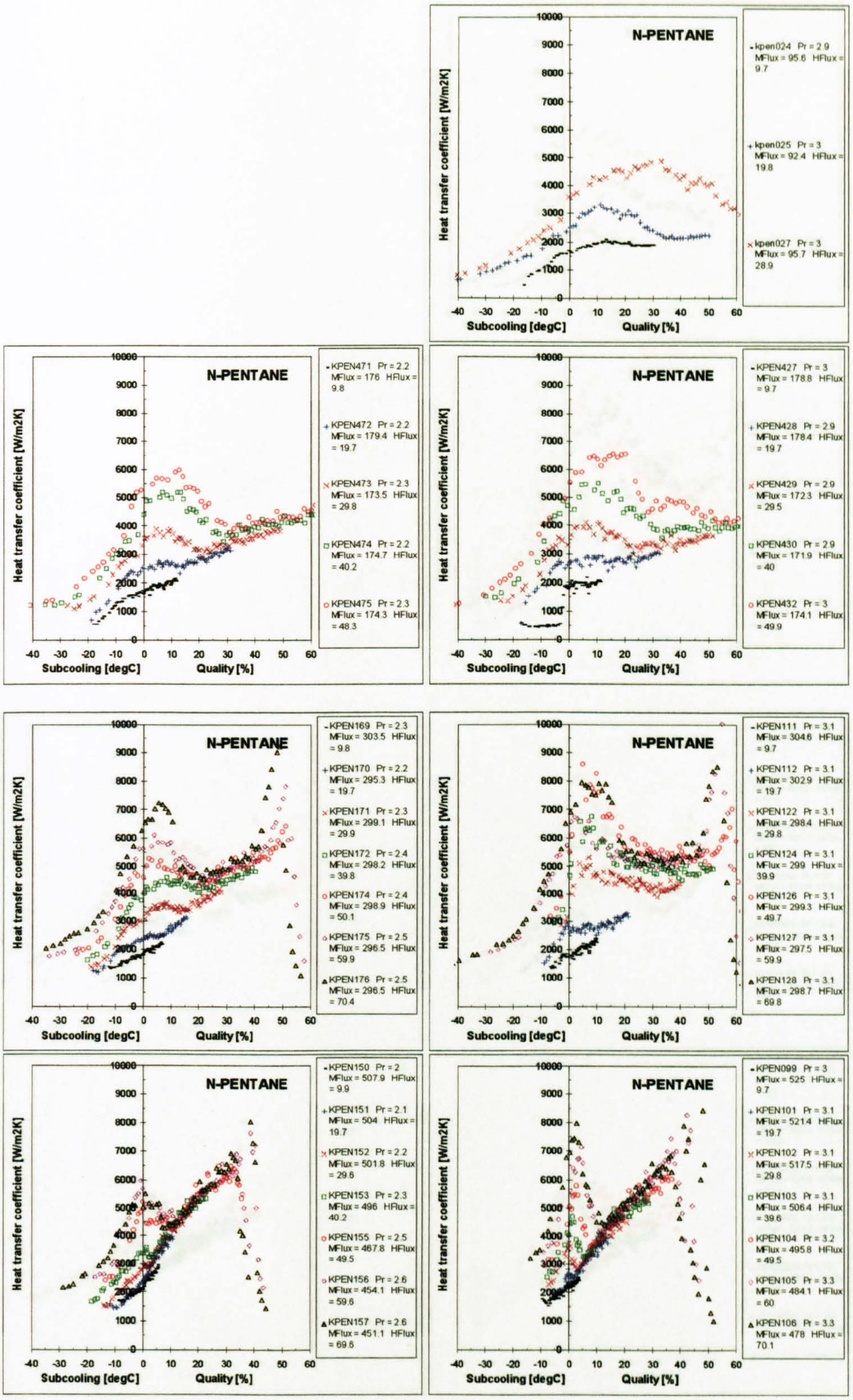


Figure 4.56: Heat transfer coefficients plotted against quality for the n-pentane boiling experiments at a pressure of 0.23 and 0.3 MPa.

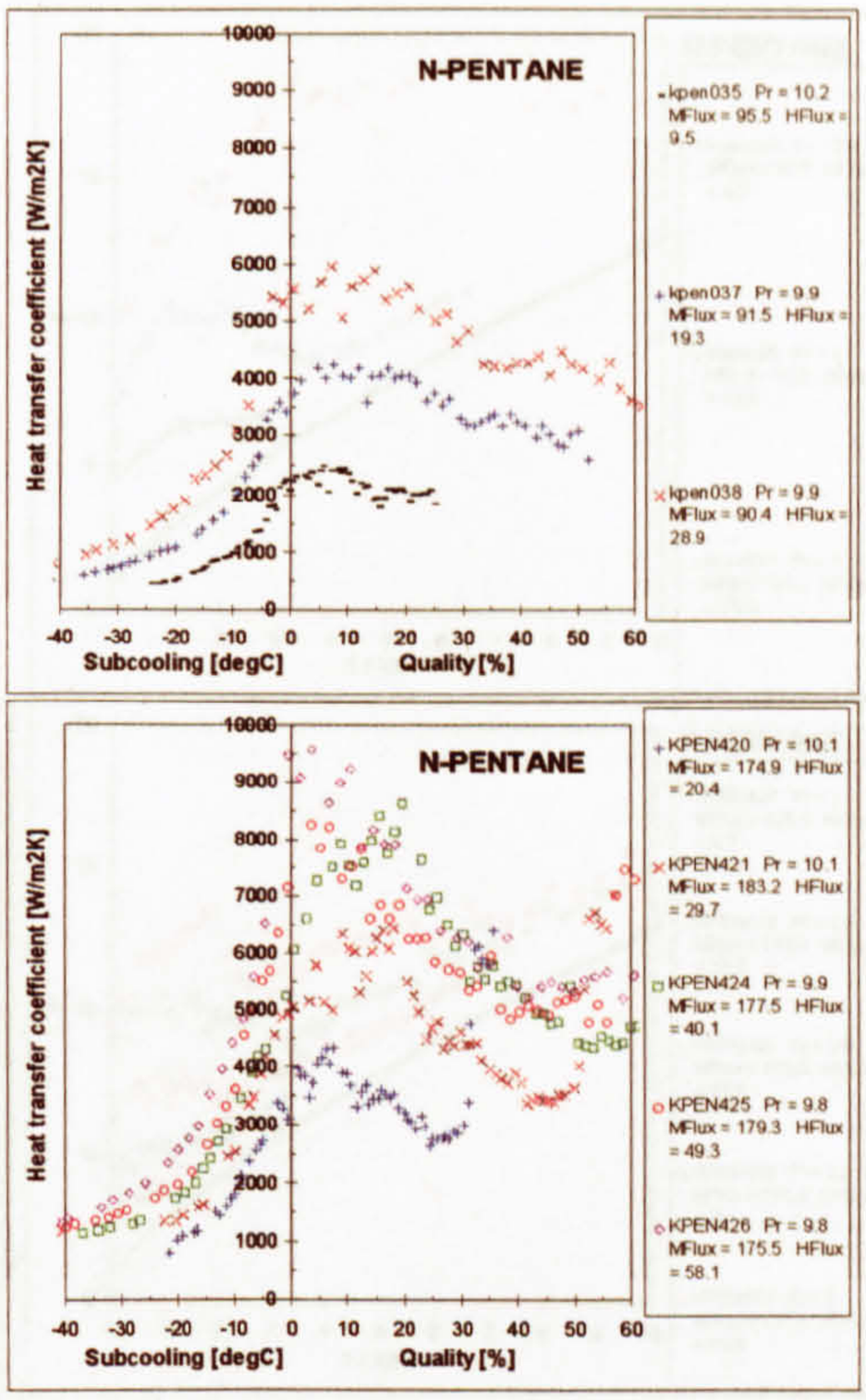
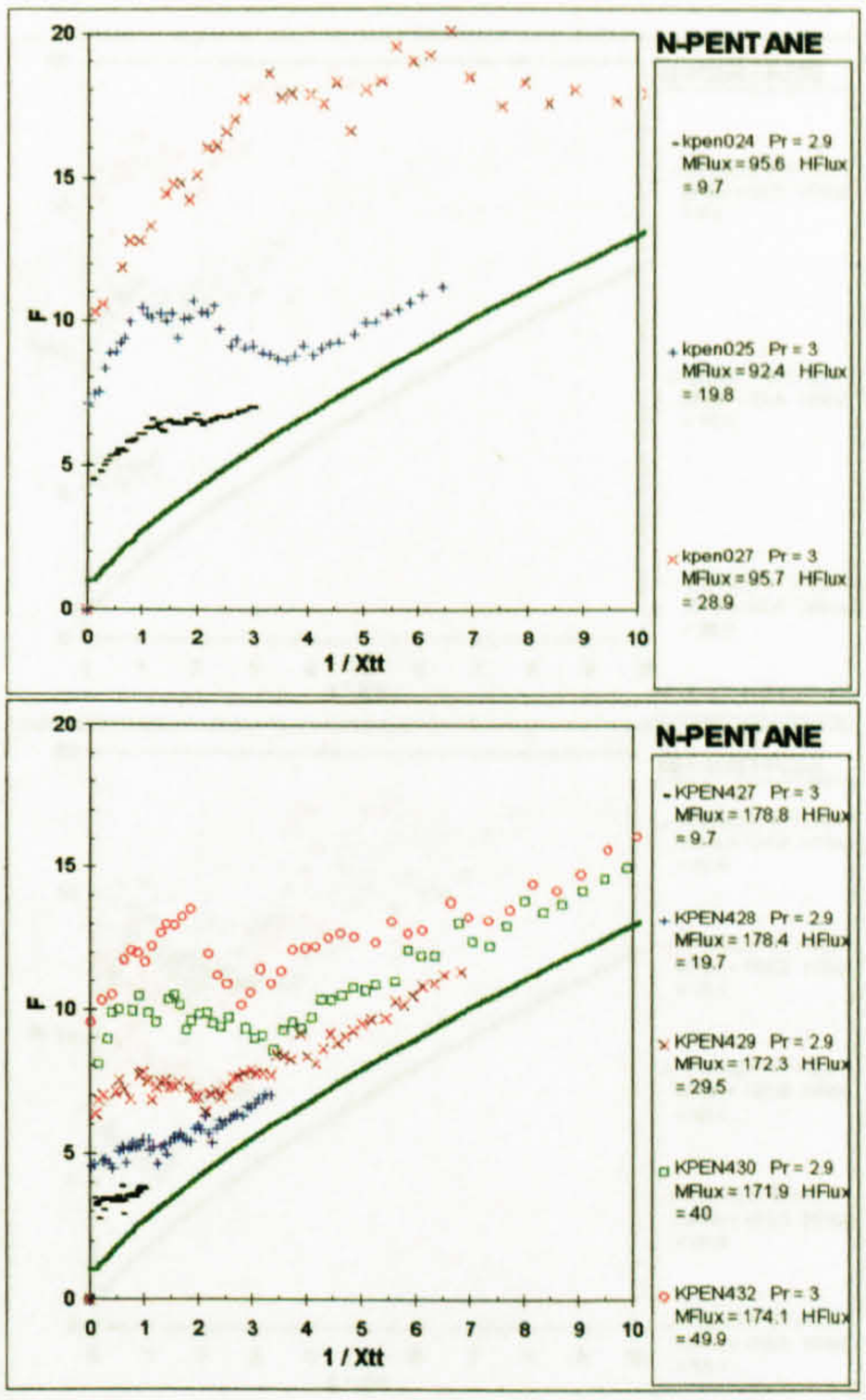
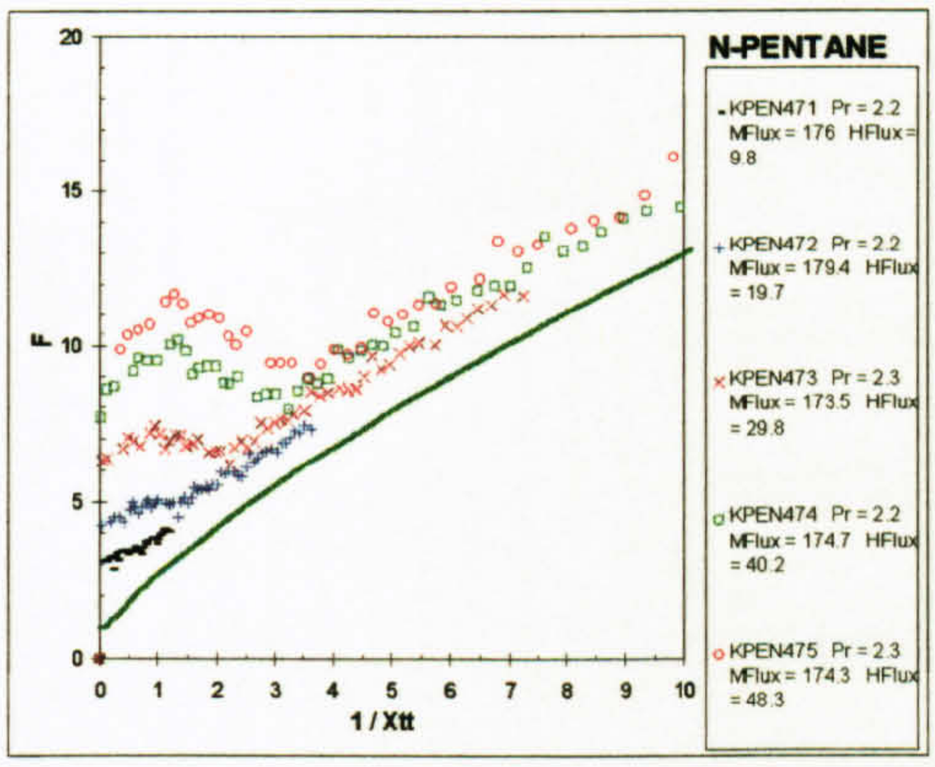
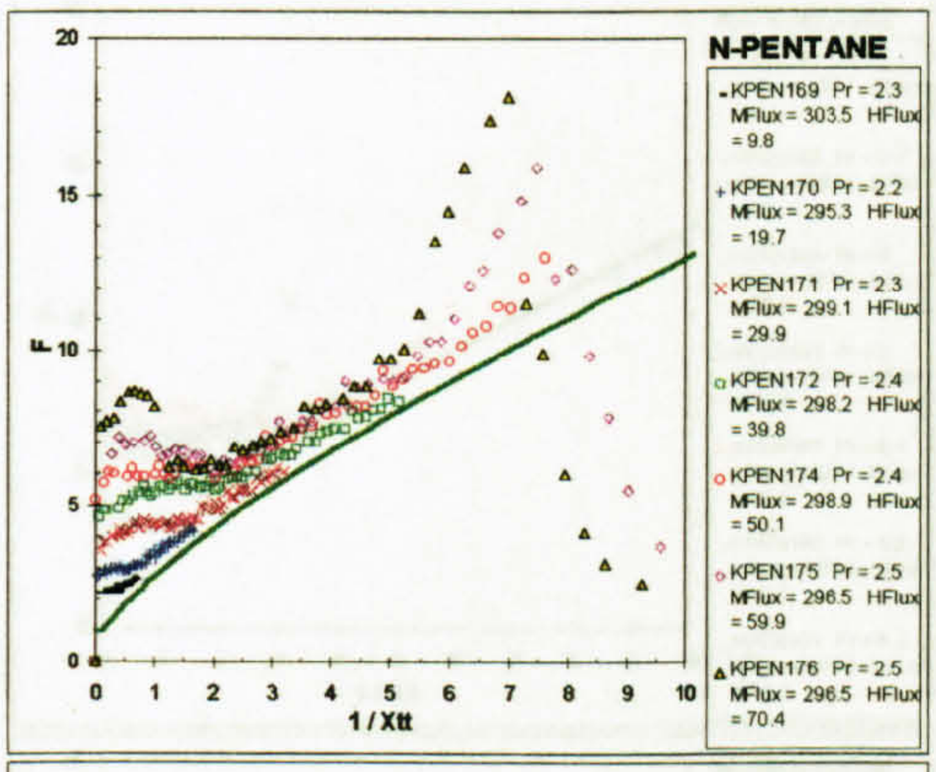
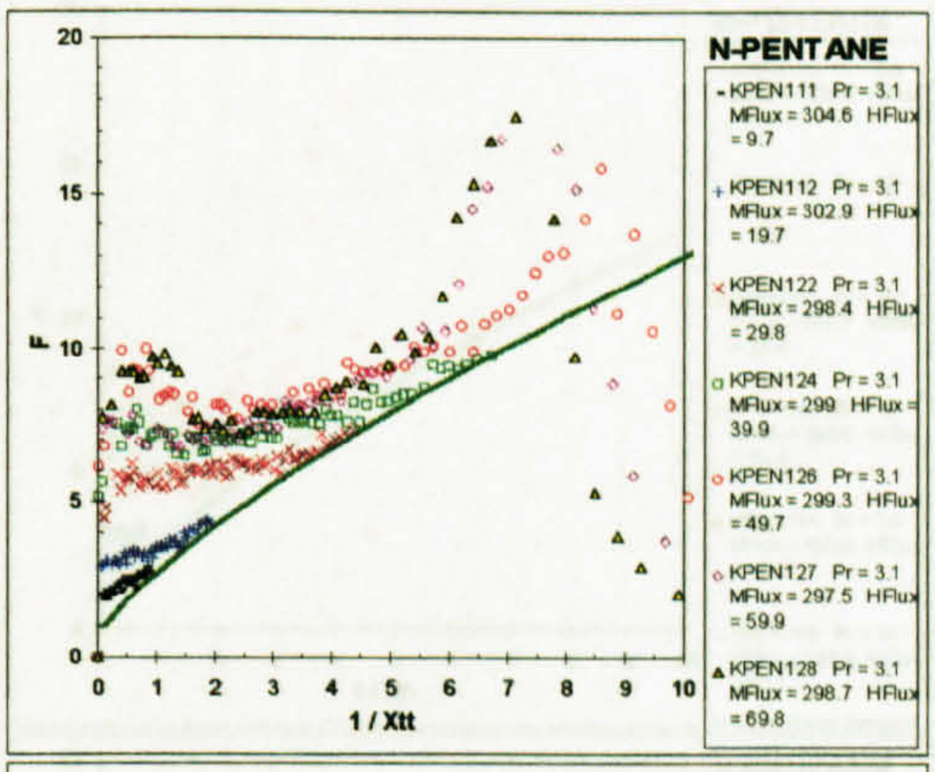


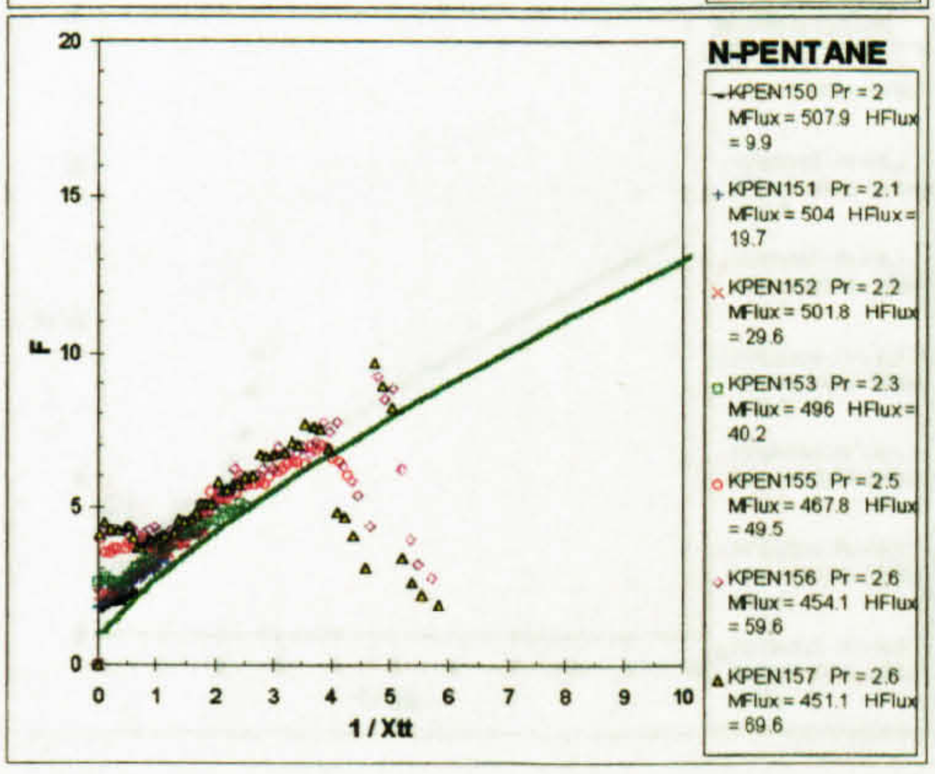
Figure 4.57: Heat transfer coefficients plotted against quality for the n-pentane boiling experiments at a pressure of 0.6 and 1 MPa.











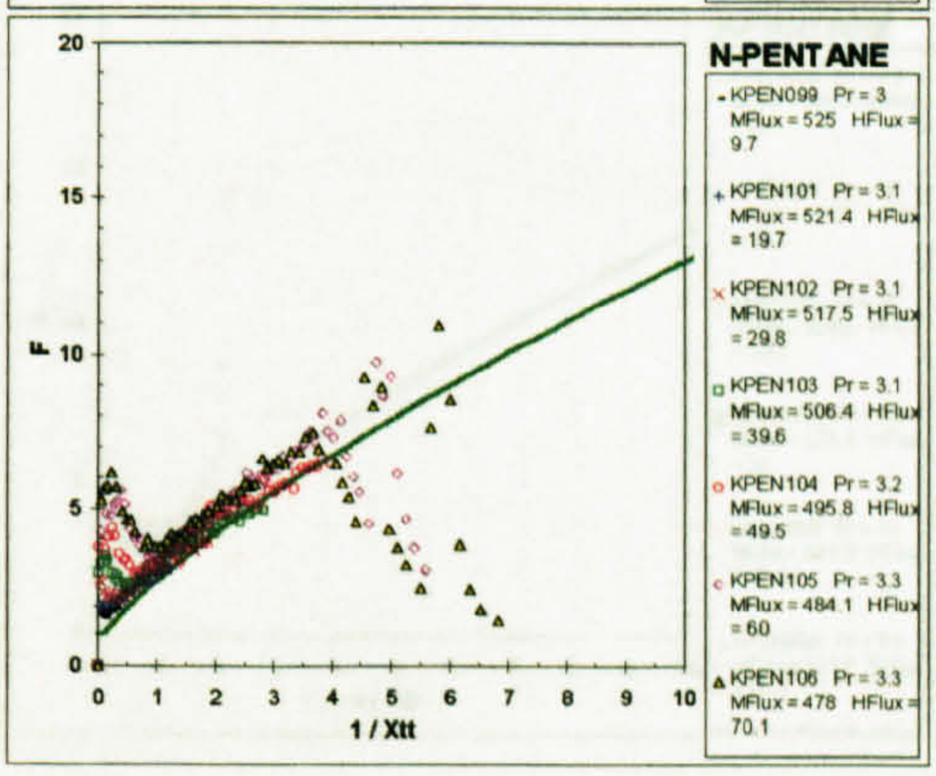


Figure 4.58: F enhancement factor plotted against $1/X_{tt}$ for the n-pentane boiling experiments at a pressure of 0.23 and 0.3 MPa.

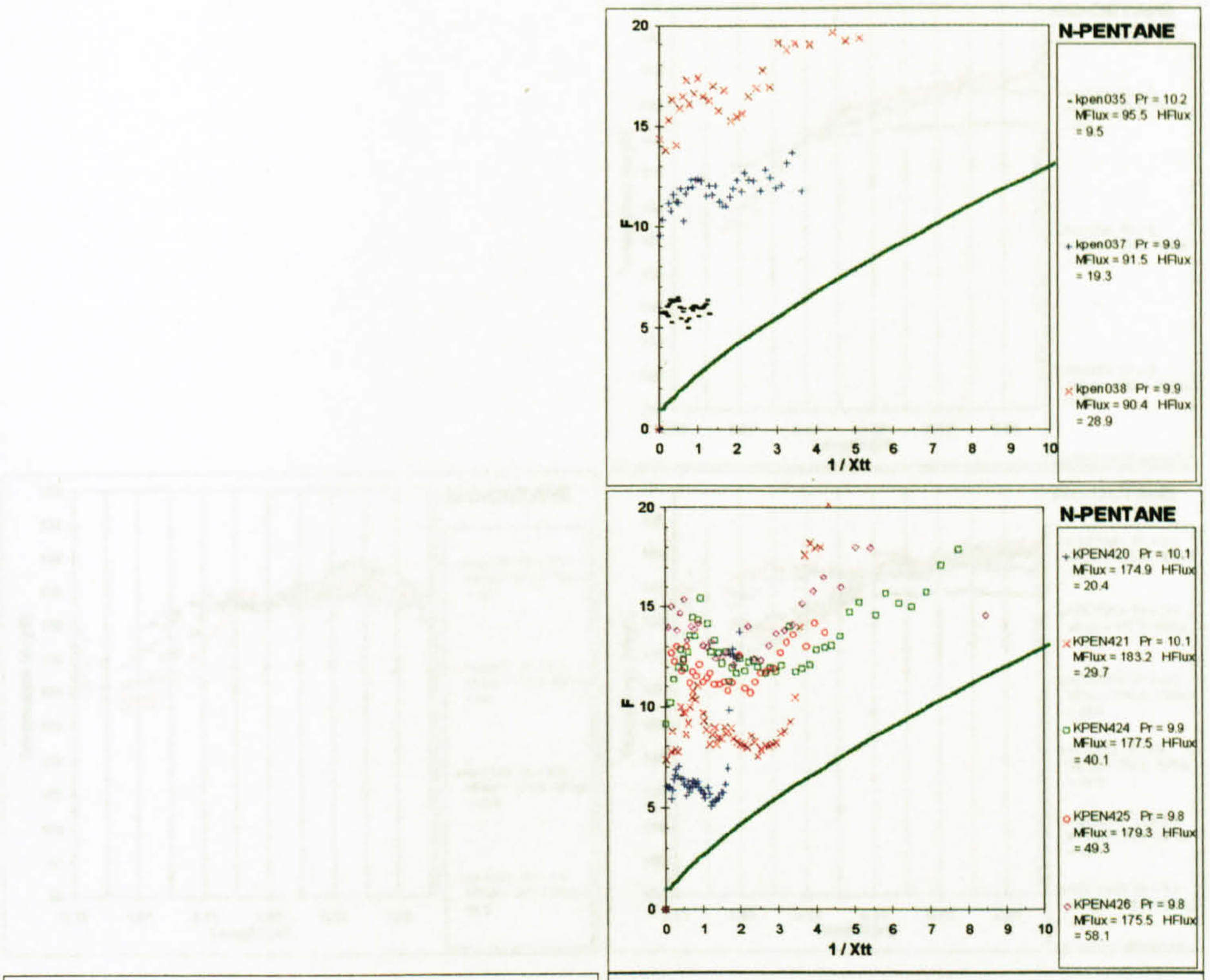


Figure 4.59: F enhancement factor plotted against $1/X_{tt}$ for the n-pentane boiling experiments at a pressure of 0.6 and 1 MPa.

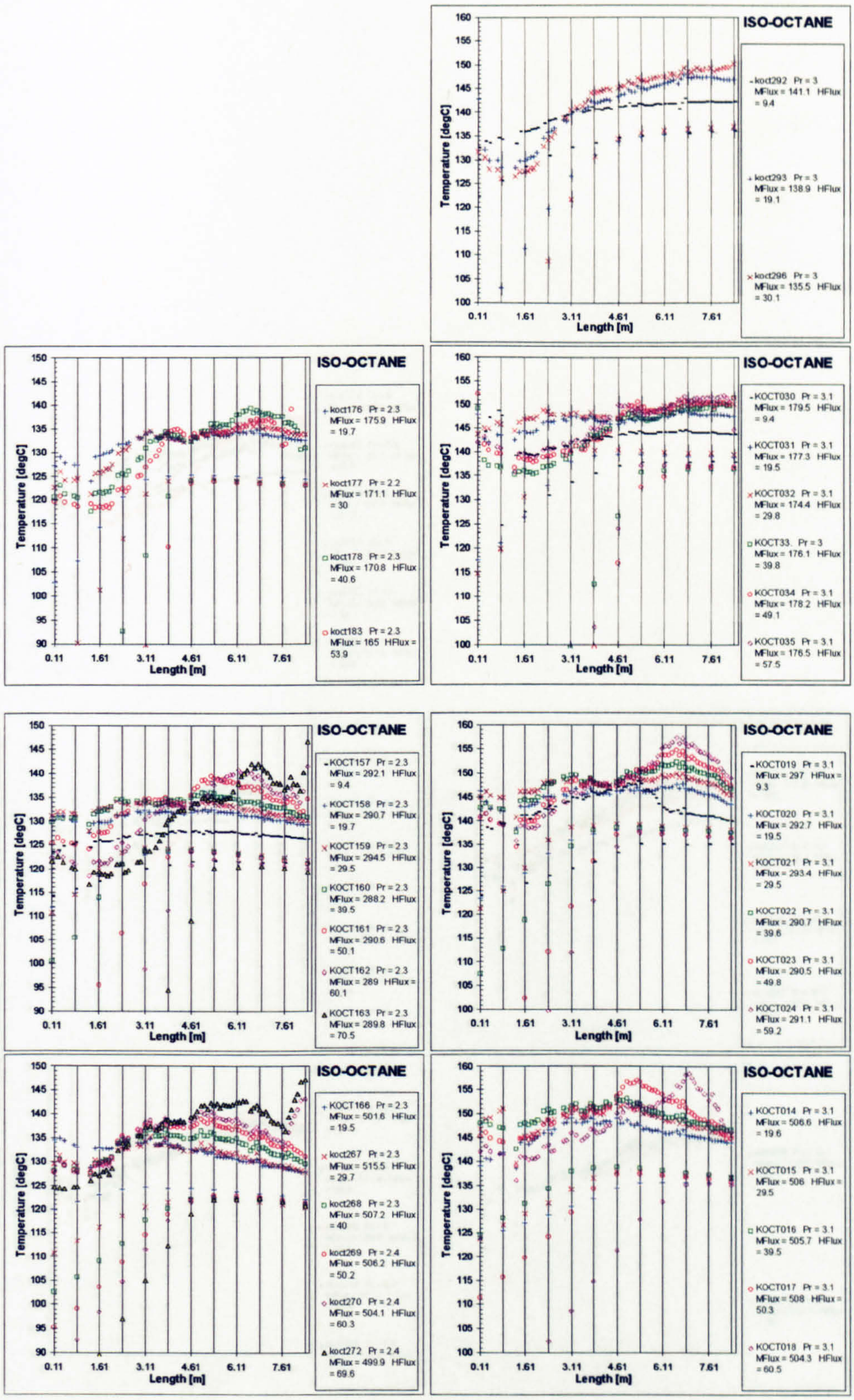


Figure 4.60: Temperature profiles plotted against tube length for the iso-octane boiling experiments at a pressure of 0.23 and 0.3 MPa.

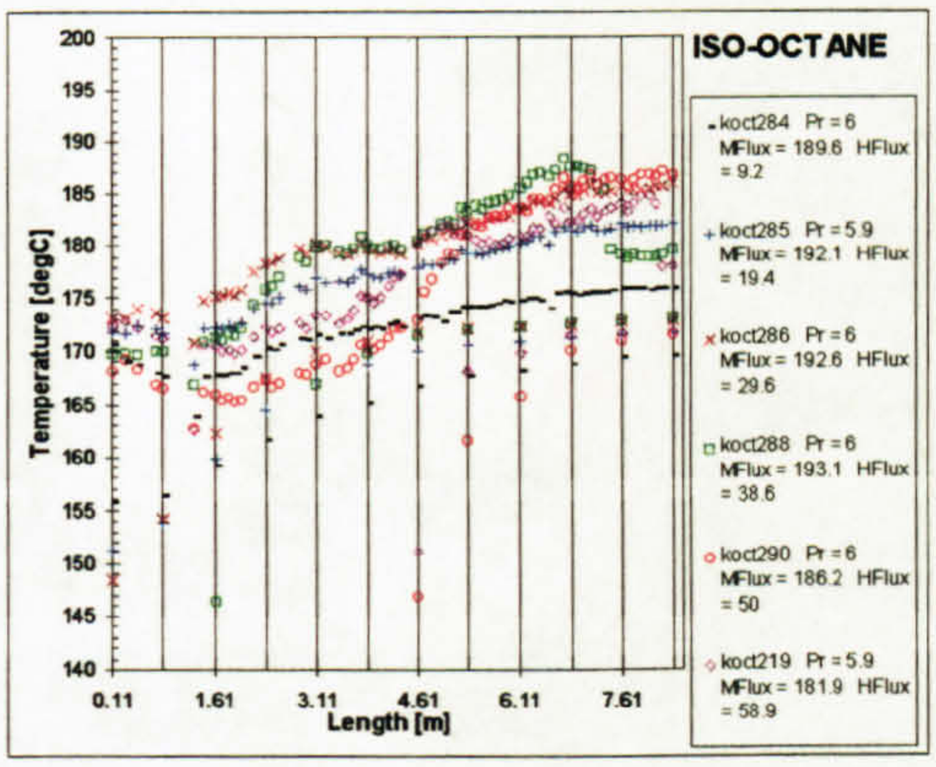


Figure 4.61: Temperature profiles plotted against tube length for the iso-octane boiling experiments at a pressure of 0.6 and 1 MPa.

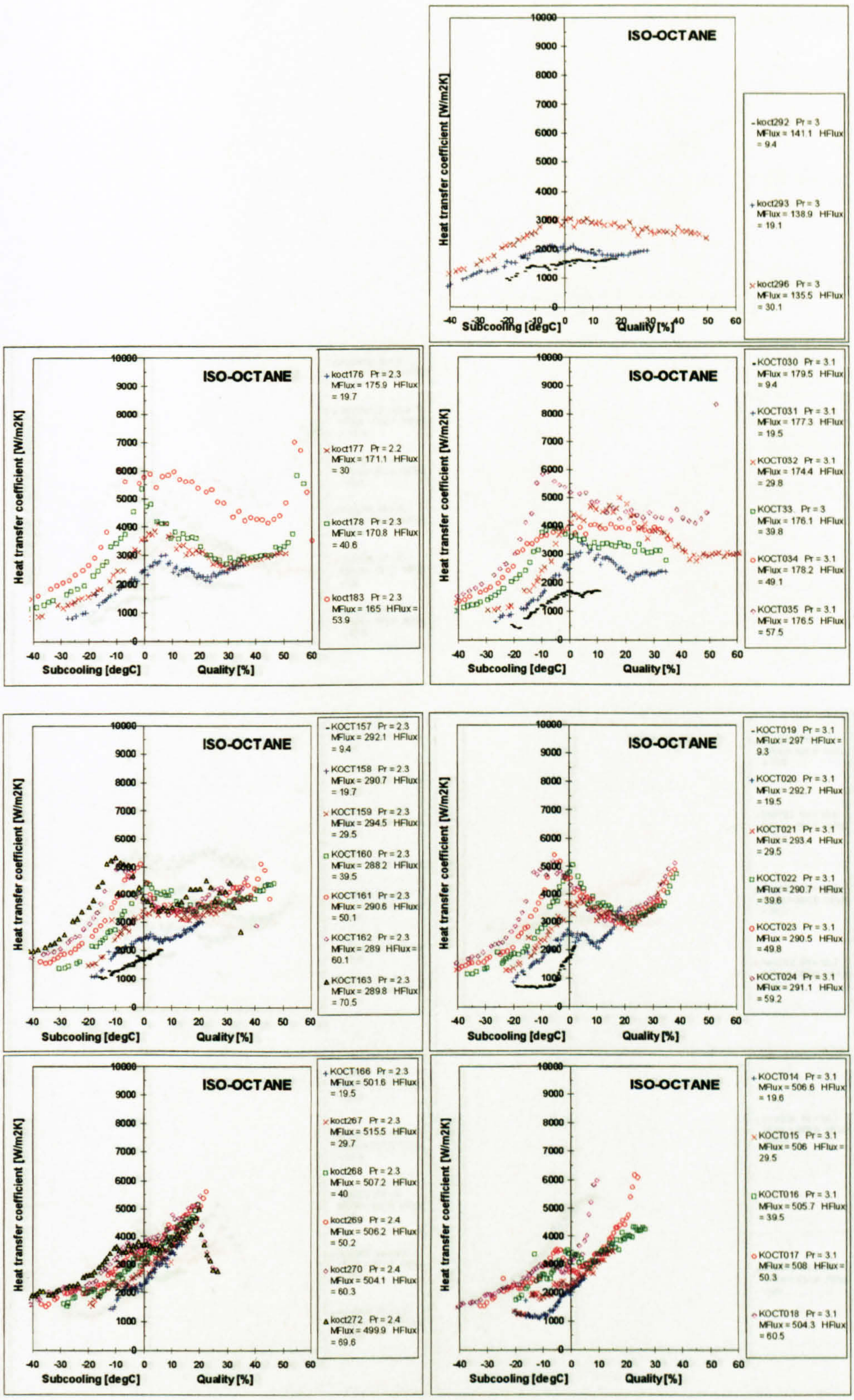


Figure 4.62: Heat transfer coefficients plotted against quality for the iso-octane boiling experiments at a pressure of 0.23 and 0.3 MPa.

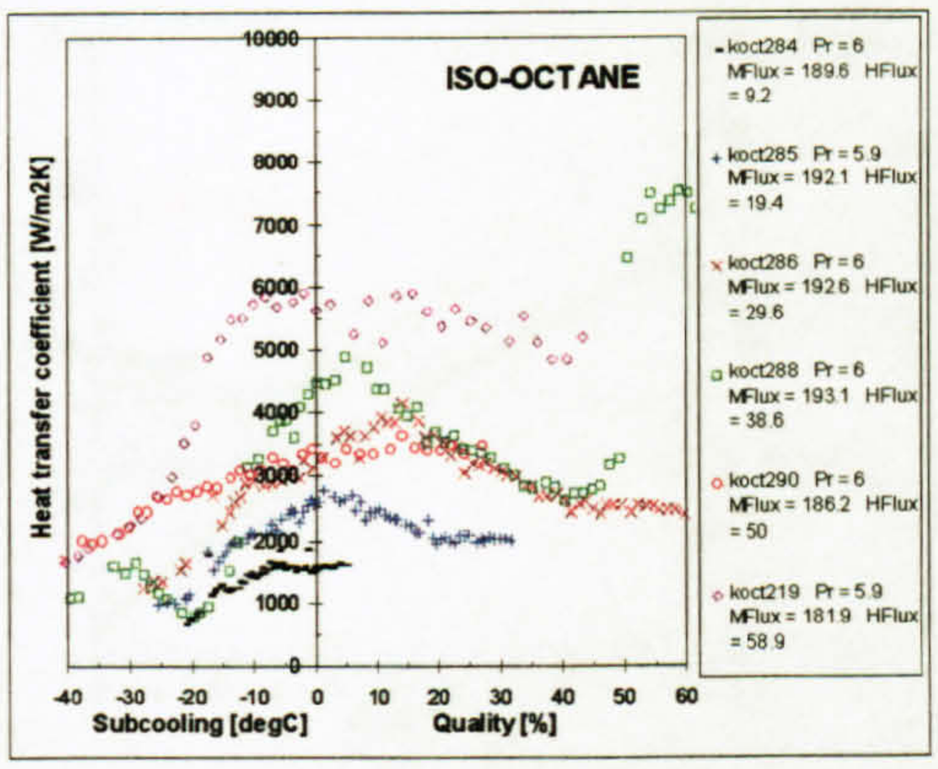


Figure 4.63: Heat transfer coefficients plotted against quality for the iso-octane boiling experiments at a pressure of 0.6 and 1 MPa.

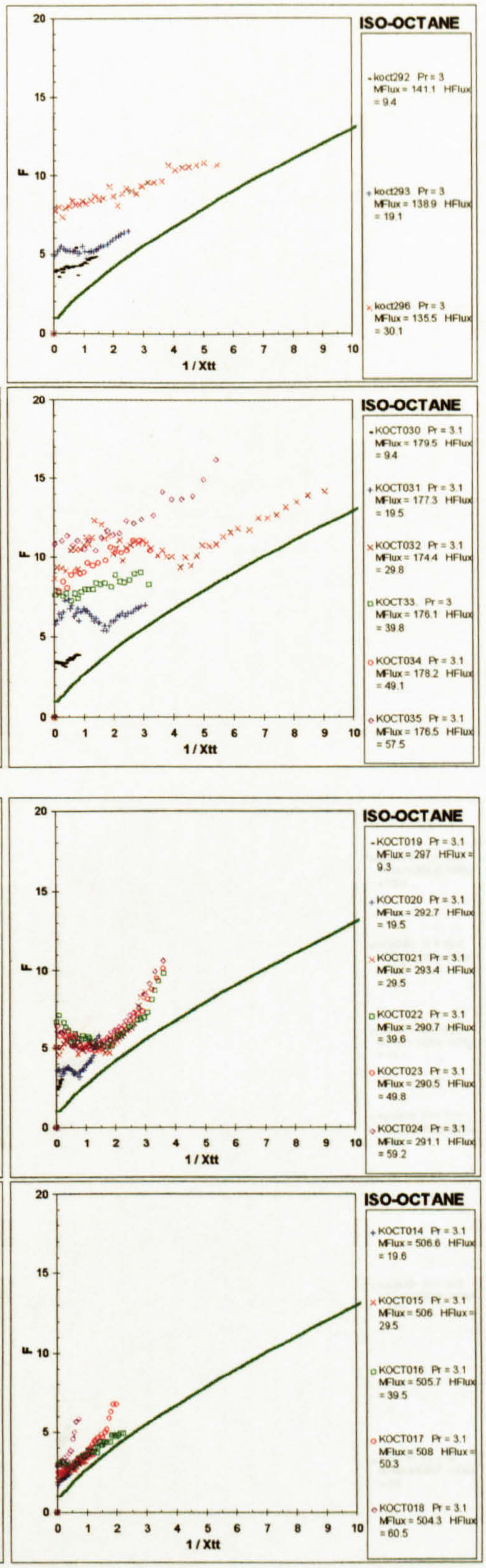
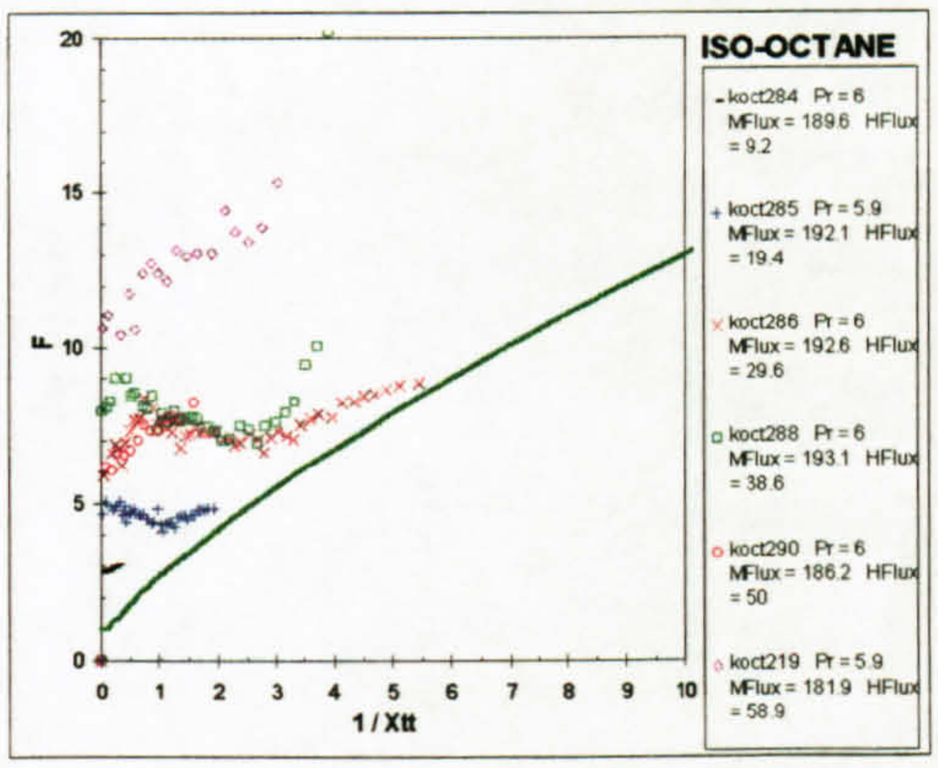
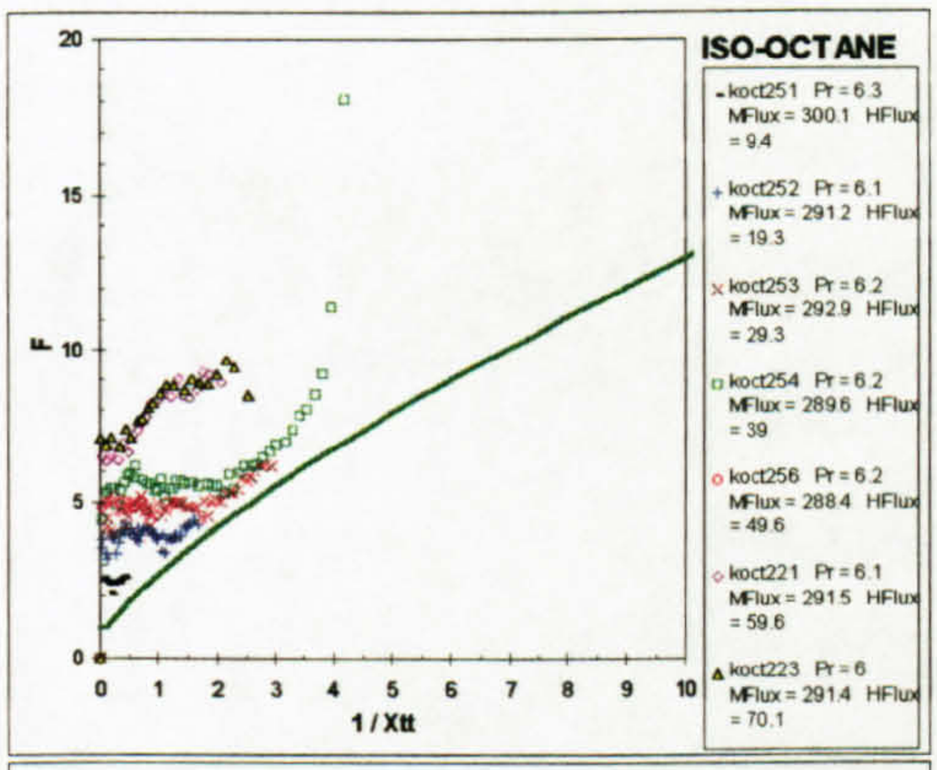
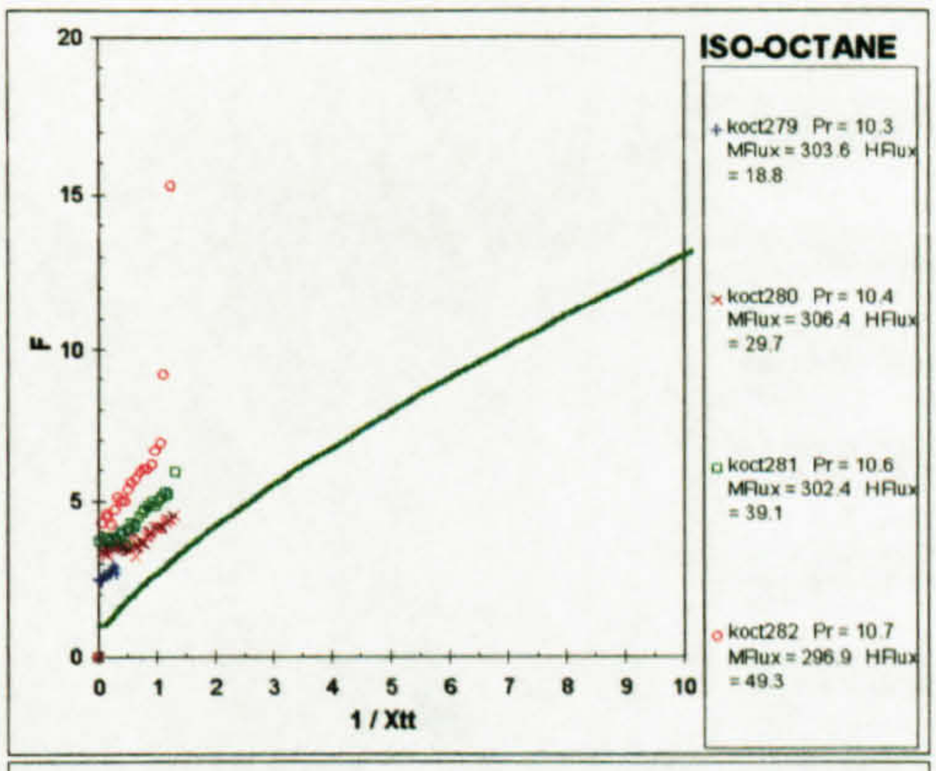
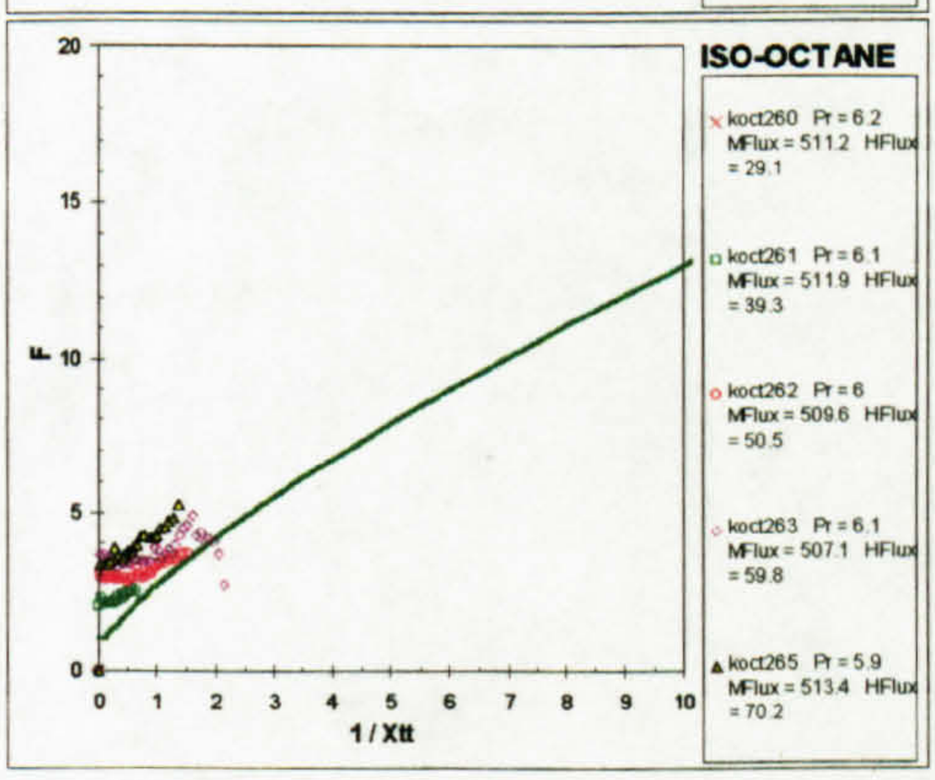


Figure 4.64: F enhancement factor plotted against $1/X_{tt}$ for the iso-octane boiling experiments at a pressure of 0.23 and 0.3 MPa.









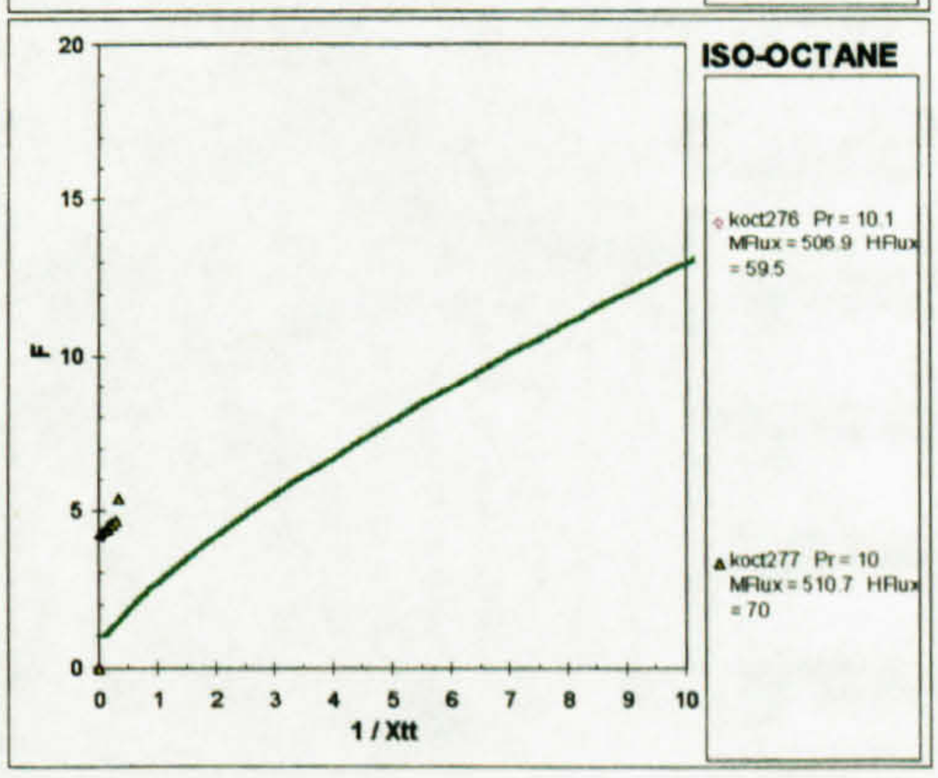


Figure 4.65: F enhancement factor plotted against $1/X_{tt}$ for the iso-octane boiling experiments at a pressure of 0.6 and 1 MPa.

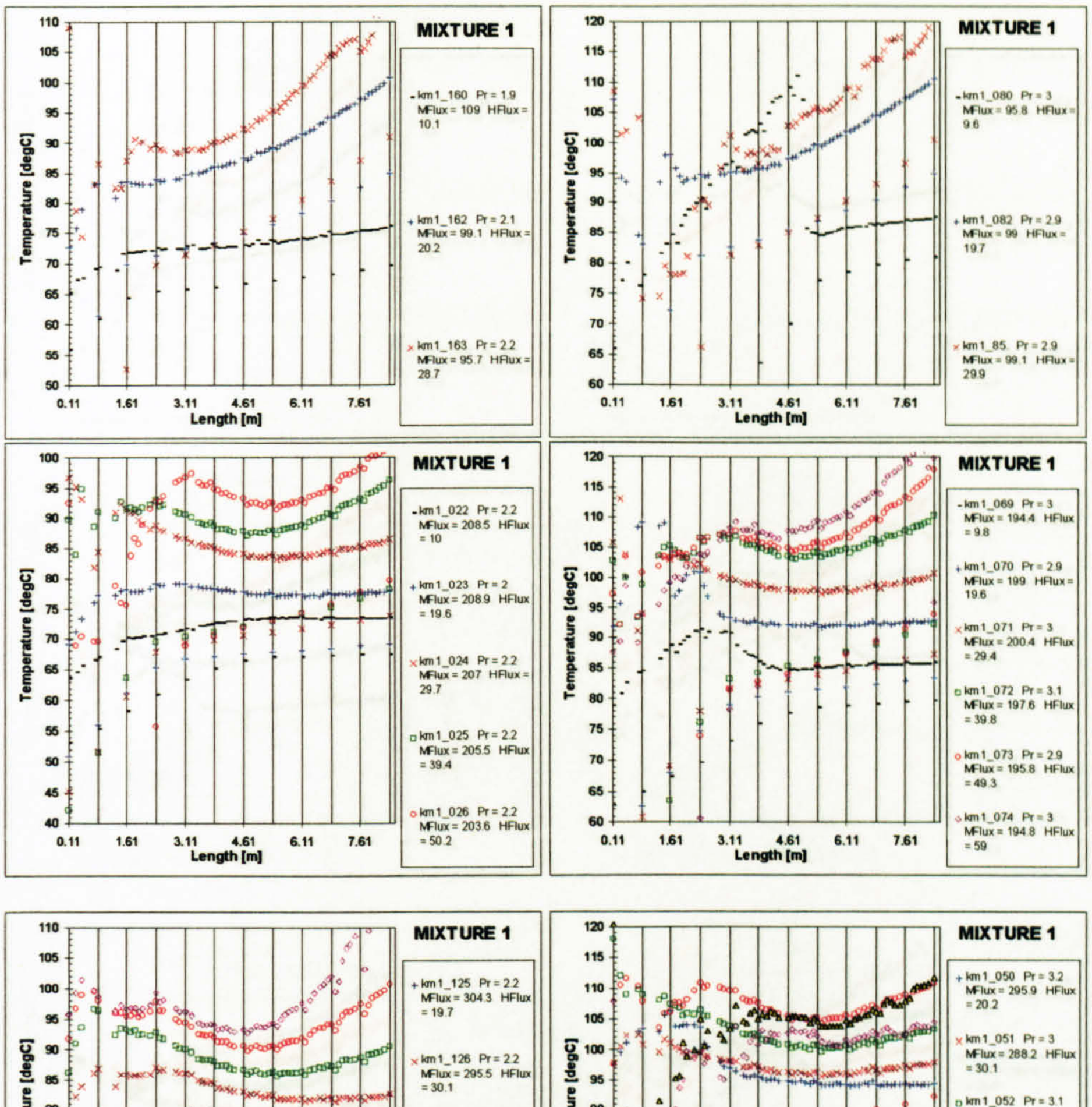


Figure 4.66: Temperature profiles plotted against tube length for Mixture 1 boiling experiments at a pressure of 0.23 and 0.3 MPa.

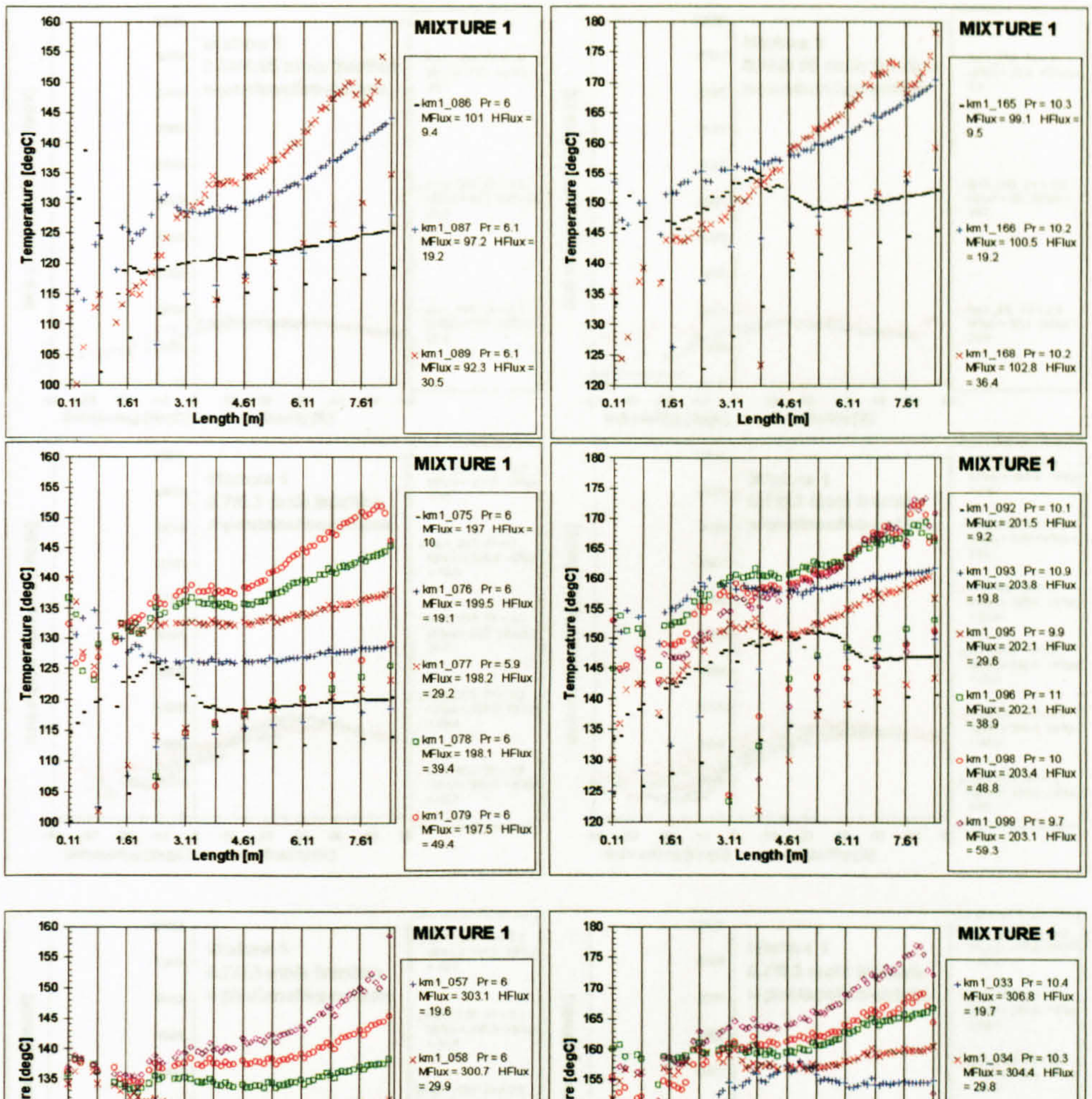


Figure 4.67: Temperature profiles plotted against tube length for Mixture 1 boiling experiments at a pressure of 0.6 and 1 MPa.

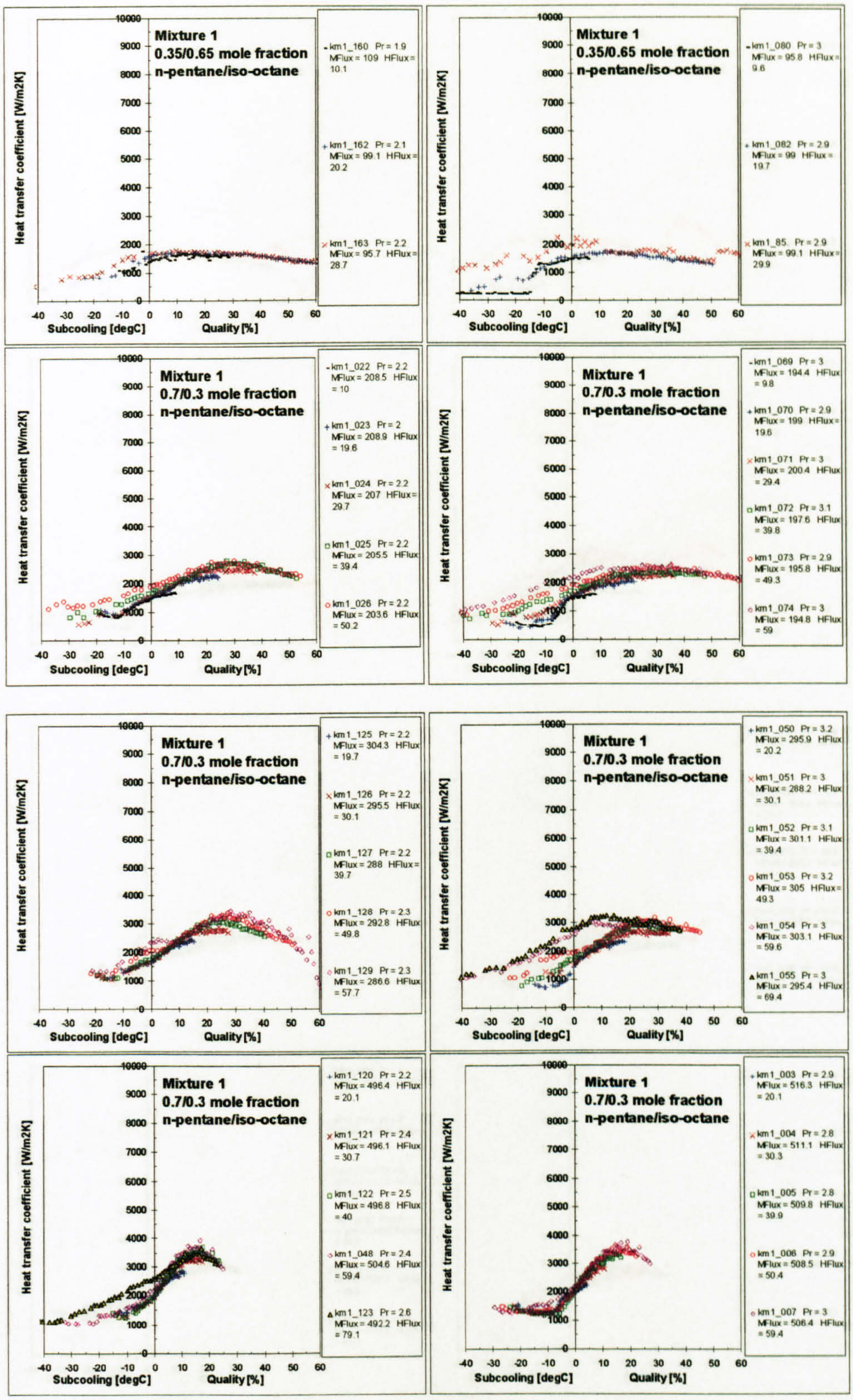


Figure 4.68: Heat transfer coefficients plotted against equilibrium quality for Mixture 1 boiling experiments at a pressure of 0.23 and 0.3 MPa.

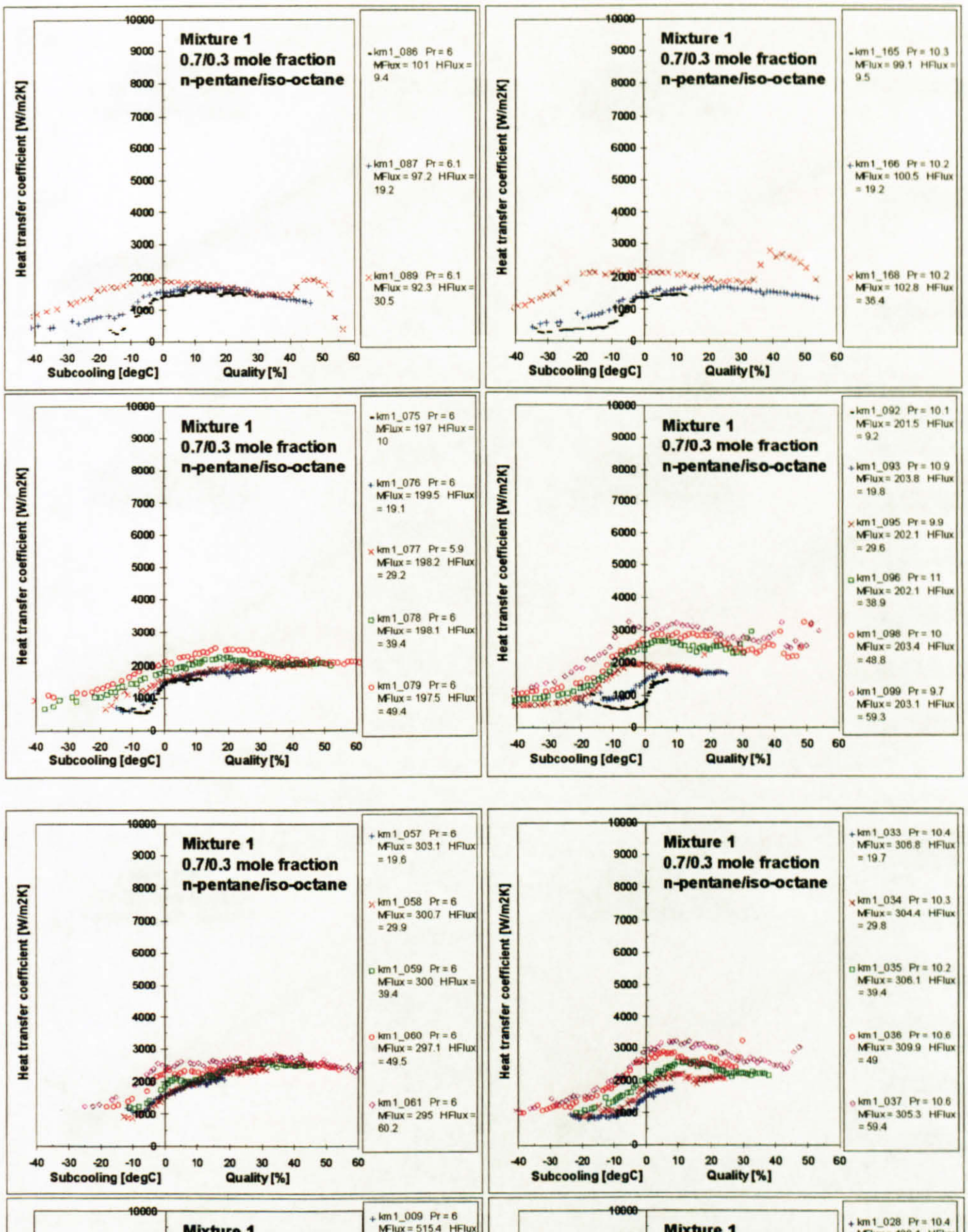


Figure 4.69: Heat transfer coefficients plotted against equilibrium quality for Mixture 1 boiling experiments at a pressure of 0.6 and 1 MPa.

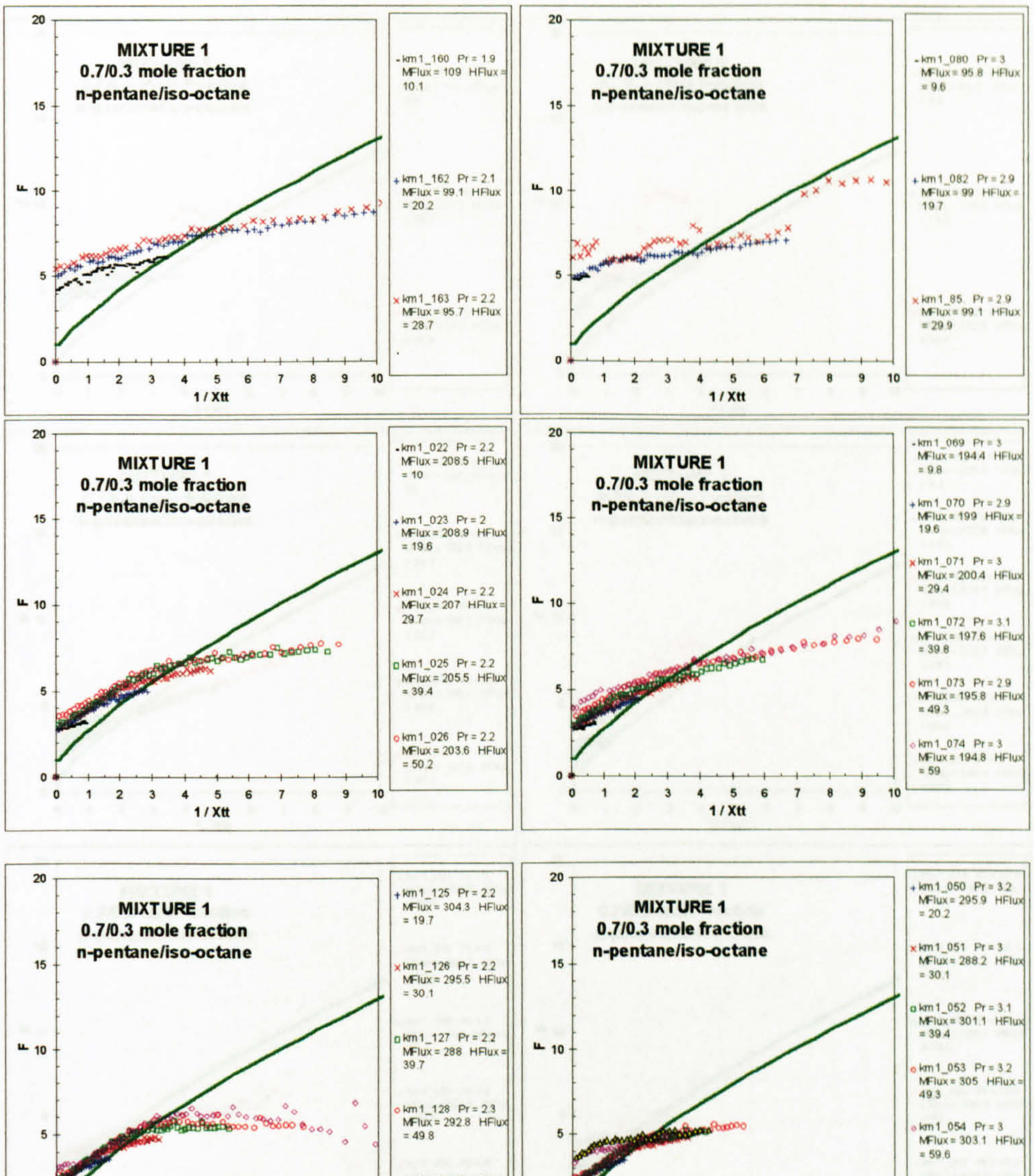


Figure 4.70: F enhancement factor plotted against $1/X_{tt}$ for the Mixture 1 boiling experiments at a pressure of 0.23 and 0.3 MPa.

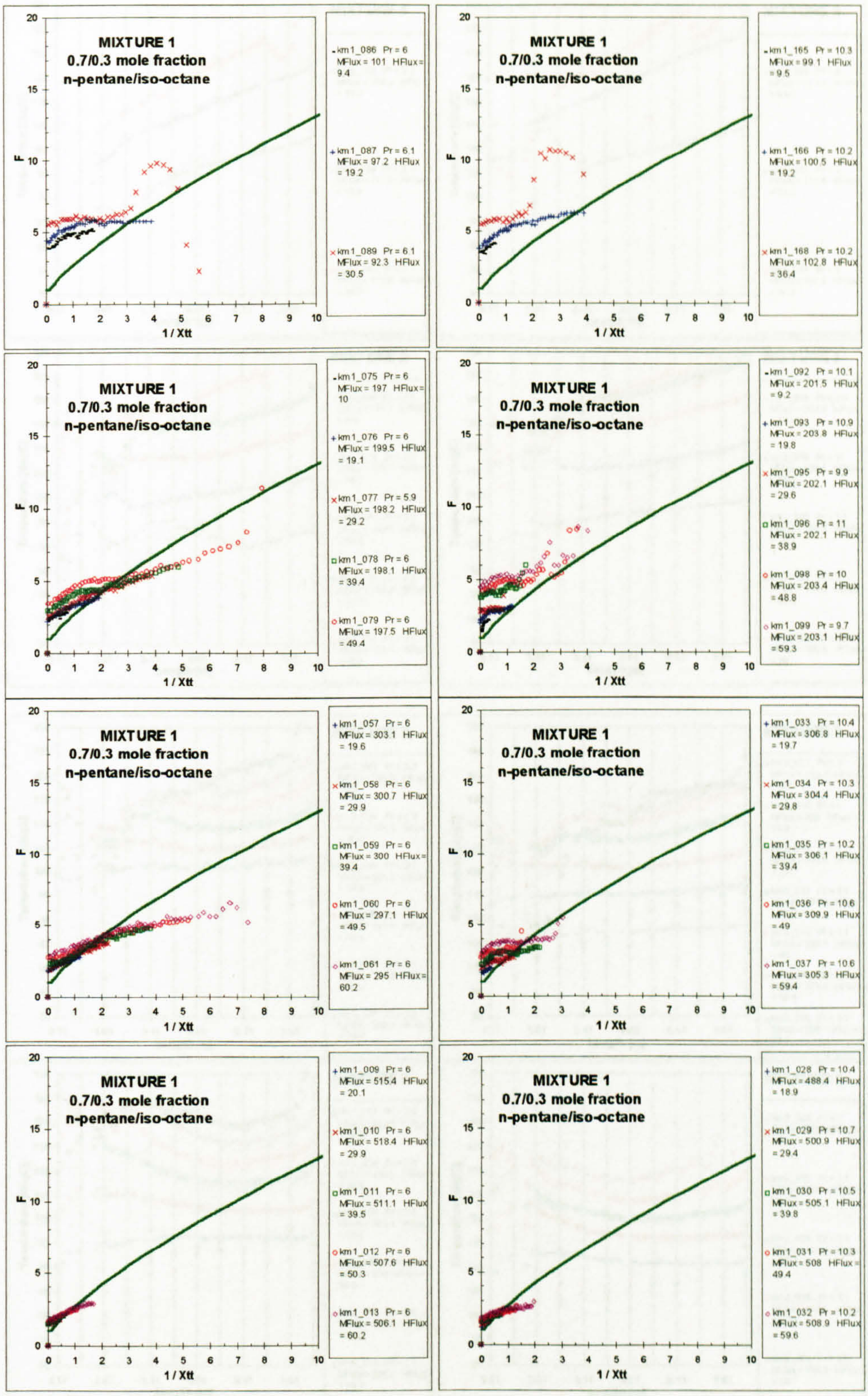


Figure 4.71: F enhancement factor plotted against $1/X_{tt}$ for Mixture 1 boiling experiments at a pressure of 0.6 and 1 MPa.

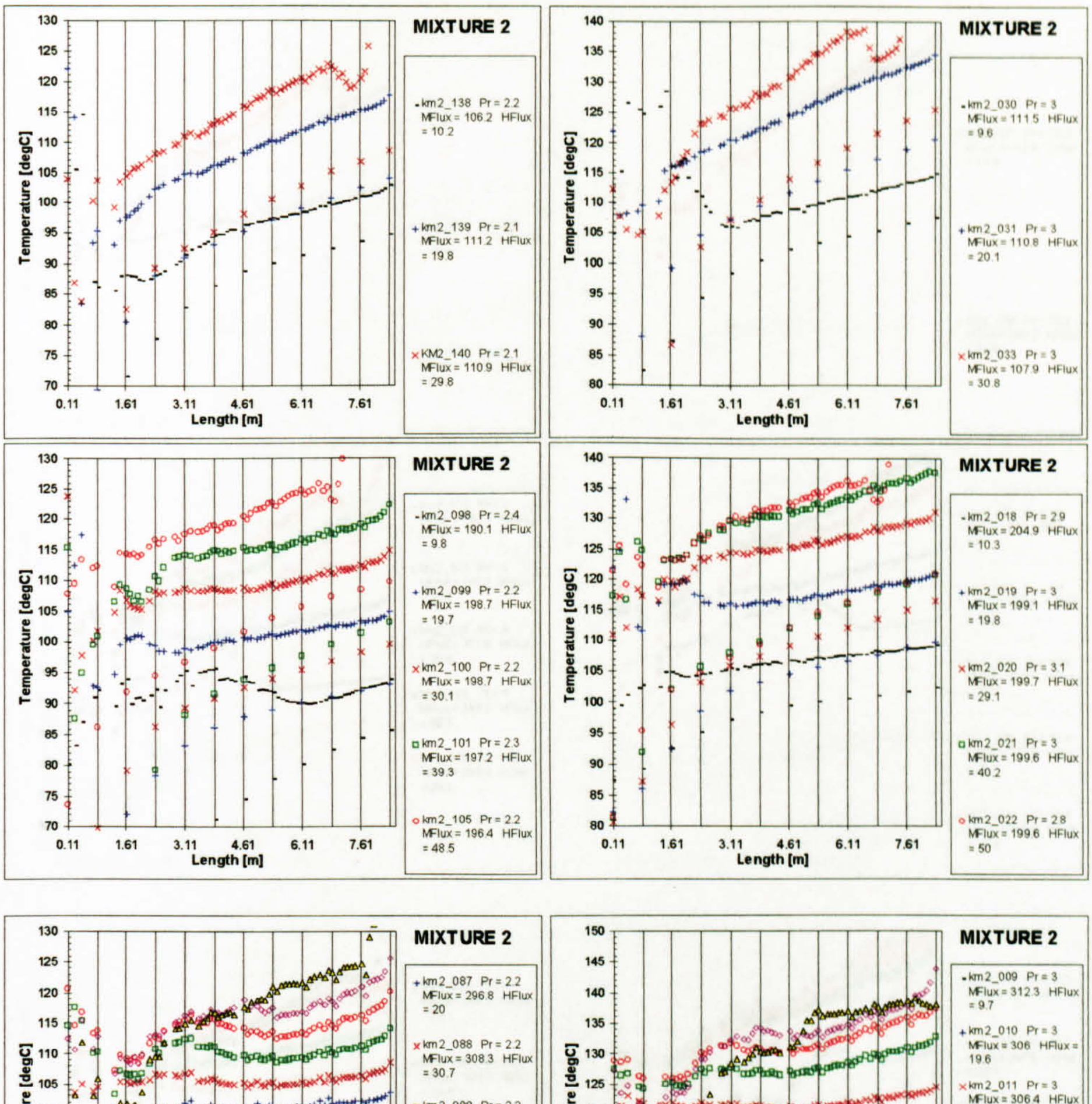


Figure 4.72: Temperature profiles plotted against tube length for Mixture 2 boiling experiments at a pressure of 0.23 and 0.3 MPa.

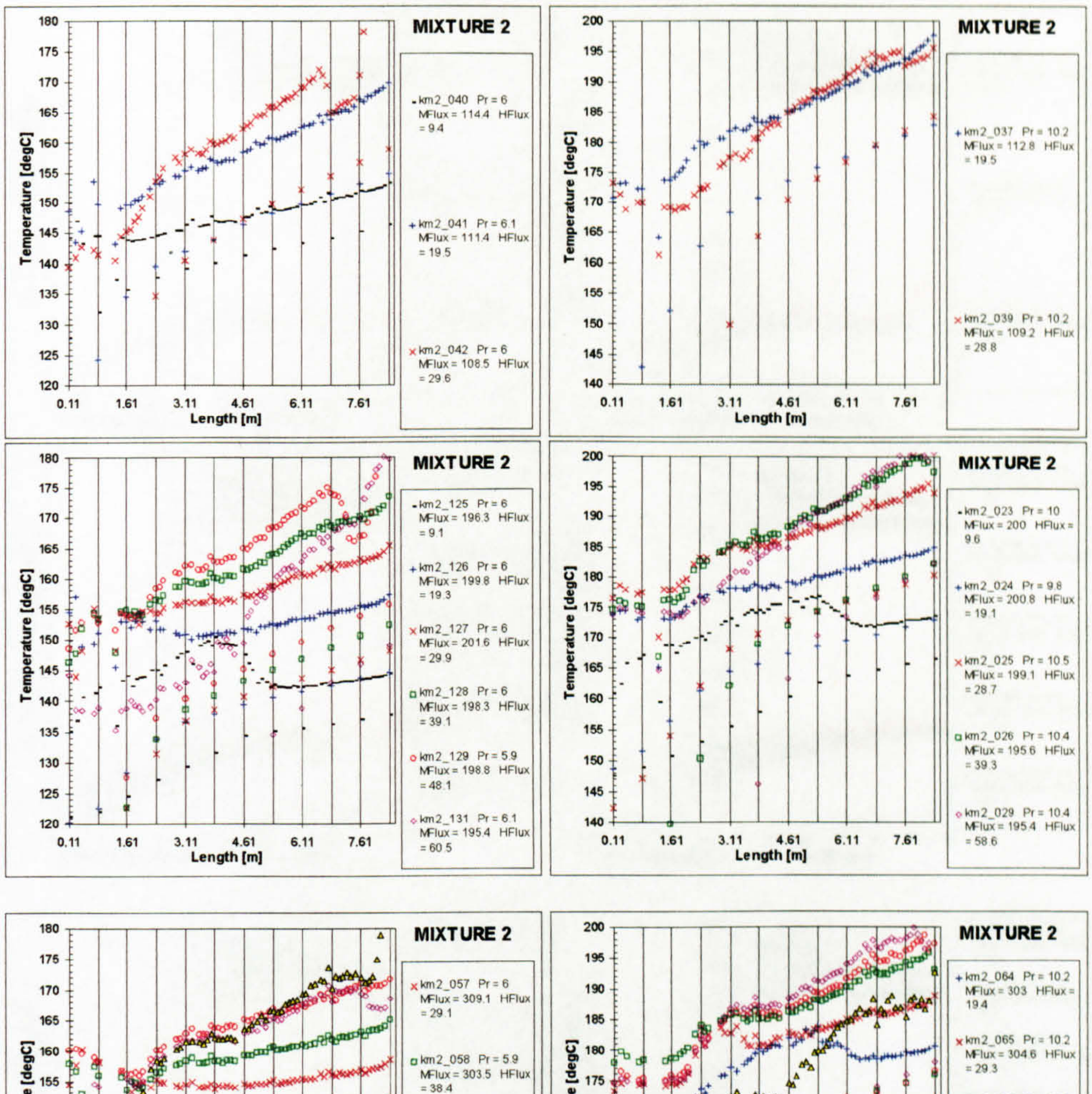


Figure 4.73: Temperature profiles plotted against tube length for Mixture 2 boiling experiments at a pressure of 0.6 and 1 MPa.

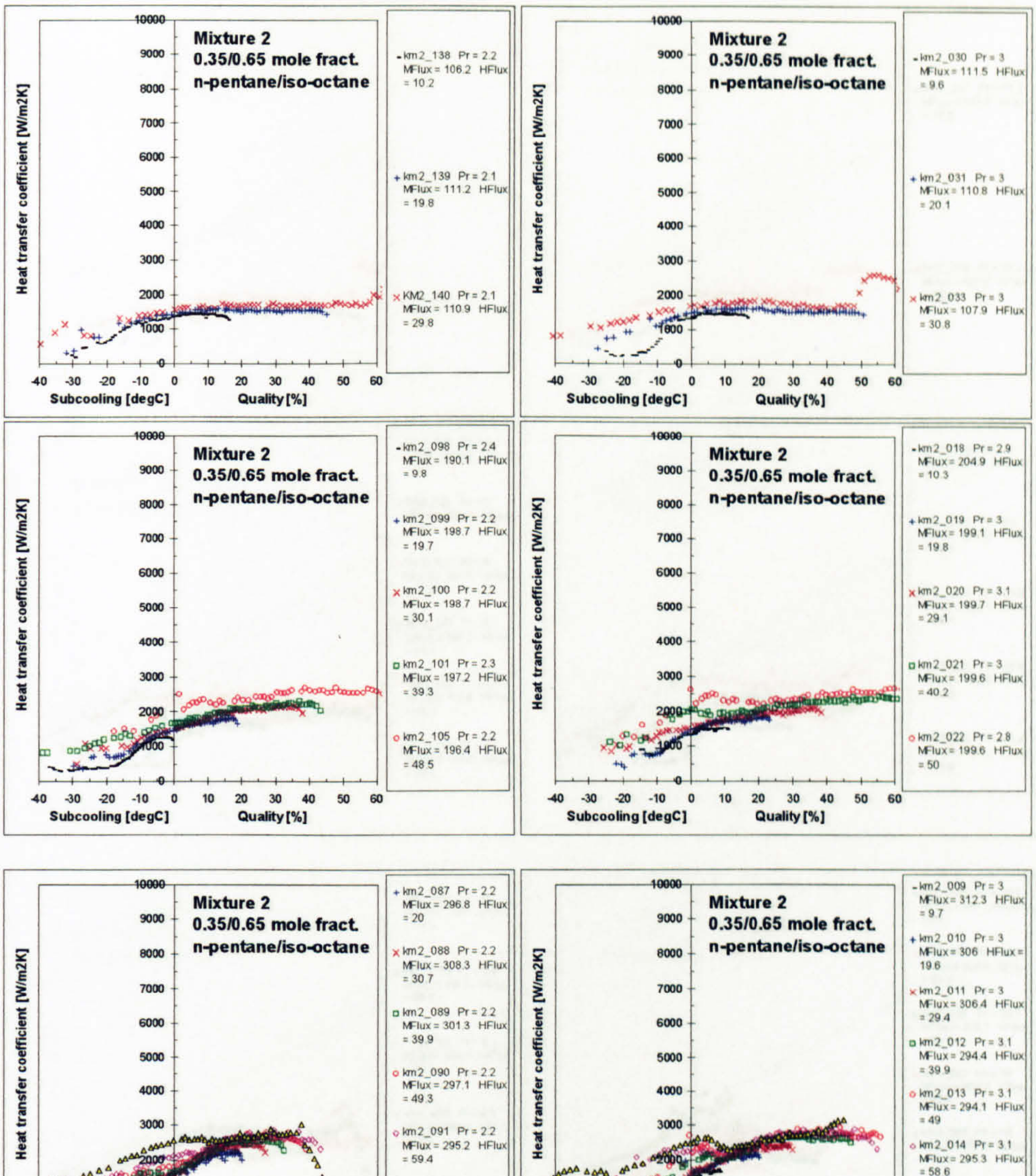


Figure 4.74: Heat transfer coefficients plotted against quality for Mixture 2 boiling experiments at a pressure of 0.23 and 0.3 MPa.

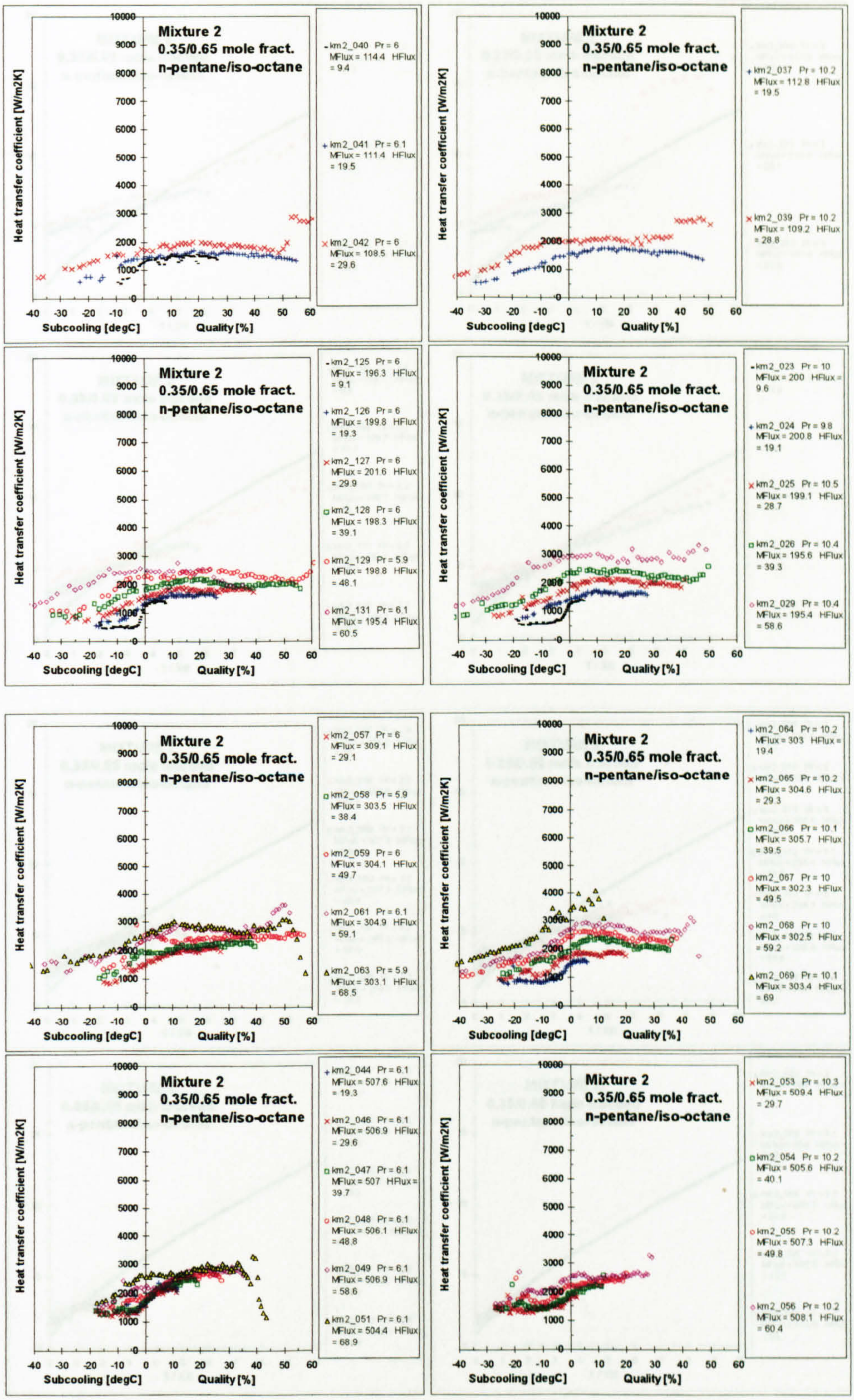


Figure 4.75: Heat transfer coefficients plotted against equilibrium quality for Mixture 2 boiling experiments at a pressure of 0.6 and 1 MPa.

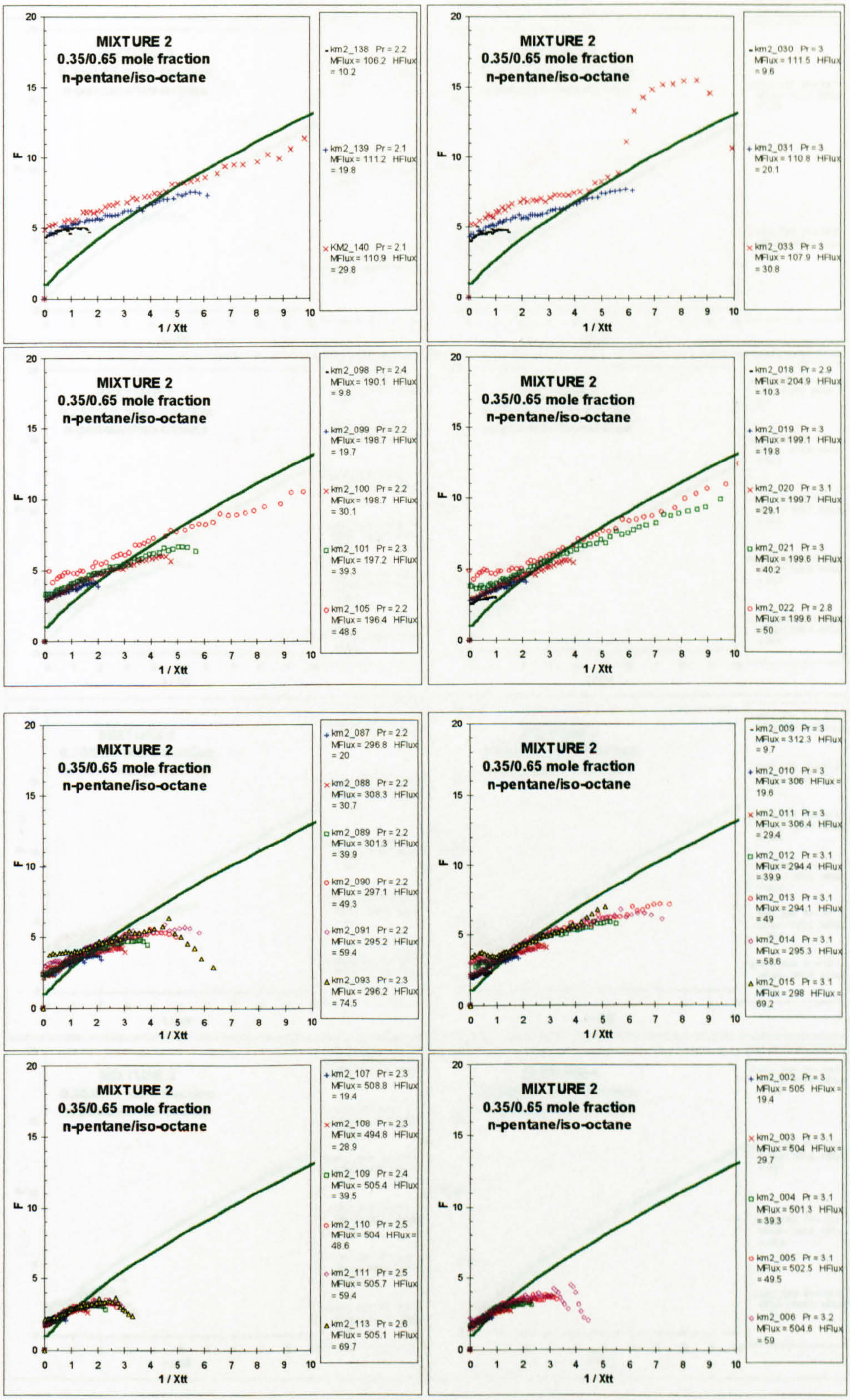


Figure 4.76: F enhancement factor plotted against $1/X_{tt}$ for the Mixture 2 boiling experiments at a pressure of 0.23 and 0.6 MPa.

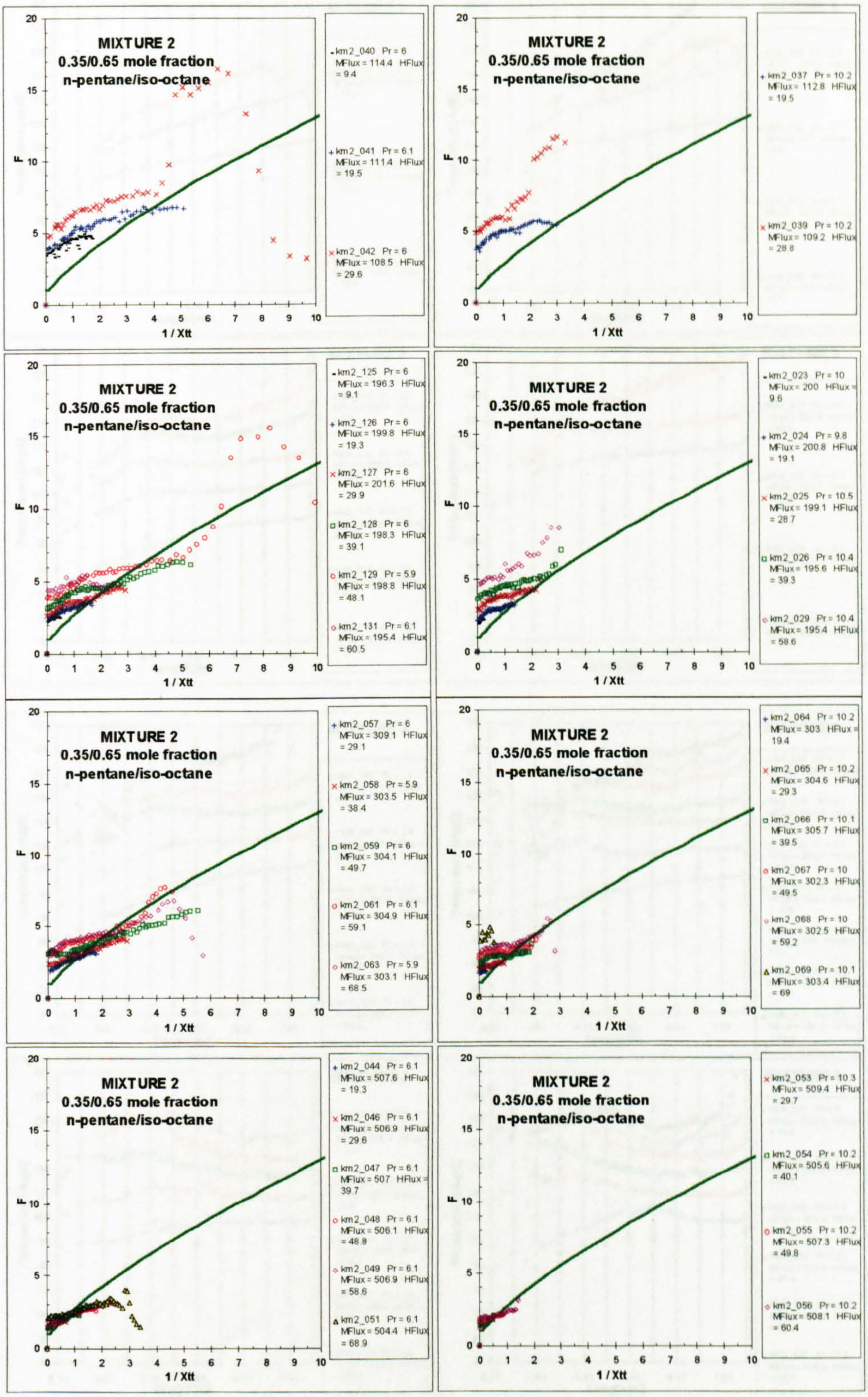


Figure 4.77: F enhancement factor plotted against $1/X_{tt}$ for the Mixture 2 boiling experiments at a pressure of 0.6 and 1 MPa.

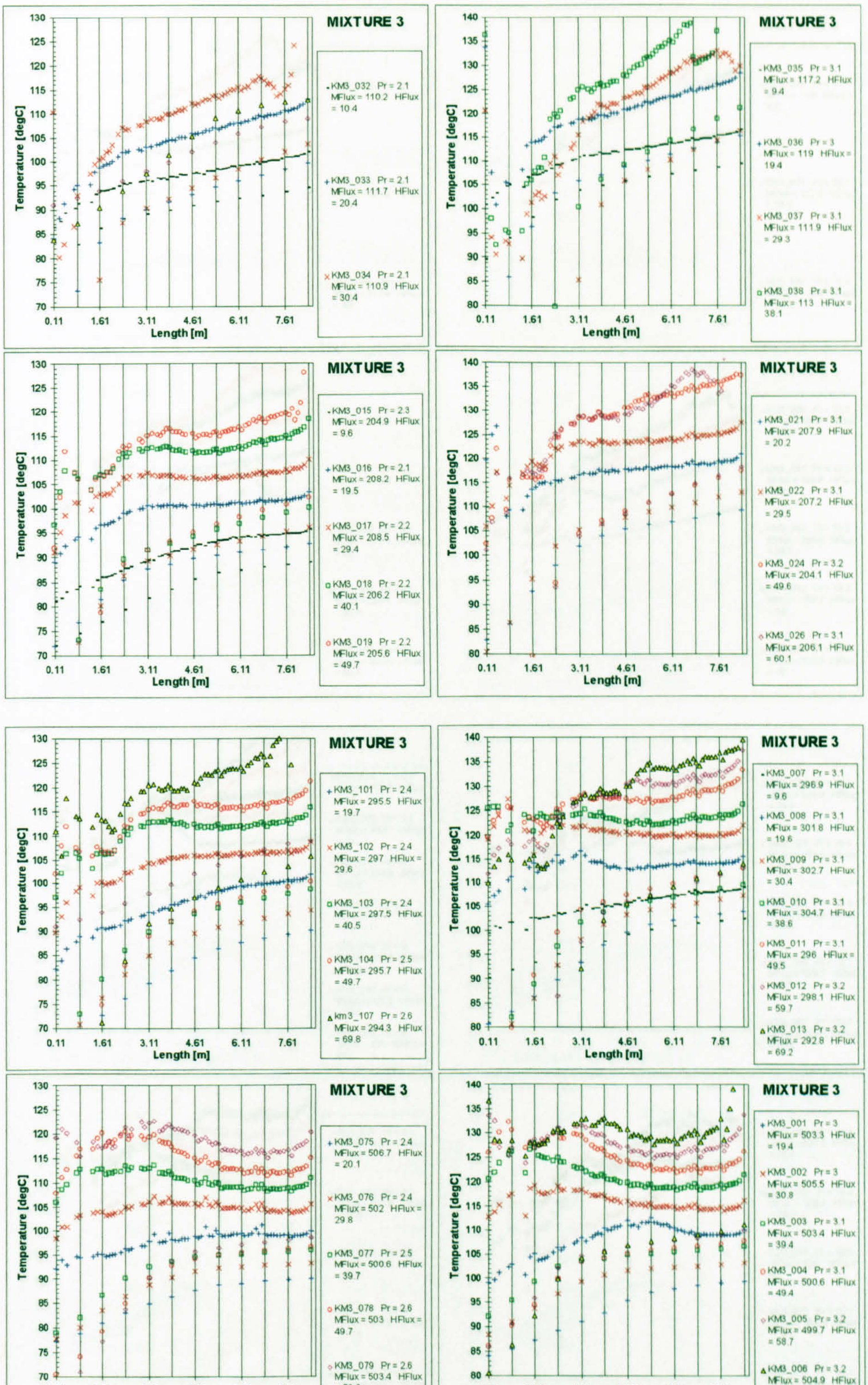


Figure 4.78: Temperature profiles plotted against tube length for Mixture 3 boiling experiments at a pressure of 0.23 and 0.3 MPa.

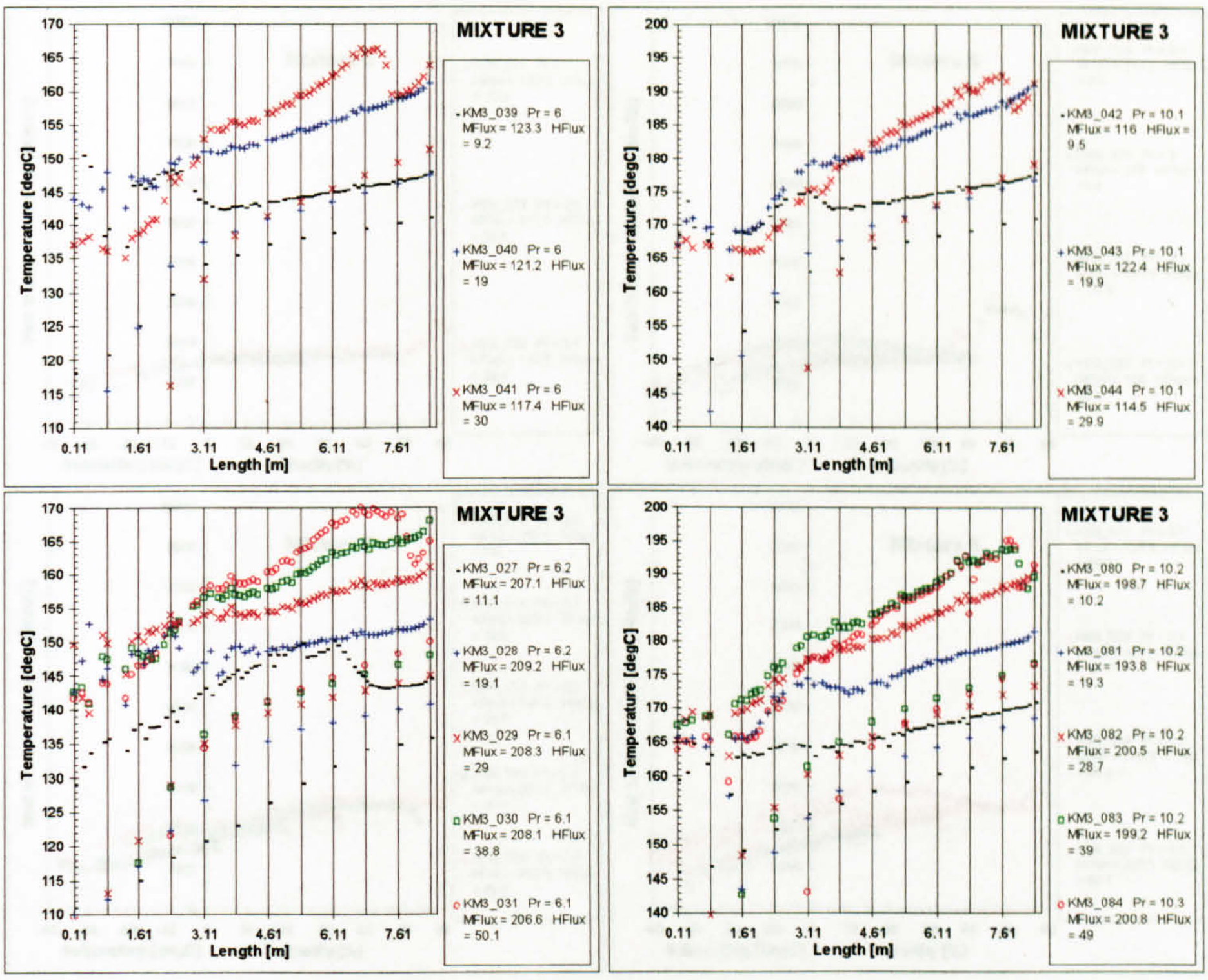


Figure 4.79: Temperature profiles plotted against tube length for Mixture 3 boiling experiments at a pressure of 0.6 and 1 MPa.

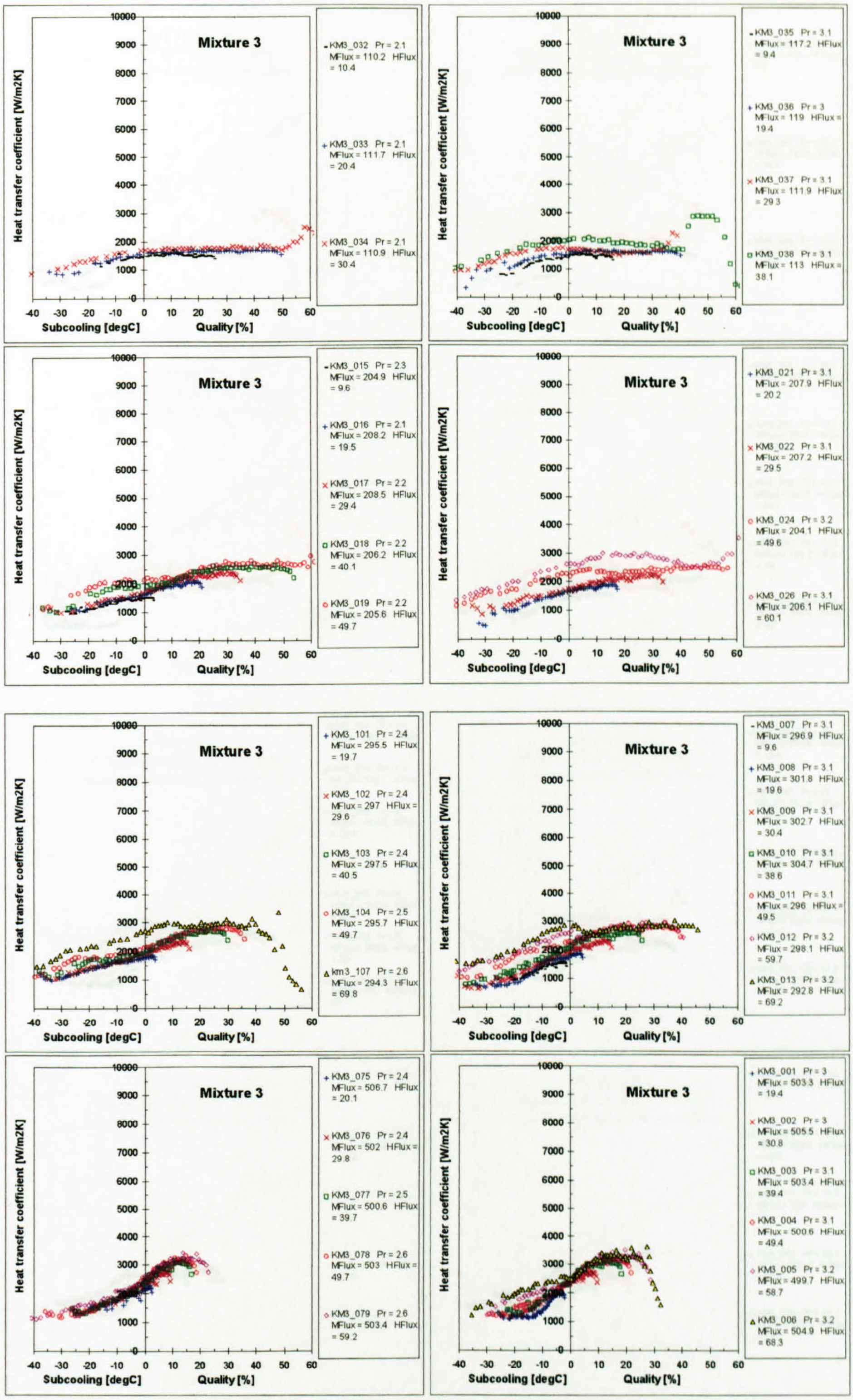


Figure 4.80: Heat transfer coefficients plotted against quality for Mixture 3 boiling experiments at a pressure of 0.23 and 0.3 MPa.

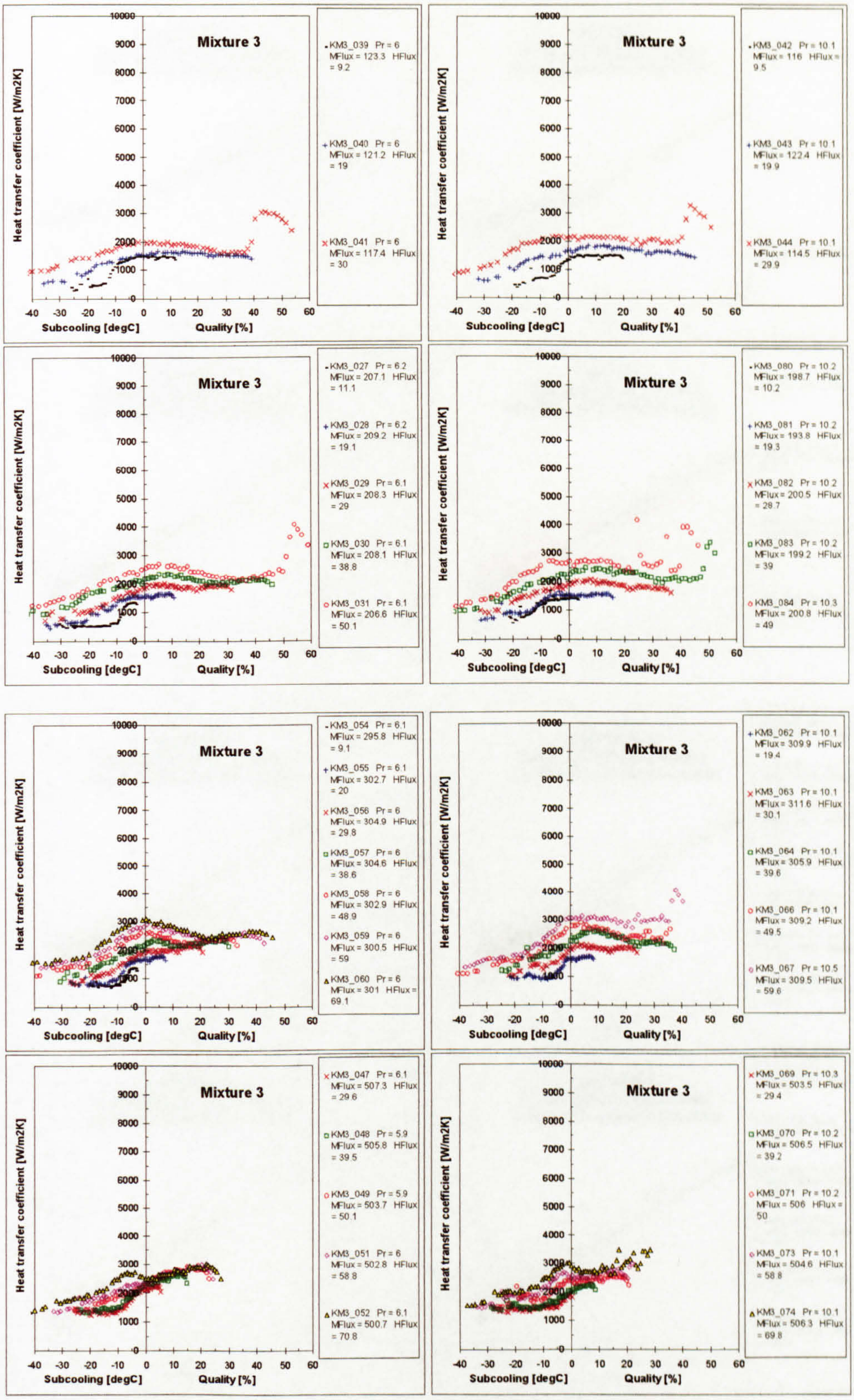


Figure 4.81: Heat transfer coefficients plotted against quality for the Mixture 3 boiling experiments at a pressure of 0.6 and 1 MPa.

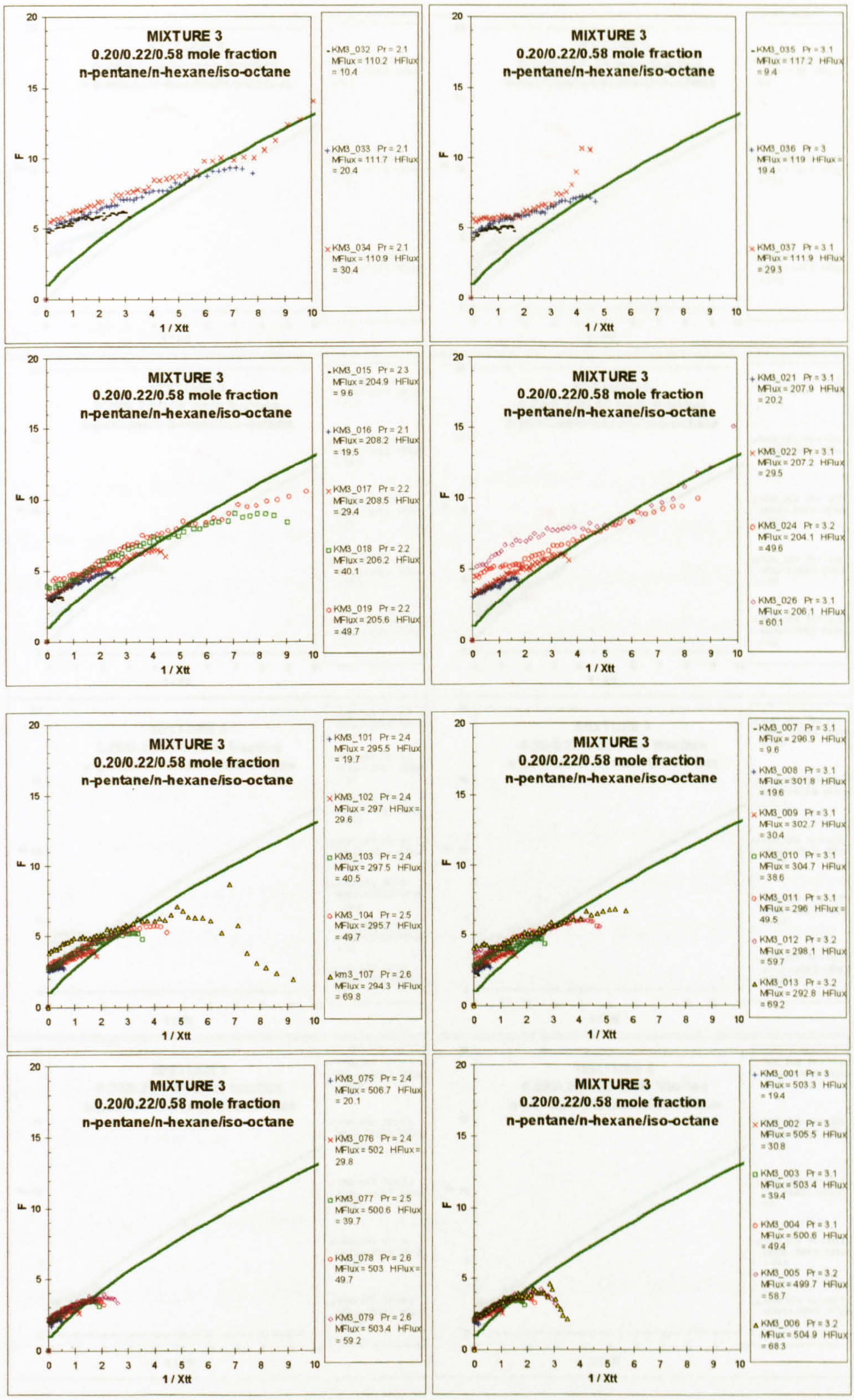


Figure 4.82: F enhancement factor plotted against $1/X_{tt}$ for Mixture 3 boiling experiments at a pressure of 0.23 and 0.3 MPa.

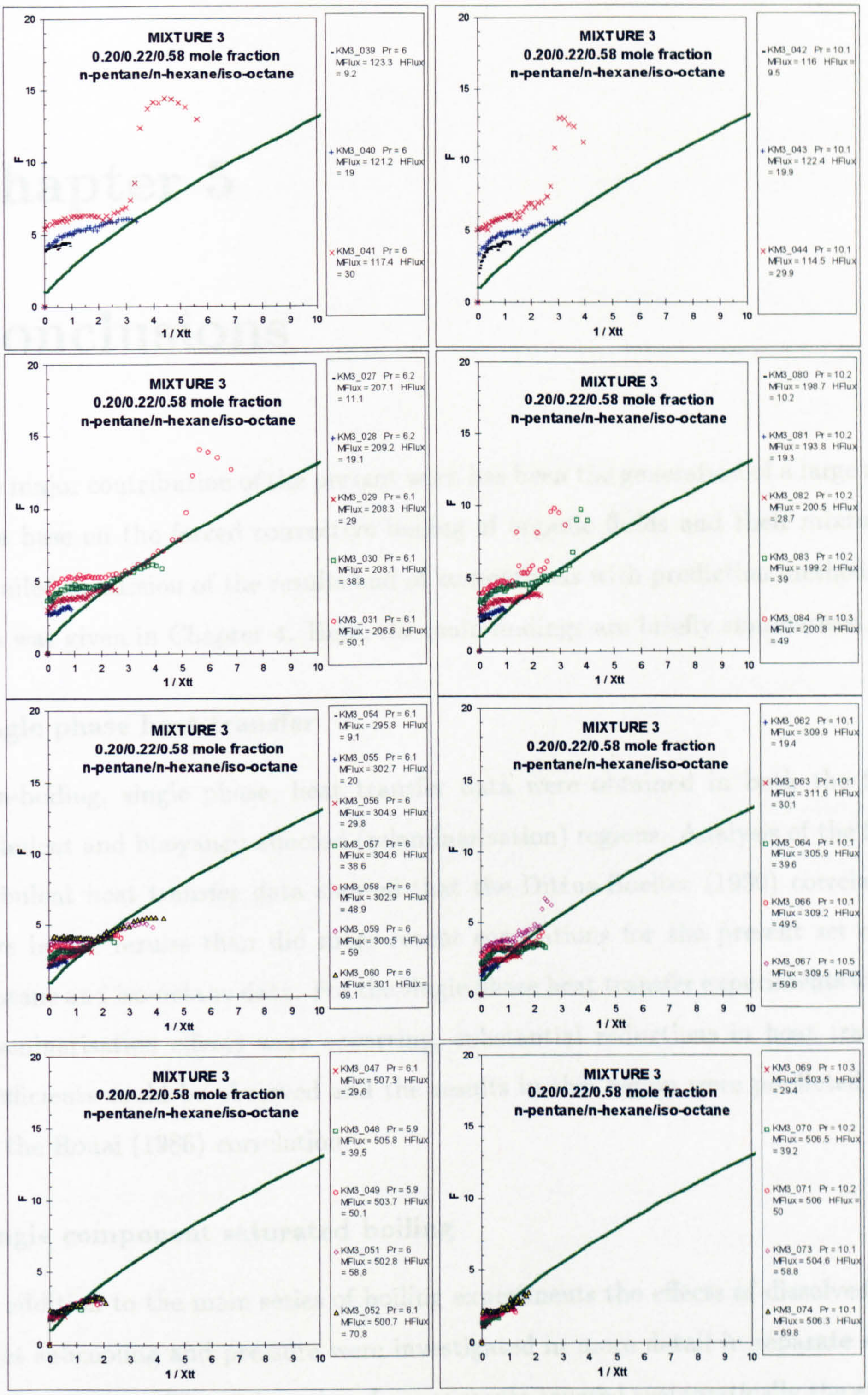


Figure 4.83: F enhancement factor plotted against $1/X_{tt}$ for Mixture 3 boiling experiments at a pressure of 0.6 and 1 MPa.

Chapter 5

Conclusions

The major contribution of the present work has been the generation of a large new data base on the forced convective boiling of organic fluids and their mixtures. Detailed discussion of the results and of comparisons with prediction methodologies was given in Chapter 4. Here, the main findings are briefly summarised.

Single phase heat transfer

Non-boiling, single phase, heat transfer data were obtained in both the fully turbulent and buoyancy-affected (relaminarisation) regions. Analysis of the fully turbulent heat transfer data showed that the Dittus-Boelter (1930) correlation gave better results than did more recent correlations for the present set of n-pentane and iso-octane data. For the single phase heat transfer experiments where relaminarisation effects were occurring, substantial reductions in heat transfer coefficients could be observed and the results in this region were predicted best by the Rouai (1986) correlation.

Single component saturated boiling

In addition to the main series of boiling experiments the effects of dissolved gas, inlet subcooling and pressure were investigated in more detail in separate series of experiments. The main series of experiments covered systematically the effects of mass flux, heat flux and pressure with a fixed (low) range of inlet subcooling.

The main conclusions that can be drawn from the single component experiments are as follows:

1. The results from the main series show a noteworthy trend of the reduction of the heat transfer coefficient with increasing quality where nucleate boiling is dominant. This trend is predicted by the Kandlikar (1990b) and the Chen (1966) correlation.

2. Dissolved gas effects were found to have negligible effect on the heat transfer in the saturated region. The wall temperatures in the subcooled region were lower for higher amounts of dissolved gas. This is expected because bubble nucleation is aided by the presence of dissolved gas.

3. Peaking of the heat transfer coefficient at near zero quality was found and occurred when inlet subcoolings were low. It was suggested that the high heat transfer coefficients were due to the thin developing thermal boundary layers which cause rapid condensation of the bubbles, analogous to micro bubble boiling.

4. The experimental results have shown that the forced convective heat transfer can be predicted fairly well with the existing methods with the correlation of Jung (1989c) giving the best fit.

5. For the tests conducted the effects of hysteresis on the heat transfer were minimal.

Dryout

The comparison of experimental data for the pure components with the annular flow model (GRAMP code) showed that experimental dryout qualities were lower than those predicted. The expected trends with mass flux and pressure were observed in the present data. For the prediction of dryout the value assumed for initial entrained fraction has little effect on the dryout quality. The phenomenon of heat transfer enhancement before dryout as discussed by Beattie (1986) was

also found in the present experiments. If the heat flux is reduced after dryout has been entered, the heat transfer coefficient in the previously dry region was greatly enhanced and this enhancement persisted for long periods. The original (pre-dryout) values of heat transfer coefficient were reinstated if the heat flux was reduced to zero and the rig held at that condition for some time before increasing the heat flux again.

Saturated boiling of mixtures

The main conclusions that can be drawn from the present data on boiling of mixtures are as follows:

1. There is much less influence of heat flux on the heat transfer coefficient for mixtures as compared to the pure components.

2. The reduction in heat transfer for mixtures relative to pure components increases with increasing heat flux.

3. The characteristic effect of inlet subcooling effect giving rise to peaks in the heat transfer coefficient at low inlet subcooling was not observed in the case of the mixtures. Growth and condensation of bubbles would be inhibited due to mixture effects.

4. At higher qualities (annular flow region), the heat transfer coefficients reach a maximum and then stay either fairly constant or reduce with increasing quality. It is postulated that this effect could be due to differential concentrations of the heavier phase in the liquid film, leading to increased effective temperature differences.

Chapter 6

Future work

The main focus of the present work has been the development of a large new data base on forced convective boiling. Although extensive analysis of this data has been carried out (and in particular comparison of the data with a wide variety of prediction methodologies), there is clearly scope for more work in developing generic prediction methods. These developments could be based on the present data but there is also scope for further experimental work. Suggestions for further analytical work are given in Section 6.1 and for further experimental work in Section 6.2.

6.1 Analytical work

The following possible lines of further analytical work are suggested:

1. Combining the present data base with the (more limited) existing data for both single component fluids and for mixtures and using the resultant data bank as a basis for developing new empirical correlations.

2. To develop prediction methods based on more phenomenological approaches. Examples of such possibilities include:

   (a) Extension of current methods for predicting nucleation initiation, bubble departure and void fraction in the subcooled region for single com-

ponent fluids to the case of mixtures.

(b) Extend the prediction methods for annular flow to include multicomponent effects. This extension could be based on the work of Sun and Hewitt (1996) and the previous development of annular flow prediction methods as embodied in the GRAMP code (Hawkes, 1996). Specifically, the film bubble nucleation, growth and bursting models of Sun and Hewitt (1996) could be adopted to the case of multicomponent systems and the mixing of film and drop liquid could be incorporated into the GRAMP code.

(c) Development of models for bubbly and slug flow, again including the mixture effects.

3. Analytical investigation of the postulated bubble boundary layer effects associated with the peak in heat transfer coefficient observed at low subcoolings for the single component fluids.

4. Improvement in dryout models to better represent this new data for organic fluids. A candidate for investigations in this context is the influence of heat flux on entrainment rate.

5. Extension of the work by Jayanti (1997) on CFD simulation of heat and momentum transfer in wavy annular flow to the case of simultaneous heat, mass and momentum transfer.

6.2 Experimental work

The HPBR represents a unique experimental facility in which a great deal of capital and effort has been invested. Though the amount of data generated in the present project is vast, the range of conditions covered is relatively small and there is much scope for further work. This could include:

1. Studying a wider range of mixtures. It would be particularily interesting to make measurements at smaller increments of concentration and to include

such measurements on components forming azeotropic mixtures. The work on ternary mixtures is also an obvious area for extended study.

2. Investigating more systematically the effect of dissolved gases. Here, it would be desirable to use different types of seal pumps which could operate without gas pressurisation.

3. Investigating the effect of longer hydrodynamic entrance lengths by moving the inlet end bus bar. This would allow the decoupling of the development of hydrodynamic and thermal boundary layers and this may throw further light on the inlet peaking phenomena observed with low inlet subcooling. This phenomenon could also be investigated (perhaps visually) in a separate rig if appropriate.

4. Extending the ranges of mass flux covered. The presence of the inlet strainer provides a significant restriction on the mass flux, even after it was unblocked. It should be possible to increase the mass flux considerably by removing this strainer, whose necessity is unproven.

5. Extending the studies to include other geometies. An obvious variable is tube diameter but systematic investigations of the effect of surface roughness and wetability would also be of interest.

6. Carrying out experiments with enhanced heat transfer devices such as tube inserts and porous wall coatings.

7. Improving instrumentation on the facility to allow the investigation of local phenomena. Perhaps liquid film extraction or the use of sampling or isokinetic probes in the gas core could be employed to investigate the hypothesis of relative enrichment of the liquid film in the heavier phase.

In all of the above, generic improvements in the HPBR facility would be valuable. For instance, the present volume flowmeter might be replaced by a mass flow meter to further improve the accuracy of the mass balances etc.

Appendix A

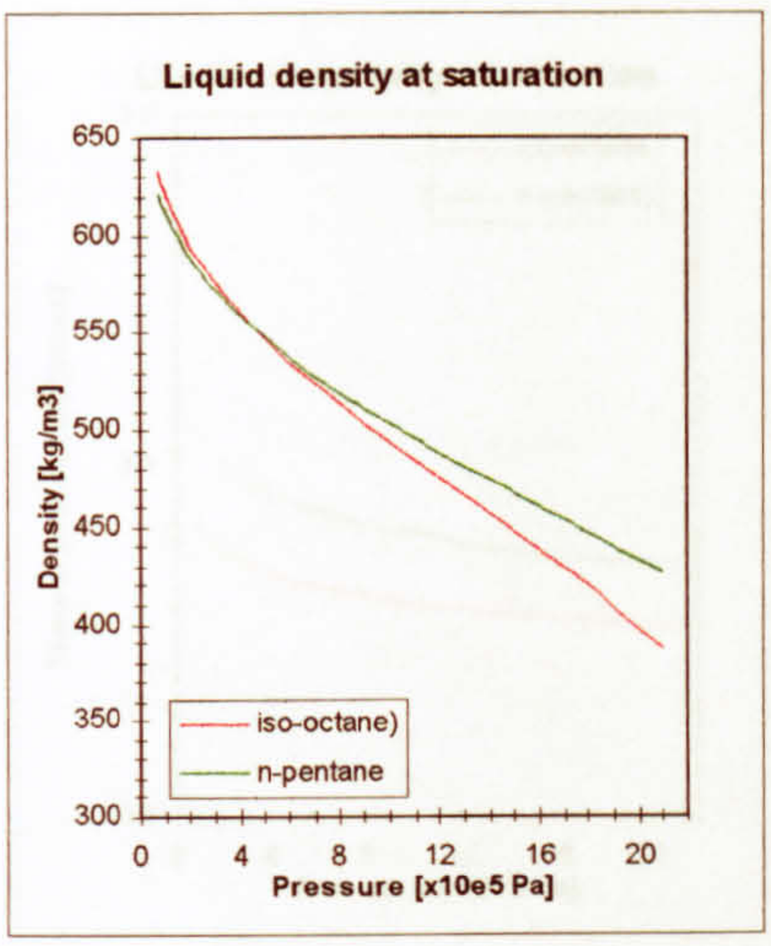
Physical properties of hydrocarbons

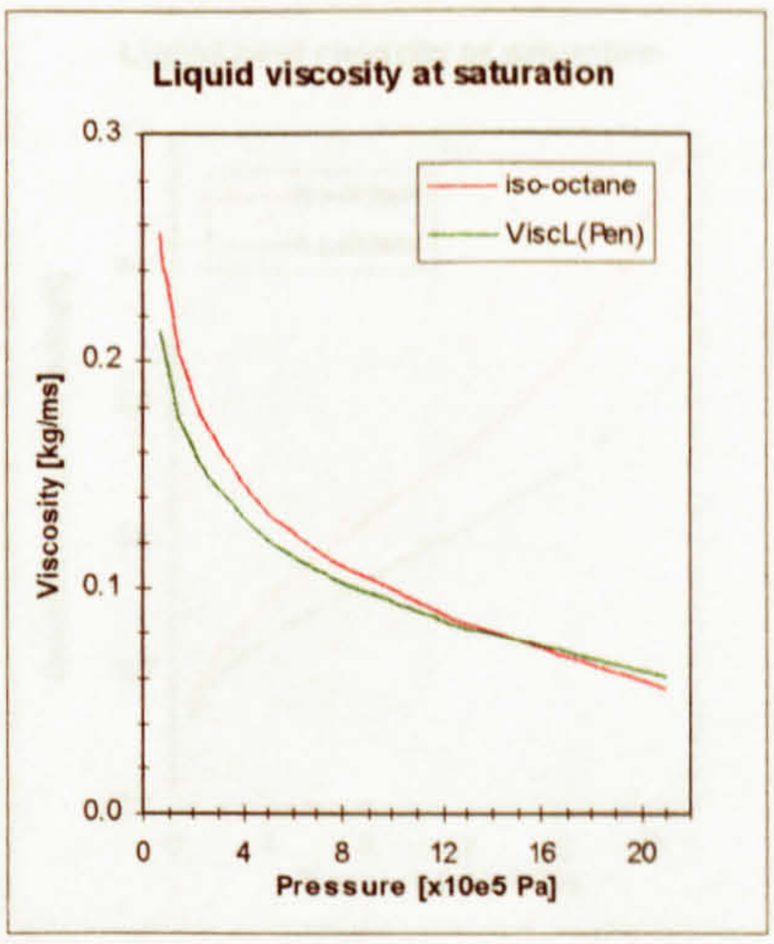
The commercially available software package PPDS (Physical Property Data Service) was used for the calculation of pure and mixture fluid properties. The vapour-liquid equilibrium (VLE) method used was that of Soave-Redlich-Kwong. In Table A.1 characteristic properties are given for the three different hydrocarbons used. Figures A.1 and A.2 show the liquid and vapour saturation properties for n-pentane and iso-octane as a function of pressure.

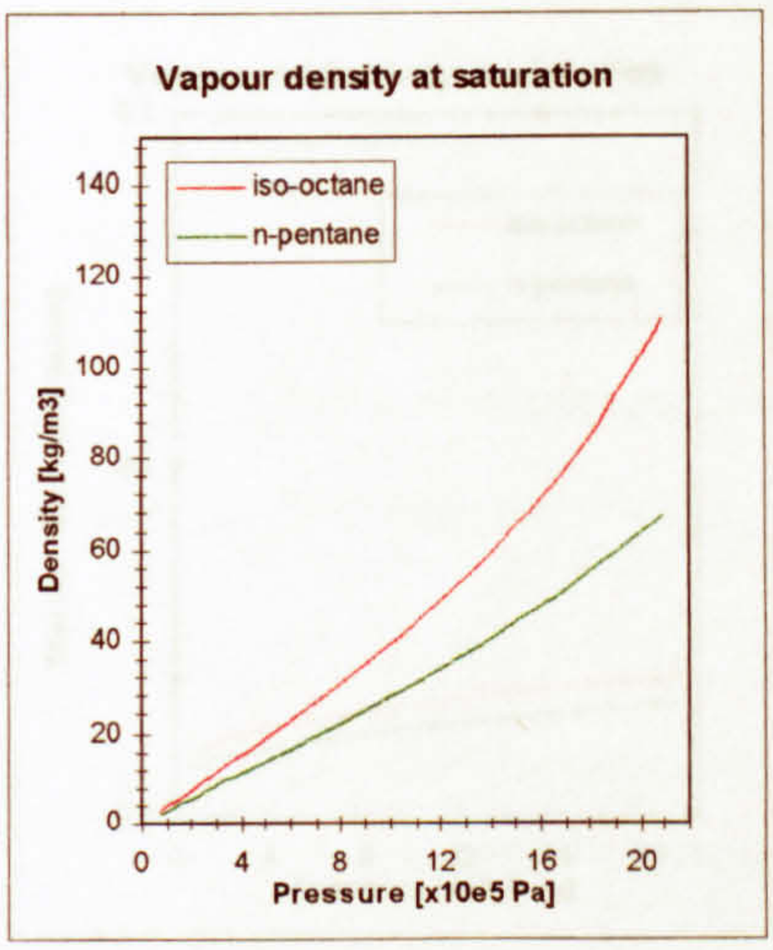
The temperature-composition diagram for the n-pentane/iso-octane mixture is given in Figure A.3. The boiling ranges of the three mixtures used are given in Figure A.4 as a function of pressure.

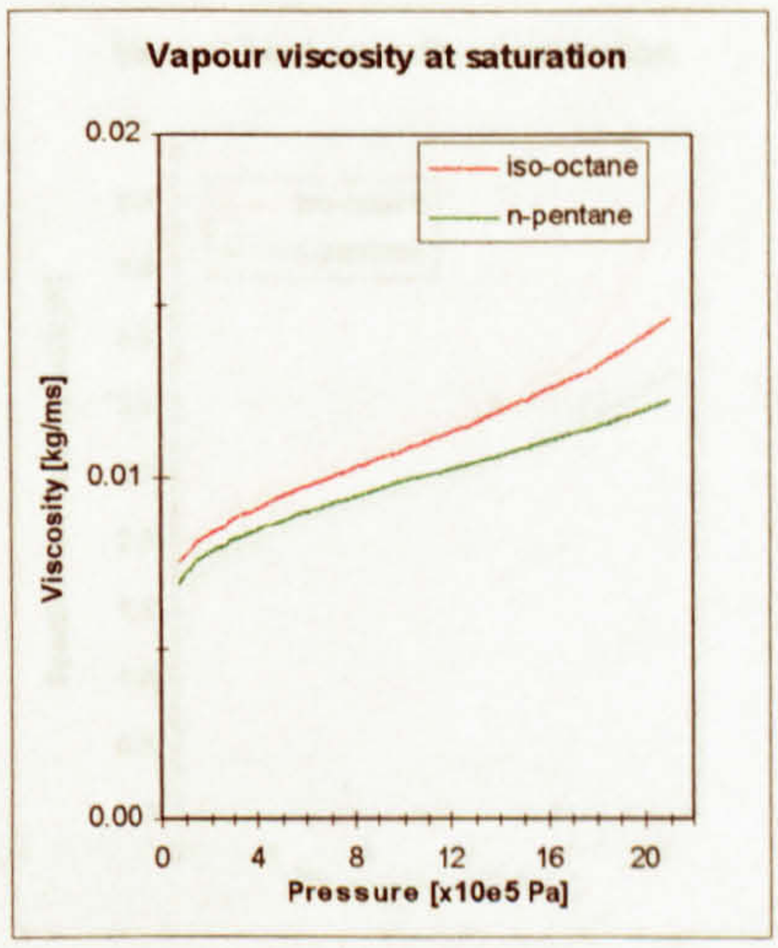
Property	Unit	n-pentane	iso-octane	n-hexane
Molecular weight	[kg/kmol]	72.15	114.23	86.18
Critical temperature	[°C]	196.59	270.81	234.75
Critical pressure	[*bara*]	33.70	25.68	30.22
Normal boiling point	[°C]	36.06	99.22	68.73

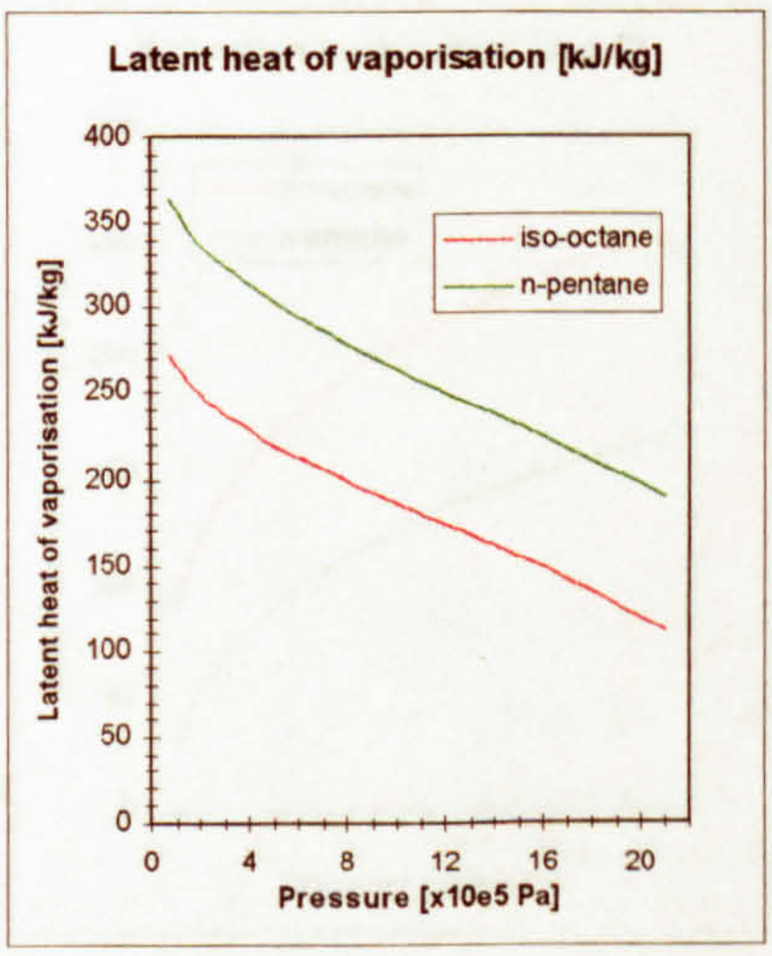
Table A.1: Properties for the pure hydrocarbons n-pentane, iso-octane and n-hexane











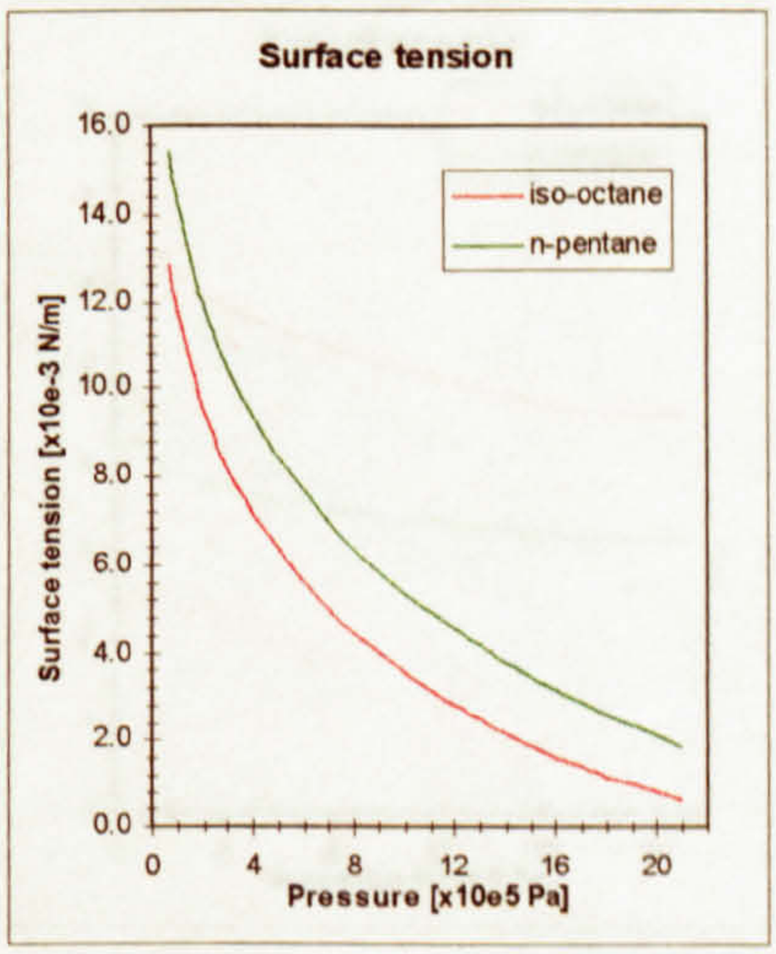
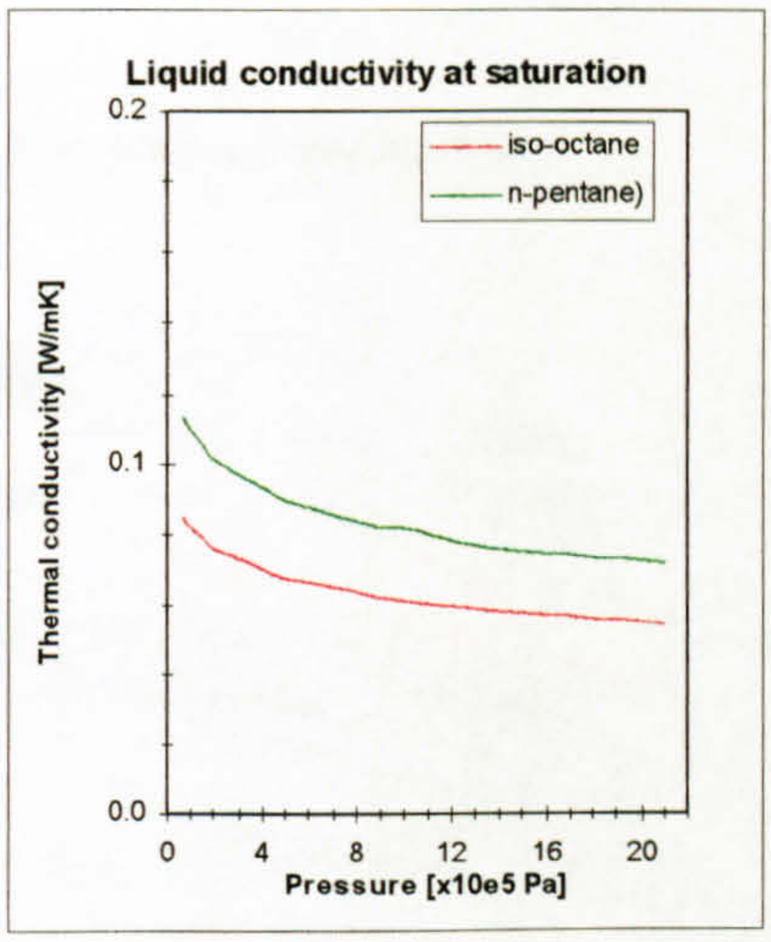
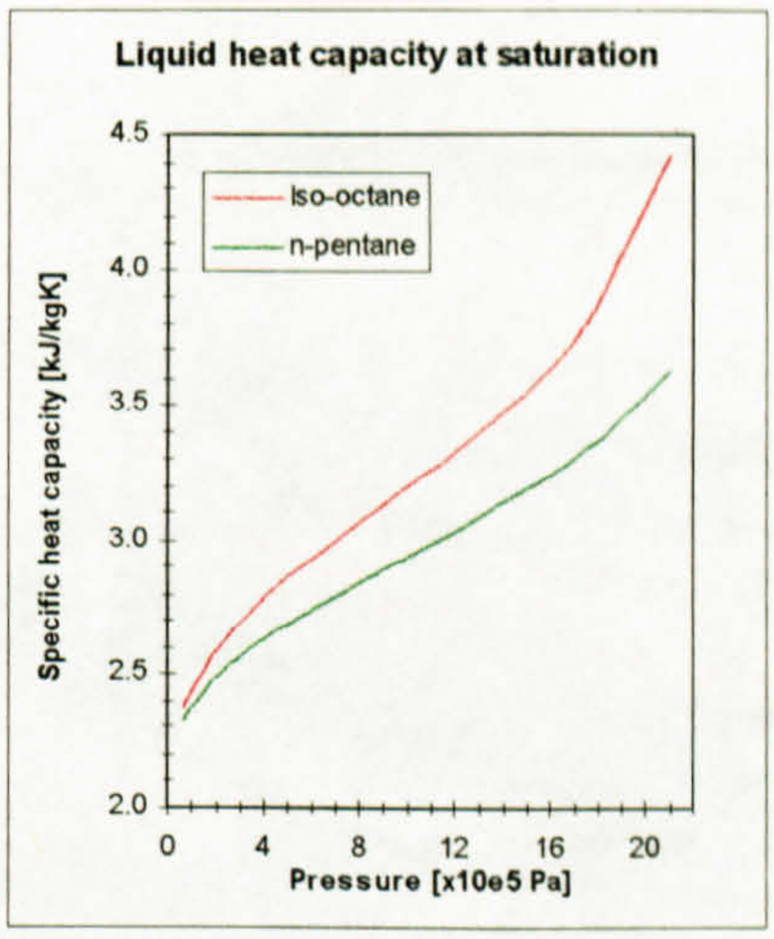
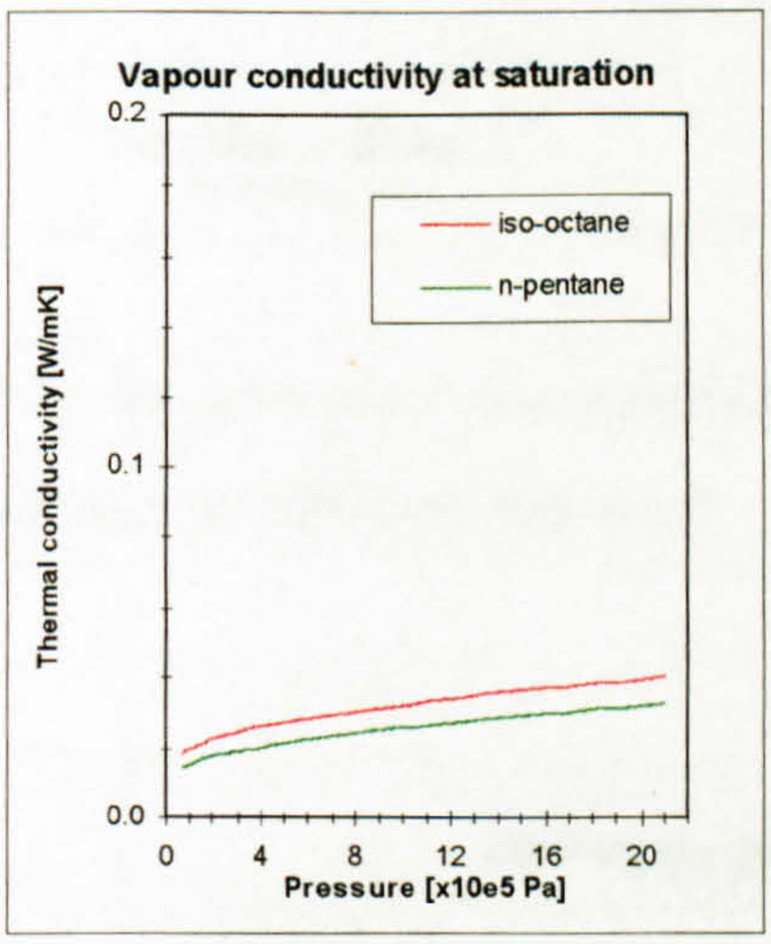
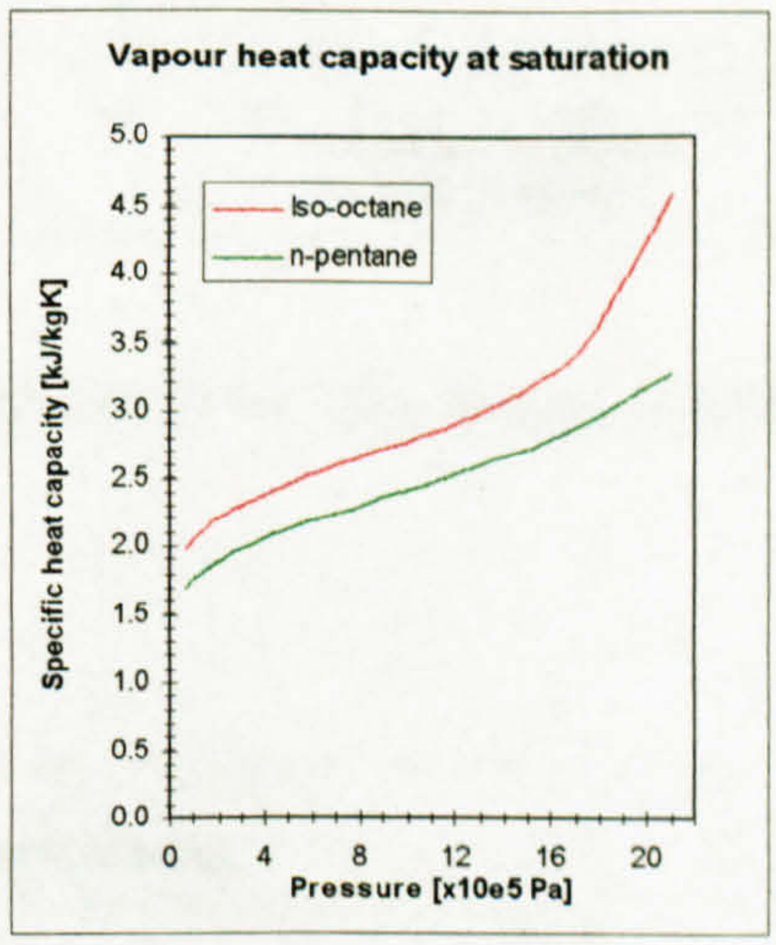


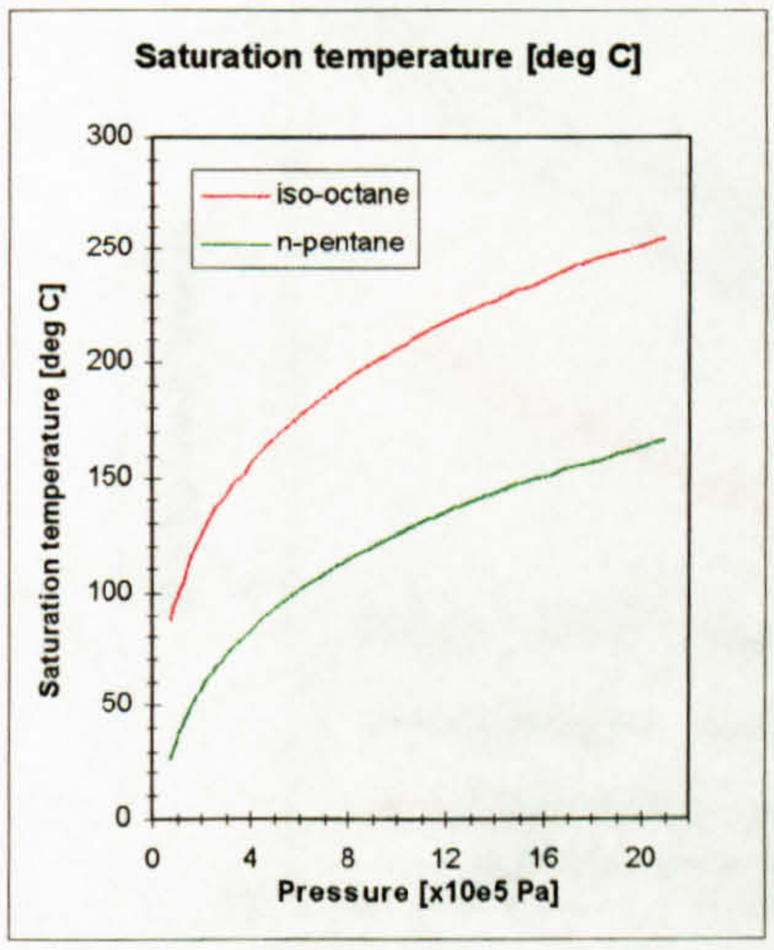
Figure A.1: Properites of n-pentane and iso-octane at saturation as a function of pressure











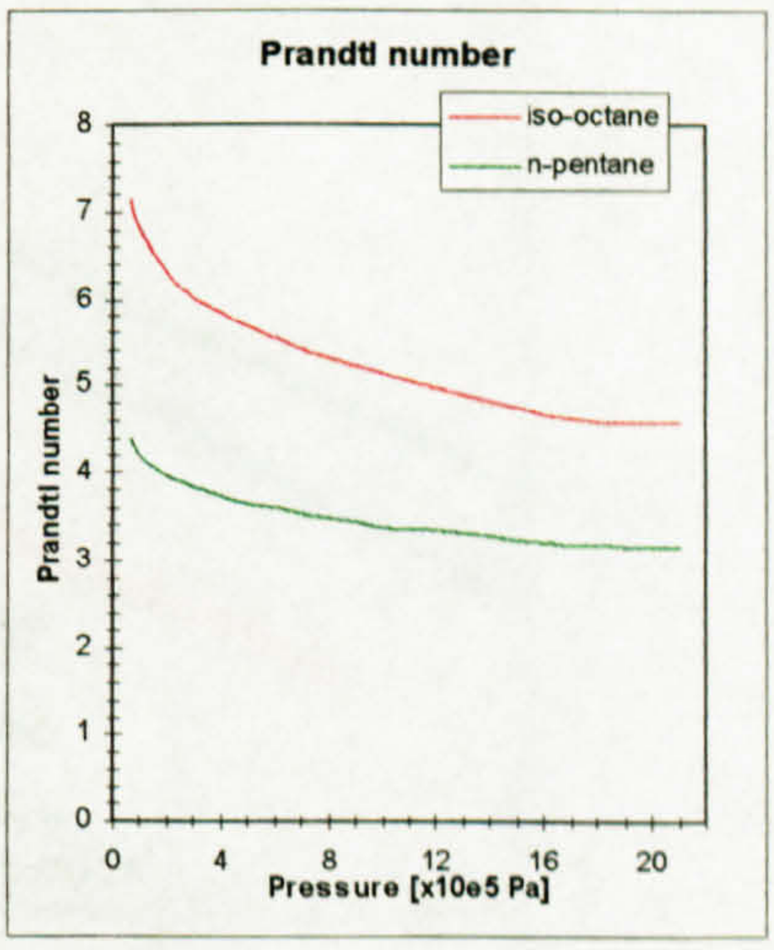


Figure A.2: Properties of n-pentane and iso-octane at saturation as a function of pressure

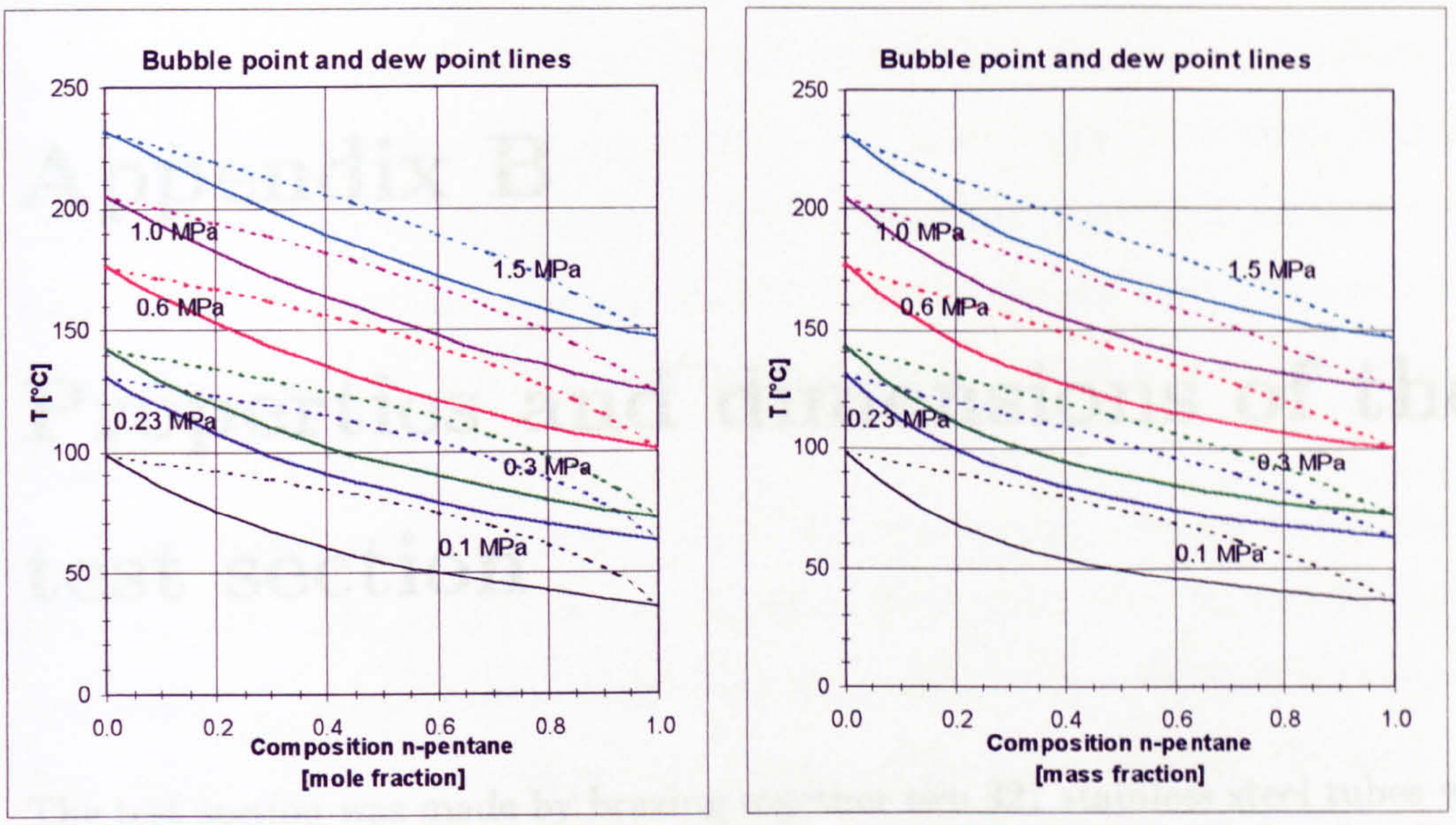


Figure A.3: Temperature–composition diagram for the binary mixture n-pentane/iso-octane at different pressures

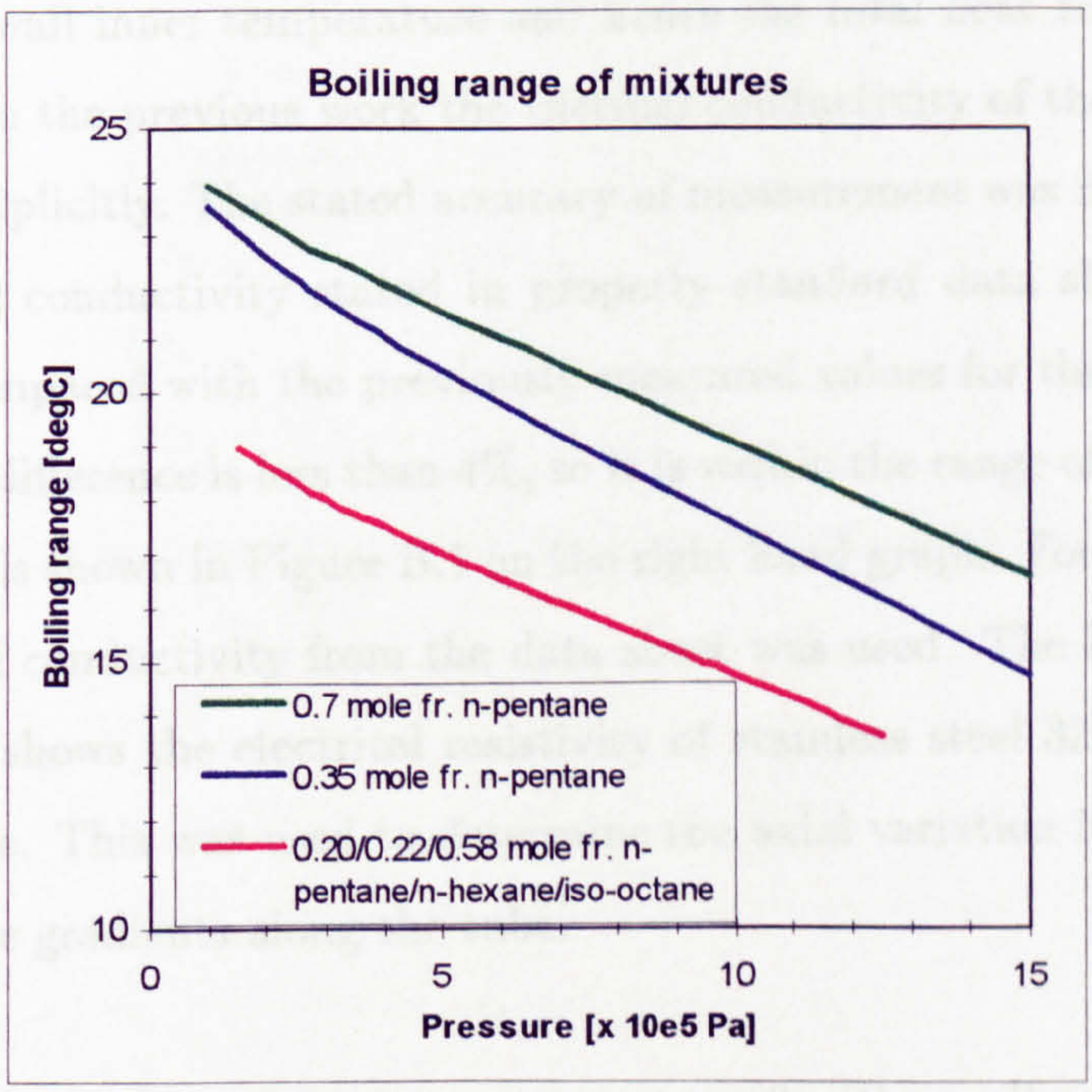


Figure A.4: Boiling ranges for the mixtures used plotted against pressure

Appendix B

Properties and dimensions of the test section

The test section was made by brazing together two 321 stainless steel tubes with a nominal inner diameter of 25.4mm (1 inch).

As described in Section 3.2.3 the wall inner temperature has to be calculated using the one-dimensional steady state heat conduction equation, in which the thermal conductivity and the wall thickness are a source for inaccurate prediction of the wall inner temperature and hence the total heat transfer coefficient. Therefore, in the previous work the thermal conductivity of the test section was measured explicitly. The stated accuracy of measurement was ±4%. In this work the thermal conductivity stated in property standard data sheets for stainless steel are compared with the previously measured values for the thermal conductivity. The difference is less than 4%, so it is within the range of the experimental error. This is shown in Figure B.1 on the right hand graph. For this present work the thermal conductivity from the data sheet was used. The left hand graph of Figure B.1 shows the electrical resistivity of stainless steel 321 as a function of temperature. This was used to determine the axial variation in heat flux due to temperature gradients along the tube.

The test section wall thickness was measured with an ultrasonic flow detector

(Wells Krautheimer USD10). An unused part of the test section tube material was tested. Measurements were taken at four locations (Positions 1 to 4) around the circumference (0, 90, 180, 270°) with an axial spacing of 100mm and with a total of 29 axial positions measured. Figure B.2 shows the wall thickness plotted against length. Each graph shows one circumferential position with the average thickness over the 4 circumferential positions. The minimum and maximum measured wall thicknesses were 6.04 and 6.35 mm respectively, with the average thickness having a variation from 6.16 to 6.23 mm. This shows that the test section tube changes slightly its eccentricity.

The roughness of an unused part of the test section was measured at two locations according to the German Standard DIN 4768. The measuring system was principally a fine needle which could sense and measure the surface structure. The results of the measurement are given in Figure B.5 showing the measured profile against length. Table B.1 lists the measured roughness parameter R_{max}, R_z and R_a, which are explained in Table B.2. The measured length is subdivided into 5 sections, (see Figure B.3). Z_1 to Z_5 are the differences between maximum and minimum peaks for each section considered.

Parameter	Unit	Position 1	Position 2
R_{max}	[μm]	7.29	4.90
R_z	[μm]	4.52	4.18
R_a	[μm]	0.70	0.66

Table B.1: Roughness parameters for the two measured locations of the test section

	Description
R_{max}	is the greatest value of Z_1 to Z_5
R_z	is calculated from $R_z = (Z_1 + Z_2 + Z_3 + Z_4 + Z_5)/5$.
R_a	is electronically calculated by the measuring device. Figure B.4 shows a surface profile with a reference line for an ideal surface (0). The area (striped) A, below and above the reference line is summed up and divided by the measured length, l_m giving R_a as A/l_m.

Table B.2: Description of the roughness parameters according to the German standard DIN 4768

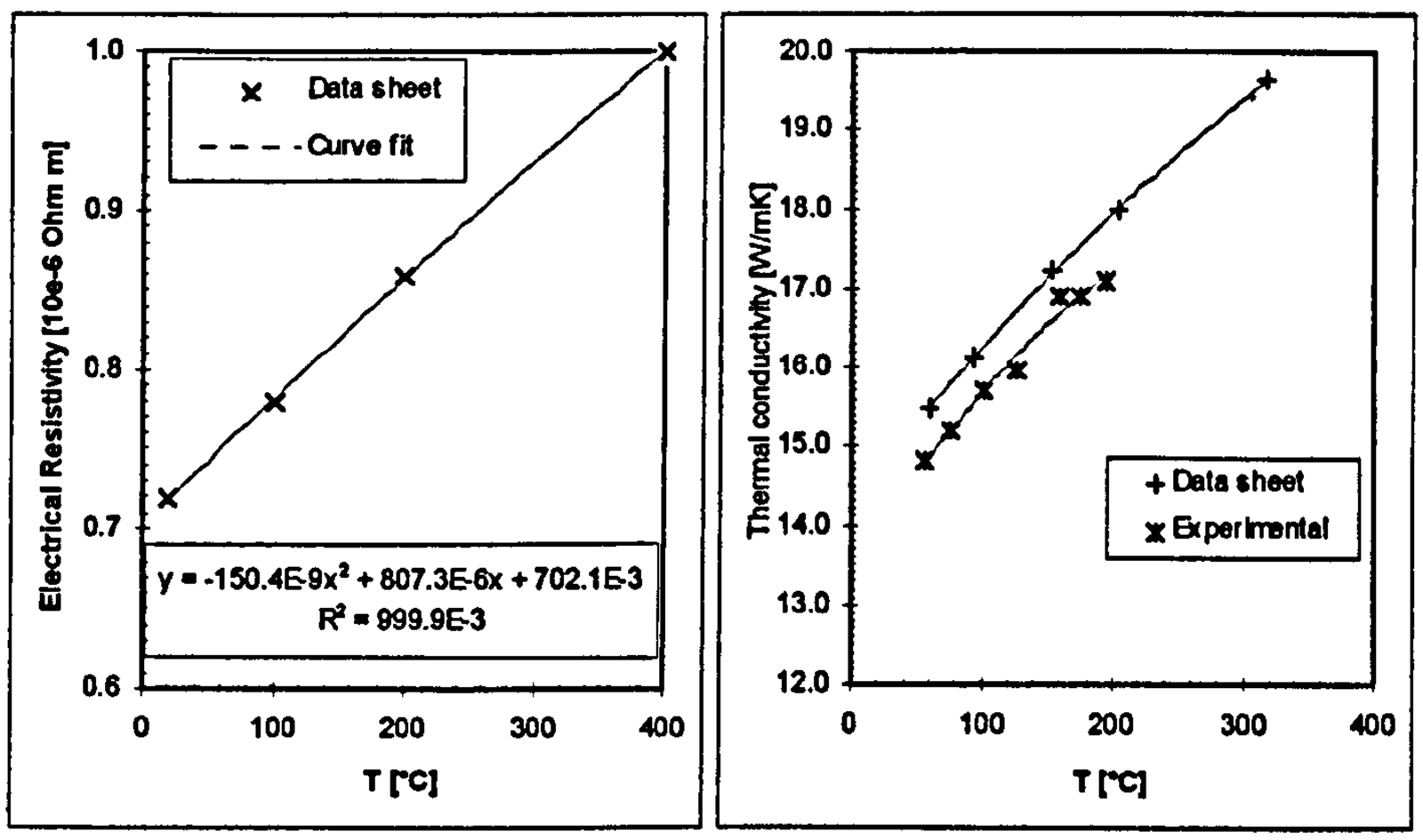


Figure B.1: Thermal conductivity and electrical resistivity of stainless steel 321

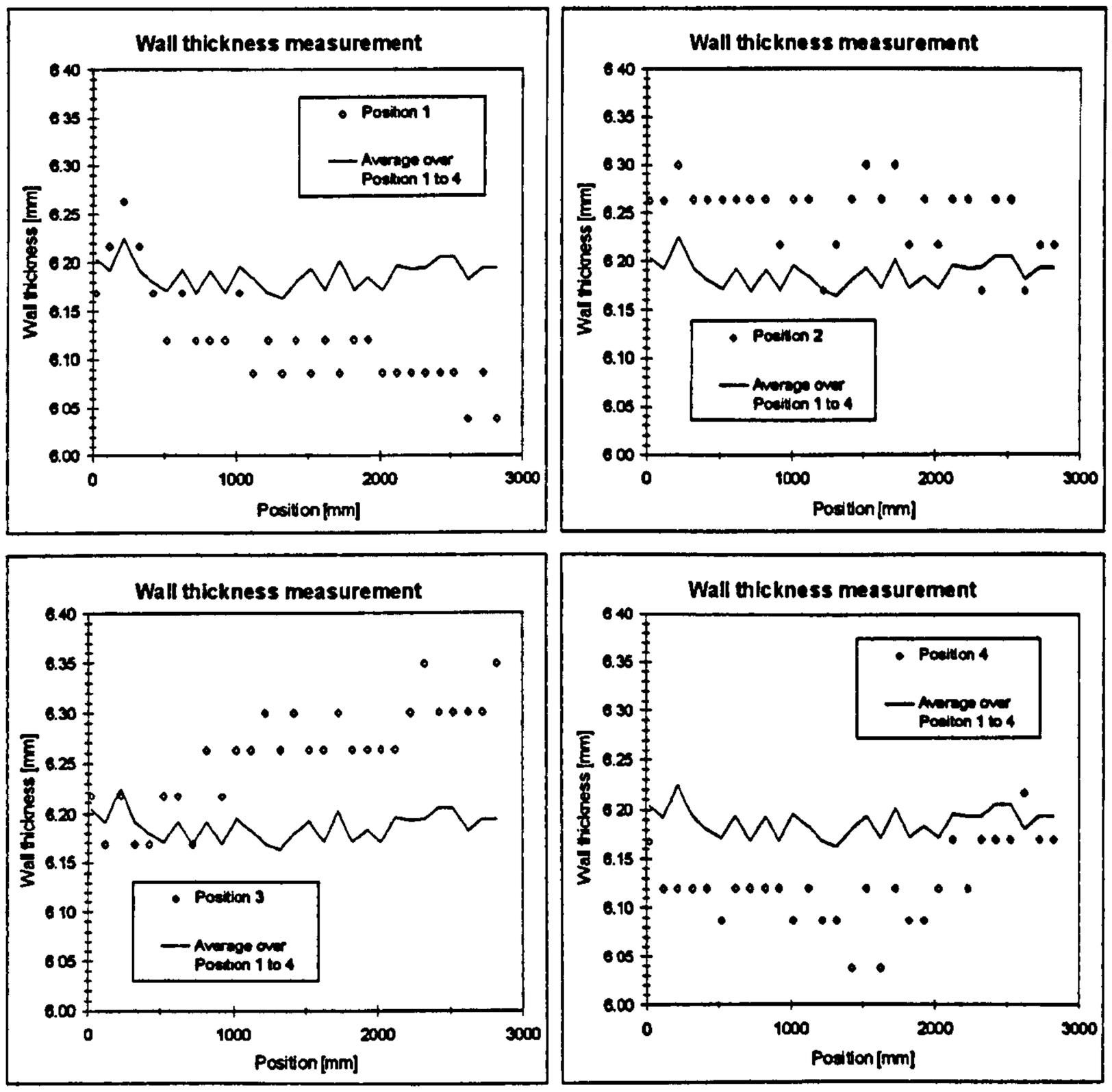


Figure B.2: Measured test section thickness

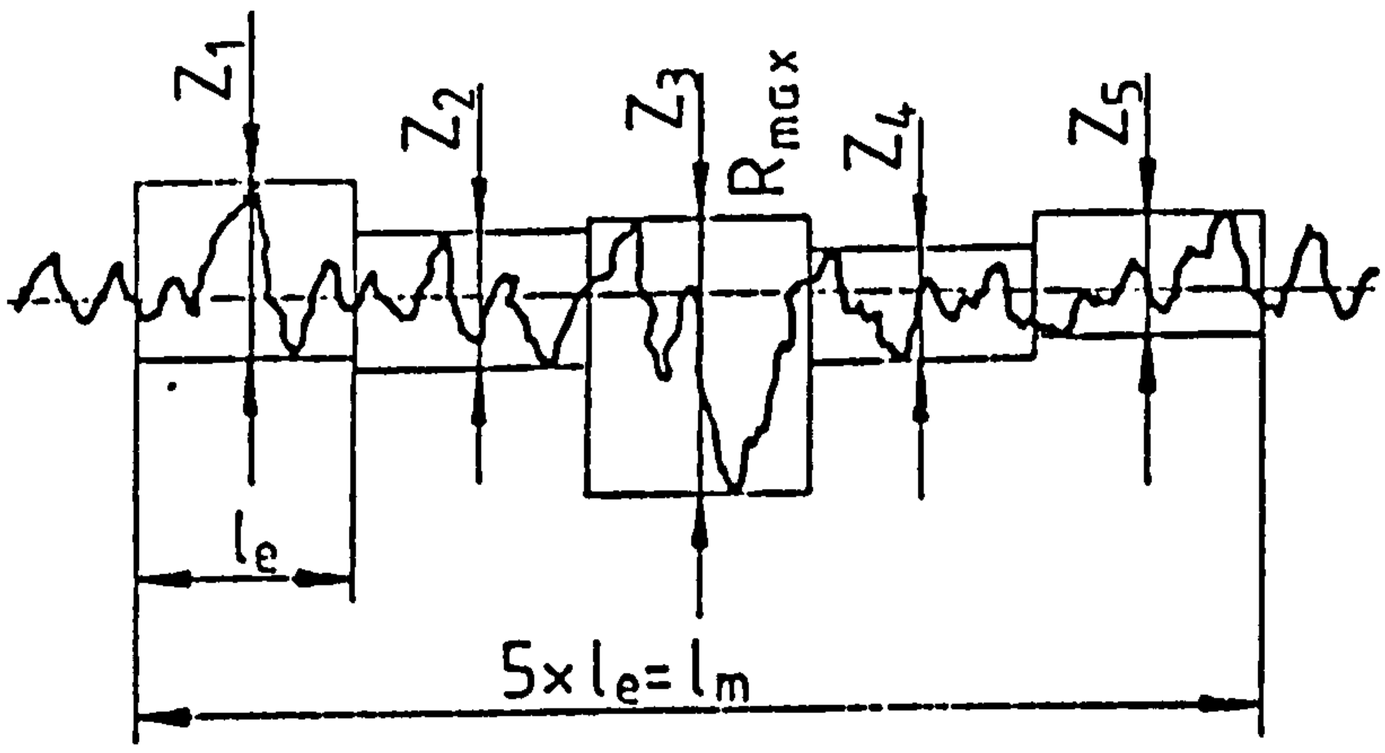


Figure B.3: The definition of the roughness parameters

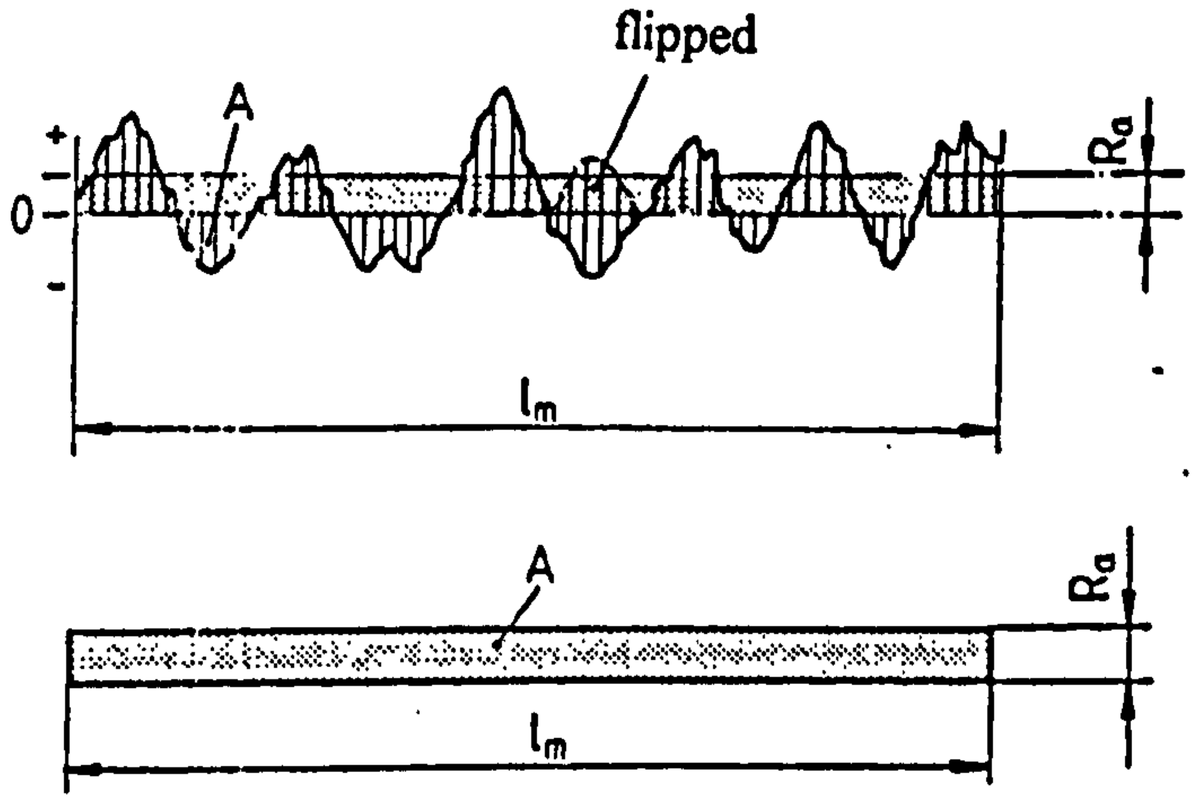


Figure B.4: Definition of roughness parameter R_a

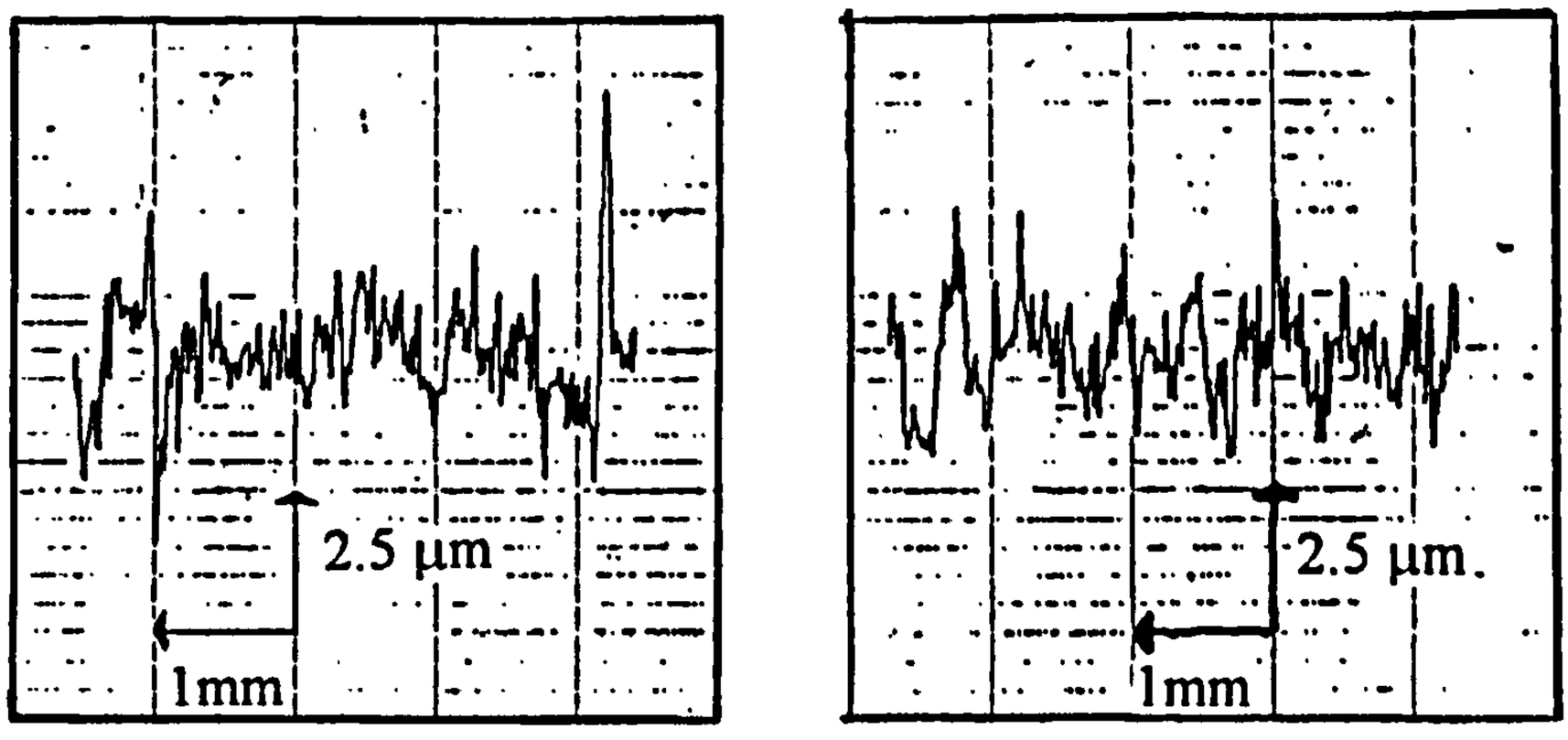


Figure B.5: Measured roughness of test section for two locations (left: Position 1; right: Position 2)

Appendix C

Statistical analysis of the experiments

This Appendix lists the equations used for the statistical analysis of performance of single phase heat transfer correlations as well as forced convective boiling correlations.

The experimental heat transfer coefficient is denoted as α_{exp}, the predicted as α_{pre} and the deviation, $e(j)$, for data point j is expressed as:

$$e(j) = \frac{\alpha_{pre} - \alpha_{exp}}{\alpha_{pre}} \qquad \text{(C.1)}$$

The average error for a set of data with m data points is calculated from

$$\text{Average error} = \frac{1}{m} \sum_{j=1}^{m} e(j) \qquad \text{(C.2)}$$

and the mean error is

$$\text{Mean error} = \frac{1}{m} \sum_{j=1}^{m} |e(j)| \qquad \text{(C.3)}$$

The root-mean-square deviation or standard deviation is calculated from

$$\text{Standard deviation} = \sqrt{\frac{1}{m} \sum_{j=1}^{m} (e(j) - \text{Average error})^2} \qquad \text{(C.4)}$$

Appendix D

Data storage

All the experimental data from the raw data file to the final output file are stored on a CD-ROM (held at HTFS, AEA Technology plc., Harwell, UK) for easy and quick access in the future. A short report was written which includes a description of the data reduction procedure, the output files with a description of each column and a summary of the experiments conducted, listing operating conditions and type of run (single phase, two-phase, heat loss and subcooled). The CD-ROM and report are held by the Heat Transfer and Fluid Flow Service (HTFS) of AEA Technology plc, Harwell, Oxfordshire, England.

References

Alferov, N. S., Balunov, B. F. and Rybin, R. A. (1973) Reduction in heat transfer in the region of supercritical state variables of a liquid, Heat transfer – Soviet Research, Vol.5, pp. 49-52.

Aounallah, Y., Kenning, D. B. R., Whalley, P. B. and Hewitt, G. F. (1982) Boiling heat transfer in annular flow, Proc. 7th Int. Heat Transfer Conf., San Francisco.

Aziz, S., Hewitt, G. F. and Kenning, D. B. R. (1986) Heat transfer regimes in forced convection film boiling on spheres, Proc. 8th Int. Heat Transfer Conf., Vol.5, p. 2149.

Beattie, D. R. H. and Lawther, K. R. (1986) An examination of the wall temperature drop phenomenon during approach to flow boiling crisis, Proc. 8th Int. Heat Transfer Conf., San Fancisco, CA, USA, 17-22 Aug., Vol.5, pp. 2215-2219.

Behar, M., Courtuad, M., Ricque, R. and Semeria, R. (1966) Fundamental aspccts of subcooled boiling with and without dissolved gases, Proc. 3rd Int. Heat Transfer Conf., Chicago, Aug.1966, Vol.4, pp. 1-11.

Bell, K. J. and Ghaly, M. A. (1973) An approximate generalized design method for multicomponent partial condensers, AIChE Symp. Ser., Vol.69, No.131, pp. 72-79.

Bennett, D. L., Davis, M. W. and Hertzler, B. L. (1980) The suppression of saturated nucleate boiling by forced convective flow, AIChE Symp. Ser., Vol.76, No.199, pp. 91-103.

Bennett, D. L. and Chen, J. C. (1980) Forced convective boiling in vertical tubes for saturated pure components and binary mixtures, AIChE Journal, Vol.26, No.3, pp. 454-461.

Bergles, A. E. and Rohsenow, W. M. (1964) The determination of forced-convection surface-boiling heat transfer, ASME J. Heat Transfer, Vol.86, pp. 365-372.

Bjorge, R.W., Hall, G.R. and Rohsenow, W.M. (1982) Correlation of forced convection boiling heat transfer, Int. J. Heat Mass Transfer, Vol.25, No.6, pp. 753-757.

Bowring, R. W. (1962) Physical model based on bubble detachment and calculation of steam voidage in the subcooled region of a heated channel, OECD Halden Reactor Project Report HPR-10.

Bräuer, H. and Mayinger, F. (1992) Onset of nucleate boiling and hysteresis effects under forced convection and pool boiling, Proc. Conf. on Pool and External Flow Boiling, Santa Barbara, 22-27 Mar, pp. 15-36.

Calus, W. F., di Montegnacco, A. and Denning, R. K. (1973a) Heat transfer in a natural circulation single tube reboiler, Part II: Binary liquid mixtures, Chem. Eng. J., Vol.6, No.3, pp. 251-264.

Calus, W. F., di Montegnacco, A. and Denning, R. K. (1973b), Heat transfer in a natural circulation single tube reboiler, Part I: Single component liquids, Chem. Eng. J., Vol.6, No.3, pp. 233-250.

Calus, W. F. and Rice, P. (1972) Pool boiling - binary liquid mixtures, Chemical Engineering Science, Vol.27, pp. 1687-1697.

Carey, V. P. (1992) Liquid-vapor phase-change phenomena, An introduction to the thermophysics of vaporisation and condensation processes in heat transfer equipment, Series in Chemical and Mechanical Engineering, Hemisphere Publication.

Celata, G. P., Cumo, M. and Setaro, T. (1995) Heat transfer in vertical forced convective boiling of mixtures, Int. Conf. on Convective Flow Boiling, Banff, Alberta, Canada, 30.April - 5.May, Paper VI-1.

Celata, G. P., Cumo, M. , Setaro, T. (1993) Forced convective boiling in binary mixtures, Int. J. Heat and Mass Transfer, Vol.36, No.13, pp. 3299-3309.

Chaddock, J. B. and Noerager, J. A. (1966) Evaporation of refrigerant 12 in a horizontal tube with constant wall heat flux, ASHRAE Trans., Vol.72, pp. 90-103.

Chawla, J. M. (1967) Wärmeübergang und Druckabfall in waagrechten Rohren bei der Strömung von verdampfenden Kältemitteln, Kältetechnik – Klimatisierung, Vol.19, No.8.

Chen, J. C. (1966) A correlation for boiling heat transfer to saturated fluids in convective flow, Ind. Eng. Chem. Process Des. Dev., Vol.5, pp. 322-329.

Cichelli, M. T. and Bonilla, C. F. (1945) Heat transfer to liquids boiling under pressure, Trans. Am. Instn. Chem. Engrs., Vol.41, pp. 755-787.

Churchill, S. W. and Usagi, R. (1972) A general expression for the correlation of rates of heat transfer and other phenomena, AIChE J., Vol.18, No.6, pp. 1121-1128.

Collier, J. G. and Thome, J. R. (1994) Convective boiling and condensation, Third Edition, Oxford University Press.

Cooper, M. G., Judd, A. M. and Pike, R. A. (1978) Shape and departure of single bubbles growing at a wall, Pres. at 6th Int. Heat Transfer Conf., Toronto, Vol.1, pp. 115-120.

Cooper, M. G. (1984) Saturation nucleate pool boiling - A simple correlation, IChem E Symp. Series, No.86(2).

Cousins, L. B. and Hewitt, G. F. (1968) Liquid phase mass transfer in annular two-phase flow: Radial liquid mixing. UKAEA Report AERE-R5693.

Davidson, W. F. (1943) Studies of heat transmission through boiler tubing at pressures from 500 to 3300 pounds, Trans. of the American Soc. of Mech.

Engineers, Vol.63, pp. 551-554.

Dhir, V. K. (1996) Pool boiling heat transfer: Recent advances and expectations for the future. In " Process, Enhanced and Multiphase Heat Transfer: Festschrift für A. E. Bergles" Ed. R. M. Manglik and A. D. Kraus, Begell House, NY.

Dittus, F. W. and Boelter, L. M. K. (1930) Heat transfer in automobile radiators of the tubular type, Publications in Engineering, Univ. of California, Vol.2, No.13, pp. 443-461; reprinted in Int. Comm. Heat Mass Transfer, Vol.12, pp. 3-22, 1985.

ESDU (1991) Forced convection heat transfer in straight tubes, Item No. 92003, Engineering Science Data Unit, London.

ESDU (1967) Forced convection heat transfer in circular tubes, Part I: Correlations for fully developed turbulent flow, Item No. 68007, Engineering Science Data Unit, London.

Forster, H. K. and Zuber N. (1955) Dynamics of vapor bubbles and boiling heat transfer, AIChE Journal, Vol.1, pp. 531-535.

Frankum, D. P. (1996) Heat transfer and flow patterns for vertical in-tube boiling of single and multicomponent fluids, PhD Thesis, University of Nottingham.

Frankum, D. P. (1991) Wall temperature measurement for the high pressure boiling rig, Internal Report, AEA Technology plc., Harwell, UK.

Fritz, W. (1935) Maximum volume of vapor bubbles, Zeitschrift für Physik, Vol.36, pp. 379-384.

Fujita, Y. and Tsutsui, M. (1995) Convective boiling of binary mixtures in a vertical tube, Int. Conf. on Convective Flow Boiling, Banff, Alberta, Canada, 30 April - 5. May, Paper VI-2.

Fujita, Y., Bai, Q. and Tsutsui, T. (1996) Heat transfer of binary mixtures in nucleate pool boiling, 2nd European Thermal-Sciences and 14th UIT Nat. H.T. Conf., 1996.

Gnielinski, V. (1983) Forced convection in ducts, Heat Exchanger Design Handbook (HEDH), Hemisphere Publishing Corporation.

Gnielinski, V. (1976) New equations for heat and mass transfer in turbulent pipe and channel flow, Int. Chem. Eng., Vol.16, No.2, pp. 359-368, April 1976.

Gorenflo, D., (1991), Abschnitt Hab Behältersieden, VDI-Wärmeatlas, 6. Aufl., VDI-Verlag, Düsseldorf, 1991.

Gorenflo, D. and Köster, R. (1997) Pool boiling heat transfer from horizontal tubes to mixtures, Conv. Flow and Pool Boiling Conf., Int. Engn. Foundation Conf., May 1997, Irsee, Germany.

Govan, A. H. (1990) Modelling of vertical annular and dispersed two-phase flows, PhD Thesis, Imperial College London, University of London, UK, 310p.

Govan, A. H. and Hewitt, G. F. (1990) Phenomenological modelling of non-equilibrium flows with phase change, Int. J. Multiphase Flow, Vol.33, pp. 229-242.

Gungor, K. E. and Winterton, R. H. S. (1986) A general correlation for flow boiling in tubes and annuli, Int. J. Heat Mass Transfer, Vol.29, No.3, pp. 351-358.

Gungor, K. E. and Winterton, R. H. S. (1987) Simplified general correlation for saturated flow boiling and comparisons of correlations with data, Chem. Eng. Res. Des., Vol.65, pp. 148-156.

Han, C. and Griffith, P. (1965) The mechanism of heat transfer in nucleate pool boiling - Part I, Int. J. Heat Mass Transfer, Vol.8, pp. 887-904.

Happel, O. and Stephan, K. (1974) Heat transfer from nucleate to the beginning of film boiling in binary mixtures, Proc. 5th Int. Heat Transfer Conf., Tokyo, Sept., Vol.6, Paper B7.8.

Hattan, A. P. and Hall, I. S. (1966) Photographic study of boiling on prepared surfaces, 3rd Int. Heat Transfer Conf., Chicago, August.

Hausen, H. (1959) Neue Gleichungen für die Wärmeübertragung bei freier oder erzwungener Strömung, Allg. Wärmetechnik, No.9, No. 4/5, pp. 75-79.

Hawkes, N. (1996) Wispy-annular flow, PhD Thesis, Imperial College London, University of London.

Hewitt, G. F. and Hall-Taylor, N. S. (1970) Annular two-phase flow, Pergamon Press.

Hewitt, G. F. (1982) Handbook of multiphase systems, Hemisphere Publishing, ed. G. Hetsroni.

Hewitt, G. F., Shires, G. L. and Bott, T. R. (1994), Process Heat Transfer, CRC Press.

Hihara, E., Tanida, K. and Saito, T. (1989) Forced convective boiling experiments of binary mixtures, JSME Int. J., Vol.32, No.1, pp. 98-106.

Hihara, E. and Saito, T. (1988) Forced convective boiling heat transfer of binary mixtures, The Japan-US Seminar on Two Phase Flow Dynamics, 15-20 July, Ohtsu, Japan, 9p.

Howell, J. R. and Siegel, R. (1966) Incipience growth and detachment of boiling bubbles in saturated water from artificial nucleation sites of known geometry and size, 3rd Int. Heat Transfer Conf., Chicago, August.

Hsu, Y. Y. and Graham, R. W. (1986) Transport Processes in Boiling and Two-Phase Systems, ANS, ISBN0894480308, Chapter 1, pp. 3-49.

Jackson, J. D., Cotton, M. A. and Axcell, B. P. (1989) Studies of mixed convection in vertical tubes, Int. J. Heat Fluid Flow, Vol.10, No.1, pp. 2-15.

Jackson, J. D. and Hall, W. B. (1979) Influences of buoyancy on heat transfer to fluids flowing in vertical tubes under turbulent conditions, Turbulent Forced Convection in Channels and Bundles Theory and Applications to Heat Exchangers and Nuclear Reactors, Vol.2 (eds. Kakac, S. and Spalding D. B.), pp. 613-640.

Jayanti, S. (1997) Hydrodynamics and heat transfer in wavy annular gas-liquid flow – A computational fluid dynamic study, Int. J. Heat and Mass Transfer, Vol.40, No.10, pp.2445-2460.

Jallouk, P. A. (1974) Two-phase flow pressure drop and heat transfer characteristics of refrigerants in vertical tubes, Ph.D. dissertation, University of Tennessee.

Jensen, M. K. and Bensler, H. P. (1986) Saturated forced-convective boiling heat transfer with twisted-tape inserts, J. Heat Transfer, Vol.108, No.1, pp. 93-99.

Johnson, M. A., de la Pena, J. and Mesler, R. B. (1966) Bubble shapes in nucleate boiling, Chem. Engng. Prog. Symp. Series, Vol.62, No.1.

Jung, D. S., McLinden, M. , Radermacher, R. and Didion, D. (1989a) A study of flow boiling heat transfer with refrigerant mixtures, Int. J. Heat Mass Transfer, Vol.32, No.9, pp. 1751-1764.

Jung, D. S., McLinden, M. and Radermacher, R. (1989b) Horizontal flow boiling heat transfer experiments with a mixture of R22/R114, Int. J. Heat Mass Transfer, Vol.32, No.1, pp. 131-145.

Jung, D. S. and Didion, D. A. (1989c) Horizontal flow boiling heat transfer using refrigerant mixtures, EPRI ER-6364 Research Project 8006-2.

Kandlikar, S. G. (1990a) Flow boiling maps for water, R-22 and R-134a in the saturated region, Proc. 9th Int. Heat Transfer Conf., Jerusalem, Israel , Paper 1-BO-03, pp. 15-20.

Kandlikar, S. G., (1990b) A general correlation for saturated two-phase flow boiling heat transfer inside horizontal and vertical tubes, J. Heat Transfer, Vol.112, No.1, pp. 219-228.

Kandlikar, S. G. (1991) Correlating flow boiling heat transfer data in binary systems, HTD-Vol. 159, Phase Change Heat Transfer, ASME.

Kattan, N. and Thome, J. R. (1995a) R-502 and two near-azeotropic alternatives: Part I – In-tube flow-boiling tests, ASHRAE Trans, Vol.101, Pt.1, pp. 491-508.

Kattan, N. and Thome, J. R. (1995b) R-502 and two near-azeotropic alternatives: Part II – Two-phase flow patterns, ASHRAE Trans, Vol.101, Pt.1, pp. 509-519.

Kenning, D. B. R. and Cooper M. G. (1989) Saturated flow boiling of water in vertical tubes, Int. J. Heat Mass Transfer, Vol.32, No.3, pp. 445-458.

Kenning, D. B. R., Shock, R. A. W. and Poon, J. Y. M. (1974) Local reductions in heat transfer due to buoyancy effects in upward turbulent flow, Proc. of the 5th Int. Heat Transfer Conf., Tokyo, Paper NC4.3.

Keshock, E. G. and Siegel, R. (1964) Forces acting on bubbles in nucleate boiling under normal and reduced gravity conditions, NASA TN-D-2299.

Klimenko, V. V. (1990) A generalized correlation for two-phase forced flow heat transfer - second assessment, Int. J. Heat Mass Transfer, Vol.33, No.10, pp. 2073-2088.

Koumoutsos, N., Moissis, R. and Spyridonos, A. (1968) A study of bubble departure in forced-convection boiling, J. of Heat and Mass Transfer, No.5, pp. 223-230.

Kröger, P. G. and Zuber, N. (1968) An analysis of the effects of various parameters on the average void fractions in subcooled boiling, Int. J. Heat Mass Transfer, Vol. 11, pp. 2111-233.

Kusumowardhoyo, M. A. and Hardianto, T. (1985) Two-phase heat transfer correlation for multi-component mixtures in the saturated flow-boiling regime, Int. J. Heat Fluid Flow, Vol.6, No.4, pp. 265-268.

Kutateladze, S. S. (1961) Boiling heat transfer, Int. J. Heat Mass Transfer, Vol.4, pp. 31-45.

Landolt-Börnstein (1976) Zahlenwerte und Funktionen, Vol.IV, Sec.4cI, Springer Verlag.

Levy, S. (1967) Forced convection subcooled boiling - prediction of vapor volumetric fraction, Int. J. Heat Mass Transfer, Vol.10, pp. 951-965.

Liu, Z. and Winterton, R. H. S., (1991), A general correlation for saturated and subcooled flow boiling in tubes and annuli, based on a nucleate pool boiling equation, Int. J. Heat Mass Transfer, Vol.34, No.11, pp. 2759-2766.

Marto, P. J. and Lepere V. J. (1982) Pool boiling heat transfer from enhanced surfaces to dielectric fluids, ASME J. of Heat Transfer, Vol.104, pp. 292-297.

Mayinger, F. and Bucher, B. (1976) Subcooled boiling, NATO Advanced Study Institute, Two-Phase Flows and Heat Transfer, 16-27 Aug., Istambul, Turkey.

Mesler, R. B. (1976) A mechanism supported by extensive experimental evidence to explain high heat fluxes observed during nucleate boiling, AIChE J., Vol.22.

Mikic, B. B. and Rohsenow, W. M. (1969) A new correlation of pool-boiling data including the effect of heating surface characteristics, J. of Heat Transfer, pp. 245-250.

Milashenko, V. I., Nigmatulin, B. I., Petukhov, V. V. and Tribunkin, N. I. (1989) Burnout and distribution of liquid in evaporative channels of various lengths, Int. J. Multiphase Flow, No.15, pp. 393-402.

Mishra, M. P., Varma, H. K. and Sharma, C. P. (1981) Heat transfer coefficients in forced convection evaporation of refrigerants mixtures, Letters in Heat Mass

Transfer, Vol.8, No.2, pp. 127-136.

Moore, D. F. and Mesler, R. B. (1961) The measurements of rapid surface temperature fluctuations during nucleate boiling of water, AIChE J., Vol.7, pp. 620-624.

Müller-Steinhagen, H., Epstein, N. and Watkinson, A. P. (1988) Effect of dissolved gases on subcooled flow boiling heat transfer, Chem. Eng. Process, Vol.23, No.2, pp. 115-124.

Murata, K. and Hashizume, K. (1993) Forced convective boiling of nonazeotropic refrigerant mixtures inside tubes, J. Heat Transfer, Vol.115, pp. 680-689.

Murata, K. and Hashizume, K. (1991) An experimental investigation on forced convection boiling of refrigerant mixtures, 18th Int. Congress of refrigeration, Montreal, 10-17 Aug. 1991.

Murata, K. and Hashizume, K. (1990) An investigation on forced convection boiling of nonazeotropic refrigerant mixtures, Heat Transfer Jap. Res., Vol.19, No.2, pp. 95-109.

Murphy, R. W. and Bergles, A. E. (1972) Subcooled flow boiling of fluorocarbons – hysteresis and dissolved gas effects on heat transfer, Proc. Heat Transfer and Fluid Mechanics Inst., Northridge, California, 14.-16. June.

Nakanishi, S., Kaji, M., Matoba, H. and Kaji, N. (1987) Flow boiling in tube of mixtures of refrigerants R11 and R113, Trans. JSME, Vol.53, No.486, pp. 2626-2632.

Niederkrüger, M., Steiner, D. and Schlünder, E.-U. (1992) Horizontal flow boiling experiments of saturated pure components and mixtures of R846-R12 at high pressures, Int. J. Refrig., Vol.15, No.1, pp.48-58.

Nishikawa, K., Fujita, Y., Ohta, H. and Hidaka, S. (1982) Effect of surface roughness on the nucleate boiling heat transfer over the wide range of pressure, Proc.

9th Int. Heat Transfer Conf., München, Germany, Sept., Vol.4, Paper PB10, pp. 61-66.

Owen, D. G. and Hewitt, G. F. (1986) A proposed entrainment correlation, AERE-R 12279, AEA Technology, Harwell, UK.

Palen, J. W. and Small, W. M. (1964) A new way to design kettle and internal reboilers, Hydrocarbon Processing, Vol.43, No.11, pp. 199-208.

Palen, J. W. and Yang, C. C. (1983) Circulation model for analysis of kettle and internal reboiler performance, Paper presented at 21st Nat. Heat Transfer Conf., Seattle, 1983.

Palen, J.W. (1983) Shell-and-tube reboilers, Thermal Design, HEDH, Hemisphere Publishing Corporation, Sec.3.6.2.

Petukhov, B. S. (1977) Turbulent flow and heat transfer in pipes under considerable effect of thermogravitational forces, Heat transfer and turbulent buoyant convection, Vol.2, D. B. Spalding and N. Afgan (Eds), Hemisphere Publishing.

Petukhov, B. S. and Popov, V. N. (1963) Theoretical calculation of heat exchange and frictional resistance in turbulent flow in tubes of an incompressible fluid with variable physical properties, High Temperature, Vol.1, No.1, pp. 69-83.

Petukhov, B. S. (1970) Heat transfer and friction in turbulent pipe flow with variable physical properties, Advances in Heat Transfer, Academic Press, Vol.6, pp. 503-564.

Radermacher, R., Ross, H. and Didion, D. (1983) Experimental determination of forced convective evaporative heat transfer coefficients for nonazeotropic refrigerant mixtures, ASME Nat. Heat Transfer Conf., ASME 83-WA/HT54.

Redlich, O. and Kwong, J. N. S. (1949) Chem. Rev., Vol.44, p.233

Reid, R. S., Pate, M. B. and Bergles, A. E. (1987) Evaporation of refrigerant 113 flowing inside smooth tubes, Nat. Heat Transfer Conf., Pittsburgh, PA, USA,

9-12 Aug., ASME Paper 87-HT-51.

Rohsenow, W. M. (1952) Heat transfer with evaporation, Heat Transfer Symposium, University of Michigan, Section 4.

Ross, H. and Radermacher, R. (1987a) Horizontal flow boiling of pure and mixed refrigerants, Int. J. Heat Mass Transfer, Vol.30, No.5, pp. 979-992.

Ross, H. and Radermacher, R. (1987b) Suppression of nucleate boiling of pure and mixed refrigerants in turbulent annular flow, Int. J. Multiphase Flow, Vol.13, No.6, pp. 759-772

Rouai, N. M. (1987) Influences of buoyancy and imposed flow transients on turbulent convective heat transfer in a tube, PhD Thesis, University of Manchester.

Saha, P. and Zuber, N. (1974) Point of net vapor generation and vapor void fraction in subcooled boiling, 5th Int. Heat Transfer Conf., Tokyo, 3-7 Sept, 5p.

Sardesai, R. G., Shock, R. A. W. and Butterworth, D. (1982) Heat and mass transfer in multicomponent condensation and boiling, Heat Transfer Eng., Vol.3, No.3-4, pp. 104-114.

Schlünder, E. U. (1983) Heat transfer in nucleate boiling of mixtures, Int. Chemical Engineering, Vol.23, No.4, pp. 589-599.

Scriven, L. E. (1959) On the dynamics of phase growth, Chemical Engineering Science, Vol.10, No.1/2.

Shah, M. M. (1976) A new correlation for heat transfer during boiling flow, ASHRAE Trans., Vol.82, No.2, pp. 66-86.

Shah, M. M. (1982) Chart correlation for saturated boiling heat transfer: Equations and further study, ASHRAE Trans., Vol.88, Part I, pp. 185-196.

Shock, R. A. W. (1976) Evaporation of binary mixtures in upward annular flow, Int. J. Multiphase Flow, Vol.2, pp. 411-433.

Shock, R. A. W. (1982) Boiling in multicomponent fluids, Multiphase Science and Technology, Vol.1, Chapter 3, Hemisphere Publishing, New York.

Shock, R. A. W. (1973) The evaporation of binary mixtures in forced convection, PhD Thesis, University of Oxford, 402pp.

Singal, L.C, Sharma, C.P. and Varma, H.K. (1983) Experimental heat transfer coefficient for binary refrigerant mixtures of R13 and R12, ASHRAE Trans., Vol.80, pp. 175-188.

Silver, L. (1947) Gas cooling with aqueous condensation, Trans. Inst. Chem. Eng., Vol.25, pp. 30-42.

Sivaniah, E. (1992) Thermocouple calibration procedure for the High Pressure Hydrocarbon Boiling Rig, Link Project Multiphase Group, Dept. Chem. Engng. and Technology, Imperial College London.

Soave, G. (1972) Chem. Eng. Sci., Vol.27, p.1197

Spindler, K. (1994) Flow boiling, 4th Int. Heat Transfer Conf., Brighton, UK, 14-18 Sept., Paper GK-12, pp. 349-368.

Steiner, D. (1991) Wärmeübertragung beim Sieden gesättigter Flüssigkeiten, VDI-Wärmeatlas, Sect. Hbb, VDI-Verlag, Düsseldorf.

Steiner, D. and Taborek, J. (1992) Flow boiling heat transfer in vertical tubes correlated by an asymptotic model, Heat Transfer Eng., Vol.13, No.2, pp. 43-69.

Stephan, K. and Körner, M. (1969) Calculation of heat transfer in evaporating binary liquid mixtures, Chemie-Ing.-Tech., Vol.41, No.7, pp. 409-417.

Stephan, K. and Abdelsalam, M. (1980) Heat transfer correlations for natural convection boiling, Int. J. Heat Mass Transfer, Vol.23, pp. 73-87.

Stephan, K. (1982) Heat transfer in boiling of mixtures, Proc. of the 7th Int. Heat Transfer Conf., München, Germany, 6-10 Sep., Paper RK14, pp. 59-81.

Stephan, K. and Preusser, P. (1978) Heat transfer in natural convection boiling of polynary mixtures, Proc. 6th Int. Heat Transfer Conf., Toronto, Canada, 7-11 Aug., Vol.1, pp. 187-192.

Stephan, K. and Auracher, H. (1981) Correlations for nucleate boiling heat transfer in forced convection, Int. J. Heat Mass Transfer, Vol.24, pp. 99-107.

Sun, G. and Hewitt, G. F. (1996) Experimental studies on heat transfer in annular flow, 2nd European Thermal-Sciences and 14th UIT Nat. H.T. Conf., 1996.

Thome, J. R. (1983) Prediction of binary mixture boiling heat transfer coefficients using only phase equilibrium data, Int. J. Heat Mass Transfer, Vol.26, No.7, pp. 965-974.

Thome, J. R. (1989) Prediction of the mixture effect on boiling in vertical thermosyphon reboilers, Heat Transfer Eng., Vol.10, No.2, pp. 29-38.

Toral, H., Kenning D. B. R. and Shock, R. A. W. (1982) Flow boiling of ethanol / cyclohexane mixtures, Proc. 7th Int. Heat Transfer Conf., München, Germany, 6-10 Sep, Paper FB14.

Toral, H. (1979) Flow boiling heat transfer in mixtures, PhD Thesis, University of Oxford, Vol.1 and 2, 603pp.

Traviss, D. P., Rohsenow, W. M. and Baron, A. B. (1972) Forced convection condensation inside tubes: A heat transfer equation for design, ASHRAE Reprint no. 2272 RP-63.

Ünal, H. C. (1986) Prediction of nucleate pool boiling heat transfer coefficients for binary mixtures, Int. J. Heat Mass Transfer, Vol.29, No.4, pp. 637-640.

Van Stralen, S. J. D. and Zijl, W. (1978) Fundamental developments in bubble dynamics, Proc. 6th Int. Heat Transfer Conf., Toronto, Canada, 7-11 Aug., Vol.6, pp. 429-450.

Van Stralen, S. J. D. (1965) The mechanism of heat transfer in nucleate pool boiling, Int. J. Heat Mass Transfer, Vol.8, pp. 887-914.

Van Sralen, S. J. D. (1970) Pres. at 4th Int. Heat Transfer Conf., Paris, Paper B7.6.

Van Stralen, S. J. D. (1966a) The mechanism of nucleate boiling in pure liquids and in binary mixtures - Part I, Int. J. Heat Mass Transfer, Vol.9, pp. 995-1020.

Van Stralen, S. J. D. (1966b) The mechanism of nucleate boiling in pure liquids and in binary mixtures - Part II, Int. J. Heat Mass Transfer, Vol.9, pp. 1021-1046.

Wadekar V. V. (1990) Flow boiling - A simple correlation for convective heat transfer component, Proc. 9th Int. Heat Transfer Conf., Vol.2, pp. 89-91.

Wadekar, V. V. and Kenning, D. B. R. (1990) Flow boiling heat transfer in vertical slug and churn flow region, 9th Int. Heat Transfer Conf., Jerusalem, Israel, pp. 449-454.

Wadekar, V. V. (1991) Vertical slug flow heat transfer with nucleate boiling, Phase Change Heat Transfer, 28th Nat. Heat Transfer Conf., Minneapolis, MN, USA, 29-31 Jul., ASME, E. Hensel et al (Ed.), ISBN 0791807282, HTD-Vol.159.

Wadekar, V.V. (1995) An alternative model for flow boiling heat transfer, 4th UK Nat. Heat Transfer Conf., UMIST, Manchester, 26-27 Sept., 1995.

Wattelet, J. P. (1995) Predicting boiling heat transfer in a small-diameter round tube using an asymptotic method, Proc. of Convective Flow Boiling, Banff, Alberta, Canada, 30 April - 5 May.

Webb, R. L. and Gupte, N. S. (1992) A critical review of correlations for convective vaporization in tubes and tube banks, Heat Transfer Eng., Vol.13, No.3, pp. 58-81.

Yagov, V.V. (1995) The principal mechanisms of flow boiling heat transfer, Int. Conf. on Convective Flow Boiling, Banff, Alberta, Canada, 30. April - 5. May, Paper IV-9.

You, S. M., Simon, T. W. and Bar-Cohen, A. (1991) Reduced incipient superheats in boiling of fluids which hold dissolved gas, Phase Change Heat Transfer, HTD-159, ASME 1991.

Zizyukin, V. K. and Aerov, M. E. (1975) Heat transfer to certain boiling hydrocarbons during their forced motion in a horizontal tube, Theor. Found. Chem. Eng., Vol.9, pp. 47-52.

BIBL.
LONDIN.
UNIV.